UNIVERSITÀ DEGLI STUDI DI MILANO
PhD Course in Molecular and Cellular Biology
XXIX Cycle

TESTING THE EFFICACY OF BRAIN CHOLESTEROL SUPPLEMENTATION AS A POSSIBLE THERAPEUTIC APPROACH FOR HUNTINGTON'S DISEASE

Eleonora Di Paolo

PhD Thesis

Scientific tutor: Elena Cattaneo

Academic year: 2015-2016
SSD: BIO/14

Thesis performed at University of Milan; Department of Biosciences;
Elena Cattaneo's Laboratory

Contents

Part I

Part II

[*]co-first authors, [§]co-second authors

Abstract

Huntington's disease (HD) is a progressive, fatal, adult-onset, neurodegenerative disorder caused by an expanded CAG repeat in the huntingtin gene, which encodes an abnormally long polyglutamine repeat in the huntingtin protein. Clinical features of Huntington's disease include progressive motor dysfunction, cognitive decline, and psychiatric disturbance. Currently, the available drugs are used only for symptomatic management of Huntington's disease, but there is no effective therapy.

Several studies indicate that brain cholesterol biosynthesis is reduced in several HD rodent models (Valenza et al. 2005) (Valenza et al. 2007) (Valenza et al. 2010) and data from HD patients also suggested a similar reduction (Leoni et al. 2008) (Leoni et al. 2013).

This dysfunction may be detrimental for neuronal cells, especially given that locally synthesized cholesterol is implicated in neurite outgrowth, synapses formation and maintenance, synaptic activity and integrity, and optimal neurotransmitter release (Pfrieger et al. 2003).

Based on these evidences, we supposed that *in vivo* supplying of exogenous cholesterol could rescue aspects of neuronal dysfunction. To verify our hypothesis we used different approaches to deliver exogenous cholesterol to the brain of R6/2 mice (Mangiarini et al. 1996), since peripheral cholesterol is not able to cross the blood brain barrier (BBB).

In our first study, the delivery of cholesterol via brain-permeable polymeric nanoparticles (g7-NPs-Chol) rescued synaptic communication, protected from cognitive decline and partially improved global activity in HD mice (Valenza et al. 2015). In a second study we tested the efficacy of increasing doses of cholesterol directly infused into mouse brain by osmotic minipumps. Results demonstrated that high amounts of cholesterol have to be delivered to observe both cognitive and motor functional recovery in R6/2 mice. More recently, we started to investigate a third innovative non-invasive strategy based on intranasal delivery of cholesterol and preliminary results will be discussed.

Introduction

1. HUNTINGTON'S DISEASE

1.1 Huntington's disease history

Huntington's disease (HD) is a fatal neurodegenerative disorder characterized by psychiatric, cognitive and motor disorders. HD was first recognized as an inherited disorder in 1872 when George Huntington, an American doctor, wrote a paper called "*On Chorea"*. The paper was published in the *Medical and Surgical Reporter* of Philadelphia and gave the first complete description of the disease based on studies of several generations of one family who exhibited similar symptoms.

"Chorea" comes from the Latin and Greek words meaning *chorus* or a *group of dances*. The term was given to many so-called "dancing disorders" that became noticed in the Middle Ages. In those days it was believed that people with chorea, like the involuntary muscle jerks and twitches characteristic of HD, were possessed by devils.

In 1968, Dr. Milton Wexler, a psychoanalyst and clinical psychologist, created the Hereditary Disease Foundation (HDF) to find treatments and cures for HD, after his wife Leonore was diagnosed with the disease. Later years a research team guided by their daughter, the geneticist Nancy Wexler, identified a region of Venezuela where the disease was prevalent. Thus, a twenty-year-long study started in 1979, which allowed to collect over 4,000 blood samples and documented 18,000 different individuals to work out a common pedigree.

The collected samples were useful in a collaborative research project of the HDF, together with the National Institute of Neurological Disorders and Stroke (NIH) to locate the gene that causes the disease. In 1983, the gene was located near the telomere of chromosome 4 and a test to identify carriers of HD was developed (Gusella et al. 1983).

From 1983, the HDF organized and funded a decade-long international collaboration of over 100 scientists named "The Gene Hunters" to find the HD gene itself and finally, in 1993, the HD gene mutation was discovered.

HD was the first genetic disorder to be mapped to a specific locus in the chromosome without prior knowledge of the gene location and one of the first diseases to have prenatal genetic testing made available.

1.2 The genetics of HD

The human HD gene (also called IT15) is located on chromosome 4p16.3 and encodes the protein huntingtin, whose proposed functions will be discussed later. The genetic alteration, which causes the disease, is an increase of the number of repetitions of three nucleic acids (C, A, and G) in the

coding region of the first exon of the HD gene. This results in an expanded polyglutamine tract in N-terminus of huntingtin protein (Htt) (Zuccato, Valenza, and Cattaneo 2010).

The distribution of CAG "triplet" repeats for Huntington's disease may be divided into four categories. Repeats of 26 or fewer are normal. Repeats between 27 and 35 are rare and are not associated with the expression of the disease. Repeats between 36 and 39 are associated with reduced penetrance whereby some individuals will develop HD at an advanced age and others will not. Repeats of 40 or larger are always associated with the expression of HD (Myers 2004).

Merritt et al. first observed that a disproportionate number of cases with juvenile onset HD (before the age of 21) had inherited the HD gene from affected fathers (Merritt, Conneally, and Rahman 1969). This phenomenon termed "anticipation", is typical of trinucleotide repeat disorders, and is explained by the meiotic instability of the HD repeat. Although meiotic instability may occur in both maternal and paternal transmission, in paternal transmission there is a propensity toward larger repeat expansion.

A recent study completed a systematic review of the literature on the prevalence of HD. Overall worldwide prevalence of HD was estimated at 2.71 per 100,000. The study has also revealed that HD prevalence is higher in North America, Europe, and Australia (5.70 per 100,000), compared to Asia and Africa (0.40 per 100,000) (Pringsheim et al. 2012). This difference can be, at least partly, explained by differences in CAG tract size and HTT haplotypes. In fact it is known that the average CAG tract size in European populations is larger than that in Asian and African populations (Squitieri et al. 1994).

Interestingly, genetic variations correlated with onset of motor signs, were recently identified by the genome-wide association (GWAS) study (Modifiers of Huntingtons Disease Consortium 2015). Two genetic loci on chromosomes 15 and 8 were found. In particular, the region on chromosome 15, harbors two independent modifier association signals in the HD population: one that anticipates and the other that delays age of onset. The region on chromosome 8 carries a modification signal that delays onset. The study also suggested a role of MLH1 gene, involved in mismatch DNA repair, in modifying the onset of disease due to an effect on somatic HTT CAG repeat instability.

1.3 Clinical manifestations of HD

One of the main focuses in HD research is the development of new therapeutic strategies, as currently there is no treatment to delay or prevent the progression of the disease. Neuronal dysfunction and death observed in HD are caused by a combination of many pathogenic processes that lead to motor, cognitive and psychiatric symptoms. Other less well-known, but prevalent features of HD include weight loss, sleep- and circadian rhythm disturbances and autonomic

nervous system dysfunction. The mean age at onset is between 30 and 50 years, with a range of 2 to 85 years. The mean duration of the disease is 17-20 years and most common cause of death is pneumonia.

Motor symptoms and signs

When HD was first discovered it was called Huntington's chorea, due to the uncontrollable, dance-like movement that is common among patients. The unwanted movements, which initially occur in the distal extremities and in small facial muscles, gradually spread to all other muscles. Choreatic movements are always present when the patient is awake, so that even walking becomes unstable. However, the pattern of motor symptoms tends to change over time: while chorea declines, dystonia (sustained or repetitive muscle contractions that result in twisting and repetitive movements or abnormal fixed postures), rigidity and akinesia (inability to initiate movement) becomes more marked leading to bradykinesia (slowness of movement). Also dysarthria (a motor speech disorder) and dysphagia (difficulty in swallowing) become very prominent during the course of the disease.

Behavior and psychiatric symptoms and signs

Psychiatric symptoms very frequently appear in the early stage of the disease, and can even anticipate the onset of motor symptoms. These symptoms and signs have a highly negative impact on family daily life (Wheelock et al. 2003). The most frequently signs are depression and anxiety. Obsessions and compulsions are also common and lead to irritability and aggression. Furthermore, HD patients manifest apathy and increasing passive behavior with the progression of the disease. Psychosis most frequently appears in the later stages and is accompanied by cognitive decline. The complete clinical picture is comparable to schizophrenia with paranoid and acoustic hallucinations. An additional aspect of the disease is the higher risk of suicide, frequently associated to the genetic test and the loss of independence in daily life.

The cognitive impairment

Although the clinical diagnosis of HD relies on the onset of motor abnormalities, patients manifest the first signs of cognitive impairments at least 15 years prior, in parallel with volume loss detected by MRI (Paulsen et al. 2004) (Aylward et al. 2011). Cognitive decline in HD is mostly due to cortico-striatal and hyppocampal dysfunctions. Patient's actions and behaviors are not more goal-directed or planned. Furthermore, HD patients are not able to distinguish what is relevant from what can be ignored and are no longer able to organize or plan their life. HD patients have difficulty in learning new information or recall previously learned information (Sadek et al. 2004) (Montoya et

al. 2006). The implicit memory, that includes those coordinated movements and skills that allow to ride a bike, play a musical instrument and even the ability to chew and swallow without choking, is compromised.

More in detail, at pre-symptomatic stages one of the most common cognitive deficits affects tasks requiring a shift in strategy (Lawrence et al. 1998) (Ho et al. 2003). Executive functions, verbal fluency (Hahn-Barma et al. 1998) (Paulsen et al. 2001), procedural learning, planning, and explicit motor learning result impaired (Lawrence et al. 1998) (Rosenberg et al. 1995) (Schneider et al. 2010). The execution of ordinary mental tasks is more tiring and requires more time.

At early symptomatic stages, HD patients show a significant deficit in discrimination and reversal learning (Lawrence et al. 1999). Moreover, attention, acquisition of psychomotor skills, planning and executive functions progressively decline (Watkins et al. 2000) (Ho et al. 2003). In early symptomatic HD patients, there are alterations in associative learning, pattern and spatial short-term memory, in spatial working memory (Lawrence et al. 2000), and there are deficits in recall and recognition memory (Montoya et al. 2006).

Middle symptomatic stage is characterized by a widespread worsening in executive function, verbal fluency, perceptual speed and reasoning (Bäckman et al. 1997) (Lemiere et al. 2004). In this stage HD patients show episodic memory and spatial memory deficits (Bäckman et al. 1997) (Lemiere et al. 2004).

Finally, at more advanced symptomatic stages, patients manifest a sub-cortical dementia with alterations in cognitive functions involving slow information processing, decreased motivation, depression, apathy and personality changes (Paulsen et al. 1995) (Zakzanis 1998). Thus, tasks relying on hippocampal and cortico-temporal integrity (declarative memories: visuospatial, spatial working memory and object and spatial perception/recognition) are altered in HD patients also if to a lesser extent than those dependent on cortico-striatal integrity (procedural learning). Finally, different findings have suggested that HD lead to alterations in the perception of time and the production of timed output (Hinton et al. 2007) (Rowe et al. 2010).

Secondary symptoms and signs

In addition to motor, psychiatric and cognitive symptoms, there are other important symptoms in HD, including weight loss, sleep disturbances and autonomic disturbances. From early on, weight loss has been reported in all patients. A recent study have described a relationship between the weight loss and the CAG tract size (Aziz et al. 2008). This can be also ascribed to decreased appetite, difficulty handling food and swallowing. An additional causative factor is hypothalamic neuronal loss (Aziz et al. 2007).

Recently, attention has been focused also on sleep and circadian rhythm disturbances of patients with HD. The first description of these type of abnormalities in HD patients came from the study of Morton (2005) showing as HD patients exhibit abnormal night-day ratios, although interestingly they do not report any major sleep difficulties. A delayed sleep phase and an increased REM latency together with circadian changes in melatonin have been reported in HD (Aziz et al. 2010). Melatonin synthesis is directly regulated by the SCN and it plays a major role in the regulation of sleep and other circadian rhythms. HD patients report insomnia and increased daytime somnolence (Goodman & Barker 2010), besides impaired quality of sleep, reduced sleep efficiency (Silvestri et al. 1995) (Mena-Segovia et al. 2002) and reduced sleep time (Silvestri et al. 1995). The progressively worsening sleep disorder appeared to be independent of CAG repeat length (Arnulf et al. 2008)

Also the autonomic symptoms are highly prevalent in patients with HD. These symptoms are related to functional disability and depression and may precede the onset of motor signs. 44% of patients, even at early stages of the disease, manifest autonomic dysfunction whereby both the sympathetic and parasympathetic system are affected (Andrich et al. 2002). Different autonomic disturbances, such as hyperhydrosis, sexual dysfunction, swallowing difficulties and dysphagia, have been reported in HD patients (Aziz et al. 2010). The origin of autonomic dysfunction is found in alterations of the central autonomic network that includes the hypothalamic region and its connections to the cortex, limbic system, brainstem, and spinal cord (Benarroch 1993). Indeed, hypothalamic damage has been found in HD patients (Aziz et al. 2007) (Politis et al. 2008).

1.4 Neuropathological features of HD

HD brain is characterized by a variable pattern of neuropathological changes (Vonsattel and DiFiglia 1998) that reflect the highly variable symptomatology of HD even among comparing cases with the same number of CAG repeats (Friedman et al. 2005) (Gómez-Esteban et al. 2006) (Tippett et al. 2006). The most affected brain area is the neostriatum, which includes the caudate nucleus and putamen, but, especially in more severe cases, also other brain regions are involved. Gross examination of postmortem HD human brains highlights a characteristic bilateral atrophy of the striatum (Vonsattel and DiFiglia 1998) (Vonsattel, Keller, and Pilar Amaya 2008). In particular, the putamen had an average 64% cross-sectional area loss compared with a 57% cross-sectional area loss in the caudate nucleus (de la Monte et al. 1988).

In 1985, JP Vonsattel developed a neuropathological grading system for HD based on the pattern of striatal neurodegeneration observed in a wide sample of HD brains (Vonsattel et al. 1985). Grade 0 comprises HD brains that show indistinguishable features from control brains. However, 30–40%

neuronal loss has been revealed in the head of the caudate nucleus upon histological examination. Grade 1 comprises HD brains in which the body of caudate nucleus shows atrophy, neuronal loss, and astrogliosis. Gross striatal atrophy is described mild to moderate in grade 2 and severe in grade 3. In Grade 4, the striatum is severely atrophic with a strong neuronal loss of about 95%. Furthermore, in Grades 1 and 2, non-striatal structures of the brain are apparently normal, or show only mild atrophy. In grades 3 and 4 also other brain regions as globus pallidus, neocortex, thalamus, subthalamic nucleus, substantia nigra, and cerebellum are smaller than normally expected.

The most affected neuronal populations in the HD striatum are the medium-sized spiny projection neurons (MSNs) that constitute 90–95% of the total striatal neuronal population. The MSNs degeneration is associated with increasing HD grade (Vonsattel et al. 1985) (Vonsattel and DiFiglia 1998) and leads to the disruption of important striatal pathways. Immunohistochemical studies also revealed differential loss of striatal projection neurons in HD. In particular, in early and middle stages of the disease, enkephalin-containing neurons, projecting to the external segment of the globus pallidus, results much more affected than substance P-containing neurons projecting to the internal pallidal segment. Furthermore, substance P-containing neurons projecting to the substantia nigra pars reticulata results more affected than those projecting to the substantia nigra pars compacta. At later stages of the disease, projections to all striatal target areas are significantly reduced, with the exception of some apparent sparing of the striatal projection to the substantia nigra pars compacta (Reiner et al. 1988). However, in most severe HD cases the extreme striatal atrophy and loss of neurons observed indicate that even the striatal interneurons are affected (Reiner et al. 2013). Cortical atrophy is another hallmark of HD brains, especially at advanced stages of the disease. Many studies highlight volume loss, cortical thinning, and neuronal loss in HD cerebral cortex (Macdonald & Halliday 2002) (Rosas et al. 2002) (Thu et al. 2010). In particular, the cortical volume loss was demonstrated to correlate with the degree of striatal atrophy and the number of CAG repeats, suggesting a relation between disease processes occurring into striatum and cortex. Neurodegeneration of cortical pyramidal neurons is also observed but in a smaller degree respect to that of MSNs (Vonsattel et al. 1985) (Hedreen et al. 1991).

An additional neuropathalogical feature of HD is the reactive gliosis, especially in the dorsal striatum (Myers et al. 1991). Gliosis involves the proliferation or hypertrophy of several types of glial cells, including astrocytes, microglia, and oligodendrocytes and form part of the inflammatory response of the diseased brain. Interestingly, activated microglia correlated with neuronal loss in the neostriatum, globus pallidus, cerebral cortex, and white matter (Sapp et al. 2001). Furthermore, astrocytes in the white matter of HD brain display intranuclear inclusions (Shin et al. 2005),

especially in advanced stages. This phenomenon may contribute to the overall metabolic dysfunctions of the HD brain.

Another HD pathological hallmark consists in the presence of intracellular aggregates of mutant Htt. Mutant Htt shows a similar expression level and regional distribution to the wild-type Htt in the brain (Aronin et al. 1995), but abnormal accumulation of its N-terminal fragments gives rise to typical aggregates/inclusions in the nucleus, cytoplasm, and dystrophic neurites in HD brains (DiFiglia et al. 1997). These protein aggregates are thought to be formed by associations of polyglutamine (polyQ) regions, which act as a "polar zipper" (Perutz 1996). The immunohistochemical analyses of postmortem human HD brain have demonstrated the presence of aggregates that can form neuronal intranuclear inclusions (NIIs) or cytoplasmic and neuropil extranuclear inclusions (NEIs), and Htt aggregates also form in axons and dendritic spines. The inclusions are already evident in the HD human brain before onset of symptoms and can be found throughout the cortex, but less frequently in the striatum (Gutekunst et al. 1999) (Maat-Schieman et al. 1999) (Herndon et al. 2009).

Finally, white matter changes have been reported in HD brains, although detailed systematic studies have not been carried out. Earlier studies measured 29–34% changes in overall white matter area in slices through HD brains (de la Monte et al. 1988). More recent studies based on neuroimaging techniques show changes in the white matter even at pre-symptomatic phase of HD, in different brain regions (Rosas et al. 2006) (Rosas et al. 2010).

1.5 Normal Htt distribution and functions

Cellular and tissue distribution

Htt is expressed ubiquitously in humans and rodents, but reaches the highest expression levels in the neuronal cells within the central nervous system (CNS) (DiFiglia et al. 1995) (Ferrante et al. 1997). Htt is particularly enriched in cortical pyramidal neurons in the layers III and V that project to the striatal neurons (Fusco et al. 1999). Within cells, mammalian Htt is associated with different organelles, including the nucleus, endoplasmic reticulum, Golgi complex, and mitochondrion (Hilditch-Maguire et al. 2000) (Kegel et al. 2002) (Panov et al. 2002) (Strehlow et al. 2006). In particular, in neuronal cells, Htt localize within neuritis and at synapses, where it associates with various vesicular structures such as clathrin-coated vesicles, endosomal compartments or caveolae and microtubules (DiFiglia et al. 1995) (Velier et al. 1998) (Hilditch-Maguire et al. 2000).

Htt interacts with proteins involved in different cellular functions including clathrin-mediated endocytosis, apoptosis, vesicle transport, cell signaling, morphogenesis, and transcriptional regulation (Li and Li 2004). Htt binds also to proteins of the synaptic complex such as protein

kinase C, casein kinase substrate in neurons 1 (PACSIN-1) and postsynaptic density 95 (PSD95), thus participating in the regulation of synaptic activity (Sun et al. 2001) (Smith et al. 2005).

Htt functions

There are solid evidence showing the critical role of Htt for embryonic development. Generation of nullizygous Htt mice ($Hdh^{-/-}$) causes embryonic death between day 8.5 and 10.5 (Zeitlin et al. 1995). The same study found that a single wt HTT allele is sufficient to carry out the developmental function of Htt in mice. Furthermore, with the progression of embryonic development, Htt levels lowering to below 50% leads to defects in the epiblast and severe cortical and striatal architectural anomalies (White et al. 1997) (Auerbach et al. 2001). Wild-type Htt plays also a critical role in brain maturation, especially in establishing and maintaining cortical and striatal neuronal identity (Reiner et al. 2001).

Interestingly, also mHtt can carry out this developmental role. In fact HD patients are born normally and the onset of symptoms occurs several years after birth. Even homozygosity for CAG mutation does not results in evident developmental defects in HD patients (Wexler et al. 1987). In addition, expression of human Htt with a pathological polyglutamine expansion (72 CAG repeats) rescues $Hdh^{-/-}$ mice from embryonic lethality (Leavitt et al. 2001).

All these evidence suggest that, despite the mutation, Htt can perform its physiological function during development.

However, more recent findings (Molero et al. 2009) suggest that developmental abnormalities occur in a knock-in mouse model of HD (HdhQ111) compared with a knock-in mouse expressing 18 CAG (HdhQ18). In particular, the striatum of HdhQ111 embryos at E17.5, show impairment in the acquisition of the cytoarchitecture of striatal subcompartments, suggesting abnormal specification and maturation of MSN.

Htt has an important prosurvival role as demonstrated by different *in vitro* and *in vivo* studies. The first *in vitro* experiment was performed using ST14A striatal cells, transfected with wild-type htt (Rigamonti et al. 2000). They found that cells expressing high levels of exogenous wt Htt protein were protected from death. On the contrary, the same cells transfected with mHtt showed a fastern viability decline, indicating that the mHtt is not able to act as a neuroprotective protein.

Additional studies confirmed the antiapoptotic role of Htt. Primary striatal neurons derived from YAC18 transgenic mice overexpressing full-length wild-type human Htt were protected from apoptosis compared with cultured striatal neurons from nontransgenic littermates or from YAC72 mice expressing human mHtt (Leavitt et al. 2006).

Different studies clarified some of the mechanisms by which wild-type Htt protects cells from apoptosis. Wild-type Htt is able to prevent the formation of a functional apoptosome complex and the consequent activation of caspase-3 and caspase-9 (Rigamonti et al. 2000) (Rigamonti et al. 2001). Furthermore, wild-type Htt physically interacting with active caspase-3, blocks its proteolytic activity and interferes with procaspase-8 activation (Hackam et al. 2000). A pro-survival role for Htt has also been demonstrated *in vivo.* Overexpression of full-length wild-type Htt in yeast artificial chromosome (YAC18) transgenic mice conferred protection against apoptosis triggered by NMDA receptor induced excitotoxicity (Leavitt et al. 2006). Moreover, it has been found that levels of endogenous Htt are reduced following ischemic injury through a caspase mediated process, while overexpression of wild-type Htt in mice protects against ischemic injury in a dose-dependent manner (Zhang et al. 2003).

WT Htt is also linked to Brain-derived neurotrophic factor (BDNF), a neurotrophin particularly important for the survival of striatal neurons and for the activity of the cortico-striatal synapses (Zuccato and Cattaneo 2007). Most of striatal BDNF is anterogradely transported from the cortex to striatum (Altar et al. 1997) via the cortico-striatal afferents (Fusco et al. 1999) in which Htt and BDNF colocalize. YAC18 mice overexpressing wild-type Htt showed a significant increase in cortical production and striatal levels of BDNF (Zuccato et al. 2001) compared with control littermates. On the contrary, reduced BDNF mRNA levels were found in brain samples from wild-type Htt-depleted mice as well as in heterozygous Htt knock-out mice (Zuccato et al. 2003). Wild-type Htt promotes cortico-striatal BDNF expression by enhancing transcription of exon II of the BDNF gene (Zuccato et al. 2001). This function is exclusive to wild-type Htt, indeed mice overexpressing mHtt show a decrease of BDNF levels compared with controls (Zuccato et al. 2001).

Wt Htt is also involved in BDNF vesicle trafficking along microtubules, through its interaction with the molecular motors dynein/dynactin and kinesin (Caviston et al. 2007). BDNF vesicle trafficking is enhanced in the presence of wild-type Htt and conversely reduced either in the presence of mHtt or when the levels of wild-type Htt are reduced by RNA interference (Gauthier et al. 2004).

Besides the BDNF vesicles, Htt transports synaptic precursor vesicles (Zala et al. 2013), v-SNARE VAMP7 protein containing vesicles (Colin et al. 2008), autophagosomes (Y. C. Wong & Holzbaur 2014), endosomes and lysosomes (Liot et al. 2013). Htt mediates the transport of organelles, in both the anterograde and retrograde directions, and in axons and dendrites within neurons.

Furthermore, Htt is also involved in endocytosis, vesicle recycling and endosomal trafficking (Waelter et al. 2001) (Harjes & Wanker 2003) (Kaltenbach et al. 2007) (Moreira Sousa et al. 2013).

Wild-type Htt can affect gene transcription in many different ways. Indeed it interacts with numerous transcription factors, as the cAMP-response element (CREB)-binding protein (CBP) (Steffan et al. 2000) and the nuclear factor-kB (NF-kB) (Takano & Gusella 2002). Htt also binds transcriptional activators and repressors as the Gln-Ala repeat transcriptional activator CA150 (Holbert et al. 2001) and the repressor element-1 transcription factor/neuron restrictive silencer factor (REST/NRSF) (Zuccato et al. 2003). Further target of Htt are nuclear receptors, including LXRa and peroxisome proliferator-activated receptor-g (PPARg) (Futter et al. 2009). Htt also activates the transcription of genes containing a conserved repressor element 1 sequence (RE1, also named the neuron-restrictive silencer element NRSE) (Zuccato et al. 2003), recognized by REST transcriptional silencer. One of the most important NRSF-regulated genes is the BDNF gene (Zuccato et al. 2001). Htt may also act as a transcriptional cofactor itself (Benn et al. 2008) and a chromatin remodeling factor (Seong et al. 2009). Finally, Htt may mediate the transport to the nucleus of transcription factors and regulators (Marcora et al. 2003).

Htt is involved in autophagy cellular process. Through its scaffolding function of the dynein/dynactin/HAP1 complex, Htt regulates the retrograde transport of autophagosomes along axons (Wong & Holzbaur 2014). Htt also participates in the clathrin coated-mediated post-Golgi trafficking to lysosomes through its interaction with optineurin/Rab8 (del Toro et al. 2009). An essential role for Htt in p62-dependent cargo recognition, required for correct sequestration of cargo into autophagosomes, has been recently identified (Rui et al. 2015). This autophagy regulatory function of HTT is conserved from flies to humans (Rui et al. 2015).

Finally, Htt play also an essential role in mitotic spindle positioning in mammary stem cells (Elias et al. 2014) and it is required for correct ciliogenesis (Keryer et al. 2011).

1.6 Molecular dysfunctions in HD

Many pathogenic mechanisms have been identified in HD including proteolysis and aggregation of mutant Htt (mHtt) (Vonsattel et al. 1985) (Poirier et al. 2002) (Legleiter et al. 2010), mitochondrial dysfunction (Gu et al. 1996) (Panov et al. 2002) (Chen et al. 2007) (Browne 2008), impaired protein degradation pathways (Bennett et al. 2007) (Martinez-Vicente et al. 2010), reduction of striatal BDNF (Gauthier et al. 2004) (Zuccato et al. 2008) (Zuccato and Cattaneo 2009).

In this introduction HD mechanisms related to altered transcriptional dysregulation, synaptic alterations and glial dysfunctions will be considered.

Transcriptional dysregulation

A large number of studies have provided evidence for transcriptional abnormalities in HD, even before the onset of symptoms (Cha 2007). These include changes in mRNA levels, direct interactions between Htt and proteins of the transcriptional machinery, and inhibition of enzymes involved in chromatin remodeling.

A whole-genome analysis, based on a microarray platform, revealed that the variety of altered genes increased with the progression of the disease (Chan et al. 2002) (Luthi-Carter et al. 2002) (Sipione et al. 2002). In particular, the altered genes were associated with transcriptional processes, neurotransmitter receptors, synaptic transmission, cytoskeletal and structural proteins, intracellular signaling, and calcium homeostasis.

In 2006, Luthi-Carter completed a gene expression profile of HD patients (Hodges et al. 2006), showing gene expression changes in the caudate and motor cortex and confirming the set of down-regulated genes previously identified in HD transgenic mice (Luthi-Carter et al. 2002). Gene expression profile studies revealed that transcriptional abnormalities occurred also in the skeletal muscles (Luthi-Carter et al. 2002) (Strand et al. 2005). It was also found that mHtt itself can repress transcription of genes binding their specific transcriptional factors (Zhai et al. 2005) (Benn et al. 2008). Indeed TFIID, TFIIF, and TAFII130, which are components of the core transcriptional machinery, are direct targets of mHtt (Shimohata et al. 2000) (Dunah et al. 2002) (Zhai et al. 2005).

One of the main transcriptional abnormalities described in HD concerns the neuronal gene repression mediated by the transcription factor REST/NRSF (Zuccato et al. 2007). REST/NRSF represses a large cohort of neuronal-specific genes, among the BDNF gene, through recruitment of the DNA regulatory motif RE1/NRSE (Ooi & Wood 2007). RE1/NRSE silencing activity is inhibited in the presence of wild-type Htt, on the contrary protein mutation induces the activation of RE1/NRSE leading to a significant decrease of BDNF levels (Zuccato et al. 2003) (Zuccato et al. 2007). By using a microarray-based survey of gene expression in a large cohort of HD patients and matched controls (Hodges et al. 2006), most of REST/NRSF target genes were found down regulated in the HD caudate (Johnson & Buckley 2009). Transcriptional dysregulation in HD was also linked to energy defects since Htt inhibits expression of PGC-1α, the main transcription coactivator involved in the regulation of cellular energy metabolism (Cui et al. 2006). Mutant Htt may interfere with gene expression also by inducing modifications in chromatin structure. The expanded polyQ can indeed directly bind CREB binding protein (CBP) and p300/CBP associated factor (P/CAF), blocking their acetyltransferase activity (Steffan et al. 2001). This results in a condensed chromatin state and reduced gene transcription.

Synaptic alterations

Survival and activity of striatal neurons, the most affected neuronal population in HD, depend on glutamate release from the cortical afferents. An increased glutamate release from cortical afferents in parallel with reduced uptake of glutamate by glial cells may contribute to the excessive activation of glutamate receptors observed in HD. Impaired clearance of glutamate from the synaptic cleft may also contribute to enhance excitotoxic neurodegeneration in HD. In some HD mouse models (R6/2 and R6/1 lines), the Na^+-dependent glial transporter of glutamate GLT1 is down-regulated and appears responsible for decreased striatal glutamate uptake (Liévens et al. 2001) (Estrada-Sánchez et al. 2009). Decreased GLT1 mRNA and deficient glutamate uptake has also been reported in post mortem brain tissues taken from HD patients (Arzberger et al. 1997) (Hassel et al. 2008). Results from electrophysiological experiments also confirmed the excitotoxic hypothesis. Enhanced NMDA receptors sensitivity to NMDA and increased NMDA evoked currents have been described in striatal neurons from full-length HD mouse models (Fan & Raymond 2007). Furthermore, altered information processing in the prefrontal cortex of HD mouse models and dysregulation of coordinated neuronal firing patterns in striatum (Miller et al. 2008) (Walker et al. 2008) suggest that the loss of connectivity between the cortex and striatum may participate in the excitotoxic process and contribute to the development of the HD phenotype.

Mutant Htt causes also the over activation (Song et al. 2003) and the trafficking impairment of NMDA receptors (Fan et al. 2007). Also changes in NMDA receptors protein level or subunits have been proposed as possible mechanisms responsible for aberrant NMDA receptors activity in HD (Cepeda et al. 2001) (Ali & Levine 2006) (Fan et al. 2007). The R6/2 transgenic mouse model displays a deficiency in metabotropic glutamate receptor mGluR2 that could lead to glutamate-mediated overstimulation of the postsynaptic striatal neurons (Cha et al. 1998) (Cha et al. 1999) (Luthi-Carter et al. 2000) (Luthi-Carter et al. 2003). Other mechanisms can contribute to excitotoxicity in HD. The polyglutamine expansion alters the interaction between Htt and post-synaptic density 95 (PSD95) scaffolding protein, resulting in the sensitization of NMDA receptors (Sun et al. 2001). In HD patients, a significant decrease in NMDA receptor (NMDAR) binding at pre- and early symptomatic stages has been detected (London et al. 1980) (Young et al. 1988) (Albin et al. 1990) (DiFiglia 1990).

Contrary to all these studies, a recent paper has shown that glutamate clearance in the striatum of R6/2 mice is normal or even accelerated (Parsons et al. 2016). Indeed, thanks to an innovative approach based on a real-time imaging technique using a fluorescent reporter as glutamate sensor (iGluSnFR) it was possible to quantify real-time glutamate dynamics in R6/2 mouse models. This

evidence supports the hypothesis that glutamate clearance is not the major contributor to excitotoxic cell death in HD.

Other neurotransmitter systems, controlling the activity of the corticostriatal synapse, result compromised in HD, contributing to striatal excitotoxicity. Evidence of aberrant Adenosine 2A receptor function (Tarditi et al. 2006) as well as downregulation of the dopamine transporter and D1 and D2 receptors has also been reported in HD brains (Augood et al. 1997) (Cha et al. 1998) (Cha et al. 1999).

Glial dysfunctions

Astroglia represent the major cellular component of the CNS and their dysfunction contributes to the pathogenesis of most neurological diseases. Glial cells expressing mutant HTT are characterized by compromised morphology and function that can exacerbate neurological symptoms in HD (Hebb et al. 1999) (Shin et al. 2005). Accordingly, transgenic mice that express N-terminal mHtt under the control of GFAP promoter, display age-dependent neurological phenotype and accumulation of mutant protein in astrocytes (Bradford et al. 2009).

Many studies demonstrate that one of the most important astrocyte-mediated mechanisms altered in HD is the glutamate uptake for preventing neuronal excitotoxicity.

Indeed, *in vitro* experiments have shown that the expression of mHtt in HD astrocytes results in a decreased expression of GLT-1 and GLAST glutamate transporters (Shin et al. 2005). Time-dependent reduced expression of both GLT-1 and GLAST was observed in striatal specimens from HD subjects and in an HD animal model expressing short N-terminal fragment of mHtt selectively into striatal astrocytes (Faideau et al. 2010). The same results emerged by analyzing the levels of these glutamate transporters in the R6/2 transgenic mice (Behrens et al. 2002) (Estrada-Sánchez et al. 2009). In addition to glutamate transporters abnormalities, a defect in Ca(2+)-dependent glutamate exocytosis has also been demonstrated in HD astrocytes (Lee et al. 2013).

Another well-known astrocytic homoeostatic function is to regulate extracellular potassium. A recent study found that symptom onset in R6/2 and Q175 HD mouse models was associated with decreased expression of striatal astrocytes Kir4.1 K^+ channel, leading to elevated striatal extracellular K^+ *in vivo.* Interestingly, restoration of Kir4.1 function normalized extracellular K^+, ameliorated aspects of MSN dysfunction, prolonged survival and attenuated some motor phenotypes in R6/2 mice (Tong et al. 2014). These results were recently confirmed by a new study showing early-onset astrocytes loss of Kir4.1- and Glt1-mediated homeostatic functions in R6/2 mice, which may in turn contribute to altered MSNs in the striatum (Jiang et al. 2016).

All these findings suggest that the presence of mutant Htt in astrocytes impairs glial glutamate potassium and calcium homeostasis leading to excitotoxicity that may contribute to HD pathogenesis.

Normally, astrocytes are also an important source of BDNF in the brain (Miyamoto et al. 2015) but the expression of mHtt inhibits BDNF exocytosis from these cells (Hong et al. 2016).

As described later in a dedicated paragraph, another important function of astrocytes consists in supplying cholesterol to neuronal cells by ApoE-containing lipoproteins (Lahiri 2004). A paper from our lab has shown that astrocytes bearing the Htt protein containing increasing CAG repeats secreted less apoE-lipoprotein-bound cholesterol in the medium (Valenza et al. 2015). Furthermore, conditioned media from HD astrocytes was detrimental in a neurite outgrowth assay and did not support synaptic activity in HD neurons, compared with conditioned media from wild-type (wt) astrocytes (Valenza et al. 2015).

A recent work have further investigated the role of glial cells in HD, by neonatally engrafting immunodeficient mice with mutant Htt (mHTT)-expressing human glial progenitor cells (hGPCs) (Benraiss et al. 2016). It was found that while mHTT glia impaired behavioral phenotype of healthy mice, normal glia engraftment was able to ameliorate aspects of the disease in transgenic HD mice.

All the described dysfunctions represent potential therapeutic target for HD treatment. However, the discovery of genetic cause of HD have offered the opportunity to develop genetic approaches aimed at inhibiting mutant Htt expression, which are currently considered among the most promising emerging therapeutics for HD (Garriga-Canut et al. 2012) (Magen & Hornstein 2014). The use of antisense oligonucleotides (ASOs) have been found to reduce mutant Htt-associated abnormalities in animal models of HD (Kordasiewicz et al. 2012) (Skotte et al. 2014). Ionis Pharmaceuticals, has initiated a clinical study with this “Htt lowering” strategy.

2. MOUSE MODELS OF HD

There are a variety of mouse models available for the study of HD that recapitulate many of the features of the human disease. HD animal models can be divided into two broad categories, nongenetic and genetic. Nongenetic models are easy to generate and use, and basically induce cell death by excitotoxic mechanisms or by alteration of mitochondrial metabolism.

Genetic models differ in their CAG repeat numbers (and stability of the stretch), size and species of origin (mouse or human) of the Htt protein, promoters driving the protein expression and their

background strain. As a consequence, each model exhibits a different characteristic phenotype. Genetic models can be grouped into:

- N-terminal transgenic animals, carrying the 5' portion of the human mutant HTT gene, including exon 1 that contains the CAG repeat region.
- Full-length transgenic models, expressing full-length mutant HTT.
- Knock-in models, carrying an expanded polyglutamine stretch within the mouse HTT protein.

2.1 The R6/2 transgenic model

The R6/2 is the most widely studied transgenic mouse model of HD. It allows a depth and relatively rapid evaluation of the efficacy of pre-clinical therapeutic strategies, for this reason R6/2 model is been chosen for our *in vivo* studies.

This animal model was generated by random insertion into the mouse genome of exon 1 from the 5' end of the human HTT gene, with approximately 150 CAG repeats (Mangiarini et al. 1996). In these mice the transgene expression is driven by the human Htt promoter and reach 75% of the level of the endogenous gene in all cells (Mangiarini et al. 1996). This model is characterized by a very aggressive, rapidly progressing phenotype, similar to the juvenile form of HD in humans. Most of the behavioral symptoms appear around 8-9 weeks of age and average life expectancy is around 14 weeks.

During the progression of the disease, R6/2 mice develop both motor and cognitive dysfunctions.

Motor symptoms include resting tremor, chorea-like movements, stereotypic involuntary grooming movements and clasping behavior (Mangiarini et al. 1996) (Stack et al. 2005). Starting from 3 weeks of age, mice display locomotor hyperactivity (Lüesse et al. 2001), while around 8 weeks of age they become hypoactive (Carter et al. 1999) (Stack et al. 2005). In the same period, R6/2 begin to show an abnormal paw clasping response, recognizable by dystonia of the limbs when suspended by the tail. Around 8 weeks of age, other gradual changes in motor function, such as stereotypical hindlimb grooming and involuntary movements appear. As a result, R6/2 motor coordination, assessed by the Rotarod test, progressively deteriorates by 8–12 weeks of age (Carter et al. 1999) (Lüesse et al. 2001). R6/2 mice exhibit severe cognitive abnormalities before the onset of motor defects (Lione et al. 1999). At 3.5 weeks their performance in the hippocampal dependent Morris water maze spatial learning task is impaired. Furthermore, at around 8 weeks of age, these animals completely lose the ability to learn the task, partly for the worsening in swimming ability (Lione et al. 1999) (Murphy et al. 2000). R6/2 mice also demonstrate difficulty in reversing pre-learned tasks in the two-choice swim T-maze (Lione et al. 1999). This particular test requires correct functioning of the frontostriatal circuitry that allows to subjects to replace of a previously learned strategy

(Goldberg et al. 1990) (Van Raamsdonk et al. 2005). It is known that the impairment of these neural pathways results in loss in executive function, procedural memory and psychomotor skills in HD patients (Heindel et al. 1988) (Bylsma et al. 1990) (Lange et al. 1995), therefore deficits in the T-maze may be more closely related to those seen in HD. Finally, R6/2 mice display impaired long-term memory (LTM) during disease progression (Giralt et al. 2011) as assessed by the Novel Object Recognition test (NORT), based on the spontaneous tendency of rodents to spend more time exploring a novel object than a familiar one (Antunes & Biala 2012).

R6/2 mice are also characterized by many neuropathological signs. In particular, this animal model demonstrate robust brain atrophy (about 20% brain weight loss at 12 weeks) (Davies et al. 1997) but only moderate cerebral cell death. Since only a small number of cortical and striatal neurons undergo "dark cell degeneration" (Turmaine et al. 2000), probably the significant reduction in brain volume is the result of atrophy of individual neurons and massive decrease in neuropil. Indeed, the cell bodies of striatal medium-sized spiny neurons have been described to shrink by around 20% in surface area and the size of their dendritic fields is also reduced (Klapstein et al. 2001). Another frequently used pathological endpoint in R6/2 mice is the presence of mutant Htt-containing nuclear inclusions (NIs) and neuropil aggregates (NAs) in different brain regions. Aggregates and inclusions first appear in the striatum and the cortex around 3–4 weeks of age and progressively increase until late symptomatic phase in which around 98% of the striatal projection neurons (calbindin positive) exhibit Htt inclusions (Meade et al. 2002). Glial cells do not appear to develop these protein inclusions (Davies et al. 1997). In R6/2 mouse model an alteration in gene expression is also evident. Within the striatum, the levels of mRNAs encoding components of the neurotransmitter, calcium and retinoid signaling pathways are decreased at both early and late symptomatic time points (6 and 12 weeks of age). Conversely some genes associated with cell stress and inflammation appear to be upregulated in striatum but also in cerebellum and in peripheral tissues of R6/2 mice (Luthi-Carter et al. 2000) (Luthi-Carter et al. 2002). In addition, increases in markers for oxidative damage to DNA (Bogdanov et al. 2001) and mitochondrial dysfunctions (Tabrizi et al. 2000) have been found in R6/2 striatum.

Different studies revealed an abnormal neurotransmission in R6/2 mice that may account for striatal neuronal vulnerability. Starting from 8 weeks of age, to advanced stages of the disease, cortico-striatal LTP results impaired in R6/2 mice (Kung et al. 2007). Striatal neurons exhibit more depolarized resting potentials (Levine et al. 1999) and increased intracellular calcium levels (Hansson et al. 2001). Furthermore, alterations in the firing patterns of cortico-striatal fibers have been demonstrated in the brains of R6/2 mice (Cepeda et al. 2003) together with changes in neurotransmitter release (Behrens et al. 2002). At specific stages of the disease R6/2 mice show

reduced synthesis of neurotransmitters such as dopamine (Hickey et al. 2002) (Johnson et al. 2006) and serotonin (Reynolds et al. 1999) (Yohrling IV et al. 2002), but also severe alterations in the levels of synaptic proteins (Morton et al. 2001) and deficits in glial glutamate uptake (Liévens et al. 2001). At the postsynaptic sites R6/2 mice display a progressive reduction in dopamine and glutamate receptors expression (Cha et al. 1998) (Cha et al. 1999) (Zucker et al. 2005).

R6/2 mice also suffer from epileptic seizures and spontaneous shuddering movements. Starting from 9weeks of age their body weight progressively decline and at the end of their life is approximately 70% less than their wild-type littermates (Mangiarini et al. 1996).

3. BRAIN CHOLESTEROL

3.1 Brain cholesterol in physiologic condition

The brain is the most cholesterol-rich organ, with about 25% of the whole body's cholesterol (Bjorkhem 2004) (Dietschy 2004). The content of cholesterol within the brain is 15–30 mg/g tissue, whereas the average in other tissues is at 2–3 mg/g tissue (Dietschy 2009). Essentially all brain cholesterol (>99.5%) is unesterified, but small amounts of desmosterol and cholesteryl ester are also present. Brain cholesterol is a basic component of myelin sheaths and plasma membranes of both astrocytes and neurons (Dietschy and Turley 2001). Moreover, brain cholesterol is a necessary precursor of neurosteroids (Zwain & Yen 1999).

All brain cholesterol is *de novo* locally synthetized, since the blood–brain barrier (BBB) efficiently prevents exchange with circulating lipoprotein cholesterol. This allows to keep constant the levels of cholesterol within the brain. Overall, brain cholesterol homeostasis is maintained by the dynamic equilibrium among *de novo* synthesis, transport, storage, removal and recycle.

The larger pool (about 70%–80%) of brain cholesterol is produced by oligodendrocytes, with a very slow turnover (half-life of approximately 5 years) (Russell et al. 2009), to form myelin sheaths, an electrically insulating layer surrounding neuronal cells. Indeed, during the period of active myelination the rate of cholesterol synthesis reaches the highest levels. With the conclusion of brain maturation and myelin formation phases, the production of cholesterol drops by 90%. Brain cholesterol half-life has been estimated to be at least 5 years in humans and 4-6 months in mice (Björkhem et al. 1998) (Dietschy and Turley 2001).

While in the developing brain a minor pool of cholesterol is synthesized by neurons (Saito et al. 2009), in adulthood neurons completely rely on glia-derived cholesterol (Nieweg et al. 2009). This strategy allows to avoid costly cholesterol synthesis. Indeed, more than 100 mol of ATP are required for the synthesis of one mole of cholesterol (Poirier et al. 1993).

As it will be described in a more detailed paragraph, brain cholesterol actively contributes to synapse formation and synaptic transmission.

Cholesterol synthesis in the brain

The first step of *de novo* brain cholesterol biosynthesis consists in the conversion of acetyl-CoA into 3-hydroxyl-3-methylglutaryl-CoA, catalyzed by HMG-CoA synthetase. Then 3-hydroxyl-3-methylglutaryl-CoA is converted into mevalonate by HMG-CoA reductase. The HMG-CoA reductase-catalyzed reaction is considered an irreversible and rate-limiting step of cholesterol biosynthesis.

There are two cholesterologenic pathways in the brain (Fig. 1): the Kandutsch-Russel cholesterol synthetic pathway, and the Bloch pathway typical of neurons and astrocytes respectively (Leoni and Caccia 2015).

The intracellular machinery for cholesterol synthesis is located in the endoplasmic reticulum (ER). Transcriptional regulation of cholesterol synthesis and uptake depends on sterol regulatory element binding proteins (SREBPs) (Ye & DeBose-Boyd 2011), a class of transcription factors of the basic helix–loop–helix leucine zipper (bHLH-Zip) family. Three distinct SREBP isoforms have been identified: -1a, -1c and -2. SREBP-1a is constitutively expressed in the cell as a 'low-specificity' regulator, targeting all genes containing sterol response elements (SRE) (Eberlé et al. 2004). By contrast, the inducible SREBP-1c and SREBP-2 promote the expression of genes involved in fatty-acid and cholesterol metabolism respectively (Eberlé et al. 2004). In particular, the SREBP-2 transcription factor directly interacts with the cholesterol sensor SREBP cleavage-activating protein (SCAP). In conditions of high cholesterol concentrations, the SREBP-2/SCAP complex is retained in the ER membranes by the retention insulin-induced proteins 1 and 2 (INSIG-1 and -2). On the contrary, cholesterol depletion results in the loss of interaction between the INSIG retention complex and SREBP-2/SCAP, allowing SCAP to escort SREBP-2 to the Golgi compartment. Within the Golgi apparatus, SCAP releases the N-terminal domain of SREBP-2, which can translocate to the nucleus and bind to the sterol regulatory elements (SRE) in the promoter regions of target genes involved in cholesterol biosynthesis (Dietschy 2009) (Leoni and Caccia 2015).

The critical role of SCAP is confirmed by evidences of a substantial (30–40%) reduction in brain cholesterol synthesis, with deleterious effects on synaptic transmission and cognitive function, in SCAP knockout mice (Suzuki et al. 2013). Furthermore, mice in which SCAP is mutated in schwann cells exhibit congenital hypomyelination and neuropathy-related behavior, tremor and abnormal gait (Verheijen et al. 2009).

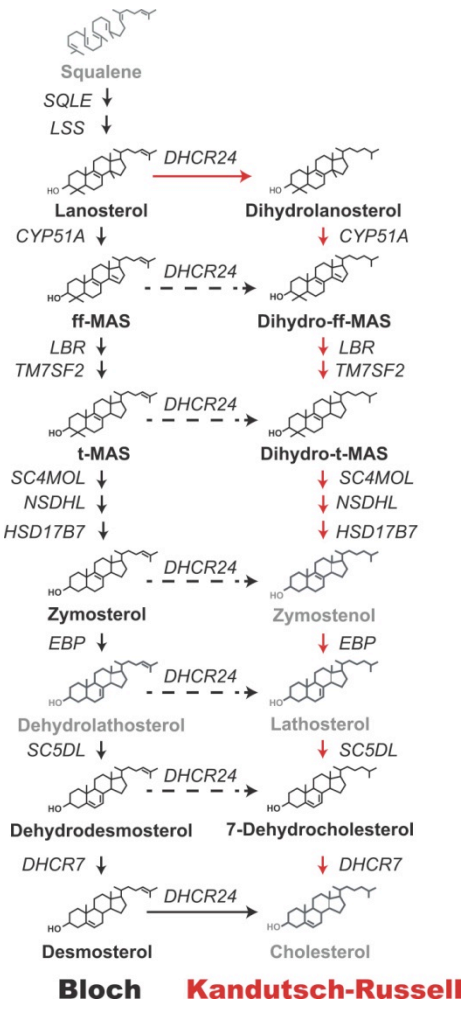

Figure 1. *Schematic representation of the Bloch and Kandutsch-Russel pathways for cholesterol synthesis. Broken arrows indicate potential sites of crossover from the Bloch to Kandutsch-Russel pathway. (From: Mitsche, Matthew et al. 2015. "Flux Analysis of Cholesterol Biosynthesis in Vivo Reveals Multiple Tissue and Cell-Type Specific Pathways." eLife 4.)*

Brain cholesterol storage

Typically, esterified cholesterol represents ~1% of the total cholesterol pool. The enzyme responsible for cholesterol esterification is acylcoenzyme A: cholesterol acyltransferase 1 (ACAT1/SOAT1). ACAT1/SOAT1 is located in ER and is upregulated in response to intracellular high cholesterol levels that induce cholesterol movement from the plasma membrane to the ER (Cheng et al. 1995) (Chang et al. 1997). ACAT1/SOAT1 is generally more active in neurons than in glial cells (Sakashita et al. 2000) although, following impaired cholesterol efflux or exogenous cholesterol surplus, the astrocytic enzyme become more active (Karten, Robert B. Campenot, et al. 2006).

Regulators of intercellular and intracellular cholesterol trafficking

In adult brain, astrocytes represent the major producers of cholesterol, which is transported to neurons via apolipoproteins and lipids. Astrocytes are also the major source of apolipoprotein E (ApoE) (Mahley et al. 2006), a key apolipoprotein required for extracellular transport of cholesterol and other lipids between astrocytes and neurons or oligodendrocytes (Lahiri 2004). The synthesis of ApoE by glial cells increase up to 150 fold in case of nerve injury (Boyles et al. 1990). The stability of ApoE in the brain depends from the association with lipids. In particular, lipidation and secretion of ApoE are mediated by one or several ATP-binding cassette transporters (ABC), such as ABCA1, ABCG1, and ABCG4 (Hayashi 2011). The major classes in the brain are ABCA and ABCG, critical transporters for lipid homeostasis (Dean et al. 2001) (Puglielli et al. 2003). The initial transfer of lipids into lipid-free apolipoproteins, including ApoE, is catalyzed by ABCA1 whereas ABCG1 mediates lipidation in a second phase (Vaughan & Oram 2006). ABCA1 is expressed in both neurons and glial cells (Wellington et al. 2002).

In ABCA1 knockout mice a significant decrease of ApoE lipidation, with consequent decline of cholesterol and ApoE levels, are observed in brain and cerebrospinal fluid (CSF) (Hirsch-Reinshagen et al. 2004) (Wahrle et al. 2004). These mice exhibit also cortical astrogliosis, increased inflammatory gene expression, altered synaptic transmission and sensomotor behavior (Karasinska et al. 2013).

The Low-Density Lipoprotein receptor (LDLR) and the Low Density Lipoprotein Receptor-related Protein 1 (LRP1) are the main receptors responsible for the uptake of ApoE-containing lipoproteins in the brain. In particular LDLR is highly expressed in glial cells than in neurons, on the contrary LRP1 is mainly found in neurons (Rebeck et al. 1993) and transports ApoE in a more efficiently way, due to the elevated rates of endocytic recycling (Li et al. 2001). The interaction between ApoE-particles and these receptors activate signaling pathways essential for neuronal survival and correct activity (Hayashi 2011) (Lane-Donovan et al. 2015). The crucial role of LRP1 is confirmed by the evidence that its ablation in neuronal cells leads to global impairment of cholesterol homeostasis and neurodegeneration (Liu et al. 2010).

Externally uptaken low-density lipoproteins are rapidly transported to late endosomal/lysosomal compartments where they are hydrolyzed. Consequently free cholesterol can reach subcellular membrane compartments whereas lipoproteins are recycled to the plasma membrane (Rensen et al. 2000) (Soccio 2004).

Cholesterol intracellular movement can be vesicle-dependent or vesicle-independent (Maxfield & Wüstner 2002). Cholesterol vesicle-mediated trafficking, along cytoskeletal tracks, involves ATP-dependent proteases. Conversely, non-vesicular transport can be mediated by diffusible carrier

proteins characterized by hydrophobic cavities for cholesterol binding and transport across the aqueous cytosol. A key player of non-vesicular trafficking is the cholesterol transport protein steroidogenic acute regulatory protein (StAR) (Alpy 2005). The intracellular trafficking of cholesterol is also related to Niemann-Pick type C1 (NPC1) and C2 (NPC2) proteins, expressed in both neurons and glial cells (Prasad et al. 2000) (German et al. 2002). In particular, NPC1 is a transmembrane protein with a sterol-sensitive domain (Carstea et al. 1997) and NPC2 is an intralumenal component that binds cholesterol (Soccio 2004). Both these proteins are essential to avoid unesterified cholesterol accumulation in the late endosome/lysosome, condition that could leads to pathologic changes in neurons and glial cells (Baudry et al. 2003) (Reid et al. 2004).

Cholesterol efflux from the brain

As cholesterol-recycling mechanisms are not sufficient to maintain steady state within the brain, excess cholesterol needs to be removed.

A minor mechanism for cholesterol removal consists in ApoE-bound cholesterol excretion through the CSF (Pitas et al. 1987). According to the CSF cholesterol content and the rate of CSF renewal, this mechanism allows to eliminate about 1-2 mg of cholesterol per day.

However, the most important removal mechanism is based on cholesterol conversion into 24S-hydroxycholesterol (24OHC), catalyzed by cholesterol 24-hydroxylase (encoded by CYP46A1, a member of the cytochrome p450 family). CYP46A1 is normally expressed in neuronal cells bodies and dendrites (large pyramidal cells of cortical areas, hippocampal cells, amygdale cells, putamen cells, thalamic cells, Purkinje cells), suggesting that a strict regulation of cholesterol content is required in these cells (Russell et al. 2009). Conversely, only a little expression of CYP46A1 was observed in glial cells (Ramirez et al. 2008).

Contrary to cholesterol, 24-OHC is able to cross the blood–brain barrier (Lütjohann et al. 1996) (Björkhem et al. 1997) (Björkhem et al. 1998).

The rapid transfer of 24-OHC, over lipophilic membranes, is due to an energetically favorable reordering of membrane phospholipids in parallel with an increase in the membrane surface area, induced by the hydroxyl group in the side chain (Kessel et al. 2001) (Meaney et al. 2002). The direction of the net flux across the membrane is probably influenced by oxysterol concentration gradient. The estimated amount of 24-OHC moving from the brain into the circulation is 6-7 mg per day (Lütjohann et al. 1996) (Björkhem et al. 1998). Interestingly, CYP46 knockout mice showed a dramatic decrease (about 64%) in sterol export from the brain in parallel to a reduction (about 40%) in cholesterol synthesis, suggesting a close relation between synthesis and metabolism of

cholesterol within the brain (Lund et al. 2003). Once in the circulation, 24-OHC binds to LDL, is taken up by hepatocytes and finally excreted in bile salts (Russell et al. 2009).

Whereas in mice, 24-OHC production has been reported also in the liver, human 24-OHC is exclusively of cerebral origin (Lund et al. 1999) (Lund et al. 2003). Consequently, 24-OHC can represent a useful marker of brain cholesterol homeostasis in humans. In different neurological diseases an alteration of plasma levels of 24-OHC is observed (Lütjohann et al. 2000) (Leoni et al. 2002) (Leoni et al. 2013).

The brain-derived cholesterol metabolite 24-OHC, as other oxysterols, can activate the nuclear liver-X receptors (LXR), ligand-activated transcription factors, recognized as master regulators of cholesterol homeostasis in the CNS (Janowski et al. 1996) (Lehmann et al. 1997) (Edwards et al. 2002). LXRs, directly interact with the retinoid X receptors (RXRs), forming heterodimers that regulate the expression of target genes, by binding to LXR-response elements within genes regulatory regions. There are two isoforms of LXRs: LXRα, prominently expressed in the liver, kidney and other peripheral tissues, and LXRβ, expressed in the brain and liver (Zhao & Dahlman-Wright 2010).

LXRs are considered key cholesterol sensors. Following excessive increase of cholesterol, cellular oxysterols, including 24-OHC, accumulate, activating LXR. Consequently, LXR positively regulate ApoE transcription in astrocytes and increase the expression of its lipidating transporters ABCA1 and ABCG1, in neurons and glia, protecting cells from cholesterol overload (Fukumoto et al. 2002) (Pfrieger and Ungerer 2011) (Vitali et al. 2014).

LXRs are also involved in cellular cholesterol uptake, downregulating lipoprotein receptor cell surface expression through the inducible degrader of LDLR (IDOL) pathway (Zelcer et al. 2009).

The complex mechanism of cholesterol homeostasis within the brain is summarized in Fig. 2.

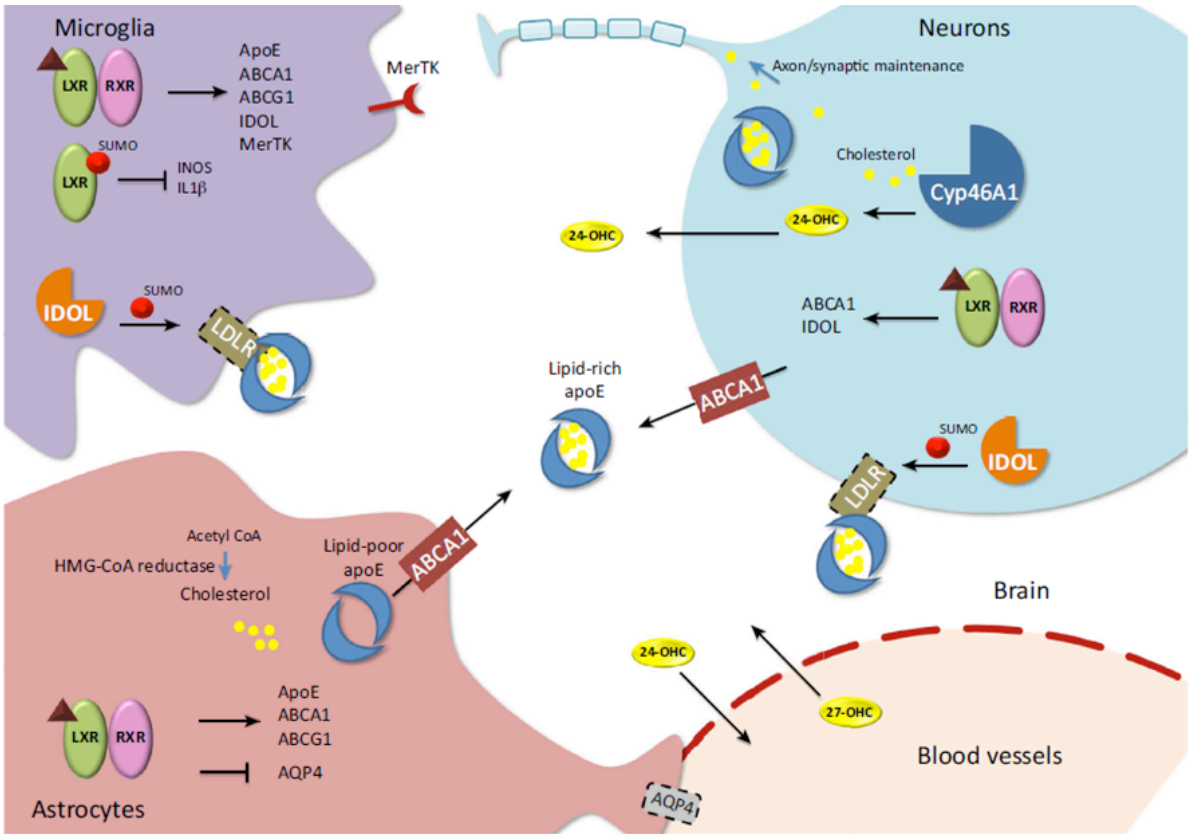

Figure 2. *Schematic representation of brain cholesterol metabolism. (From: Courtney, Rebecca, and Gary E. Landreth. 2016. "LXR Regulation of Brain Cholesterol: From Development to Disease." Trends in Endocrinology and Metabolism.)*

Cholesterol and synaptic transmission

Cholesterol is an essential component of cells membranes, able to affect their biophysical properties (Yeagle 1985). Cholesterol is particularly enriched in the cytosolic leaflet of the plasma membranes (Mondal et al. 2008), within micro-domains named "lipid rafts". Lipid rafts are considered highly dynamic scaffolding regions, which connect multiple signal transduction pathways (Martens et al. 2004) (Lingwood & Simons 2010) involving ion channels, transporters and receptors (Burger et al. 2000). Notably, in neuronal cells, lipid rafts and their enclosed cholesterol play a crucial role in both pre- and postsynaptic terminals (Gil et al. 2006) (Allen et al. 2007). Brain cholesterol regulates multiple processes, important for the maintenance of synapse organization, synaptogenesis, and synaptic vesicles recycling (Mauch et al. 2001) (Hering et al. 2003) (Pfrieger 2003) (Rohrbough & Broadie 2005). In particular, at presynaptic site, cholesterol is the major component of vesicle membranes. It is required for synaptic vesicle fusion, since it ensures the appropriate membrane curvature during the process (Chen & Rand 1997). Furthermore, cholesterol promotes membrane fusion by interacting with the synaptic vesicles integral membrane protein synaptophysin (Thiele et al. 2000), and by concentrating, at fusion-competent sites, other integral membrane proteins named

SNAREs (Lang et al. 2001) (Chamberlain & Gould 2002). Different studies reveal fusion inhibition, and impaired synaptic vesicle exocytosis and transmission, following cholesterol removal from membranes (Lang et al. 2001) (Linetti et al. 2010).

At postsynaptic site cholesterol is involved in composition, localization and trafficking/internalization of neurotransmitter receptors (Burger et al. 2000) (Sooksawate & Simmonds 2001), mediating learning and memory processes (Bliss & Collingridge 1993) (Plant et al. 2006). Poor availability of cholesterol results in impaired lateral mobility and endocytosis of AMPA receptors that accumulate in neuronal lipid rafts (Martin et al. 2014). Cholesterol depletion also prevents NMDA-dependent Ca2+ influx in neuronal cells (Frank et al. 2004) and inhibits NMDA-induced hippocampal long-term potentiation (LTP) (Frank et al. 2008). Accordingly, age-dependent decrease in hippocampal cholesterol content, leads to deficits in glutamate receptor internalization and consequent long-term depression (LTD) impairment, through a mechanism mediated by PI3K/Akt. Intracerebral infusion of cholesterol rescues age-related hippocampal LTD decrease and improves hippocampal-related learning and memory processes in aging animals (Martin et al. 2014). This study has further confirmed the crucial role of cholesterol in neuronal function.

3.2 Brain cholesterol defect in HD

Evidences in animal models and patients

The first evidence of brain cholesterol dysfunction in HD emerges from a microarray study of immortalized murine striatal cell lines, characterized by an inducible expression of mutant Htt N-terminal fragment. In this inducible cellular model of HD, a downregulation of genes related to cholesterol biosynthesis was observed in presence of mHtt (Sipione et al. 2002). A subsequent study performed in R6/2 mice, an HD animal model expressing exon 1 of human mutant HTT (Mangiarini et al. 1996), confirmed the transcriptional deregulation of cholesterogenic genes within mice striatum and cortex and highlighted a significant decrease in brain sterol content (Valenza et al. 2005). The decrease in cerebral cholesterol content was also found in other HD animal models (Valenza et al. 2010) such as yeast artificial chromosome (YAC) transgenic mice, expressing full length human mutant HTT (Hodgson et al. 1999), with progressively increased CAG repeats (YAC46, YAC72, YAC128), and HdhQ111 knock-in mice, carrying an expanded CAG tract within the mouse HD protein (Menalled 2005). Other studies in these animal models described brain cholesterol accumulation (Trushina et al. 2006) (Del Toro et al. 2010). This discrepancy was due to the low sensitive, colorimetric and enzymatic, methods used for cholesterol content detection,

instead of more reliable analytical method such as gas chromatography-mass spectrometry (Marullo et al. 2012).

Importantly, reduced levels of brain cholesterol biosynthesis were also observed in four different HD rodent models (R6/2 mice, YAC mice, HdhQ111 knock-in mice and transgenic HD rats) (Valenza et al. 2007) (Valenza et al. 2010). These studies revealed reduced activity of HMGCoAR, the rate-controlling enzyme of cholesterol biosynthesis pathway, together with reduced levels of cholesterol precursors (Valenza et al. 2007 a, b). These molecular abnormalities worsened in YAC mice carrying progressively increased CAG repeats (Valenza et al. 2010), whereas HMGCoAR activity and levels of cholesterol and its precursors increased in brain of YAC18 mice, overexpressing normal HTT (Valenza et al. 2010) (Valenza et al. 2007).

In R6/2 and YAC128 mice brain cholesterol biosynthesis dysfunction is evident even before the onset of behavioral symptoms, conversely significant reductions in cholesterol content are measurable only in advanced symptomatic stages (Valenza et al. 2007) (Valenza et al. 2010).

Furthermore, a new study in heterozygous knock-in Q175 mice (Menalled et al. 2012) quantified the rate of *de novo* brain cholesterol biosynthesis, by heavy water (2H2O) labeling method. From early stages of the disease, the striatal daily synthesis rate of cholesterol was found significantly reduced. Additionally, isotope mass spectrometry analysis revealed an inverse correlation between the levels of lathosterol, the direct precursor of cholesterol, and the CAG size in an allelic series of knock-in mice (Q7, Q20, Q80, Q111, Q175), at symptomatic stages. A significant correlation between the fractional synthesis rates of total cholesterol and 24OHC in brain of wt and Q175 mice was also observed, supporting the evidence that plasma 24OHC may reflect cholesterol synthesis in the adult brain (Shankaran et al. 2017).

All these studies performed in multiple HD animal models reinforce the potential relevance of brain cholesterol dysfunction to human pathology.

There are evidences of potential alterations in cholesterol biosynthetic pathway also in human HD patients. Initial studies performed on post-mortem caudate specimens from human HD patients and on patients-derived fibroblasts indicated reduced expression of cholesterogenic genes, compared to controls (Valenza et al. 2005).

Additional evidence in HD patients revealed that total plasma cholesterol levels decline (Markianos et al. 2008) according to disease progression (Leoni et al. 2008). A recent study confirmed these findings in both pre-manifest and manifest HD subjects (Wang et al. 2014). Also two cholesterol precursors, lanosterol and lathosterol, and the cholesterol metabolites 27OHC and 24OHC, respectively of cerebral and peripheral origin, are lower in plasma from HD patients respect to controls, at any disease stage (Leoni et al. 2011). These data suggest that whole body cholesterol

homeostasis is disturbed in HD patients. In particular, the decrease in plasma 24OHC, an indirect marker of metabolically active brain neurons (Lütjohann & von Bergmann 2003), was proportional to the degree of caudate atrophy (measured as reduction of caudate volume at MRI) and to the motor impairment in HD patients (Leoni et al. 2008). Finally, an additional study, revealed a definitive correlation between decreasing concentration of 24OHC and the progression of striatum atrophy and striatal volumes reduction at MRI (Leoni et al. 2013).

Molecular mechanisms of cholesterol dysfunction in HD

One of the possible mechanisms underlying cholesterol metabolism defect in HD is the reduction of SREBP activity, linked to mHtt expression. Indeed, in HD cellular models and in R6/2 mice striata a reduced nuclear translocation of SREBP is observed (Valenza et al. 2005).

Brain cholesterol homeostasis could be also impaired due to mutant Htt inability to bind some nuclear receptors involved in lipid metabolism such as LXRs (Futter et al. 2009a).

A further potential interconnection exists between cholesterol dysfunction, BDNF signaling and synaptic transmission alterations in HD. BDNF signaling in neuronal cells leads to the activation cholesterol synthetic pathway, increases the cholesterol content in lipid rafts and facilitates the development of a readily releasable pool of presynaptic vesicles (Suzuki et al. 2007). Mutant Htt, by affecting both BDNF transport and release (Zuccato, Valenza, and Cattaneo 2010), could inhibit neuronal cholesterol synthesis.

An additional key mechanism is the cross-talk between neurons and astrocytes. In adulthood astrocytes produce and secrete cholesterol bound to ApoE lipoproteins, which is available to neurons, but this process is altered in HD. Indeed, the expression of cholesterol biosynthesis genes is reduced in primary astrocytes cultured from two HD mouse models (R6/2 and YAC128) compared to control littermates (Valenza et al. 2010). Primary astrocytes from YAC128 mice also displayed reduced mRNA levels of ABCA1, ATP binding cassette sub-family G member 4 (another ATP binding cassette transporter highly expressed in the brain) and ApoE compared with controls (Valenza et al. 2010). Furthemore, ApoE was predominantly associated with smaller lipoprotein particles in CSF from HD mice (Valenza et al. 2010). These findings suggest that reduced cholesterol biosynthesis and efflux occur in HD astrocytes, along with reduced transport in the HD brain (Valenza et al. 2010). Accordingly, a recent study confirmed that astrocytes derived from both neural stem knock-in cells, carrying increasing CAG repeats, and from R6/2 mice secrete lower levels of cholesterol bound to ApoE in the culture medium, leading to a reduced availability of cholesterol to HD neurons (Valenza et al. 2015). Glia-conditioned medium (GCM) from wt astrocytes is able to rescue neurite outgrowth defect in NS-derived HD neurons, as well as

cholesterol administration. This beneficial effect of wt GCM is abolished following silencing of ABCA1 or SREBP2 in wt astrocytes (Valenza et al. 2015). Conversely, GCM derived from HD astrocytes fails to support neurite outgrowth in NS-derived HD neurons. However, the induced ABCA1 or SREBP2 N-terminal fragment over-expression in HD astrocytes makes the relative GCM able to promote efficient neurite outgrowth in HD neurons (Valenza et al. 2015). The same study proved that a reduced supply of glial-derived cholesterol from HD astrocytes affects synaptic related activities (number of synapses, synaptic proteins, electrophysiological parameters) in primary neurons cultured from R6/2 mice but this condition may be reversed by cholesterol or wt GCM supplementation (Valenza et al. 2015).

Taken together, these observations suggest that in HD there is a reduced ApoE mediated cholesterol transport and supply from astrocytes to neurons that might be due to a combination of reduced activity of LXRs and a reduced SREBP activation.

Other mechanisms that can concur to perturb brain cholesterol homeostasis are the deficiency of metabolic intermediates for cholesterol biosynthesis associated with HD mitochondrial dysfunction (Leoni and Caccia 2015) and the alteration of membrane properties and fluidity (Muratore 2013) that can contribute to affect the transfer of cholesterol between cells.

3.3 Brain cholesterol alterations in other neurodegenerative diseases

Dysregulation of brain cholesterol homeostasis is being linked to different chronic neurodegenerative disorders over HD, including Niemann-Pick type C (NPC) disease, Smith-Lemli Opitz syndrome (SLOS) and Alzheimer's disease (AD).

Cholesterol and NPC disease

NPC is a fatal, autosomal, recessive, inherited disorder characterized be massive loss of neurons, often accompanied by hepatosplenomegaly and lung disease (Vanier & Millat 2003). NPC disease is directly related to cholesterol metabolism impairment, since it is caused by mutations in either the NPC1 or NPC2 gene resulting in unesterified cholesterol and glycosphingolipids sequestration and accumulation within the endocitic pathway (Karten et al. 2002) (Karten et al. 2005). Consequently, a deficiency in the intracellular trafficking of cholesterol towards plasma membrane and endoplasmic reticulum is observed. NPC1 and NPC2 are involved in recycling endosomes in presynaptic nerve terminals thus synaptic vesicle morphology and composition are also impaired by NPC1 dysfunction (Karten et al. 2006).

There is currently no definitive cure for NPC, but treatments based on cyclodextrin gave encouraging results (Rosenbaum et al. 2010) (Aqul et al. 2011) (Peake & Vance 2012).

Cholesterol and SLOS

SLOS is an, autosomal recessive, neurodegenerative and developmental disease caused by mutations in the gene encoding for 7-dehydrocholesterol reductase, the enzyme that catalyzes the final step in the cholesterol biosynthetic pathway. This condition leads to increased levels of 7-dehydrocholesterol in parallel with a dramatic decrease in cholesterol amounts within the cells, plasma and the brain (Porter 2006) (Porter and Herman 2011). It remains unclear whether these disease-related processes are caused by the low level of cholesterol in the brain or by the abnormal accumulation of the potentially toxic cholesterol precursor, 7-dehydrocholesterol. The developmental abnormalities observed in SLOS patients might also be caused by reduced activity of the sonic hedgehog (SHH) linked to alterations in cholesterol metabolism. Indeed SHH signaling pathway is involved in embryonic development of the CNS, limbs and facial features (Maity et al. 2005). SHH correct activity is only ensured by the covalent attachment of a cholesterol molecule to the protein (Porter, Young, and Beachy 1996) (Mann & Beachy 2000).

Cholesterol and AD

AD is a progressive neurodegenerative disorder that leads to memory loss and cognitive decline. The brains of individuals affected by AD are characterized by the presence of extracellular deposits of β-amyloid (Aβ) plaques, as well as intracellular neurofibrillary tangles that contain hyperphosphorylated tau, a microtubule-associated protein. The accumulation of Aβ plaques and the loss of neurons play a critical role in the development of AD (Selkoe 2002).

Although, on the contrary of NPC and SLOS disorders, a direct causal relationship has not been found, different experimental evidences have indicated that alterations in brain cholesterol metabolism might contribute to the pathogenesis of AD (Simons et al. 1998).

Interestingly, the secretases responsible for the generation of the Aβ peptides from the amyloid precursor protein (APP) are located in cholesterol-enriched microdomains of the plasma membranes (Simons et al. 1998) (Ehehalt et al. 2003). Moreover, intracellular cholesterol levels can influence the production of the Aβ peptides (Bodovitz & Klein 1996) (Simons et al. 1998).

APOE associates with Aβ peptides, facilitating their degradation (Sanan et al. 1994). A recent study performed in a mouse model of AD demonstrated that the induced increased production of APOE enhanced Aβ degradation reducing Aβ plaque area within the brain (Cramer et al. 2012). Other contrasting data have suggested that low APOE levels are associated with reduced amount of Aβ in the brain (Bien-Ly et al. 2012). These differences could be due to the expression of different isoforms of ApoE. The most common isoform allele is APOE3. The less widespread allele in the human population is APOE4 whose inheritance is recognized as the strongest genetic risk factor for

the development of late-onset AD (Corder et al. 1993). In contrast, inheritance of the APOE2 allele seems to protect against AD (Corder et al. 1994).
Finally, evidences in AD mice show that ABCA1 deficiency can lead to increased amyloid deposition (Wahrle et al. 2005), while its overexpression have the opposite effect (Wahrle et al. 2008).

4. OUR THREE SELECTED STRATEGIES FOR CHOLESTEROL DELIVERY TO THE BRAIN

Considered the critical role of brain cholesterol for correct synaptic transmission (described in paragraph 3.1), we hypothesized that HD synaptic dysfunction could be, at least in part, due to reduced brain cholesterol production and availability, described in different animal models (Valenza et al. 2007) (Valenza et al. 2010) (Shankaran et al. 2017). We were interested in investigating the therapeutic potential of brain cholesterol supply in R6/2 mice. To this end, we tested three drug delivery strategies that allowed to overcome the obstacle of the blood-brain barrier (BBB) in different ways.

4.1 Surface-Modified Poly(lactic-co-glycolic acid) (PLGA) Nanoparticles (NPs) (Strategy 1)

PLGA is one of the most successfully used synthetic polymers in biomedical devices. Indeed, it has been approved by the US Food and Drug Administration (FDA) and European Medicine Agency (EMA) due to its high biodegradability (Mundargi et al. 2008). Once in the body, PLGA is degraded by non-enzymatic hydrolysis leading to the formation of lactic acid (LA), glycolic acid (GA), CO2 and H2O (Yoo et al. 2005).
The biomedical and therapeutic applications of PLGA NPs as drug delivery devices were deeply investigated for vaccines (des Rieux et al. 2006), neurological disorders (Tosi et al. 2008) (Tosi, Ruozi, and Belletti 2012) and cancer (Bala et al. 2004) (Taurin et al. 2012). NPs biodistribution and interaction with living cells, tissues, organs or blood constituents depend on their chemico-physical features (shape, size, surface properties) (Alexis et al. 2008) (Minchin 2008).
Recent studies performed in rodents revealed that surface engineering with a glycosylated hepta-peptide, called g7, confers to PLGA NPs the ability to cross the BBB at a concentration of up to 10% of the injected dose (Costantino et al. 2005) (Tosi et al. 2007) (Tosi et al. 2011a) (Tosi et al. 2011b). Conversely to un-modified PLGA NPs, systemically administered peptide-conjugated NPs (g7-NPs) are able to cross the BBB and reach the brain bypassing the hepatic uptake (Costantino et

al. 2005) (Tosi et al. 2005). Further studies investigated the g7-NPs ability to act as drug carriers. In particular, Loperamide, an opioid drug generally not able to cross the BBB, was loaded into systemically administered NPs inducing antinociceptive effects in treated rats (Tosi et al. 2007). The ability of g7-NPs to reach the brain following different routes of administration (intraperitoneal, intravenous, nasal, oral) was also confirmed by other *in vivo* studies (Tosi et al. 2013).

Endocytosis mechanism of NPs

In order to understand the mechanism of BBB crossing, it is important to consider that g7 peptide derives from the native opioid peptide MMP-2200 (Polt & Palian 2001). Consequently, g7 peptide ability to cross the BBB could be related to the mechanism used by the β-endorphines. These peptides maintain helical amphipathic conformation in presence of BBB luminal wall lipid bilayers, for which they have a high affinity (Dhanasekaran et al. 2005). More in general, rigid proteins stabilize the membrane curvature inserting their amphipathic moieties or helices between the polar head-groups of lipid molecules (Zimmerberg & Kozlov 2006). g7-NPs could elicit the same BBB membrane curvature, since they are characterized by a rigid polymeric matrix structure conjugated to an amphiphatic glycopeptides (g7), having a helix-like conformation. Following *in vivo* systemic administration, a clear interaction between g7-NPs and BBB was highlighted (Tosi et al. 2011b). In particular, electron photomicrographs proved that g7-NPs ability to reach the brain is related to the peculiar amphipathic character of g7-peptide that promote endocytosis at BBB level mediating NPs translocation to the CNS and macropinocytotic processes (Tosi et al. 2011b). Taken together, these evidences suggest that BBB crossing of g7-NPs is a consequence of multiple pathways, mainly membrane–membrane interaction and macropinocytosis-like mechanisms.

g7-NPs Trafficking inside the CNS

Very recently, cellular and intracellular destiny of g7-NPs was analyzed (Tosi et al. 2014) (Vilella et al. 2014). Once crossed the BBB, g7-NPs can target specific cell populations within the brain. Evidence clearly show that g7-NPs are transported intra- and inter-cellularly within vesicles, after vesicular internalization. Moreover, *in vitro* studies indicate that g7-NPs cell-to-cell transport is mediated by tunneling-nanotube (TNT)-like structures, in glial and neuronal cells. This transport is dependent on F-actin.

4.2 Intrastriatal administration via Alzet osmotic pumps (Strategy 2)

Alzet osmotic pumps were developed in the seventies (Theeuwes and Yum 1976) and are considered today one of the most important examples of miniature pumps operating without need of electric energy. They are commercially available by DURECT Corp., Cupertino, CA, USA. Alzet osmotic pumps can be surgically implanted subcutaneous, intraperitoneally, intravenous or used for brain infusion, in multiple species of laboratory animals. These rate-controlled release systems ensure continuous and constant pumping rate of drugs or test agents, over prolonged periods, without the need of external connections. ALZET osmotic pumps are cylindrically shaped and comprise different components (Fig. 3).

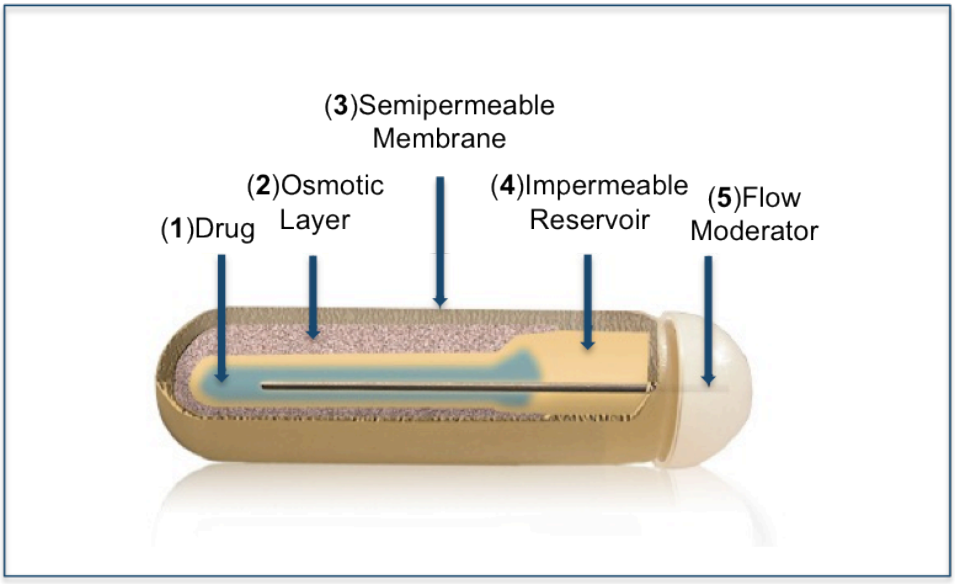

Figure 3. *Schematic representation of Alzet osmotic minipumps. The inner, collapsible, reservoir is made of impermeable thermoplastic hydrocarbon elastomer (**4**) and is surrounded by a coating layer of osmotic driving agent (**2**). The semi-permeable membrane (**3**) that covers the osmotic layer is based on a cellulose ester blend and forms the outer surface of the pump. Finally, a cannula working as flow moderator (**5**) is inserted into the drug-filled pump (**1**). (www.alzet.com)*

Osmotic minipumps geometry together with the presence of a flow moderator hinders diffusive release and prevents accidental spill of drug content. In particular, ALZET pumps operate because of the osmotic pressure generated by inflowing water from tissue environment in which the pump is implanted. As the water enters it compresses the flexible reservoir, displacing the test solution from the pump at a controlled, predetermined rate. Because the compressed reservoir cannot be refilled, the pumps are designed for single-use only. The rate of delivery by an Alzet pump is regulated by the water permeability of the pump's outer membrane while is independent from the drug formulation or its physical and chemical properties. The Alzet pumps are available with three

different reservoir capacities of 100 µL, 200 µL, and 2 mL with, delivery rates ranging from 0.11 µL/h to 10 µL/h. Depending on the chosen pump model and the delivery rate, these devices can operate from 1 day to 6 weeks. Since many agents do not cross the BBB, direct intracerebral infusion of drugs or compounds could be required. The Alzet brain infusion kits (Fig. 4) have been specifically designed for a targeted delivery to the CNS. In particular, brain infusion kits can be used for:

- Infusion into the cerebral ventricles resulting in infusate diffusion in multiple brain regions, via the cerebrospinal fluid.
- Direct microperfusion of discrete brain structures resulting in localized distribution of infusate.

The commercially available brain infusion kit models (www.Alzet.com) can differ for the maximum depth reached by their intracerebral inserted cannula.

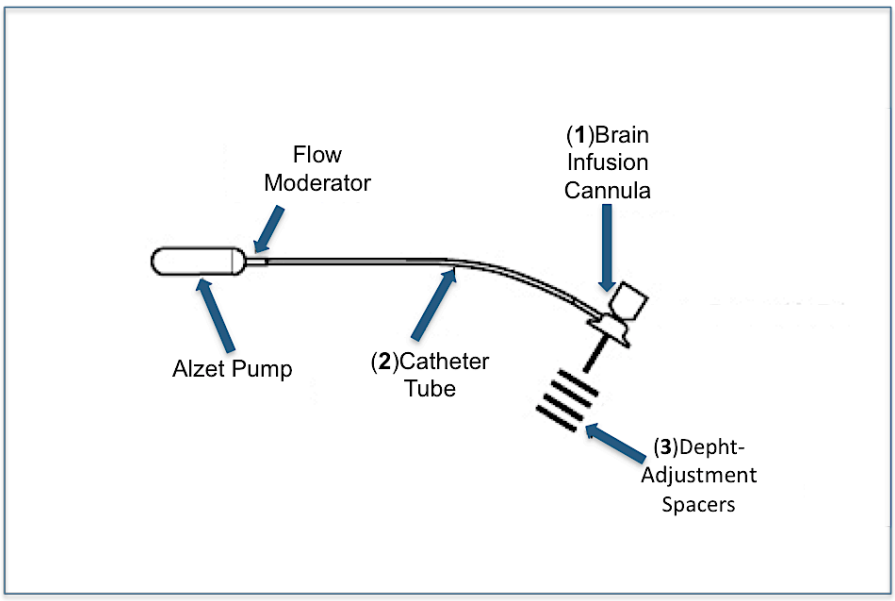

Figure 4. *Representation of the brain infusion kit. Brain infusion kits are composed by a brain infusion cannula (1) connected to the osmotic minipump through a catheter (2). Appropriate spacers (3) allow to adjust the cannula length, to target desired brain regions. (*www.alzet.com*)*

Overall, despite being considered an invasive method due to required surgery for their implantation, Alzet osmotic minipumps represent a reliable, rate-controlled, delivery strategy that avoids animal's frequent handling.

4.3 Intranasal route of administration (Strategy 3)

Intranasal transport is the direct transport of therapeutic agents from the nasal cavity to the brain. It mainly relies on extracellular and transcellular transport mechanisms, involving the olfactory and

respiratory regions of the nasal cavity. Traditionally, the nasal route has been exploited for delivery of drugs for the treatment of local diseases like nasal allergy, sinusitis and nasal congestion. In the last few decades, the nasal route emerged as a reliable, safe, non-invasive and convenient route to accomplish faster and higher levels of drug absorption (Pardeshi et al. 2012). Importantly, this non-invasive method facilitates patient compliance and comfort compared with other route of administration.

Macroscopical anatomy of the nasal cavity

The nasal cavity consists in three functionally regions: the vestibular, the respiratory and the olfactory regions (Graziadei 1970). Generally the nasal vestibule is covered in stratified squamous epithelium and is located at the opening of the nasal passages. The vestibular area contains hairs for filtering airborne particles. Largest of the three regions in humans is the respiratory area containing an epithelium made up of ciliated cells, whose function is to remove particles deposited in the mucous layer. The olfactory mucosa is located at the most dorsal and caudal region of the nasal cavity and contains a surface area of highly convoluted turbinates. Structurally, it is composed of the olfactory epithelium on the luminal side of the basal lamina and an underlying lamina propria. Different pathways connecting the nasal passages to the brain and spinal cord have been identified.

Pathways relevant for nose-to-brain transport

Following intranasal administration, therapeutics can reach the CNS, from the nasal cavity, along olfactory nerve pathways. Olfactory nerve pathways represent the major component of intranasal delivery, as illustrated by fluorescent tracers-based studies (Jansson & Björk 2002). Olfactory pathways originate in the olfactory region, a modified columnar, pseudo-stratified epithelium, containing olfactory receptor neurons (ORNs). The olfactory epithelium is located at the top of the mammalian nasal cavity, under the cribriform plate of the ethmoid bone, which divides cranial and nasal cavities. Beneath the epithelium of the olfactory region, is located the lamina propria that contains mucus secreting Bowman's glands, axons, blood vessels, lymphatic vessels, and connective tissue. ORNs are surrounded by supporting cells, microvillar cells and basal cells (Fig. 5A) and their principal function is to mediate the sense of smell (Hadley et al. 2004). ORNs are bipolar neurons extending their dendrites into the mucous layer of the olfactory epithelium. Conversely, ORNs axons reach the subarachnoid space containing CSF and terminate on mitral cells in the olfactory bulbs, passing through the lamina propria and the cribriform plate of the ethmoid bone (Fig. 5A). From the olfactory bulbs, neural projections extend to multiple brain regions including the olfactory tract, anterior olfactory nucleus, piriform cortex, amygdala, and

hypothalamus (Carmichael et al. 1994) (Kandel et al. 2000). Due to the direct contact with toxins in the external environment, ORNs regenerate in few weeks from basal cells residing in the olfactory epithelium (Whitman & Greer 2009). Special Schwann cell-like cells called olfactory ensheathing cells (OECs) envelope ORNs axons of and play a key role in axonal regeneration, regrowth, and remyelination (Field et al. 2003). In addition to ORNs, chemosensory neurons located in the nasal cavity in the Grueneberg ganglion lead into the olfactory bulbs (Koos & Fraser 2005). Intranasally administered therapeutics can reach the CNS via extracellular or intracellular mechanisms of transport along olfactory nerves. Extracellular transport mechanisms are relatively rapid and involve the movement of molecules between cells in the nasal epithelium. It has been proved that within 30 minutes intranasally administered drug reach the olfactory bulbs and other brain areas (Balin et al. 1986), probably through bulk flow mechanisms (Thorne et al. 2004). Intracellular transport mechanisms involve the uptake of molecules into ORNs by passive diffusion, receptor-mediated or adsorptive endocytosis. In this case, a slower axonal transport, requiring several hours to days for drug delivery to CNS is observed (Baker & Spencer 1986).

Another important pathway connecting nasal passages to the CNS involves the trigeminal nerve, which innervates the respiratory epithelium (Schuenke, Schulte, and Schumacher 2010) (Chapman et al. 2013). The nasal respiratory epithelium represents approximately 50% of the nasal cavity in rats and 80–90% in humans. It is a pseudostratified columnar secretory epithelium, which warms and humidifies inspired air in addition to removing particulates, microorganisms, and allergens. The human respiratory epithelium is comprised of goblet cells, ciliated cells distributed among mucus secreting goblet cells, (Fig. 5B) intermediate cells, and basal cells (Jafek 1983). Basal cells function as progenitors to the other cell types in the nasal respiratory epithelium. The trigeminal nerve conveys sensory information from the nasal cavity, the oral cavity, the eyelids, and the cornea, to the CNS via the ophthalmic division (ophthalmic nerve, V1), the maxillary division (maxillary nerve, V2), or the mandibular division (mandibular nerve, V3) of the trigeminal nerve (Standring 2009). The three branches of the trigeminal nerve come together at the trigeminal ganglion and ramify centrally to enter the brain at the level of the pons, terminating in the spinal trigeminal nuclei in the brainstem. A unique feature of the trigeminal nerve is that it enters the brain from the respiratory epithelium of the nasal passages at two sites: (1) through the anterior lacerated foramen near the pons and (2) through the cribriform plate near the olfactory bulbs, creating entry points into both caudal and rostral brain areas following intranasal administration (Schaefer et al. 2002).

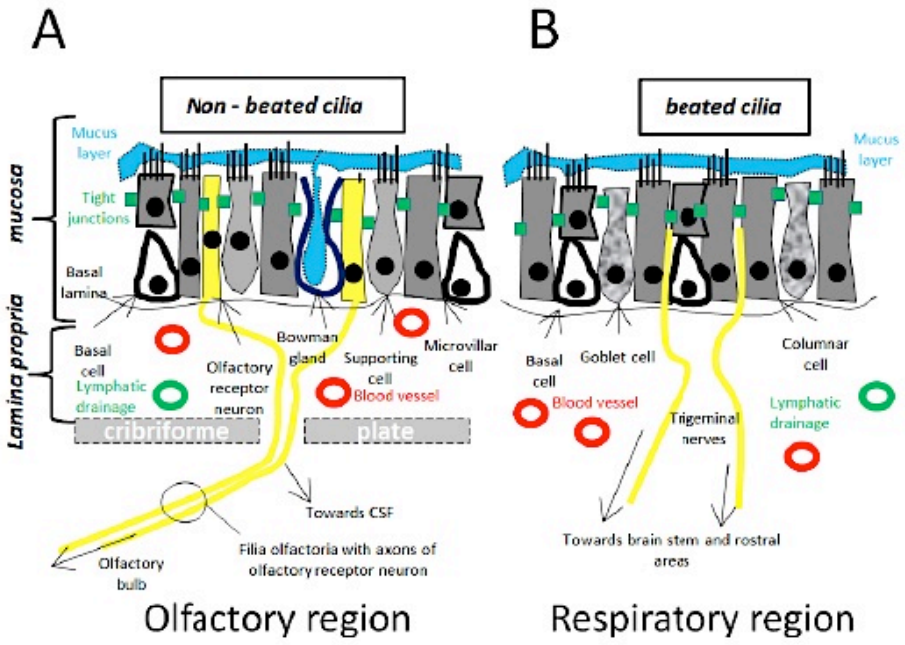

Figure 5. *Schematic representation of the olfactory (**A**) and respiratory (**B**) regions of the nasal cavities. (From: van Woensel, Matthias et al. 2013. "Formulations for Intranasal Delivery of Pharmacological Agents to Combat Brain Disease: A New Opportunity to Tackle GBM?" Cancers.)*

The vascular pathway provides a further connection between the nose and the brain. The olfactory and respiratory mucosa receives blood supply from small branches of the ophthalmic artery and from arterial branch of the maxillary artery, respectively (Coulston & DeSesso 1993). The vasculature in the respiratory region contains a mix of continuous and fenestrated endothelia, (Grevers & Herrmann 1987) allowing both small and large molecules to enter the systemic circulation following nasal administration. This pathway preferentially facilitates small, lipophilic drugs delivery to the CNS. Increasing evidence is emerging suggesting that perivascular channels, are involved in intranasal drug delivery to the CNS (Thorne et al. 2008) (Dhuria et al. 2009). Perivascular spaces surround perforating arterioles and venules (Kwee & Kwee 2007) and represent an important drainage conduit for cerebral interstitial fluid (Weller et al. 1992) (Abbott 2004). They do not have a direct connection with the subarachnoid space. Perivascular transport is not only due to diffusion but also to bulk flow mechanisms (Groothuis et al. 2007). Furthermore, arterial pulsations are considered a driving force for perivascular transport (Rennels et al. 1990). The resulting ''perivascular pump'' can account for the rapid distribution of therapeutics throughout the brain (Hadaczek et al. 2006). Perivascular transport mechanisms are also responsible for the widespread distribution within the CNS of intranasally applied drugs (Thorne et al. 2004). Direct transport from the nasal cavity to the cerebrospinal fluid (CSF) has also been reported (Johnston et al. 2004) (Walter et al. 2006). Finally, absorption of the intranasally applied substance in the

lymphatic vessels, located just under the basal lamina and draining the deep cervical lymph nodes of the neck is been observed (Yoffey & Drinker 1938).

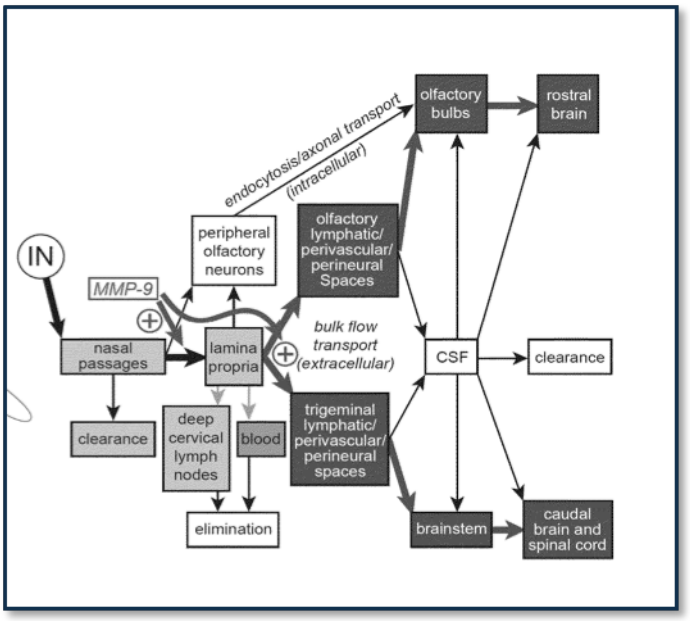

Figure 6. *Schematic representation of the olfactory and trigeminal pathways for nasal targeting of the CNS. (Modified from: Methods and Compositions for Enhancing Intranasal Delivery of Therapeutic Agents US 20140050718 A1).*

Many evidences prove the efficacy of the intranasal delivery method for the administration of variety of growth factors, hormones, neuropeptides and therapeutics including insulin, oxytocin, orexin and even stem cells. Hence, this could represent a promising strategy for the treatment of CNS associated disease, such as Alzheimer's disease, Parkinson's disease, Huntington's disease, depression, anxiety, autism spectrum disorders (Chapman et al. 2013) (Meredith et al. 2015).

Aim of the Project

The aim of our study is to explore whether cholesterol administration to the HD brain is able to rescue neurobehavioral and synaptic defects in a transgenic mouse model of the disease.

This study will also allow to further understanding the relevance of cholesterol defects in HD.

Locally synthesized brain cholesterol plays a critical role in synapse formation, synaptic activity and integrity (Pfrieger 2003). Many evidences show that brain cholesterol biosynthesis is reduced in several HD rodent models (Valenza et al. 2005) (Valenza et al. 2007) (Valenza et al. 2010). These data were recently confirmed in Q175 knock-in mice, in which consistent decrease in daily synthesis rate of cholesterol (by $^{2}H_2O$ labeling) and reduced lathosterol and cholesterol levels were found (Shankaran et al. 2017). Due to the blood-brain barrier (BBB), brain cholesterol metabolism is independent from that in peripheral tissues (Dietschy & Turley 2004). As a consequence, eventual brain cholesterol dysfunction cannot be compensated by diet.

We decided to exploit alternative routes for cholesterol delivery to the brain of R6/2 transgenic mouse model of HD (Mangiarini et al. 1996), each one presenting different advantages and limitations:

(i) Systemic injection of biodegradable polymeric nanoparticles, loaded with cholesterol, and modified with specific glycopeptides to cross the BBB (Strategy 1 - Polymeric g7-NPs-Chol).

(ii) Osmotic minipumps, attached to a stereotaxically implanted brain cannula, to infuse increasing doses of cholesterol at continuous and controlled rates, directly in the striatum (Strategy 2 - Osmotic minipumps).

(iii) Intranasal administration of cholesterol-containing liposome formulations (Strategy 3 - Intranasal rout of administration).

A combination of neurobehavioral tests, biochemical and functional assays will allow to assess how such treatments influence neuronal activity and neurobehavioral anomalies in HD mice.

Results

Strategy 1 – Surface-Modified PLGA NPs

With this first series of studies, we tested the therapeutic potential of brain cholesterol supplementation, via polymeric NPs, in R6/2 mice. **Table 1** summarizes the features of the unloaded (u) and cholesterol (chol) loaded Polymeric Poly(lactic-co-glycolic acid)-nanoparticles (PLGA-NPs) used in this work, provided and characterized by G. Tosi (University of Modena and Reggio Emilia) (Tosi et al. 2005) (Tosi et al. 2007) (Tosi et al. 2011). We decided to use g7-PLGA-NPs for their multiple attractive properties: (i) biodegradability and biocompatibility; (ii) protection of drug from degradation; (iii) successful brain targeting (due to the conjugation with the glyco-heptapetide (g7), 10% of g7-NPs reach the brain once systemically injected in rodents (Costantino et al. 2005) (Tosi et al. 2007); (iv) PLGA is approved by FDA and EMA as drug delivery system for parenteral administration in humans (Mundargi et al. 2008).

Sample	Chol/PLGA (mg/mg)	Z-Average nm (± S.D.)	PDI value (± S.D.)	D(i)10 nm (± S.D.)	D(i)50 nm (± S.D.)	D(i)90 nm (± S.D.)	ζ-pot mV (± S.D.)	% PVA residual (± S.D.)	mg Chol/100 mg form. LC%	EE%
u-NPs		181±11	0.08±0.01	139±12	187±12	205±12	-12±3	4.8±1.2		
NPs-Chol1	1:100	192±15	0.09±0.01	136±11	195±12	283±23	-9±4	5.1±0.4	0.7±0.1	68±5

Table 1. Chemical-physical properties of g7-PLGA-NPs used in the study.
Z-Average value (nm) indicates the dimensions of samples; Polydispersity Index (PDI) indicates homogeneity of the samples; Di (nm) indicates intensity distribution; ζ-pot (mV) expresses surface charge; %PVA expresses as percentage the polyvinyl alcohol residual; mg of Chol per 100 mg of formulation (LC%) and percentage of encapsulation efficiency (EE%) represent drug loading values. Standard Deviation is reported as SD.

Characterization of g7-NPs distribution in vivo

First of all, we performed immunohistochemical analysis to investigate g7-NPs distribution following a single intraperitoneal injection into both R6/2 and wild-type (wt) mice, at 8 weeks of age. Results showed both rhodamine-labeled control (unmodified) NPs (C-NPs) and g7-NPs signals, in the liver (**Fig. 1A**) and in other peripheral tissues (data not shown) of mice sacrificed few hours after the injection. On the contrary, only the g7-NPs signal was detected in the brain (**Fig. 1B**). Successive quantification of g7-NPs, determined normalizing the red spots on the mean size of NPs, yielded an approximate ratio of ~10:1 in liver compared to striatum and cortex of wt mice (**Fig. 1C**). The same quantification was also performed in R6/2 mice revealing reduced propensity of g7-NPs to reach the brain despite greater liver accumulation, compared to the wt. These results suggest an influence of HD-related mechanism in g7-NPs BBB crossing. Interestingly, g7-NPs signal was still present into mice brain 24 h and 2 weeks after a single (**Fig. 1D**) or multiple

intraperitoneal injections performed in the same week (**Fig. 1E**). Further analysis performed on high-magnification confocal images indicated the presence of g7-NPs in different brain regions and in different cells types such as IBA1 immunoreactive microglial cells (**Fig. 1F**), GFAP positive astrocytes (**Fig. 1G**) and calbindin (**Fig. 1H**) and DARPP-32 (**Fig. 1I**) positive neurons.

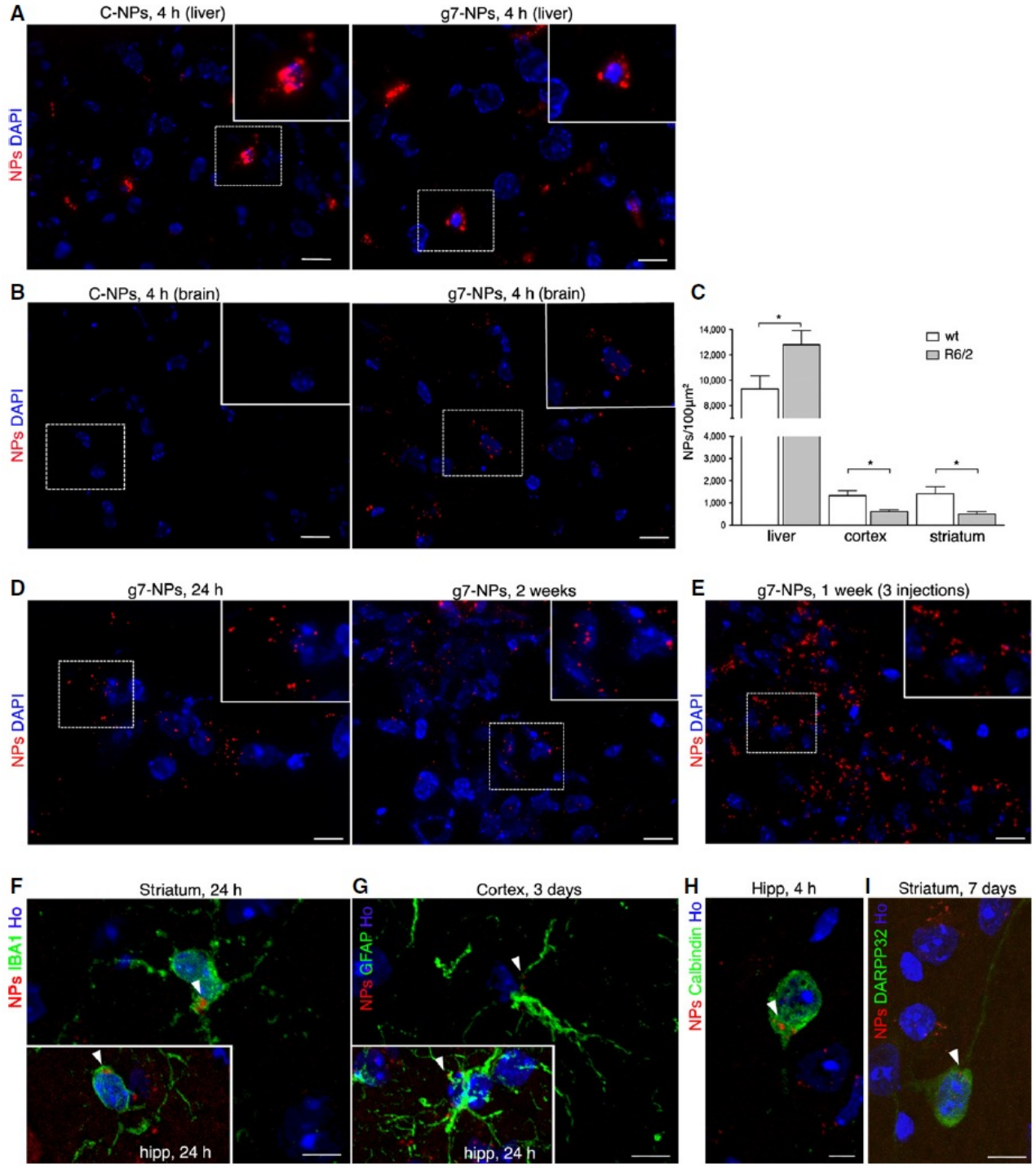

Figure 1. g7-NPs localize within different cells types in R6/2 mice brain.
*(A, B) Representative confocal images of liver (A) and brain (B) slices from R6/2 mice intraperitoneally injected with C-NPs (left) or with g7-NPs (right) and sacrificed after 4 h. (C) Quantification of g7-NPs localized in the liver, striatum, and cortex of wt (n = 3) and R6/2 mice (n = 3). Data are expressed as the number of g7-NPs for 100 µm2 ± SEM. Statistics: *P < 0.05 was determined by Student's t-test. (D, E) g7-NPs in brain slices from R6/2 mice 24 h (D, left) or 2 weeks (D, right) after a single intraperitoneal injection and 1 week (E) after multiple injections. (F-I) Representative confocal images of IBA1 (F), GFAP (G), calbindin (H), and DARPP-32 (I) positive cells, on brain coronal sections from R6/2 mice intraperitoneally injected with g7-NPs and sacrificed at indicated time points. White arrowheads indicate g7-NPs within different cells types. DAPI (A, B, D) or Hoechst 33258 (Ho) (F–I) was used to counterstain nuclei. Scale bars: 20 µm (A); 10 µm (B, D, E); 5 µm (F–I).*

Delivery and release of cholesterol by g7-NPs in the R6/2 brain

To track cholesterol delivery and intracellular release by g7-NPs, we performed specific experiments using rhodamine-labeled g7-NPs (Vergoni et al. 2009) loaded with the fluorescent analog NBD cholesterol (g7-NPs-NBD-Chol). NBD cholesterol closely resembles the structure of native cholesterol, localizes in the membrane's interior and is commonly used to study lipid transport processes as well lipid-protein interactions (Gimpl & Gehrig-Burger 2007). Accordingly, NBD cholesterol, stereotaxically injected into mice brain ventricles, co-localized with the plasma membrane Ca^{2+} ATPase (PMCA), confirming that exogenous cholesterol is incorporated on brain cells' membranes *in vivo* (**Fig. 2**).

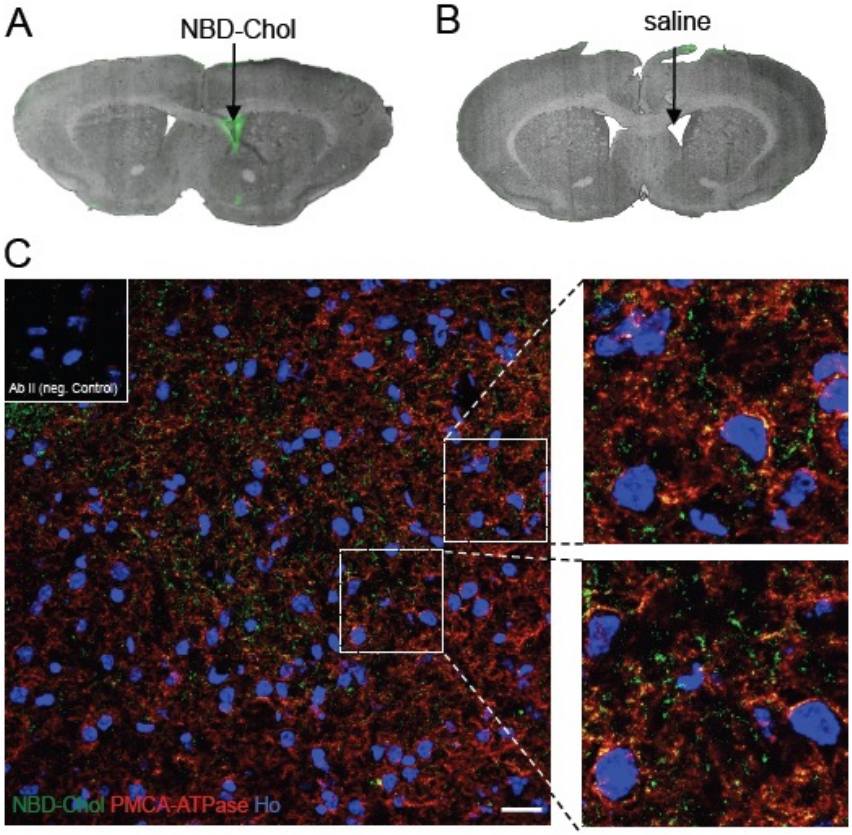

Figure 2. Co-localization of NBD-Cholesterol with PMCA in vivo.
Representative confocal images of brain slice from wt mice stereotaxically injected in the lateral ventricle with NBD-Cholesterol (10ug) and sacrificed after 7 h. (A, B) low-magnification images of brain slices from mice injected with NBD-Cholesterol (A) or with saline (B) (see arrows). (C) Representative 63x confocal image of co-localization (yellow signal) between NBD-Cholesterol (green signal) and the plasma membrane marker PMCA (red signal), in brain slices of injected wt mice (scale bar: 10μm). The Hoechst 33342 dye (Ho; blue) was used to counterstain nuclei.

We next monitored g7-NPs degradation and consequent NBD cholesterol release following the red spots and the green signal respectively. 12 and 24 h after a single intraperitoneal injection of g7-NPs-NBD-Chol, g7-NPs and NBD cholesterol signals co-localized in brain cells as indicated by the scatterplot of red and green pixel intensities (**Figs. 3A and B**). However, successive analysis performed 7 days (not shown) and 14 days after the injection highlighted a separation between g7-NPs and NBD-Chol signals (**Fig. 3C)**. These findings demonstrated a release of NBD-Chol from NPs starting from 1–2 weeks after injection, in parallel with a reduction in g7-NPs signal, probably due to their degradation. g7-NPs quantification in brain slices from injected mice confirmed a decrease in the number of NPs over time (**Fig. 3D**).

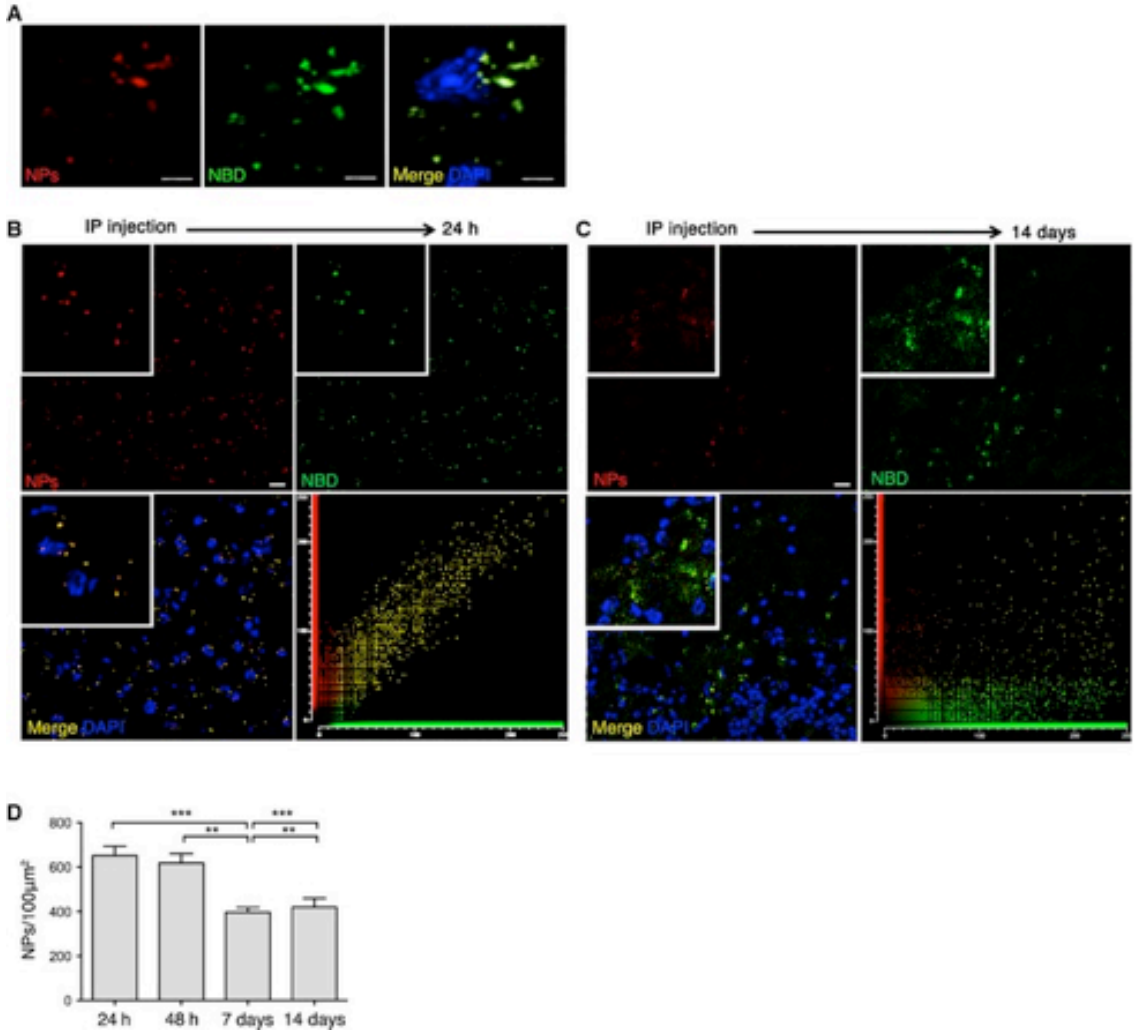

Figure 3. Cholesterol delivery and release in the R6/2 brain.
*(A) Representative confocal image (crop) of brain slices from R6/2 mice 12 h after the intraperitoneal injection of rhodamine-labeled g7-NPs-NBD-Chol, showing co-localization of NBD-Chol (green signal) and rhodamine (NPs, red signal). Scale bar: 5 µm. (B, C) Representative confocal image (low magnification) of brain slices from R6/2 mice treated with g7-NPs-NBD-Chol and sacrificed after 24 h (B) or 2 weeks (C), with the relative, decreasing, co-localization (yellow signal) of NBD-Cholesterol and g7-NPs. Scale bar: 10 µm. (D) g7-NPs quantification in brain slices at the same time points in (B, C). Data are expressed as number of g7-NPs (evaluated based their size) for 100 µm2 ± SEM. Statistics: **P < 0.01 (48 h vs. 7 days; 7 days vs. 14 days), ***P < 0.001 (24 h vs. 7 days; 7 days vs. 14 days) was determined by one-way ANOVA followed by Newman–Keuls multiple comparison test. DAPI was used to counterstain nuclei.*

g7-NPs-Chol rescue synaptic activity in R6/2 mice

As R6/2 mice typically show alterations in striatal medium spiny neurons (MSNs) synaptic transmission with disease progression (Cepeda et al. 2003) (Cepeda et al. 2004), we next explored whether cholesterol supplementation to the brain, via systemic injection of g7-NPs-Chol, was able to ameliorate synaptic parameters in HD mice. Pilot experiments in R6/2 animals treated only with 1 or 2 injections of g7-NPs-Chol did not show any significant modifications in electrophysiological properties (data not shown). We therefore redesigned the experimental paradigm in order to provide sustained and prolonged delivery of cholesterol to the HD brain (**Fig. 4**).

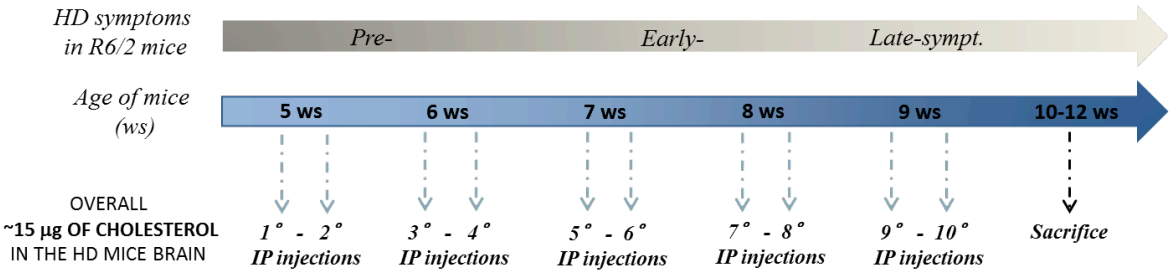

Figure 4. Scheme of the experimental paradigm.
Saline solution or g7-NPs were intraperitoneally injected, twice a week, from pre-symptomatic stage (5 weeks of age) to late-symptomatic stage (9 weeks of age), delivering an estimated dose of 15µg of cholesterol in g7-NPs-Chol treated mice.

R6/2 mice were treated starting from pre-symptomatic stage (5 weeks of age) to the symptomatic stage (9 weeks of age). 0.15 mg of g7-NPs per gram body weight were intraperitoneally injected twice a week, delivering approximately 15 µg of cholesterol to HD brain. We compared: wt and R6/2 mice treated with saline (referred to as wt and R6/2 respectively), R6/2 mice injected with empty g7-NPs (referred to as R6/2-emp) and R6/2 mice injected with g7-NPs-Chol (referred to as R6/2-Chol). In different HD animal models, robust defects have been described in striatal MSNs,

such as a reduced membrane capacitance, a decrease in spontaneous excitatory postsynaptic current (EPSC) and an increase in spontaneous inhibitory postsynaptic current (IPSC) frequencies (Cepeda et al. 2003). Therefore, in collaboration with the group of professor M. Levine (University of California, Los Angeles), we tested whether cholesterol supply, achieved by our experimental scheme, could reverse any of these phenotypes. Using the whole-cell patch-clamp recording technique, we examined MSNs properties in brain slices. Results showed that MSNs membrane capacitance, a parameter directly proportional to the membrane surface area, was significantly reduced in R6/2 mice treated with saline or empty g7-NPs (as no differences were detected between these groups, relative data were pooled in R6/2-untreated group), compared to wt mice (treated with saline) (**Table 2**). Conversely, in MSNs from R6/2 mice treated with g7-NPs-Chol (R6/2-Chol), cell capacitance was not significantly different to that of wt cells, suggesting a mild rescue of cell membrane surface area (**Table 2**). Input resistance, a parameter that reflects the extent to which membrane channels are open, was not influenced by cholesterol treatment, in fact it resulted increased in both R6/2-untreated and R6/2-Chol recorded neurons compared to wt. Interestingly, in cells from R6/2-Chol mice a significant decrease in the decay time constant was observed, compared to cells from wt or R6/2 mice treated with saline or empty g7-NPs (**Table 2**).

group	Capacitance (pF)	Input Resistance (MΩ)	Time constant (ms)
WT	68.7 ± 2.27	51.6 ± 2.73	1.9 ± 0.07
R6/2-untreated	59.8 ± 2.40*	179.3 ± 14.91***	1.9 ± 0.09
R6/2-Chol	62.9 ± 3.60	180.2 ± 24.27***	1.4 ± 0.12***###

Table 2. Summary of MSNs passive membrane properties from wt, R6/2-untreated and R6/2-chol mice. *Capacitance (pF), Input Resistance (MΩ) and Time constant (ms) registered in MSNs from wt mice treated with saline (wt), R6/2 mice treated with saline or with empty g7-NPs (R6/2-untreated) and R6/2 treated with g7-NPs-Chol (R6/2-Chol). *** R6/2-Chol vs wt; ### R6/2-Chol vs R6/2-untreated.*

This result suggests possible changes in membrane fluidity induced by cholesterol supplementation. The average frequency of spontaneous IPSCs was also significantly higher in MSNs from R6/2-untreated mice compared to wt mice (**Figs. 5A and B**), as previously demonstrated (Cepeda et al. 2004). In contrast, R6/2-Chol mice displayed a significant reduction in the frequency of IPSCs compared to R6/2-untreated mice (**Fig. 5B**), in particular for small-amplitude events (< 40 pA),

while the cumulative inter-event interval histogram showed a decreased release probability in R6/2-Chol compared to R6/2-untreated cells (**Fig. 5C**). We analyzed also the frequency of spontaneous excitatory postsynaptic currents (EPSCs) (**Fig. 5D**) that was significantly reduced in R6/2-untreated mice compared to wt mice (**Fig. 5E**). Although the decrease in the average frequency of EPSCs was not significantly rescued in R6/2-Chol mice, the cumulative inter-event interval indicated a significantly increased release probability in R6/2-Chol cells versus R6/2-untreated cells (**Fig. 5F**). Altogether, these findings demonstrate that cholesterol supplementation through g7-NPs strategy resulted in a rescue of specific membrane and synaptic parameters typically altered in MSNs of HD mice.

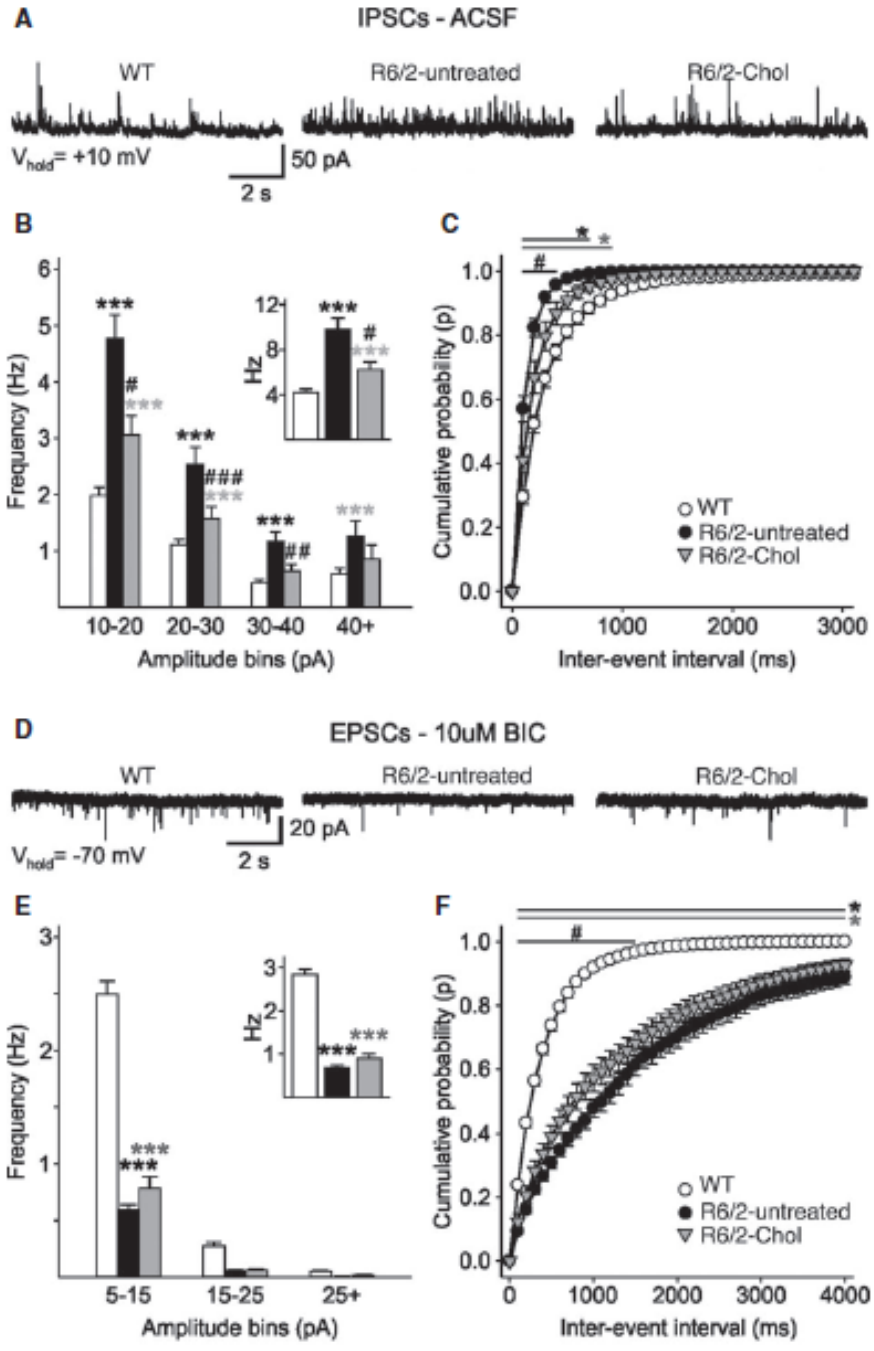

Figure 5. Systemic injections of g7-NPs-Chol rescue synaptic deficits in R6/2 mice.
*(A) Spontaneous IPSCs were recorded from striatal MSNs (wt = 52; R6/2-untreated = 27; R6/2-Chol = 29) at a holding potential of +10 mV. Data from R6/2 mice treated with saline (R6/2) or with empty g7-NPs (R6/2-emp) were pooled, as no differences were found. (B) Amplitude–frequency histogram and average frequency (inset) of IPSCs from R6/2-Chol, R6/2-untreated, and wt mice MSNs. (C) Cumulative inter-event histogram showing the release probability of IPSCs in all the experimental groups. (D) Spontaneous EPSCs were recorded from striatal MSNs (wt = 52; R6/2-untreated = 27; R6/2-Chol = 29) at a holding potential of -70 mV. Data from R6/2 mice treated with saline (R6/2) or with empty g7-NPs (R6/2-emp) were pooled, as no differences were found. (E) Amplitude–frequency histogram and average frequency (inset) of EPSCs from R6/2-Chol, R6/2-untreated, and wt MSNs. (F) Cumulative inter-event histogram showing the release probability of EPSCs in all the experimental groups. Data information: (B, D–F) Data represent mean ± SEM. P < 0.05 was calculated by one-way ANOVA followed by Newman–Keuls multiple comparison tests (#P < 0.05, ##P < 0.01, ###P < 0.001 R6/2-untreated mice vs. R6/2-Chol mice; *P < 0.05, **P < 0.01, ***P < 0.001 WT mice vs R6/2-untreated or R6/2-Chol mice).*

g7-NPs-Chol rescue cognitive dysfunction in R6/2 mice

R6/2 mice develop a progressive neurological phenotype characterized by cognitive and motor symptoms resembling those seen in HD (Carter et al. 1999) (Murphy et al. 2000) (Lüesse et al. 2001) (Giralt et al. 2011). For this reason, we investigated the impact of cholesterol supplementation on behavioral abnormalities in that HD mouse model by using standard motor and cognitive tasks. The experimental paradigm employed in these behavioral studies is shown in **Fig. 4**. To evaluate mice motor skills, we performed both rotarod and activity cage tests. We chose rotarod test since is widely used to evaluate motor coordination in rodents. Mice are first trained to walk on a rotating bar at constant speed and their motor performance is then evaluated in accelerating speed. In the rotarod test, R6/2 mice treated with saline or empty g7-NPs exhibited typical impaired motor coordination compared to wt mice, as indicated by the significantly shorter latency to fall (**Fig. 6A**). This deficit was not improved in R6/2-Chol mice (**Fig. 6A**).

Activity Cage test determines global activity, locomotion activity and exploration habits and is often used to assess motor abilities in rodent models of central nervous system (CNS) disorders. Animals are placed in the center of the testing arena and allowed to freely move while being tracked by an automated tracking system. In the activity cage, reduced rearing activity, a form of vertical exploration, was not rescued by cholesterol supplementation at 10 weeks of age (**Fig. 6B**). At the same time point, the hypokinetic phenotype (indicated by reduced global activity in the activity cage) was less dramatic in R6/2-Chol mice (**Fig. 6C**) in comparison to R6/2-untreated mice, suggesting that cholesterol supplementation partially ameliorates locomotion-related behavior in a novel environment.

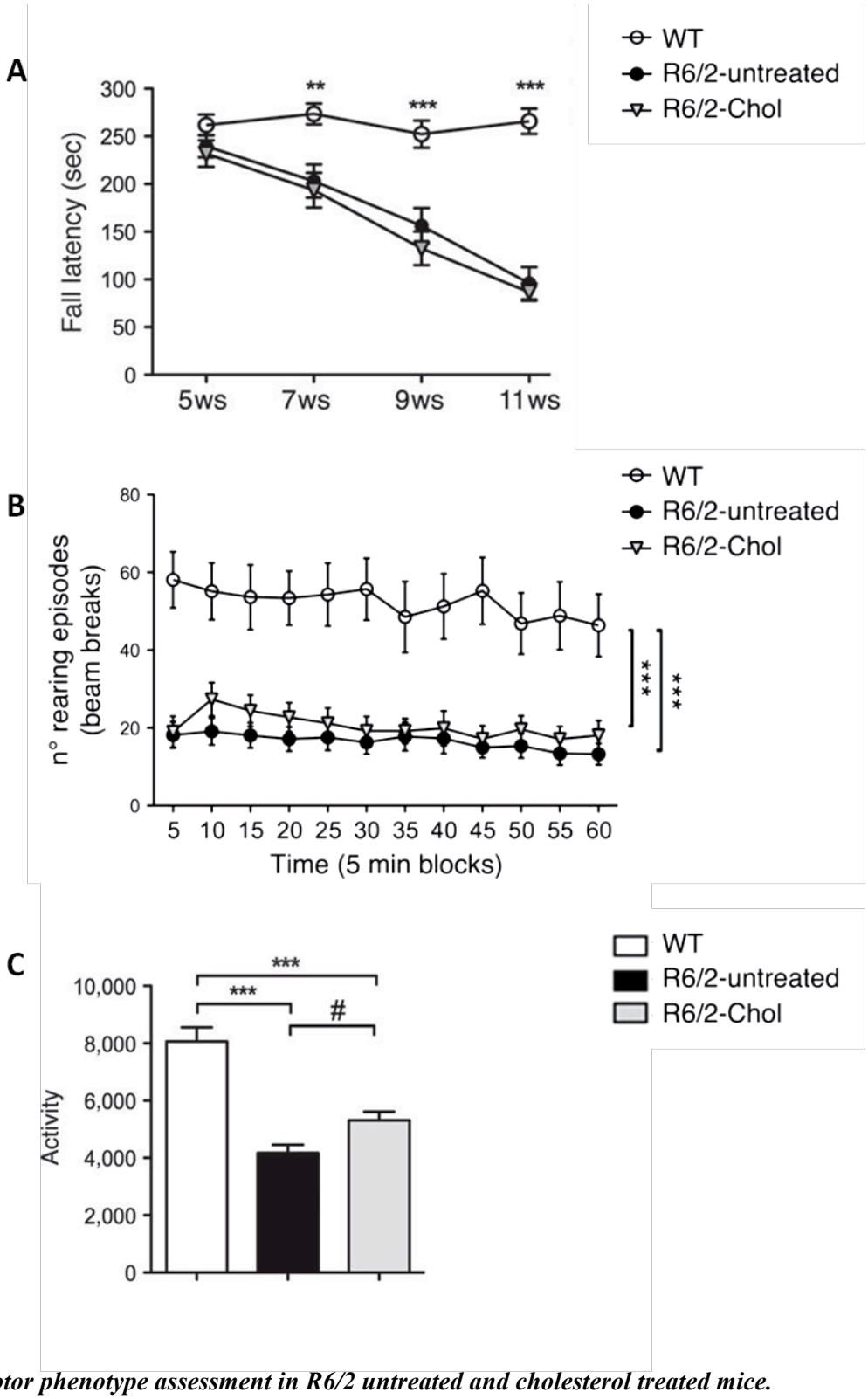

Figure 6. Motor phenotype assessment in R6/2 untreated and cholesterol treated mice.

*(A) Fall latency from an accelerating rotarod for 5- to 11-week-old wt and R6/2 mice (wt = 17; R6/2-untreated = 21; R6/2-Chol = 13). (B) Rearing episodes in the activity cage at 10 weeks of age (wt = 14; R6/2-untreated = 21; R6/2-Chol = 15). (C) Global activity in the activity cage test at 10 weeks of age (wt = 14; R6/2-untreated = 21; R6/2-Chol = 15). Data information: data are from three independent trials and represent mean ± SEM. P < 0.05 was calculated by one-way ANOVA followed by Newmann–Keuls multiple comparison tests (#P < 0.05, ##P < 0.01, ###P < 0.001 R6/2-untreated mice vs. R6/2-Chol mice; *P < 0.05, **P < 0.01, ***P < 0.001 wt mice vs. R6/2-untreated or R6/2-Chol mice).*

Finally, we evaluated cognitive tasks in HD mice after cholesterol supplementation, since changes in cholesterol synthesis/levels are associated with cognitive decline (Suzuki et al. 2013). To evaluate cognitive performance, we used the novel object recognition test (NORT), a low-stress task aimed at evaluating recognition memory. This is a cognitive test particularly attractive also because it requires no external motivation, reward, or punishment. NORT is based on the spontaneous tendency of rodents to spend more time exploring a novel object than a familiar one. The choice to explore the novel object reflects the learning and recognition memory. Importantly, object memory is impaired in patients with HD (Lawrence et al. 1996) (Lawrence et al. 2000). Behavioral analysis showed a progressive inability to discriminate novel from familiar objects in R6/2-untreated mice, from 8 weeks of age (**Fig. 7**). On the contrary, R6/2-Chol mice performance was absolutely comparable to that of wt mice, indicating that cholesterol supplementation is sufficient to complete rescue memory defect (**Fig. 7**). Importantly, this beneficial effect on recognition memory was observed at all the time points tested, even at 12 weeks of age, that is 3 weeks after the last injection (**Fig. 7**).

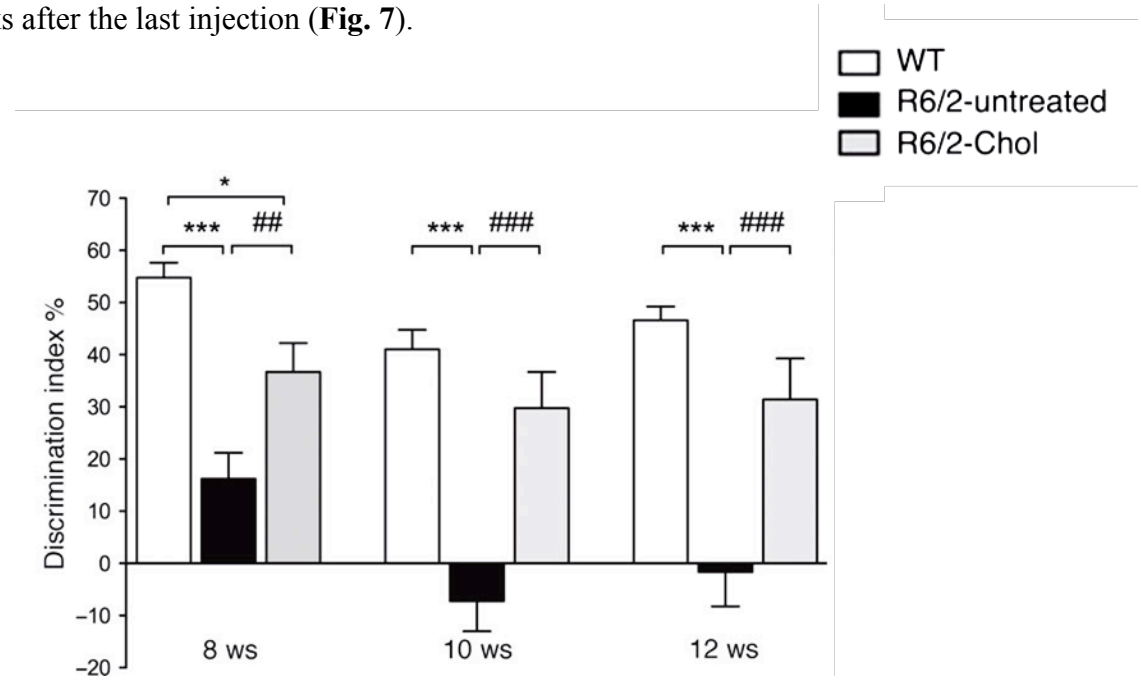

Figure 7. Cognitive phenotype assessment in R6/2 untreated and cholesterol treated mice.
*Index of discrimination (%) in wt, R6/2-untreated, and R6/2-Chol mice, at 8 weeks of age (wt = 24; R6/2-untreated = 36; R6/2-Chol = 21), at 10 weeks of age (wt = 25; R6/2-untreated = 35; R6/2-Chol = 20), and at 12 weeks of age (wt = 24; R6/2-untreated = 30; R6/2-Chol = 19). A DI above zero indicates a preference for the novel object; on the contrary the index below zero indicates a preference for the familiar object. Data from R6/2 mice treated with saline (R6/2) or with empty g7-NPs (R6/2-emp) were pooled, as no differences were found. Data information: data are from three independent trials and represent mean ± SEM. P < 0.05 was calculated by one-way ANOVA followed by Newmann–Keuls multiple comparison tests (#P < 0.05, ##P < 0.01, ###P < 0.001 R6/2-untreated mice vs. R6/2-Chol mice; *P < 0.05, **P < 0.01, ***P < 0.001 wt mice vs. R6/2-untreated or R6/2-Chol mice).*

Cholesterol supplementation influences the protein levels of synaptic machinery

To determine whether the cognitive improvement observed in R6/2 mice after cholesterol supplementation was related to a positive modulation of synaptic protein machinery, we purified synaptic protein enriched triton-insoluble fractions (TIF) from the brain of wt, R6/2-untreated and R6/2-Chol mice. Next, we performed semiquantitative Western blotting for scaffolding proteins such as PSD95 and gephyrin and NMDA receptor subunits (GluN1 and GluN2B) (**Fig. 8A**). Reduced PSD95, as well as a reduction in GluN1 and GluN2B, were found in R6/2-untreated mice compared to wt mice, as expected (**Fig. 8B**). Importantly, cholesterol supplementation normalized or increased the levels of these proteins (**Fig. 8B**), suggesting a rescue of the molecular composition of the synaptic machinery contributing to synaptic structure.

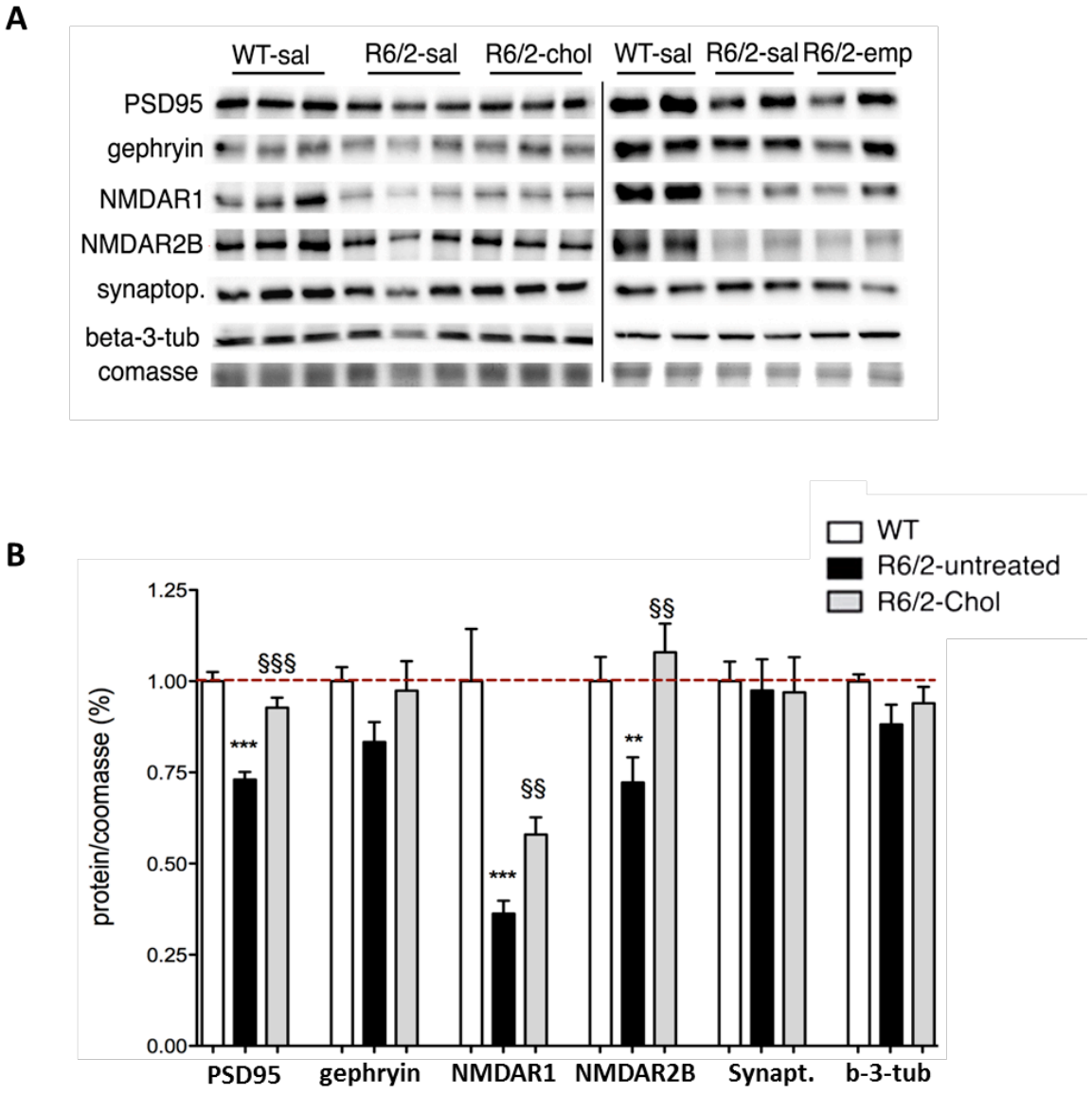

Figure 8. Systemic injections of g7-NPs-Chol increase the levels of synaptic machinery proteins.
*Protein levels (A) and relative densitometry quantification (B) of several synaptic proteins analyzed in triton-insoluble (synaptic enriched) fractions purified from total brains from wt (n = 5), R6/2-untreated (n = 5) and R6/2-Chol (n = 3) mice. Cholesterol supplementation rescued the levels of PSD95 and NMDA receptor subunits GluN1 and GluN2B in R6/2 mice. Data information: Data in B represent mean ± SEM. P < 0.05 was determined by one-way ANOVA followed by Newman–Keuls multiple comparison tests (§P < 0.05, §§P < 0.01, §§§P < 0.001 R6/2-untreated mice vs. R6/2-Chol mice; *P < 0.05, **P < 0.01, ***P < 0.001 wt mice vs. R6/2-untreated or R6/2-Chol mice).*

Anatomical examination of R6/2 brains revealed several age-related alterations in brain morphology such as progressive reduction in striatal volume and increase in ventricular volume, compared with controls (Stack et al. 2005). To investigate whether cholesterol supplementation was able to ameliorate neuropathological deficits in R6/2 mice, we performed unbiased stereological analyses at 12 weeks of age, in collaboration with Marina Boido (Neuroscience institute Cavalieri Ottolenghi, Torino). A significant enlargement of ventricles was observed in R6/2 mice treated with saline (R6/2) compared to wt mice (**Fig. 9A**), as already reported in the literature. Surprisingly, systematic injections of both empty g7-NPs and g7-NPs-Chol led to a reduction of the ventricular volume (**Fig. 9B**). We hypothesized that the effect induced by both types of NPs could be related to degradation of PLGA in lactic and glycolic acids. Altogether, these findings suggest that cholesterol supplementation via g7-NPs is not sufficient to contrast brain atrophy in R6/2 mice, at least with this experimental paradigm, although it does restore the physiological levels of specific synaptic proteins altered in HD mice.

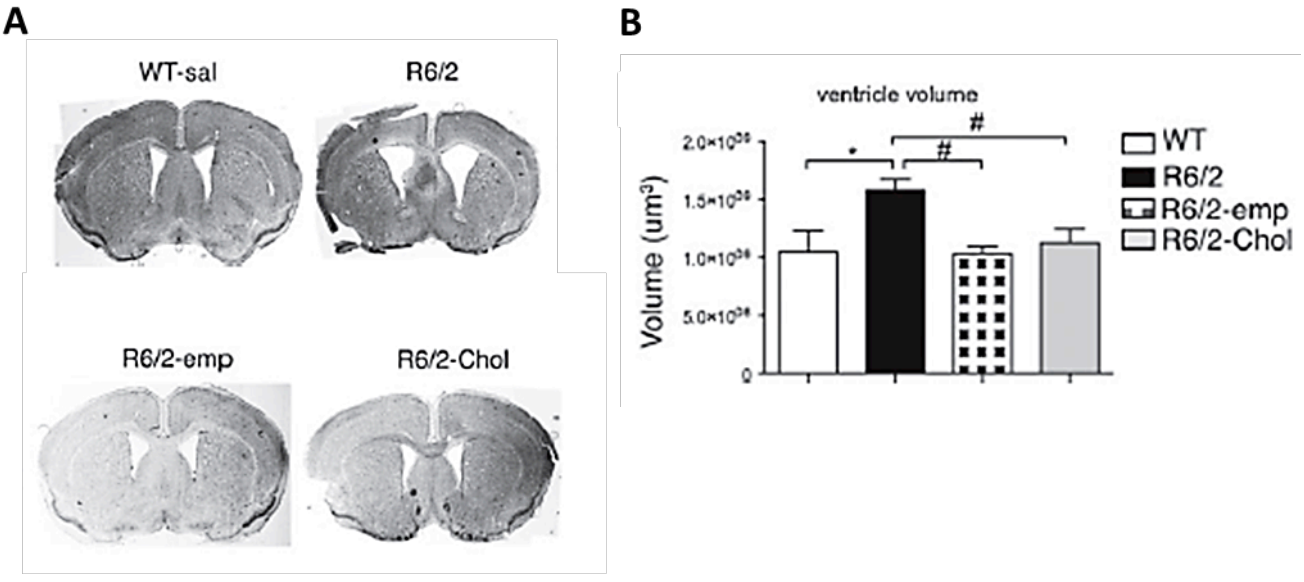

Figure 9. Systemic injections of g7-NPs-Chol do not rescue a typical neuropathological feature of R6/2 mice.

*Representative images of Nissl staining (A) and ventricle volume analyzed using Neurolucida 3D reconstruction software, at 12 weeks of age (B) in wt (n = 7), R6/2 (n = 7), R6/2-emp (n = 6), and R6/2-Chol (n = 8) mice. Data information: Data in B represent mean± SEM. P < 0.05 was determined by one-way ANOVA followed by Newman–Keuls multiple comparison tests (#P < 0.05, ##P < 0.01, ###P < 0.001 R6/2-untreated mice vs. R6/2-Chol mice; *P < 0.05, **P < 0.01, ***P < 0.001 wt mice vs. R6/2-untreated or R6/2-Chol mice).*

Safety evaluation of g7-NPs in R6/2 mice

It is known that cholesterol supplementation to the brain might lead to a further reduction in cholesterol synthesis, already compromised in R6/2 mice (Valenza et al. 2007b). We therefore analyzed by MS the levels of cholesterol precursors and the brain-specific cholesterol catabolite 24OHC in the brain of treated mice, at 12 weeks of age. Lathosterol, a marker of cholesterol synthesis, was found equally reduced in both R6/2-untreated and R6/2-Chol mice compared to wt mice (**Fig. 10A**), suggesting that exogenous cholesterol supplemented via g7-NPs does not further decrease the endogenous biosynthetic pathway. Similarly, 24OHC, an indicator of brain cholesterol catabolism that usually mirrors cholesterol biosynthesis in brain (Lund et al. 2003), was found similarly reduced in both R6/2 groups compared to wt mice (**Fig. 10B**). Furthermore, we also measured mRNA levels of cholesterol biosynthetic genes (hmgcr and fdft1) in liver and lung of R6/2 mice to verify if the injected NPs that localized in periphery altered endogenous cholesterol metabolism. The mRNA expression of both cholesterol genes was similar in both tissues in all groups, even in the presence of g7-NPs-Chol (**Figs. 10C and D**). All these results suggest that the exogenous cholesterol delivered to the brain or accumulated in peripheral tissues does not lead to significant alterations of endogenous cholesterol homeostasis in the time frame analyzed in this study. Although the PLGA NPs employed in this study are considered biocompatible and biodegradable, an immunogenicity study of these NPs *in vivo* is missing. PLGA, released after degradation of empty or cholesterol-loaded g7-NPs, and cholesterol itself might influence immune responses. Therefore, we analyzed mRNA levels of two pro-inflammation genes encoding for Tumor Necrosis Factor (TNF)-alpha and interleukin-6 (IL-6), in peripheral tissues from our cohorts. As shown in **Figs. 10E** and **F**, TNF-alpha and Il6 mRNA levels were significantly increased in the liver and in lung of R6/2 mice treated *w*ith saline (R6/2) compared to wt mice, supporting the available evidence that peripheral inflammation is associated with HD (Trager et al. 2014). Similar results were found in R6/2-emp and R6/2-Chol mice, suggesting that multiple administrations of g7-NPs (empty or loaded with cholesterol) per se do not affect peripheral inflammation in R6/2 mice.

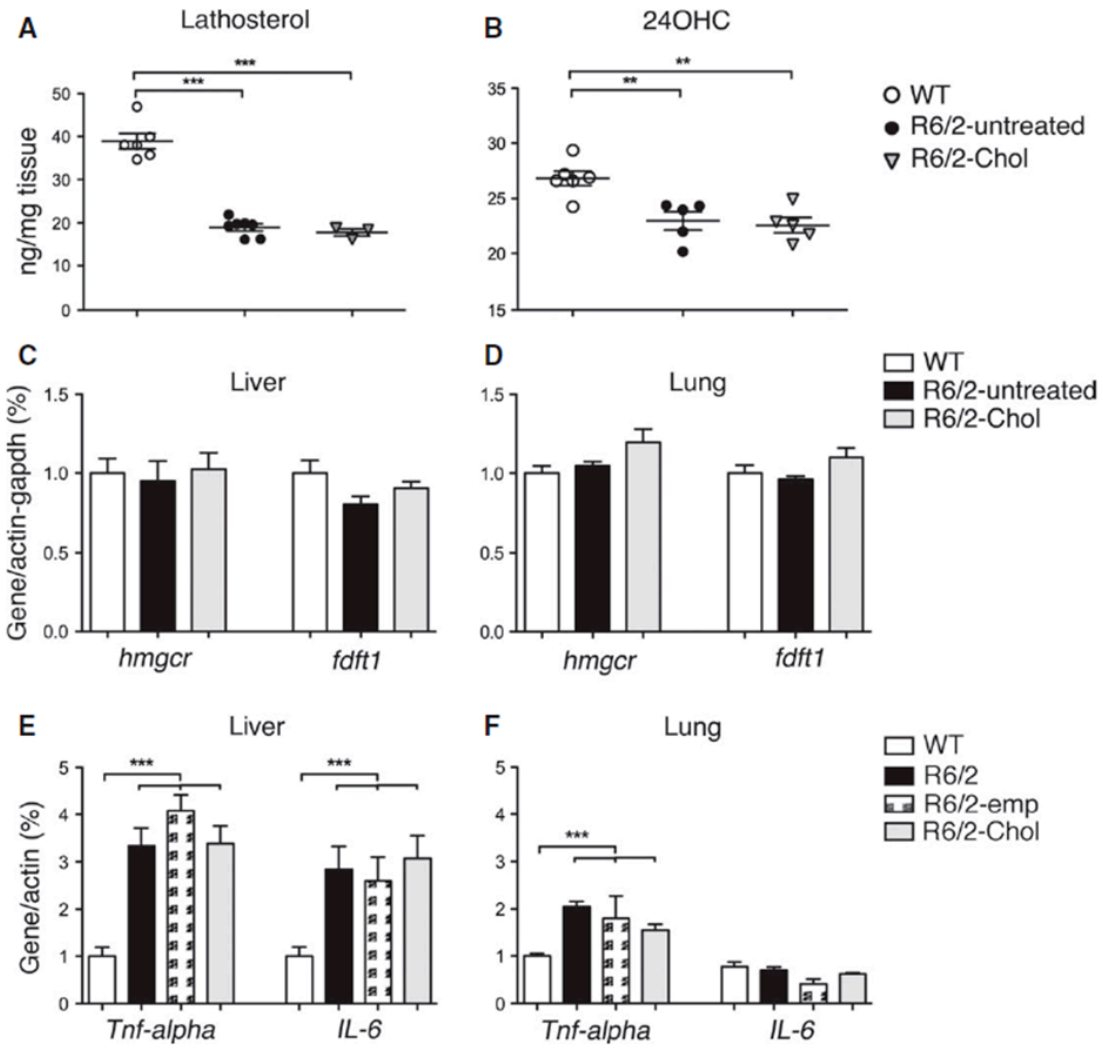

Figure 10. Exogenous cholesterol or g7-NPs per se do not affect endogenous cholesterol biosynthesis or inflammatory genes expression.

*Lathosterol (A) and 24OHC (B) measured by MS in the brain of wt (n = 6), R6/2-untreated (n = 7) and R6/2-Chol (n = 5) mice. mRNA levels of hmgcr and fdft1 in liver (C) and lung (D) of wt (n = 7), R6/2-untreated (n = 8) and R6/2-Chol (n = 4) mice. Data from R6/2 mice treated with saline (R6/2) or with empty g7-NPs (R6/2-emp) were pooled, as no differences were found. mRNA levels of inflammatory genes in liver (E) and lung (F) of wt (n = 7), R6/2 (n = 4), R6/2-emp (n = 4) and R6/2-Chol (n = 5) mice. Data information: Data in (A–F) represent mean ± SEM. *P < 0.05, **P < 0.01, ***P < 0.001 was determined by one-way ANOVA followed by Newman–Keuls multiple comparison tests.*

All these data have been published in: Valenza M., Chen J.Y.*, Di Paolo E.[§], Ruozi B.[§], Belletti D., Ferrari Bardile C., Leoni V., Caccia C., Brilli E., Di Donato S., Boido M.M., Vercelli A., Vandelli M.A., Forni F., Cepeda C., Levine M.S., Tosi G., Cattaneo E. (2015) Cholesterol-loaded nanoparticles ameliorate synaptic and cognitive function in Huntington's disease mice. EMBO Molecular Medicine, 7(12), 1547–1564. http://doi.org/10.15252/emmm.201505413. *co-first authors, [§]co-second authors.*

Strategy 2 – Alzet Osmotic Minipumps

To define the most efficacious dose of cholesterol in contrasting neurobehavioral defects in R6/2 mice and to avoid potential confounding effects from peripheral administration and limited blood–brain barrier permeability, we performed a second series of studies employing osmotic minipumps (Alzet). Conversely to g7-NPs, this second strategy allowed us to investigate the effects of chronic, unilateral, infusion of increasing doses cholesterol into mice striatum. This is of great importance given that the striatum is one of the most affected brain areas in HD, in which cholesterol dysfunction is higher and more precocious respect to other areas (Valenza et al. 2005) (Valenza et al. 2007). In all the trials performed, the animals were treated with the same experimental paradigm showed in **Fig. 11**.

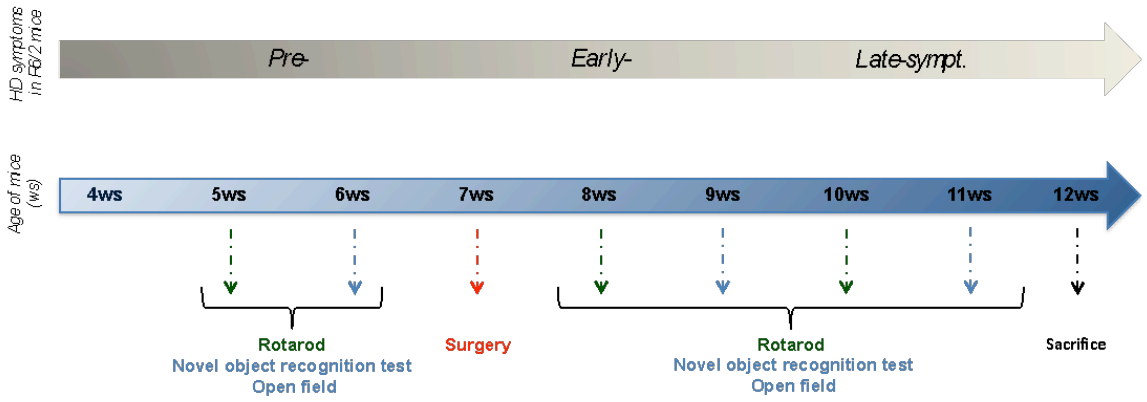

Figure 11. Scheme of the experimental paradigm.
Minipumps were surgically implanted in 7 weeks old mice and a battery of behavioral tests is performed before and after surgery, to assess motor and cognitive abilities of mice.

Cholesterol levels increase in the brain of wt animals, after minipump infusion

To verify if the delivery of exogenous cholesterol, via osmotic minipumps, led to a detectable variation in the amount of brain cholesterol, we performed initial MS studies in collaboration with the Carlo Besta Neurological Institute of Milan. Analysis of MS data, from wt mice intrastriatally infused with 500µg of cholesterol, indicated a significant increase in total cholesterol levels into both infused (right) and contralateral (left) striata of cholesterol treated wt mice, respect to controls (untreated or ACSF infused wt mice) (**Fig. 12A**). Interestingly, a detectable increase in cholesterol levels was also found into cortex of both right and left hemispheres from cholesterol treated mice, indicating cholesterol diffusion into the surrounding brain areas from the site of infusion (**Fig. 12B**).

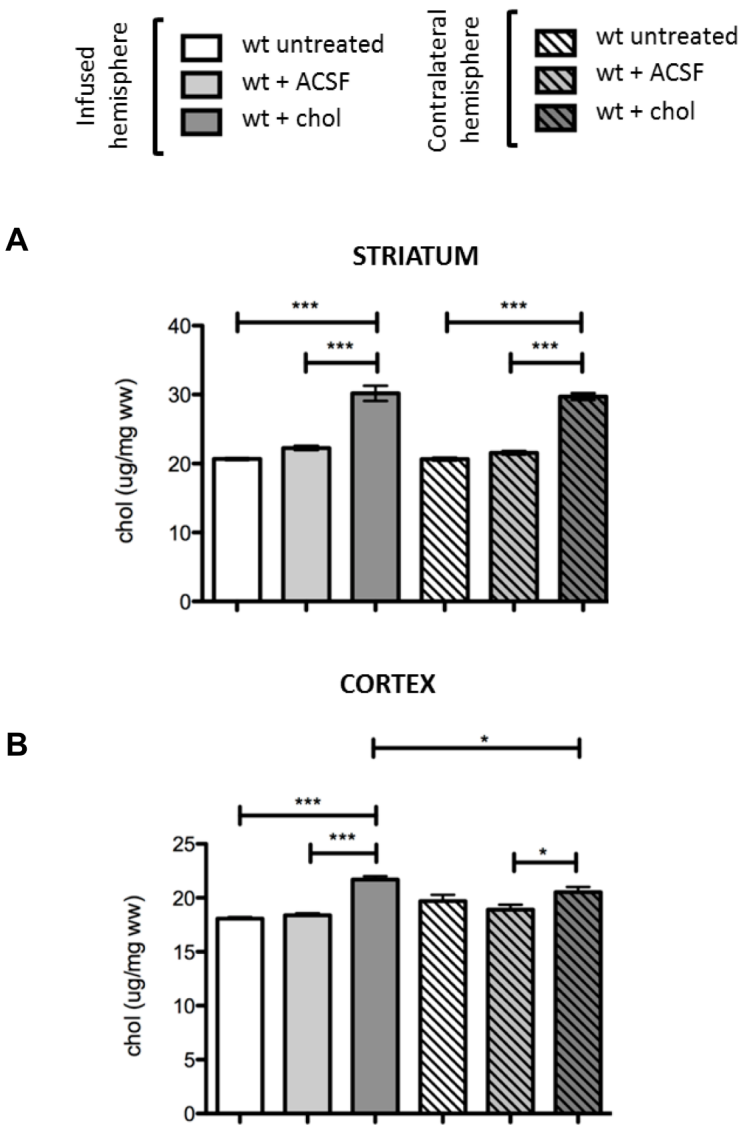

Figure 12. Intrastriatal infusion of exogenous cholesterol induces an increase in brain cholesterol levels. *Cholesterol levels measured by MS in striatum (A) and cortex (B) of wt mice at 11 weeks of age, after 4 weeks of continuous infusion (pumping rate 0.11 µl/h). Data information: data in (A–B) represent the mean from n = 2 untreated, n = 3 ACSF treated and n = 4 cholesterol treated mice ± SEM. *P < 0.05, **P < 0.01, ***P < 0.001 was determined by one-way ANOVA followed by Newman–Keuls multiple comparison tests. All data are normalized above weight tissue.*

Surgical implantation of osmotic minipumps per se does not influence behavioral phenoytpe in healthy mice

In a first trial, wt mice were subjected to surgical implantation of artificial cerebrospinal fluid (ACSF)-containing minipumps and compared to untreated (unoperated) mice, in order to investigate possible side effects associated with the procedure. Animal's behavioral phenotype was evaluated before (6 weeks of age) and after surgery (8-11 weeks of age) by using the same motor

and cognitive test described before. At each time point tested, both motor (**Fig. 13**) and cognitive (**Fig. 14**) performances of ACSF infused mice were comparable to that of unoperated (control) wt mice. Assessment of post-operative pain and distress was performed using a specific table for pain scoring based on behavioral indicators of well-being and monitoring mice body weight (Lloyd and Wofenshohn 1998). To obtain reliable results in the following cognitive and motor tests it was necessary to avoid any kind of bias based on potential mice suffering. No obvious signs of pain or distress or significant changes in body weight were detected in all the animals over the infusion period (data not shown).

Overall these data indicate that minipumps implantation does not influence the behavioral phenotype of healthy mice, consequently the experimental group of ACSF treated wt mice was not included in the successive trials.

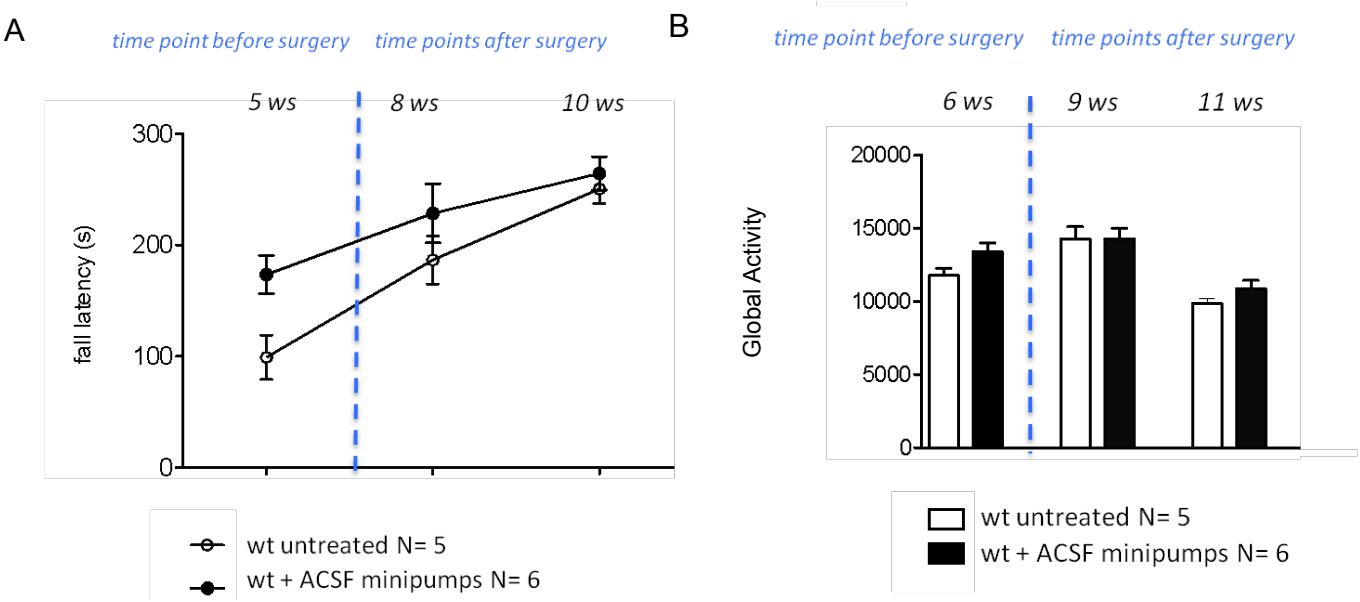

Figure 13. Motor phenotype assessment in operated and unoperated wt mice.
(A) Fall latency from an accelerating rotarod for 5- to 10-week-old wt mice. (B) Global activity in the activity cage test for 6- to 11-week-old wt mice. Data information: data in (A–B) represent the mean from n = 5 untreated and n = 6 ACSF treated wt mice ± SEM.

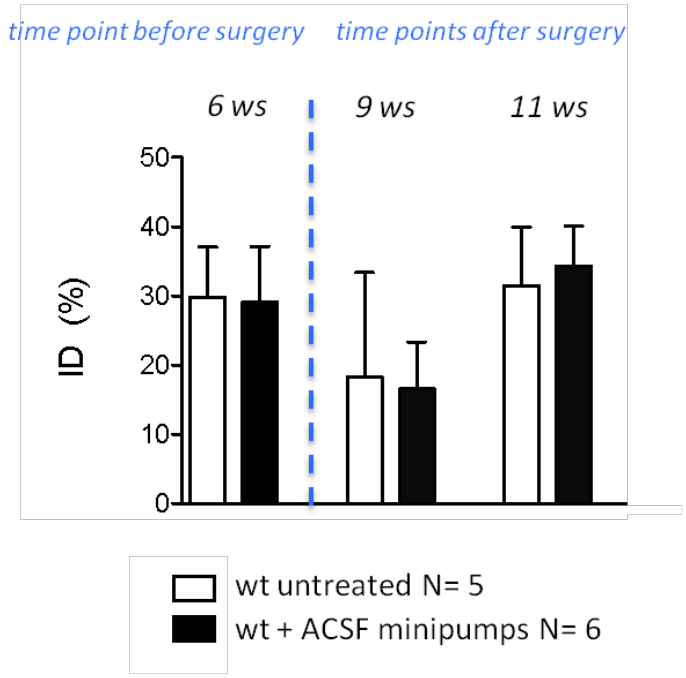

Figure 14. Cognitive phenotype assessment in operated and unoperated control wt mice.
Index of discrimination (%) for 6- to 11-week-old wt mice. Data information: data represent the mean from n = 5 untreated and n = 6 ACSF treated wt mice ± SEM.

Intrastriatal infusion of cholesterol leads to a dose-dependent rescue of motor and cognitive deficits in R6/2 mice

To provide definitive evidence of the therapeutic potential of brain cholesterol supplementation and identify the most efficacious dose in contrasting HD neurobehavioral defects, we implanted osmotic minipumps in R6/2 mice. Five independent *in vivo* trials were completed comparing:

- unoperated wt mice
- unoperated R6/2 mice
- R6/2 mice + ACSF loaded minipumps
- R6/2 mice + ACSF-cyclodextrin loaded minipumps
- R6/2 mice + 20µg-cholesterol loaded minipumps (low dose, near to the amount delivered with g7-NPs-Chol treatment)
- R6/2 mice + 250µg-cholesterol loaded minipumps (intermediate dose)
- R6/2 mice + 500µg-cholesterol loaded minipumps (high dose)

In each trial, the animals were tested following the same experimental paradigm shown in **Fig. 11**. As expected, untreated and ACSF treated R6/2 mice showed a progressive deterioration in fine motor coordination assessed by an accelerating rotarod test, from pre-symptomatic stage (5 weeks of age) (**Fig. 15A**) to symptomatic stage (10 weeks of age) (**Fig. 15B**). All the administered doses

of cholesterol failed to induce a significant amelioration in rotarod performance of R6/2 mice at 8 weeks of age (data not shown) and 10 weeks of age (**Fig. 15B**).

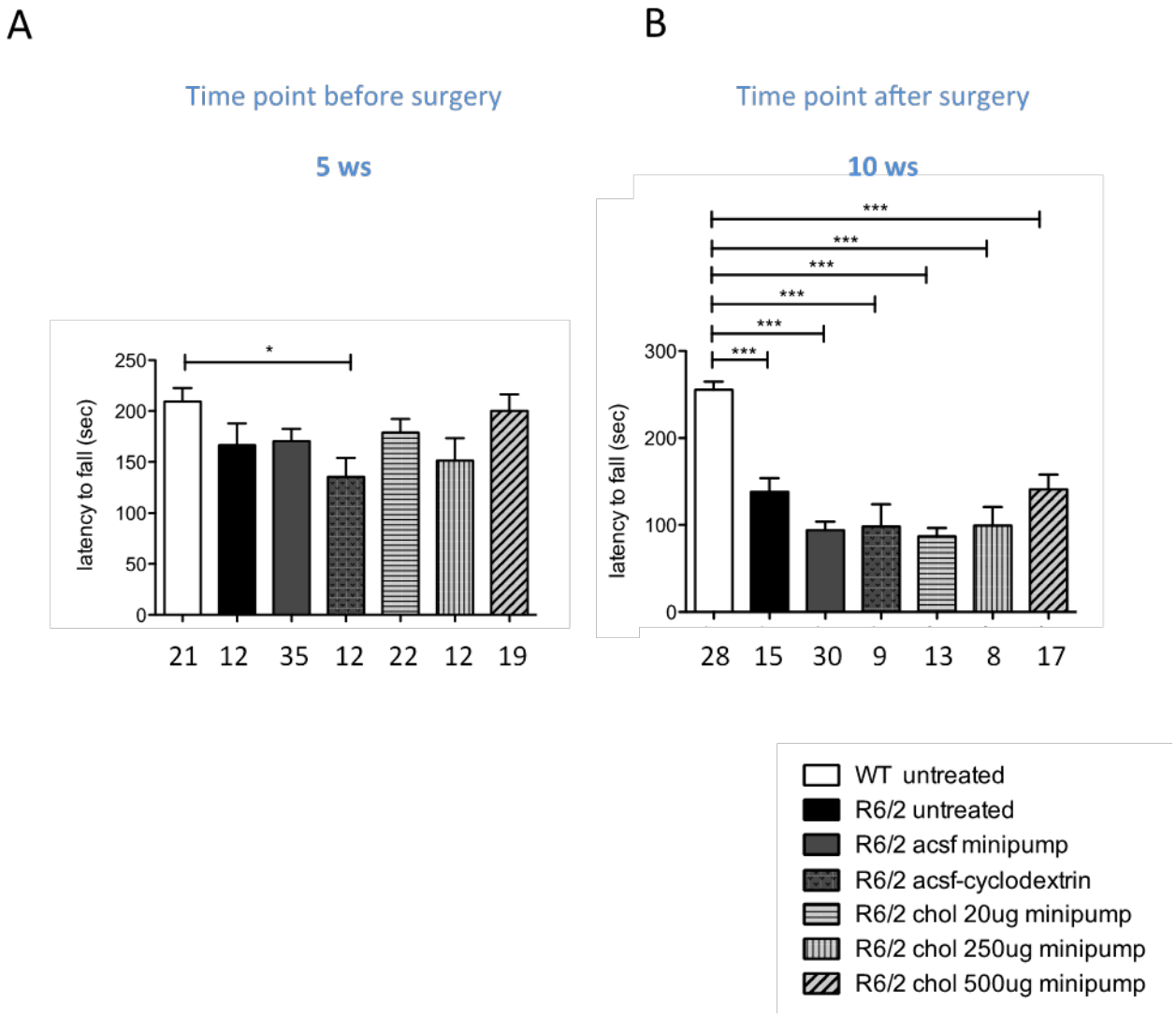

Figure 15. Motor coordination assessment in cholesterol infused R6/2 mice.
*Fall latency from an accelerating rotarod at pre-symptomatic time point (5 weeks of age) (A) and at symptomatic time point (10 weeks of age) (B) in R6/2 mice. Data information: data represent the mean ± SEM. The number of animals analyzed is reported under each column group. *P < 0.05, **P < 0.01, ***P < 0.001 was determined by one-way ANOVA followed by Newman–Keuls multiple comparison tests.*

To evaluate mice motor abilities, we performed also the activity cage test at 6 (**Fig. 16A**), 9 (data not shown) and 11 weeks of age (**Fig. 16B**). In this test R6/2 mice typically exhibit a severe hypokinetic phenotype with disease progression (Luesse et al. 2001), as confirmed in our experiments (**Fig. 16A and B**). Only the intrastriatal infusion of the high dose of cholesterol (500µg) resulted also in a rescue of spontaneous locomotor activity, that remained comparable to

that of wt mice at all the time points tested (**Fig. 16A and B**). A beneficial effect on spontaneous locomotor activity was also observed after cholesterol supplementation via g7-NPs, but in that case R6/2 mice displayed only a partial rescue at 10 weeks of age (Valenza et al. 2015).

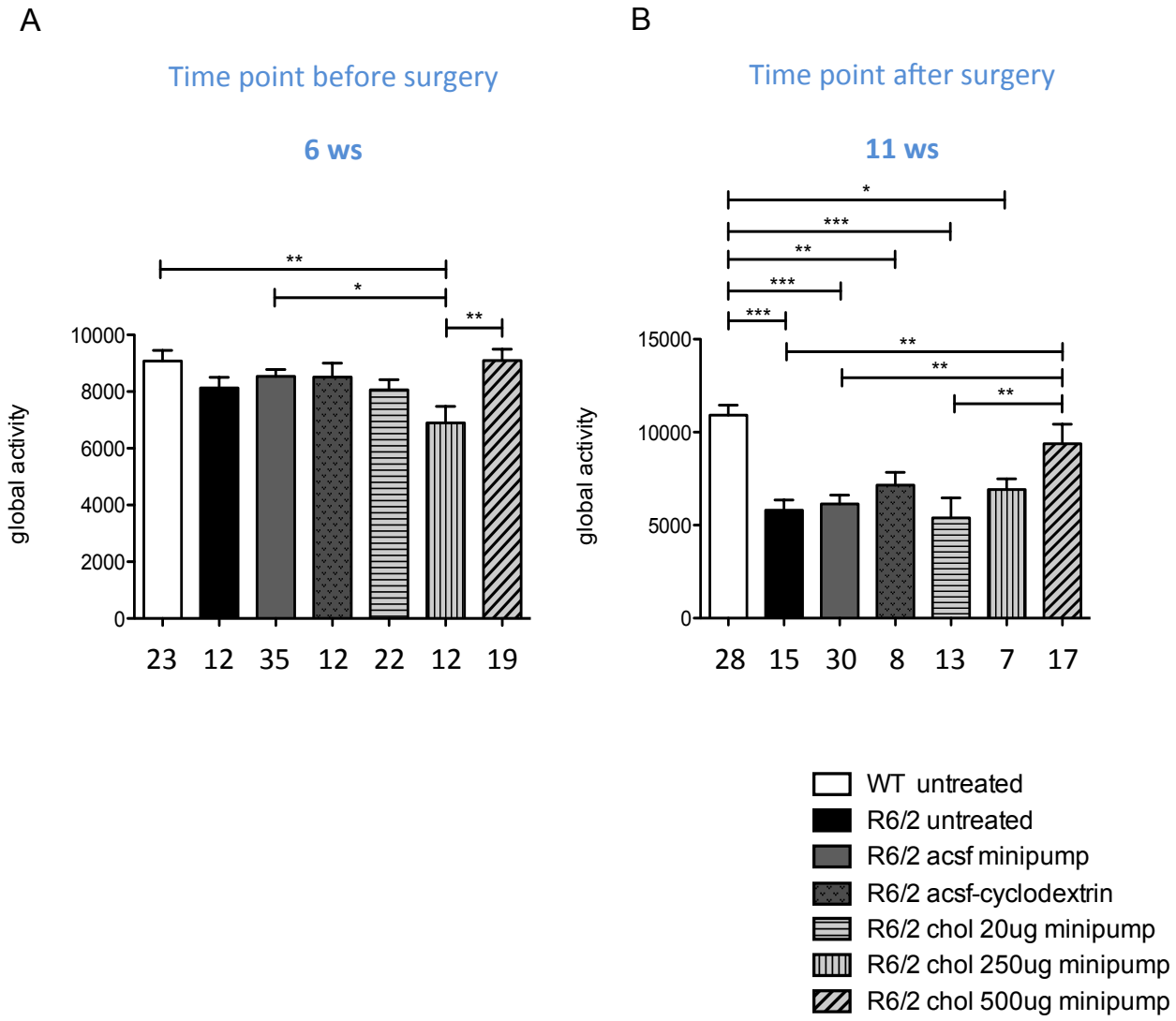

Figure 16. Spontaneous global activity assessment in cholesterol infused R6/2 mice.
*Global activity in the activity cage test at pre-symptomatic time point (6 weeks of age) (A) and at late-symptomatic time point (11 weeks of age) (B) in R6/2 mice. Spontaneous locomotor activity of 11 weeks-old R6/2 mice infused with 500μg of cholesterol was comparable to that of age-matched wt mice (B). Data information: data represent the mean ± SEM. The number of animals analyzed is reported under each column group. *P < 0.05, **P < 0.01, ***P < 0.001 was determined by one-way ANOVA followed by Newman–Keuls multiple comparison tests.*

To assess mice cognitive abilities we performed the novel object recognition test (NORT), as previously done in Valenza et al. 2015. Untreated and ACSF treated R6/2 mice cognitive abilities declined during disease progression, with a marked inability to discriminate the novel object from the familiar one evident at symptomatic time points of 9 (data not shown) and 11 weeks of age (**Fig. 17B**), but not at 6 weeks of age (**Fig. 17A**). R6/2 mice treated with all doses of cholesterol performed as well as wt mice at 11 weeks of age (**Fig. 17B**), indicating that cholesterol infusion into the striatum completely prevents memory deficits in HD mice, as previously observed with chol-g7-NPs administration (Valenza et al. 2015).

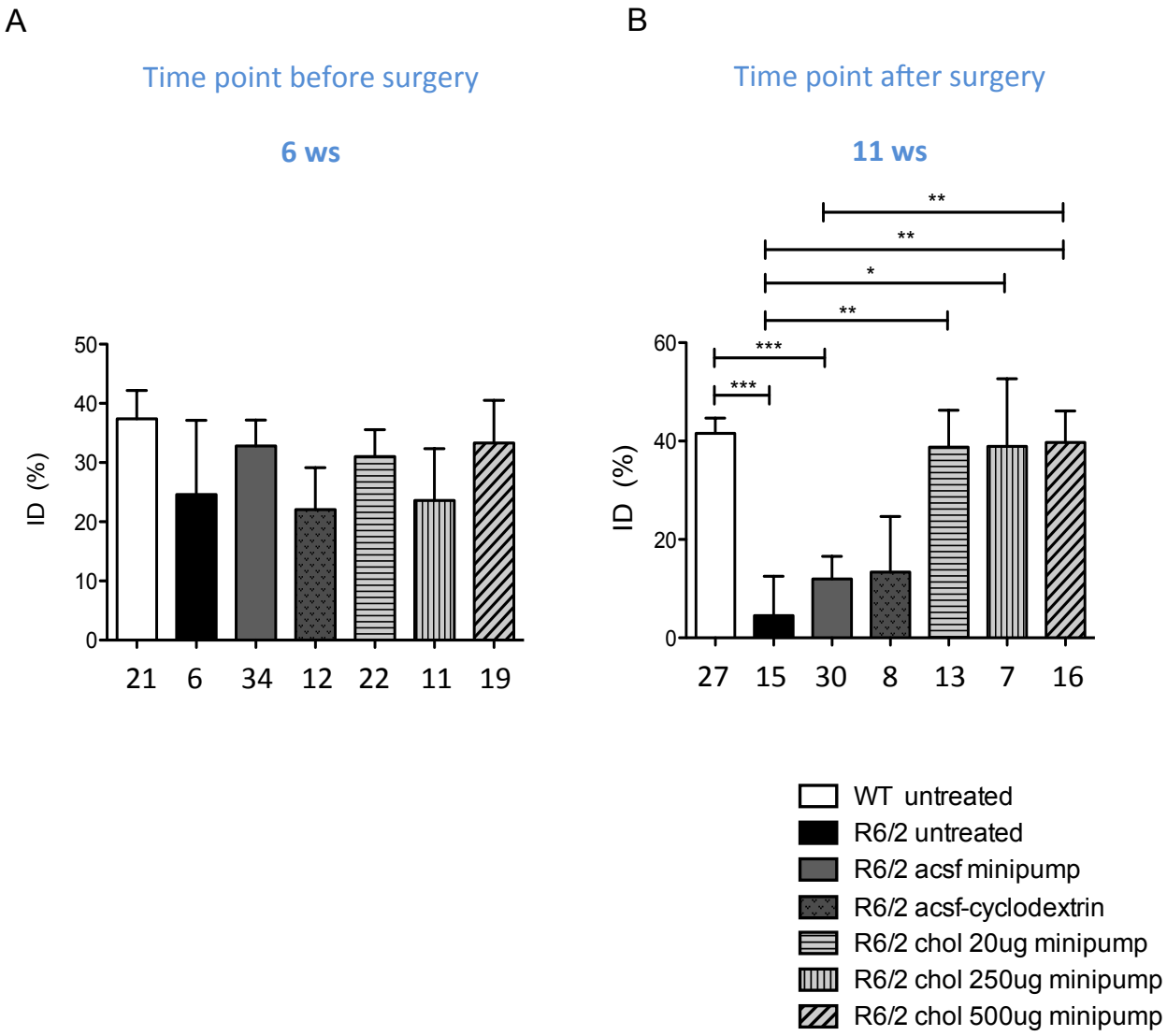

Figure 17. Cognitive phenotype assessment in cholesterol infused R6/2 mice.
*Index of discrimination (%) in NOR test at pre-symptomatic time point (6 weeks of age) (A) and at late-symptomatic time point (11 weeks of age) (B) in R6/2 mice. ID is significantly increased in R6/2 mice treated with three different doses of cholesterol at 11 weeks of age (B). Data information: data represent the mean ± SEM. The number of animals analyzed is reported under each column group. *P < 0.05, **P < 0.01, ***P < 0.001 was determined by one-way ANOVA followed by Newman–Keuls multiple comparison tests.*

All these results confirm that low doses of cholesterol are already sufficient to totally contrast cognitive decline in R6/2 mice. On the contrary, highest doses of cholesterol are required to ameliorate motor performances of HD mice.

Since in these experiments we used Methyl-β-cyclodextrin (MBCD)-balanced *water-soluble cholesterol dissolved in ACSF (see material and methods),* an additional control group of R6/2 mice treated with MBCD cyclodestrin (ACSF-cyclodestrin) was tested. However, the behavioral phenotype of this R6/2 group was comparable to that of untreated and ACSF treated R6/2 mice (**Figs. 15, 16, 17B**).

Preliminary analysis of EPSC in MSNs from R6/2 mice infused with high dose of cholesterol

Also in this case we investigated whether changes in synaptic-transmission parameters, typically altered in MSNs of HD mice, were implicated in the behavioral recovery observed in cholesterol treated mice.

In collaboration with the group of professor G. Biella (University of Pavia), we compared EPSC frequency in MSNs from R6/2 mice, following ACSF or cholesterol (500µg) infusion. It is known that the frequency of spontaneous EPSCs progressively decreases in MSNs of R6/2 mice (Cepeda et al. 2003) (Cepeda et al. 2004), however intrastriatal infusion of cholesterol partially restored this synaptic defect (**Fig. 18**).

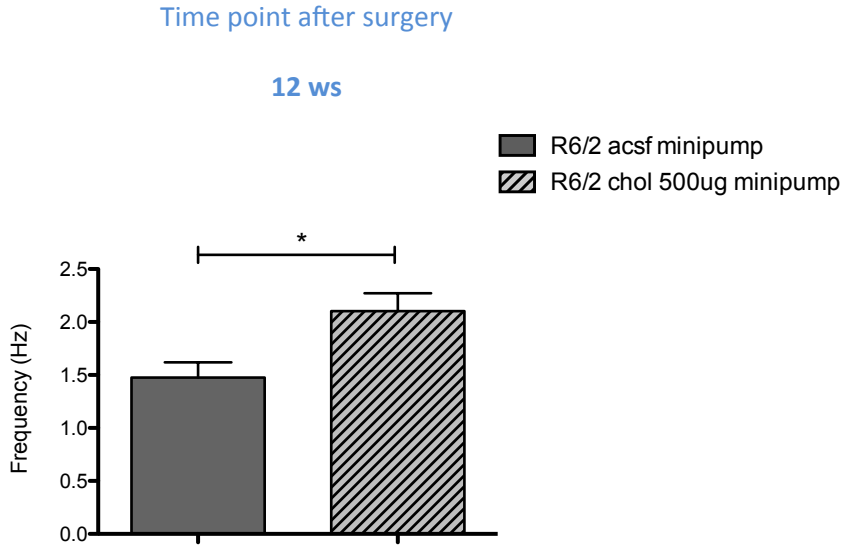

Figure 18. Intrastriatal infusion of cholesterol led to a significant increase in the frequency of EPSCs. *Spontaneous EPSCs recorded from striatal MSNs (R6/2 ACSF minipumps = 5; R6/2 chol 500µg minipumps = 5) at a holding potential of -70 mV. Data represent mean ± SEM. Statistics: *P < 0.05 was determined by Student's t-test.*

Strategy 3 – Intranasal rout of administration

In a third approach we attempted to deliver exogenous cholesterol to mice brain using intranasally administered liposomes. We were interested in this route of administration since it has recently emerged as a non-invasive, promising, approach for drug delivery to the brain (Meredith et al. 2015). Intranasally applied drugs are rapidly transported into the central nervous system by the peripheral olfactory and trigeminal systems. In collaboration with M. Salmona (Mario Negri Institute), we performed preliminary *in vivo* experiments in order to verify the validity of this further strategy for cholesterol delivery to the brain. To supply exogenous cholesterol to the mice brain through the intranasal rout, we chose to employ liposomes based formulations. Liposomes are spherical, self-closed structures formed by one or several concentric lipid bilayers with an aqueous phase inside, which were first proposed and tested as a drug delivery system in the early 1970s. Since then, they have been adopted as vehicle for drug delivery and targeting, due to their very unique and attractive biological and physical chemical properties. Liposomes are biocompatible and can both entrap and protect water-soluble (hydrophilic) molecules in their internal water compartment and water-insoluble (hydrophobic) into their membranes. Moreover, they provide a unique opportunity to deliver pharmaceuticals into cells or even inside individual cellular compartments (Bozzuto & Molinari 2015).

Intranasally administered D6-cholesterol is detectable into mice brain after 6 and 24 hours, but chronic intranasal administration of unlabeled cholesterol containing liposomes leads to undetectable variation in brain cholesterol levels

We performed a first experiment using unilamellar liposomes containing deuterated (D6) cholesterol in 6 weeks old wt and R6/2 mice. To avoid the use of any anesthesia, mice were acclimated to handling for a period of two weeks before the onset of intranasal dosing (Hanson et al. 2013). This procedure helps ensure a correct body position and avoid anxiety reaction for maximum effectiveness of awake intranasal drug delivery. All the animals received a single intranasal administration and then were sacrificed at different time points (1h, 3h, 6h, 24h; n = 2 mice/genotype/time point) (**Fig. 19**).

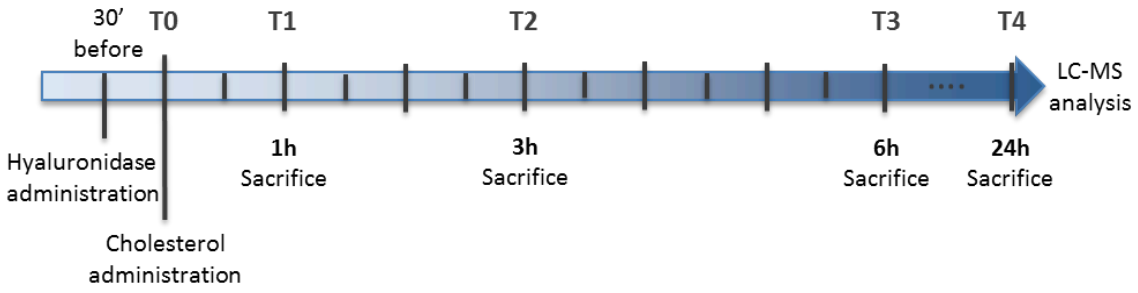

Figure 19. Scheme of the experimental paradigm.
6 weeks old animals received a single intranasal administration after hyaluronidase pretreatment. Mice were then sacrificed at different time points (1h, 3h, 6h, 24h; n = 2 mice/genotype/time point).

Subsequently, the group coordinated by Prof M. Salmona performed liquid chromatography–mass spectrometry on brain tissues isolated from treated mice. Collected data revealed that D6-cholesterol (distinguishable from the native one) reached measurable, increasing, levels in the olfactory bulb and in the brain, respectively after 6 and 24 hours (**Fig. 20**), suggesting the validity of the strategy in both wt and R6/2 mice.

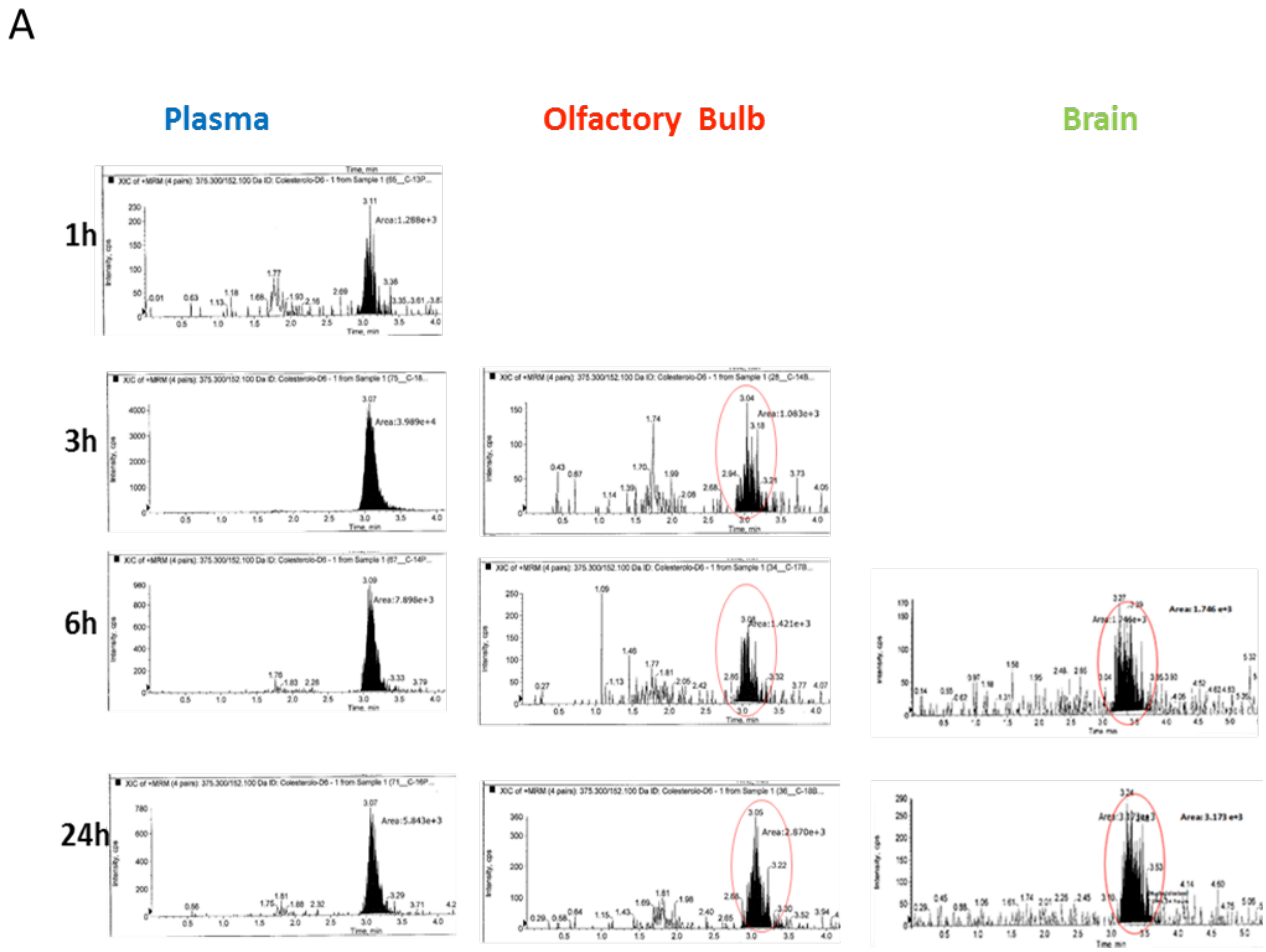

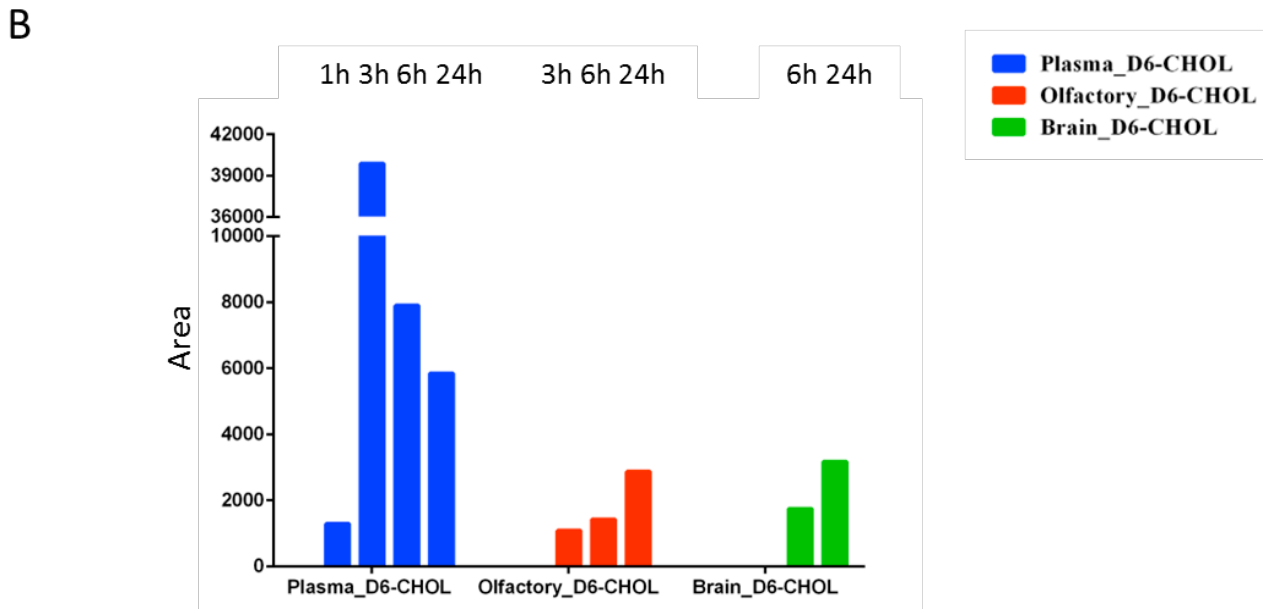

Figure 20. Deuterated cholesterol (D6-chol) levels in mice plasma, olfactory bulbs and brain.
D6-chol signal was determined in plasma 1h after intranasal administration (A) and decreased overtime from 3h to 24h (B). Detectable levels of D6-chol were found in olfactory bulbs and brain after 3h and 6h respectively (A) and increased overtime (B).

The successive trial performed in wt mice had different aims: (i) to test if repeated intranasal administrations of liposomes containing native cholesterol resulted in an increased content of cholesterol in the brain; (ii) to evaluate the effectiveness of different liposome based cholesterol formulations. On the basis of their size and number of bilayers, liposomes can also be classified into multilamellar vesicles (MLVs) and unilamellar vesicles (ULVs). In unilamellar liposomes, the vesicle has a single phospholipid bilayer sphere enclosing the aqueous solution, while in multilamellar liposomes, vesicles have an onion structure. ULVs and MLVs have different release kinetics due overall to the number of phospholipid. We compared ULVs (n = 18 wt mice) and MLVs (n = 18 wt mice) containing native hydrophobic cholesterol and cholesteryl hemisuccinate (CHEMS) within their lipid membranes and their aqueous core, respectively. In particular, CHEMS consists of succinic acid esterified to the beta-hydroxyl group of cholesterol. This chemical modification results in the ability of CHEMS to adopt a lamellar assembly in suitable aqueous media.

Following a 14-day acclimation period (Hanson et al. 2013), 6 weeks-old mice were treated three times weekly until 12ws when the animals were sacrificed to collect brain tissues (**Fig. 21**).

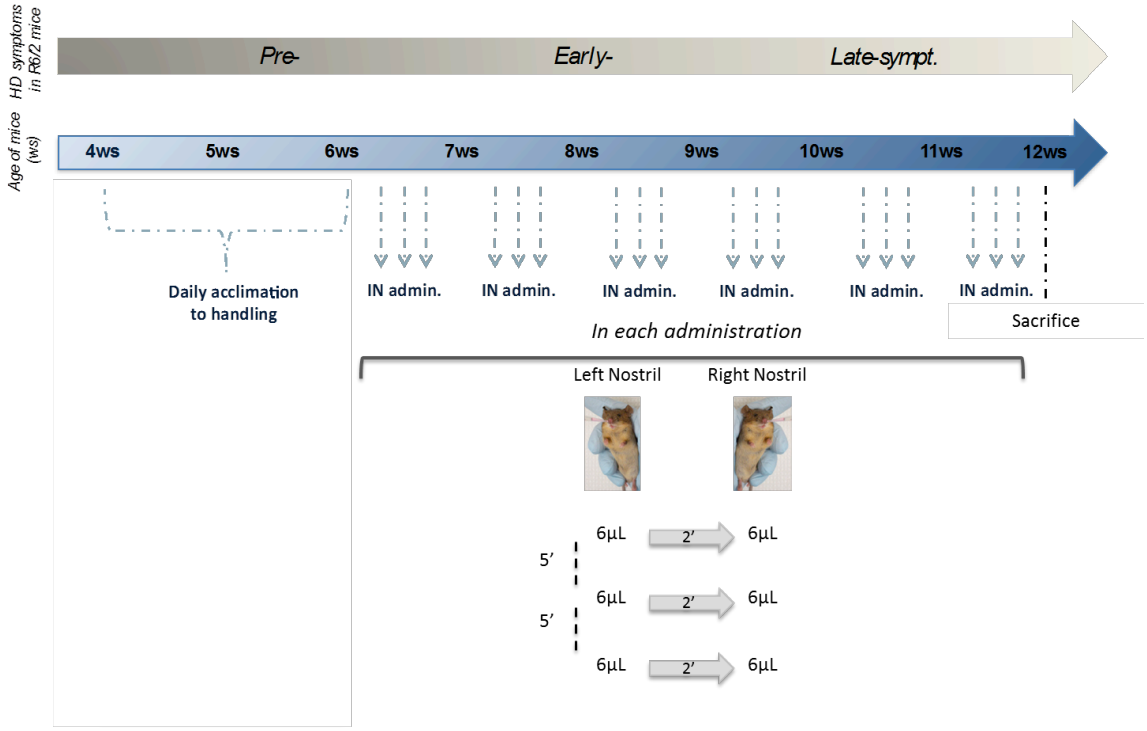

Figure 21. Scheme of the experimental paradigm followed in the first intranasal trial in wt mice.
After two weeks of acclimation to handling, wt mice were intranasally treated three times a week from 6 to 11 weeks of age. Each treatment consisted in three sequential administrations of 6µl of liposomes for a total of 18µl/nostril.

Unfortunately, we didn't find a detectable increase in the total amount of cholesterol, measured by MS, in brain tissues of treated mice respect to controls (**Fig. 22**). Probably the total amount of cholesterol delivered by DRV and MLV liposomes, with this experimental paradigm, was too low to detect an increase in the total content of cholesterol.

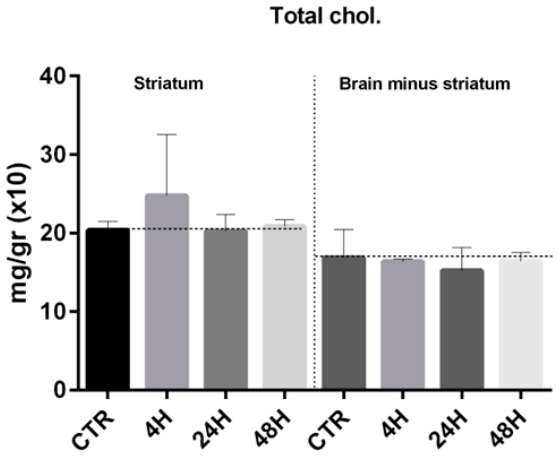

Figure 22. Total cholesterol levels measured in striatum and resting brain areas.
Total cholesterol levels measured by MS in cerebral tissues collected from wt mice sacrificed ad different time points (4h, 24h, 48h) after the last intranasal administration. All data were normalized above weight tissue.

Finally, during my PhD, I had also the opportunity to contribute to two recently published papers:

- *Valenza M., Marullo M., Di Paolo E., Cesana E., Zuccato C., Biella G., Cattaneo E. "Disruption of Astrocyte-Neuron Cholesterol Cross Talk Affects Neuronal Function in Huntington's Disease." Cell Death and Differentiation. 2015.*
- *Shankaran M., Di Paolo E., Leoni V., Caccia C., Ferrari Bardile C., Mohammed H., Di Donato S., Kwak S., Marchionini D., Turner S., Cattaneo E.*, Valenza M.* 2017. "Early and brain region-specific decrease of de novo cholesterol biosynthesis in Huntington's disease: a cross-validation study in zQ175 knock-in mice." Neurobiology of Disease. 2017. *corresponding authors.*

Discussion

Brain cholesterol homeostasis appears severely compromised in HD.

Data from our previously published papers reveal a reduction in cholesterol biosynthesis, cholesterol precursors and cholesterol levels within the brain of different HD rodent models (Valenza et al. 2005) (Valenza et al. 2007) (Valenza et al. 2010). Recently, by measuring the rate of *de novo* brain cholesterol biosynthesis in the Q175 knock-in model we further confirmed this reduction (Shankaran et al. 2017). Furthermore, the decreased plasma levels of the brain-specific cholesterol catabolite 24OHC suggest a similar dysfunction in HD patients (Leoni et al. 2008) (Leoni et al. 2013). However, others studies, performed in some of these HD models, show brain cholesterol accumulation (Thrushina et al. 2006) (Del Toro et al. 2010) (Boussicault et al. 2016). It has already been demonstrated that these opposite results might be attributable to the different methods used for sample preparation and cholesterol measurement. In particular, saline perfusion prior to tissue dissection is essential to avoid any contamination of blood-derived cholesterol (Liu et al. 2010) as well as the use of reliable analytical method such as gas chromatography-mass spectrometry is necessary to properly quantify cholesterol content (Marullo et al. 2012).

Cerebral cholesterol is fundamental for neurite outgrowth, synapses formation and maintenance, synaptic activity and integrity and optimal neurotransmitter release (Pfrieger 2003), so its deficiency may be injurious especially for neuronal cells. Given that peripheral cholesterol does not pass the BBB, we tested different strategies to deliver exogenous cholesterol to the HD brain.

Results from our studies using g7-NPs and Alzet osmotic minipumps highlight the therapeutic potential of brain cholesterol supplementation in contrasting disease-related neurobehavioral impairments in the most widely used transgenic mouse model of HD.

Our findings from g7-NPs study demonstrate for the first time that cholesterol supplementation is able to completely prevent cognitive decline and to partially rescue hypokinetic phenotype in R6/2 mice. The improvement in animal's behavioral phenotype was correlated with increased levels of scaffold synaptic proteins and ameliorations in synaptic transmission abnormalities in striatal MSNs of R6/2 mice, confirming the critical role of cholesterol in synaptic integrity and neuronal function (Pfrieger 2003). We also found that the beneficial effect of exogenous cholesterol is dose-dependent, indeed higher doses of cholesterol are required to observe a significant functional recovery of both cognitive and motor abilities. Even at late-symptomatic stages (11 weeks of age), R6/2 mice intrastriatally infused with 500μg of cholesterol performed similarly to age-matched nontransgenic wt mice in NORT and activity cage tests. In contrast, we did not observe a significant amelioration in rotarod performance. We believe that these contrasting results obtained from

rotarod and activity cage can be ascribed to the different nature of these motor tests. While the first one is based on forced motor activity and measures primarily mice coordination, the second one assesses spontaneous, global, motor activity.

NORT results indicate that low doses of cholesterol are sufficient to promote the formation of long-term memory for the familiar object in R6/2 mice, normally impaired in this HD model starting from 8 weeks of age (Giralt et al. 2011). Other works analyzed this memory aspect in R6/2 mice using the NORT, but not at advanced time points (Bissonnette et al. 2013). In particular, the group of Bissonnette et al. observed a significant increase in short- but not in long-term memory in 8 weeks old-R6/2 mice, in parallel with a partial rescue of spontaneous locomotor activity after striatal overexpression of pre-enkephalin (pENK).

Our preliminary electrophysiological analysis also suggest that behavioral recovery observed in R6/2 mice following intrastriatal cholesterol infusion mediated by osmotic minipumps, may be related to an improvement in synaptic transmission, as previously observed in our g7-NPs studies.

The encouraging results from g7-NPs and minipumps strategies, prompted us to investigate also the intranasal route of administration as an alternative, non–invasive, strategy for cholesterol delivery to the HD brain (in collaboration with M. Salmona, Mario Negri Institute). Because of their biocompatibility, biodegradability and low toxicity features, we used liposomal formulations as cholesterol-delivery vehicles in these experiments. However in our experimental conditions, measurable variations in brain cholesterol levels were not observed after repeated intranasal administrations of both DRV and MLV liposomes containing unlabeled cholesterol. Ongoing investigations are aimed at understanding the percentage of intranasally administered cholesterol that effectively reaches the brain.

Thinking to a possible clinical translation of the therapeutic approach based on brain cholesterol supplementation, other studies are necessary to better characterize and optimize g7-NPs and intranasal non-invasive strategies. g7-PLGA-NPs used in this study already present many interesting advantages. First, PLGA has been approved by FDA and EMA for drug delivery, diagnostics and clinical applications (Mundargi et al. 2008). PLGA NPs are totally biodegradable, since their physiological hydrolysis into the body produce lactic acid and glycolic acid, which are easily metabolized via the Krebs cycle (Yoo et al. 2005). A significant toxicity associated to PLGA has not been described (Athanasiou, Niederauer, and Agrawal 1996) and our studies confirmed this result as our NPs do not induce any inflammatory response in peripheral tissues in which they preferentially accumulate (liver and lung). PLGA NPs are able to sustain the release of the encapsulated therapeutic agent over a period of days to several weeks (Panyam and Labhasetwar

2003), protecting them from the body excretion and metabolism. Furthermore, due to their sub-micron size, NPs delivery systems are taken up efficiently by the cells (Vinogradov, Bronich, and Kabanov 2002).

Despite all these advantages, NPs based strategies present some limitations. Their small size and large surface area can result in particle aggregation and allow limited drug loading. Indeed, g7-NPs formulations used in this study only achieve 1% drug loading. Consequently, with our experimental paradigm we delivered only about 15 μg of cholesterol to the mouse brain, without the possibility to test the effects of higher doses of cholesterol.

In collaboration with G. Tosi (University of Modena) our future efforts will be orientated to optimize this promising, non invasive, CNS delivery system, with the goal of increasing the amount of cholesterol loaded into g7-NPs, without affecting their chemical–physical properties. This will also allow to reduce the number of injections/week in order to minimize handling stress in mice.

Additional experimental investigations are also required to optimize the intranasal strategy. Currently, the main limiting factors associated with nasal drug delivery are the limited capacity of the nasal cavity along with the rapid mucociliary clearance that hinders complete drug absorption (Soane et al. 1999). Furthermore, nasal mucosa contains a number of enzymes responsible for the degradation of intranasally applied drugs (Chung and Donovan 1996).

Common utilized approaches to improve nasal drug absorption include the use of protease and peptidase inhibitors (Bernkop-Schnürch 1998). Moreover, to enhance the retention of liposomes containing cholesterol on nasal mucosal surface, mucoadhesive polymers can be used. Owing to their properties, in situ gelling formulations undergo gelation upon contact with the nasal cavity, as they respond to physiological stimuli like nasal temperature and mucous pH (Chonkar, Nayak, and Udupa 2015). These “smart” polymers not only are able to enhance the retention of the drug in nasal cavity but also provide controlled release, ease of administration, enhanced permeation and protection of the drug from mucosal enzymes. Liposomes in situ gelling system (LIGS) have also been developed and characterized (Tiwari et al. 2009) and could represent a valid formulation for intranasal cholesterol delivery.

Although it is considered an invasive delivery system, osmotic minipumps allowed us to test the therapeutic potential of increasing doses of cholesterol directly administered into mice striatum, overcoming current limitations of g7-NPs strategy. Furthermore, a clinical translation of this brain targeting drug delivery system should not be excluded, considering that the Company Medtronic is developing these devices for human application. Indeed Alnylam Pharmaceuticals and the CHDI Foundation started a collaboration with Medtronic, to develop implantable infusion system for CNS

delivery of RNAi therapeutics targeting huntingtin ("Industry Update, The Latest Developments in Therapeutic Delivery" 2011).

Finally, an additional strategy to counteract the reduction in cholesterol available for synaptic function and neurotransmission consists in promoting its endogenous synthesis and efflux in astrocytes, which emerged to be defective in the HD brain (Valenza et al. 2010) (Valenza et al. 2015). Our *in vitro* data indicate that stimulation of endogenous biosynthesis in astrocytes results in increased availability of newly synthetized cholesterol for neuronal activities (Valenza et al. 2015). Based on this evidence, our ongoing *in vivo* studies aim to directly enhance endogenous cholesterol biosynthesis in striatal astrocytes relies on the overexpression of the active form of SREBP2, through glia-targeted viral vectors, in HD mice. More recently, an alternative indirect approach has been adopted in Boussicault et al. 2016. In this study, the viral-induced overexpression of CYP46A1 in the striatum of R6/2 mice stimulated the production of 24OHC and led to increased levels of lanosterol and desmosterol, indirect indicators of brain cholesterol biosynthesis in neurons and astrocytes respectively (Nieweg et al. 2009). The increase of 24OHC likely activates LXR-dependent cholesterol efflux from astrocytes to neuronal cells (Abildayeva et al. 2006) and indirectly glial cholesterol synthesis (i.e. increase of desmosterol), resulting in a rescue of some HD phenotypes (Boussicault et al. 2016).

Our findings together with data from Boussicault et al. (2016) highlight the beneficial effect of strategies able to stimulate endogenous biosynthesis both directly (Valenza et al. 2015) and indirectly (Boussicault et al. 2016) or, alternatively, aimed at supplying exogenous cholesterol to the HD brain (data herein described). All these studies pave the way for clinical translation and develop new possible therapeutic strategies for HD patients.

General Conclusions and Prospects

All these studies have provided clear evidence that cholesterol administration to the brain represents a promising therapeutic approach for HD.

Our future primary goals will be to better analyze the cognitive rescue promoted by cholesterol supplementation and to deepen our understanding of mechanisms underlying cholesterol-mediated behavioral recovery (Valenza et al. 2015). To reach these goals, additional cognitive tests will be performed on treated mice to investigate different aspects of learning and memory (i.e. fear conditioning test). Furthermore, molecular (RNA sequencing), biochemical, electrophysiological and neuropathological analyses will be completed on the tissues collected from mice implanted with minipumps.

Since our findings revealed that high doses of exogenous cholesterol are required to observe a significant recovery of both cognitive and motor functions in R6/2 mice, we will work to increase cholesterol encapsulation efficacy of g7-NPs and, on the other hand, we will attempt to identify more efficacious formulations for cholesterol intranasal delivery.

Moreover, pharmacokinetic and biodistribution studies will be performed, using D6-cholesterol, in order to quantify the amount and cellular localization of exogenous cholesterol delivered in the different brain regions with our non-invasive delivery systems.

Finally the potential validity of brain cholesterol supplementation–based therapeutic approach will be evaluated in another HD animal model, chosen among them that closely mimic the genetic context of patients with HD.

Material and Methods

Colony management

All the *in vivo* experiments were carried out in accordance with Italian Governing Law (D.lgs 26/2014; Authorisation n.324/2015-PR issued May 6, 2015 by Ministry of Health); the NIH Guide for the Care and Use of Laboratory Animals (2011 edition) and EU directives and guidelines (EEC Council Directive 2010/63/UE).

Our R6/2 colony lifespan was approximately of 13 weeks and it was maintained through the male line exclusively (Mangiarini et al. 1996). Transgenic R6/2 male were paired with non-carrier females (B6CBAF1/J, supplied by Charles River). Mice were weaned and then genotyped at 3 weeks of age (+/- 3 days). R6/2 colony was continually monitored for any changes that could affect strain productivity, general behavior, litter size, pup survival, genotype frequency, phenotype and other strain characteristics.

Mice were housed under standard conditions (22 ± 1°C, 60% relative humidity, 12 hour light/dark schedule, 3–4 mice/cage, with free access to food and water).

After PCR genotyping, by method of Mangiarini et al. (1996), animals were randomly divided into experimental groups. Male and female mice will be included and matched in experimental groups.

Animal treatments

- NPs injections: mice were treated with two intraperitoneal injections at week, from 5 to 9 weeks of age, receiving 0.15 mg g7-NPs/g body weight in each injection (NPs stock concentration was 12.5 mg/ml; 0.7 mg in 100 mg of NPs).
- Surgical implantation of osmotic minipumps: mice were anesthetized with Avertin 2.5%. Avertin 100% was prepared diluting 5 g of 2,2,2-Tribromoethanol (Sigma Aldrich, #T48402-25G) in 5 mL of 2-methyl-2-butanol (Sigma Aldrich, #240486). 16 µL of Avertin 2.5% per gram of weight was used to anesthetize mice. Once responses to tail/toe pinches and intactness of the ocular reflex were assessed, scalp was shaved and mice were placed into a stereotaxic apparatus (2-Biological Instrument). After disinfecting the scalp with iodine tincture, a midline sagittal incision about 2.5 cm long was made, starting slightly behind the eyes. A subcutaneous pocket was made on the back of the animals, in the midscapular area, to insert the osmotic pump. The brain infusion microcannula, connected to the pump through a catheter, cannula (brain infusion kit n°3, Alzet, #0008851) was stereotaxically implanted into mice right striatum (stereotaxic coordinates 1.75 mm mediolateral, 0.5 mm anteroposterior, 3 mm dorsoventral; from Paxinos G and Watson C. The Rat Brain in Stereotaxic Coordinates. Academic Press, San Diego). Loctite 454 instant adhesive gel (Alzet, #0008670) was spread on the base of the cannula in order to fix it to the skull. Once the skull surface was dried, the cannula and the entre implantation site were

covered with dental cement (Heraeus, #647079) and the scalp was closed with sutures (bLife, #668H). Following surgery mice were removed from the stereotaxic apparatus and placed on a warm cover to awaken from anesthesia. In each trial animals were operated at 7 weeks of age to implant minipumps (Alzet, pump model 1004, #0009922) loaded with artificial cerebrospinal fluid (ACSF), with methyl-β-cyclodextrin (Sigma Aldrich, #M7439-1G) diluted in ACSF, or with water-soluble cholesterol (Sigma Aldrich, #C4951-30MG) supplemented with 5μM free cholesterol diluted in ACSF. ACSF was prepared mixing two solutions (A and B) in a 1:1 ratio. Solution A was prepared by diluting 8,66 g of NaCl (Sigma Aldrich, #53014), 0,224 g of KCl (Sigma Aldrich, #P9333), 0,206 g of CaCl2 2H2O (Sigma Aldrich, #C3881) and 0,163 g of MgCl2 6H2O (Sigma Aldrich, #M9272) in 500 mL of sigma water. Solution B was prepared by diluting 0,214 g of Na2HPO4 7H2O (Sigma Aldrich, #59390) and 0,027 g of NaH2PO4 H2O (Sigma Aldrich, #59638) in 500 mL of sigma water.

- Intranasal administrations: animals were treated as described in Hanson et al. 2013.

Methods relative to g7-NPs studies and behavioral analysis

Please for detailed description of this part see material and methods in the paper in attached (Valenza et al. 2015).

Electrophysiological analysis relative to osmotic minipumps studies

Experiments were performed on submerged brain slices obtained from R6/2 adult mice (12 weeks of postnatal life) treated with ACSF or cholesterol (500μg) in the 4 weeks preceding the experiment. Animals were dissected using the standard procedure preceded by the intracardiac perfusion of a saline solution containing (mM): Sucrose 70; NaCl 80; KCl 2.5; NaHCO3 26; Glucose 15; MgCl2 7; CaCl2 1; NaH2PO4 1.25. The intracardiac perfusion was necessary to preserve the vitality of brain tissue in adult mice. Coronal slices (300 μm- thickness) containing the striatum were collected from the hemisphere ipsilateral to the insertion site and were kept for 1 h in a saline solution containing (mM): NaCl 125; KCl 2.5; NaHCO3 26; Glucose 15; MgCl2 1.3; CaCl2 2.3; NaH2PO4 1.25. After the recovery, slices were transferred to a submerged-style recording chamber at room temperature (23-25°C) for the electrophysiological analysis.

Experiments were performed on striatal projection medium spiny neurons (MSNs). The cell selected for recording was approached with a glass patch pipette filled with a solution iso-osmotic with cytosol and containing (mM): Cs-methanesulphonate 120; KCl 5; CaCl2 1; MgCl2 2; EGTA 10; Na2ATP 4; Na3GTP 0.3; lidocaine N-ethylbromide 5; Hepes 8 (pH adjusted to 7.3 with KOH). During the approach, the tip of the pipette was brought in close proximity to the neuron in order to

create a very high resistance seal (1 GΩ or more - 'giga seal'): this configuration is called 'cell-attached'. After the application of brief strong suctions inside the pipette, the small patch under the tip was broken: in this used configuration (called 'whole-cell') the interior of the pipette becomes continuous with the cytoplasm of the cell, allowing the measurement of electrical potentials and currents flowing through the entire cell membrane.

Statistics

Prism 5 (GraphPad software) was used to perform all statistical analyses. Data are presented as means ± standard error of the mean (SEM). Grubbs' test was applied to identify outliers. Each set of data was normally distributed consequently we used parametric statistical tests. Differences were considered statistically if the p-value was less than 0.05. The specific statistical test used is indicated in the legend of all results figures. No statistical methods were used to pre-determine sample sizes, but our sample sizes are similar to those reported in the literature.

References

Abbott, N.J., 2004. Evidence for bulk flow of brain interstitial fluid: Significance for physiology and pathology. *Neurochemistry International*, 45(4), pp.545–552.

Abildayeva, K., P. J. Jansen, V. Hirsch-Reinshagen, V. W. Bloks, A. H. F. Bakker, F. C. S. Ramaekers, and others, '24(S)-Hydroxycholesterol Participates in a Liver X Receptor-Controlled Pathway in Astrocytes That Regulates Apolipoprotein E-Mediated Cholesterol Efflux', Journal of Biological Chemistry, 281 (2006), 12799–808 <https://doi.org/10.1074/jbc.M601019200>

Albin, R.L. et al., 1990. Abnormalities of Striatal Projection Neurons and N-Methyl-D-Aspartate Receptors in Presymptomatic Huntington's Disease. *New England Journal of Medicine*, 322(18), pp.1293–1298. Available at: http://dx.doi.org/10.1056/NEJM199005033221807\nhttp://www.nejm.org/doi/full/10.1056/NEJM199005033221807\nhttp://www.nejm.org/doi/pdf/10.1056/NEJM199005033221807.

Alexis, F. et al., 2008. Factors affecting the clearance and biodistribution of polymeric nanoparticles. In *Molecular Pharmaceutics*. pp. 505–515.

Ali, N.J. & Levine, M.S., 2006. Changes in Expression of N-Methyl-<i>D</i>-Aspartate Receptor Subunits Occur Early in the R6/2 Mouse Model of Huntington's Disease. *Developmental Neuroscience*, 28(3), pp.230–238. Available at: http://www.ncbi.nlm.nih.gov/pubmed/16679770 [Accessed December 28, 2016].

Allen, J. a, Halverson-Tamboli, R. a & Rasenick, M.M., 2007. Lipid raft microdomains and neurotransmitter signalling. *Nature reviews. Neuroscience*, 8(2), pp.128–140.

Alpy, F., 2005. Give lipids a START: the StAR-related lipid transfer (START) domain in mammals. *Journal of Cell Science*, 118(13), pp.2791–2801. Available at: http://jcs.biologists.org/cgi/doi/10.1242/jcs.02485 [Accessed November 7, 2016].

Altar, C. a et al., 1997. Anterograde transport of brain-derived neurotrophic factor and its role in the brain. *Nature*, 389(6653), pp.856–860.

Andrich, J. et al., 2002. Autonomic nervous system function in Huntington's disease. *Journal of neurology, neurosurgery, and psychiatry*, 72(6), pp.726–31. Available at: http://www.ncbi.nlm.nih.gov/pubmed/12023413 [Accessed October 23, 2016].

Anon, 2011. Industry Update The latest developments in therapeutic delivery. *Therapeutic Delivery*, 2(1), pp.9–14.

Antunes, M. & Biala, G., 2012. The novel object recognition memory: neurobiology, test procedure, and its modifications. *Cognitive Processing*, 13(2), pp.93–110. Available at: http://link.springer.com/10.1007/s10339-011-0430-z [Accessed November 21, 2016].

Aqul, A. et al., 2011. Unesterified Cholesterol Accumulation in Late Endosomes/Lysosomes

Causes Neurodegeneration and Is Prevented by Driving Cholesterol Export from This Compartment. *Journal of Neuroscience*, 31(25), pp.9404–9413. Available at: http://www.jneurosci.org/cgi/doi/10.1523/JNEUROSCI.1317-11.2011 [Accessed November 14, 2016].

Arnulf, I. et al., 2008. Rapid Eye Movement Sleep Disturbances in Huntington Disease. *Archives of Neurology*, 65(4), p.482. Available at: http://archneur.jamanetwork.com/article.aspx?doi=10.1001/archneur.65.4.482 [Accessed November 2, 2016].

Aronin, N. et al., 1995. CAG expansion affects the expression of mutant Huntingtin in the Huntington's disease brain. *Neuron*, 15(5), pp.1193–201. Available at: http://www.ncbi.nlm.nih.gov/pubmed/7576661 [Accessed November 2, 2016].

Arzberger, T. et al., 1997. Changes of NMDA receptor subunit (NR1, NR2B) and glutamate transporter (GLT1) mRNA expression in Huntington's disease--an in situ hybridization study. *Journal of Neuropathology and Experimental Neurology*, 56(4), pp.440–454. Available at: http://www.ncbi.nlm.nih.gov/entrez/query.fcgi?cmd=Retrieve&db=PubMed&dopt=Citation&list_uids=9100675.

Athanasiou, K.A., Niederauer, G.G. & Agrawal, C.M., 1996. Sterilization, toxicity, biocompatibility and clinical applications of polylactic acid/ polyglycolic acid copolymers. *Biomaterials*, 17(2), pp.93–102.

Auerbach, W. et al., 2001. The HD mutation causes progressive lethal neurological disease in mice expressing reduced levels of huntingtin. *Human molecular genetics*, 10(22), pp.2515–2523.

Augood, S.J., Faull, R.L. & Emson, P.C., 1997. Dopamine D1 and D2 receptor gene expression in the striatum in Huntington's disease. *Annals of neurology*, 42(2), pp.215–21. Available at: http://www.ncbi.nlm.nih.gov/pubmed/9266732.

Aylward, E.H. et al., 2011. Longitudinal change in regional brain volumes in prodromal Huntington disease. *Journal of neurology, neurosurgery, and psychiatry*, 82(4), pp.405–10. Available at: http://www.ncbi.nlm.nih.gov/pubmed/20884680 [Accessed October 23, 2016].

Aziz, N.A. et al., 2010. Autonomic symptoms in patients and pre-manifest mutation carriers of Huntington's disease. *European journal of neurology*, 17(8), pp.1068–74. Available at: http://www.ncbi.nlm.nih.gov/pubmed/20192977 [Accessed October 23, 2016].

Aziz, N.A. et al., 2007. Hypothalamic dysfunction and neuroendocrine and metabolic alterations in Huntington's disease: clinical consequences and therapeutic implications. *Reviews in the neurosciences*, 18(3–4), pp.223–51. Available at: http://www.ncbi.nlm.nih.gov/pubmed/18019608 [Accessed October 23, 2016].

Aziz, N.A. et al., 2010. Sleep and circadian rhythm alterations correlate with depression and cognitive impairment in Huntington's disease. *Parkinsonism & Related Disorders*, 16(5), pp.345–350. Available at: http://linkinghub.elsevier.com/retrieve/pii/S1353802010000477 [Accessed November 2, 2016].

Aziz, N.A. et al., 2008. Weight loss in Huntington disease increases with higher CAG repeat number. *Neurology*, 71(19), pp.1506–1513. Available at: http://www.neurology.org/cgi/doi/10.1212/01.wnl.0000334276.09729.0e [Accessed November 2, 2016].

Bäckman, L. et al., 1997. Cognitive deficits in Huntington's disease are predicted by dopaminergic PET markers and brain volumes. *Brain : a journal of neurology*, pp.2207–17. Available at: http://www.ncbi.nlm.nih.gov/pubmed/9448576 [Accessed November 2, 2016].

Baker, H. & Spencer, R.F., 1986. Transneuronal transport of peroxidase-conjugated wheat germ agglutinin (WGA-HRP) from the olfactory epithelium to the brain of the adult rat. *Experimental brain research*, 63(3), pp.461–73. Available at: http://www.ncbi.nlm.nih.gov/pubmed/3758265.

Bala, I., Hariharan, S. & Kumar, M.N., 2004. PLGA nanoparticles in drug delivery: the state of the art. *Crit Rev Ther Drug Carrier Syst*, 21(5), pp.387–422. Available at: http://ukpmc.ac.uk/abstract/MED/15719481.

Balin, B.J. et al., 1986. Avenues for entry of peripherally administered protein to the central nervous system in mouse, rat, and squirrel monkey. *The Journal of comparative neurology*, 251(2), pp.260–80. Available at: http://www.ncbi.nlm.nih.gov/pubmed/3782501 [Accessed November 30, 2016].

Baudry, M. et al., 2003. Postnatal development of inflammation in a murine model of Niemann-Pick type C disease: Immunohistochemical observations of microglia and astroglia. *Experimental Neurology*, 184(2), pp.887–903.

Behrens, P.F. et al., 2002. Impaired glutamate transport and glutamate-glutamine cycling: downstream effects of the Huntington mutation. *Brain : a journal of neurology*, 125(Pt 8), pp.1908–22. Available at: http://www.ncbi.nlm.nih.gov/pubmed/12135980 [Accessed November 21, 2016].

Benarroch, E.E., 1993. The central autonomic network: functional organization, dysfunction, and perspective. *Mayo Clinic proceedings*, 68(10), pp.988–1001. Available at: http://www.ncbi.nlm.nih.gov/pubmed/8412366 [Accessed October 23, 2016].

Benn, C.L. et al., 2008. Huntingtin Modulates Transcription, Occupies Gene Promoters In Vivo, and Binds Directly to DNA in a Polyglutamine-Dependent Manner. *Journal of Neuroscience*,

28(42).

Bennett, E.J. et al., 2007. Global changes to the ubiquitin system in Huntington's disease (suplementary info). *Nature*, 448(7154), pp.704–8. Available at: http://www.ncbi.nlm.nih.gov/pubmed/17687326.

Benraiss, A. et al., 2016. Human glia can both induce and rescue aspects of disease phenotype in Huntington disease. *Nature Communications*, 7, p.11758. Available at: http://www.ncbi.nlm.nih.gov/pubmed/27273432 [Accessed December 27, 2016].

Bernkop-Schnürch, A., 1998. The use of inhibitory agents to overcome the enzymatic barrier to perorally administered therapeutic peptides and proteins. *Journal of Controlled Release*, 52(1–2), pp.1–16.

Bien-Ly, N. et al., 2012. Reducing human apolipoprotein E levels attenuates age-dependent Abeta accumulation in mutant human amyloid precursor protein transgenic mice. *J Neurosci*, 32(14), pp.4803–4811. Available at: http://www.ncbi.nlm.nih.gov/pubmed/22492035\nhttp://www.jneurosci.org/content/32/14/4803.full.pdf.

Bjorkhem, I., 2004. Brain Cholesterol: Long Secret Life Behind a Barrier. *Arteriosclerosis, Thrombosis, and Vascular Biology*, 24(5), pp.806–815. Available at: http://atvb.ahajournals.org/cgi/doi/10.1161/01.ATV.0000120374.59826.1b [Accessed November 5, 2016].

Björkhem, I. et al., 1998. Cholesterol homeostasis in human brain: turnover of 24S-hydroxycholesterol and evidence for a cerebral origin of most of this oxysterol in the circulation. *Journal of lipid research*, 39(8), pp.1594–1600.

Björkhem I, Lütjohann D, Breuer O, Sakinis A, W.A., 1997. Importance of a Novel Oxidative Mechanism for Elimination of. *Journal of Biological Chemistry*, 272(48), pp.30178–30184.

Bliss, T. V & Collingridge, G.L., 1993. A synaptic model of memory: long-term potentiation in the hippocampus. *Nature*, 361(6407), pp.31–39.

Bodovitz, S. & Klein, W.L., 1996. Cholesterol modulates alpha-secretase cleavage of amyloid precursor protein. *The Journal of biological chemistry*, 271(8), pp.4436–40. Available at: http://www.ncbi.nlm.nih.gov/pubmed/8626795 [Accessed November 14, 2016].

Bogdanov, M.B. et al., 2001. Increased oxidative damage to DNA in a transgenic mouse model of Huntington's disease. *Journal of neurochemistry*, 79(6), pp.1246–9. Available at: http://www.ncbi.nlm.nih.gov/pubmed/11752065 [Accessed November 21, 2016].

Boussicault, Lydie, Sandro Alves, Antonin Lamazière, Anabelle Planques, Nicolas Heck, Lara Moumné, and others, 'CYP46A1, the Rate-Limiting Enzyme for Cholesterol Degradation, Is

Neuroprotective in Huntington's Disease.', Brain : A Journal of Neurology, 139 (2016), 953–70 <https://doi.org/10.1093/brain/awv384>

Boyles, J.K., Notterpek, L.M. & Anderson, L.J., 1990. Accumulation of apolipoproteins in the regenerating and remyelinating mammalian peripheral nerve. Identification of apolipoprotein D, apolipoprotein A-IV, apolipoprotein E, and apolipoprotein A-I. *The Journal of biological chemistry*, 265(29), pp.17805–15. Available at: http://www.ncbi.nlm.nih.gov/pubmed/2120218 [Accessed November 6, 2016].

Bozzuto, G. & Molinari, A., 2015. Liposomes as nanomedical devices. *International journal of nanomedicine*, 10, pp.975–99. Available at: http://www.ncbi.nlm.nih.gov/pubmed/25678787 [Accessed December 5, 2016].

Bradford, J. et al., 2009. Expression of mutant huntingtin in mouse brain astrocytes causes age-dependent neurological symptoms. *Proceedings of the National Academy of Sciences of the United States of America*, 106(52), pp.22480–5. Available at: http://www.ncbi.nlm.nih.gov/pubmed/20018729 [Accessed December 26, 2016].

Browne, S.E., 2008. Mitochondria and Huntington's disease pathogenesis: Insight from genetic and chemical models. In *Annals of the New York Academy of Sciences*. pp. 358–382.

Burger, K., Gimpl, G. & Fahrenholz, F., 2000. Regulation of receptor function by cholesterol. *Cellular and molecular life sciences : CMLS*, 57, pp.1577–1592.

Bylsma, F.W., Brandt, J. & Strauss, M.E., 1990. Aspects of procedural memory are differentially impaired in huntington's disease. *Archives of Clinical Neuropsychology*, 5(3), pp.287–297.

Carmichael, S.T., Clugnet, M.C. & Price, J.L., 1994. Central olfactory connections in the macaque monkey. *Journal of Comparative Neurology*, 346(3), pp.403–434.

Carstea, E.D. et al., 1997. Niemann-Pick C1 disease gene: homology to mediators of cholesterol homeostasis. *Science (New York, N.Y.)*, 277(5323), pp.228–31. Available at: http://www.ncbi.nlm.nih.gov/pubmed/9211849.

Carter, R.J. et al., 1999. Characterization of progressive motor deficits in mice transgenic for the human Huntington's disease mutation. *The Journal of neuroscience : the official journal of the Society for Neuroscience*, 19(8), pp.3248–57. Available at: http://www.ncbi.nlm.nih.gov/pubmed/10191337 [Accessed November 19, 2016].

Caviston, J.P. et al., 2007. Huntingtin facilitates dynein/dynactin-mediated vesicle transport. *Proceedings of the National Academy of Sciences of the United States of America*, 104(24), pp.10045–50. Available at: http://www.ncbi.nlm.nih.gov/pubmed/17548833 [Accessed December 19, 2016].

Cepeda, C. et al., 2004. Increased GABAergic function in mouse models of Huntington's disease:

Reversal by BDNF. *Journal of Neuroscience Research*, 78(6), pp.855–867. Available at: http://www.ncbi.nlm.nih.gov/pubmed/15505789 [Accessed December 3, 2016].

Cepeda, C. et al., 2003. Transient and progressive electrophysiological alterations in the corticostriatal pathway in a mouse model of Huntington's disease. *The Journal of neuroscience : the official journal of the Society for Neuroscience*, 23(3), pp.961–9. Available at: http://www.ncbi.nlm.nih.gov/pubmed/12574425 [Accessed November 21, 2016].

Cha, J.H. et al., 1998. Altered brain neurotransmitter receptors in transgenic mice expressing a portion of an abnormal human huntington disease gene. *Proceedings of the National Academy of Sciences of the United States of America*, 95(11), pp.6480–5. Available at: http://www.ncbi.nlm.nih.gov/pubmed/9600992 [Accessed November 21, 2016].

Cha, J.H. et al., 1999a. Altered neurotransmitter receptor expression in transgenic mouse models of Huntington's disease. *Philosophical transactions of the Royal Society of London. Series B, Biological sciences*, 354(1386), pp.981–9. Available at: http://www.pubmedcentral.nih.gov/articlerender.fcgi?artid=1692608&tool=pmcentrez&rendertype=abstract.

Cha, J.H. et al., 1999b. Altered neurotransmitter receptor expression in transgenic mouse models of Huntington's disease. *Philosophical transactions of the Royal Society of London. Series B, Biological sciences*, 354(1386), pp.981–9. Available at: http://www.ncbi.nlm.nih.gov/pubmed/10434296 [Accessed November 21, 2016].

Cha, J.H.J., 2007. Transcriptional signatures in Huntington's disease. *Progress in Neurobiology*, 83(4), pp.228–248.

Chamberlain, L.H. & Gould, G.W., 2002. The vesicle- and target-SNARE proteins that mediate Glut4 vesicle fusion are localized in detergent-insoluble lipid rafts present on distinct intracellular membranes. *Journal of Biological Chemistry*, 277(51), pp.49750–49754.

Chan, E.Y.W. et al., 2002. Increased huntingtin protein length reduces the number of polyglutamine-induced gene expression changes in mouse models of Huntington's disease. *Human molecular genetics*, 11(17), pp.1939–51. Available at: http://www.ncbi.nlm.nih.gov/pubmed/12165556 [Accessed December 28, 2016].

Chang, T.Y., Chang, C.C.Y. & Cheng, D., 1997. ACYL-COENZYME A : CHOLESTEROL.

Chapman, C.D. et al., 2013. Intranasal treatment of central nervous system dysfunction in humans. *Pharmaceutical research*, 30(10), pp.2475–84. Available at: http://www.ncbi.nlm.nih.gov/pubmed/23135822 [Accessed November 30, 2016].

Chen, C.-M. et al., 2007. Increased oxidative damage and mitochondrial abnormalities in the peripheral blood of Huntington's disease patients. *Biochemical and biophysical research*

communications, 359(2), pp.335–40. Available at: http://www.ncbi.nlm.nih.gov/pubmed/17543886.

Chen, Z. & Rand, R.P., 1997. The influence of cholesterol on phospholipid membrane curvature and bending elasticity. *Biophysical journal*, 73(1), pp.267–276.

Cheng, D. et al., 1995. Activation of acyl-coenzyme A:cholesterol acyltransferase by cholesterol or by oxysterol in a cell-free system. *Journal of Biological Chemistry*, 270(2), pp.685–695.

Chonkar, A., Nayak, U. & Udupa, N., 2015. Smart Polymers in Nasal Drug Delivery. *Indian journal of pharmaceutical sciences*, 77(4), pp.367–375.

Chung, F.Y. & Donovan, M.D., 1996. Nasal pre-systemic metabolism of peptide drugs: Substance P metabolism in the sheep nasal cavity. *International Journal of Pharmaceutics*, 128(1–2), pp.229–237.

Colin, E. et al., 2008. Huntingtin phosphorylation acts as a molecular switch for anterograde/retrograde transport in neurons. *The EMBO journal*, 27(15), pp.2124–34. Available at: http://www.ncbi.nlm.nih.gov/pubmed/18615096 [Accessed December 19, 2016].

Corder, E.H. et al., 1993. Gene dose of apolipoprotein E type 4 allele and the risk of Alzheimer's disease in late onset families. *Science (New York, N.Y.)*, 261(5123), pp.921–3. Available at: http://www.ncbi.nlm.nih.gov/pubmed/8346443 [Accessed November 14, 2016].

Corder, E.H. et al., 1994. Protective effect of apolipoprotein E type 2 allele for late onset Alzheimer disease. *Nature Genetics*, 7(2), pp.180–184. Available at: http://www.nature.com/doifinder/10.1038/ng0694-180 [Accessed November 14, 2016].

Costantino, L. et al., 2005. Peptide-derivatized biodegradable nanoparticles able to cross the blood–brain barrier. *Journal of Controlled Release*, 108(1), pp.84–96. Available at: http://www.ncbi.nlm.nih.gov/pubmed/16154222 [Accessed December 2, 2016].

Coulston, F. & DeSesso, J.M., 1993. The relevance to humans of animal models for inhalation studies of cancer in the nose and upper airways. *Quality assurance (San Diego, Calif.)*, 2(3), pp.211–212.

Courtney, R. & Landreth, G. E. LXR Regulation of Brain Cholesterol: From Development to Disease. Trends Endocrinol. Metab. 27, 404–414 (2016).

Cramer, P.E. et al., 2012. ApoE-Directed Therapeutics Rapidly Clear -Amyloid and Reverse Deficits in AD Mouse Models. *Science*, 335(6075), pp.1503–1506. Available at: http://www.sciencemag.org/cgi/doi/10.1126/science.1217697 [Accessed November 14, 2016].

Cui, L. et al., 2006. Transcriptional repression of PGC-1alpha by mutant huntingtin leads to mitochondrial dysfunction and neurodegeneration. *Cell*, 127(1), pp.59–69. Available at: http://www.ncbi.nlm.nih.gov/pubmed/17018277.

Davies, S.W. et al., 1997. Formation of neuronal intranuclear inclusions underlies the neurological dysfunction in mice transgenic for the HD mutation. *Cell*, 90(3), pp.537–548.

Dean, M., Hamon, Y. & Chimini, G., 2001. The human ATP-binding cassette (ABC) transporter superfamily. *Journal of lipid research*, 42(7), pp.1007–17. Available at: http://www.ncbi.nlm.nih.gov/pubmed/11441126 [Accessed November 6, 2016].

Dhanasekaran, M. et al., 2005. Glycopeptides related to beta-endorphin adopt helical amphipathic conformations in the presence of lipid bilayers. *Journal of the American Chemical Society*, 127(15), pp.5435–5448.

Dhuria, S. V, Hanson, L.R. & Frey, W.H., 2009. Novel vasoconstrictor formulation to enhance intranasal targeting of neuropeptide therapeutics to the central nervous system. *The Journal of pharmacology and experimental therapeutics*, 328(1), pp.312–320.

Dietschy, J.M., 2009. Central nervous system: cholesterol turnover, brain development and neurodegeneration. *Biological Chemistry*, 390(4). Available at: http://www.degruyter.com/view/j/bchm.2009.390.issue-4/bc.2009.035/bc.2009.035.xml [Accessed November 5, 2016].

Dietschy, J.M., 2004. Thematic review series: Brain Lipids. Cholesterol metabolism in the central nervous system during early development and in the mature animal. *The Journal of Lipid Research*, 45(8), pp.1375–1397. Available at: http://www.jlr.org/cgi/doi/10.1194/jlr.R400004-JLR200 [Accessed November 5, 2016].

Dietschy, J.M. & Turley, S.D., 2001. Cholesterol metabolism in the brain. *Current opinion in lipidology*, 12, pp.105–112.

DiFiglia, M. et al., 1997. Aggregation of huntingtin in neuronal intranuclear inclusions and dystrophic neurites in brain. *Science (New York, N.Y.)*, 277(5334), pp.1990–3. Available at: http://www.ncbi.nlm.nih.gov/pubmed/9302293 [Accessed November 2, 2016].

DiFiglia, M., 1990. Excitotoxic injury of the neostriatum: a model for Huntington's disease. *Trends in Neurosciences*, 13(7), pp.286–289.

DiFiglia, M. et al., 1995. Huntingtin is a cytoplasmic protein associated with vesicles in human and rat brain neurons. *Neuron*, 14(5), pp.1075–81. Available at: http://www.ncbi.nlm.nih.gov/pubmed/7748555 [Accessed November 2, 2016].

Dunah, A.W. et al., 2002. Sp1 and TAFII130 transcriptional activity disrupted in early Huntington's disease. *Science (New York, N.Y.)*, 296(5576), pp.2238–2243.

Eberlé, D. et al., 2004. SREBP transcription factors: master regulators of lipid homeostasis. *Biochimie*, 86(11), pp.839–848. Available at: http://linkinghub.elsevier.com/retrieve/pii/S0300908404001658 [Accessed November 7,

2016].

Edwards, P.A., Kennedy, M.A. & Mak, P.A., 2002. LXRs;: Oxysterol-activated nuclear receptors that regulate genes controlling lipid homeostasis. *Vascular Pharmacology*, 38(4), pp.249–256.

Ehehalt, R. et al., 2003. Amyloidogenic processing of the Alzheimer β-amyloid precursor protein depends on lipid rafts. *The Journal of Cell Biology*, 160(1), pp.113–123. Available at: http://www.jcb.org/lookup/doi/10.1083/jcb.200207113 [Accessed November 14, 2016].

Elias, S. et al., 2014. Huntingtin regulates mammary stem cell division and differentiation. *Stem Cell Reports*, 2(4), pp.491–506.

Estrada-Sánchez, A.M. et al., 2009. Glutamate toxicity in the striatum of the R6/2 Huntington's disease transgenic mice is age-dependent and correlates with decreased levels of glutamate transporters. *Neurobiology of Disease*, 34(1), pp.78–86. Available at: http://www.ncbi.nlm.nih.gov/pubmed/19168136 [Accessed December 20, 2016].

Faideau, M. et al., 2010. In vivo expression of polyglutamine-expanded huntingtin by mouse striatal astrocytes impairs glutamate transport: a correlation with Huntington's disease subjects. *Human Molecular Genetics*, 19(15), pp.3053–3067. Available at: http://www.ncbi.nlm.nih.gov/pubmed/20494921 [Accessed December 22, 2016].

Fan, M.M.Y. et al., 2007. Altered NMDA receptor trafficking in a yeast artificial chromosome transgenic mouse model of Huntington's disease. *The Journal of neuroscience : the official journal of the Society for Neuroscience*, 27(14), pp.3768–3779.

Fan, M.M.Y. & Raymond, L.A., 2007. N-Methyl-d-aspartate (NMDA) receptor function and excitotoxicity in Huntington's disease. *Progress in Neurobiology*, 81(5–6), pp.272–293.

Ferrante, R.J. et al., 1997. Heterogeneous topographic and cellular distribution of huntingtin expression in the normal human neostriatum. *The Journal of neuroscience : the official journal of the Society for Neuroscience*, 17(9), pp.3052–3063.

Field, P.M., Li, Y. & Raisman, G., 2003. Ensheathment of the olfactory nerves in the adult rat. *Journal of Neurocytology*, 32(3), pp.317–324.

Frank, C. et al., 2008. Cholesterol depletion inhibits synaptic transmission and synaptic plasticity in rat hippocampus. *Experimental Neurology*, 212(2), pp.407–414.

Frank, C. et al., 2004. Cholesterol perturbing agents inhibit NMDA-dependent calcium influx in rat hippocampal primary culture. *FEBS Letters*, 566(1–3), pp.25–29.

Friedman, J.H. et al., 2005. Monozygotic Twins Discordant for Huntington Disease After 7 Years. *Archives of Neurology*, 62(6). Available at: http://archneur.jamanetwork.com/article.aspx?doi=10.1001/archneur.62.6.995 [Accessed November 2, 2016].

Fukumoto, H. et al., 2002. Induction of the cholesterol transporter ABCA1 in central nervous system cells by liver X receptor agonists increases secreted A?? levels. *Journal of Biological Chemistry*, 277(50), pp.48508–48513.

Fusco, F.R. et al., 1999. Cellular localization of huntingtin in striatal and cortical neurons in rats: lack of correlation with neuronal vulnerability in Huntington's disease. *The Journal of neuroscience : the official journal of the Society for Neuroscience*, 19(4), pp.1189–202. Available at: http://www.ncbi.nlm.nih.gov/pubmed/9952397 [Accessed December 19, 2016].

Futter, M. et al., 2009a. Wild-type but not mutant huntingtin modulates the transcriptional activity of liver X receptors. *Journal of Medical Genetics*, 46(7), pp.438–446. Available at: http://jmg.bmj.com/cgi/doi/10.1136/jmg.2009.066399 [Accessed November 13, 2016].

Futter, M. et al., 2009b. Wild-type but not mutant huntingtin modulates the transcriptional activity of liver X receptors. *Journal of medical genetics*, 46(7), pp.438–46. Available at: http://jmg.bmj.com/content/46/7/438.abstract.

Garriga-Canut, M. et al., 2012. Synthetic zinc finger repressors reduce mutant huntingtin expression in the brain of R6/2 mice. *Proceedings of the National Academy of Sciences*, 109(45), pp.E3136–E3145. Available at: http://www.ncbi.nlm.nih.gov/pubmed/23054839 [Accessed December 29, 2016].

Gauthier, L.R. et al., 2004. Huntingtin Controls Neurotrophic Support and Survival of Neurons by Enhancing BDNF Vesicular Transport along Microtubules. *Cell*, 118(1), pp.127–138. Available at: http://www.ncbi.nlm.nih.gov/pubmed/15242649 [Accessed December 19, 2016].

German, D.C. et al., 2002. Neurodegeneration in the Niemann-Pick C mouse: Glial involvement. *Neuroscience*, 109(3), pp.437–450.

Gil, C. et al., 2006. Synaptic proteins associate with a sub-set of lipid rafts when isolated from nerve endings at physiological temperature. *Biochemical and Biophysical Research Communications*, 348(4), pp.1334–1342.

Gimpl, G. & Gehrig-Burger, K., 2007. Cholesterol reporter molecules. *Bioscience Reports*, 27(6), pp.335–358.

Giralt, A. et al., 2011. Increased PKA signaling disrupts recognition memory and spatial memory: role in Huntington's disease. *Human Molecular Genetics*, 20(21), pp.4232–4247. Available at: http://www.hmg.oxfordjournals.org/cgi/doi/10.1093/hmg/ddr351 [Accessed November 20, 2016].

Goldberg, T.E. et al., 1990. Regional cerebral blood flow and cognitive function in Huntington's disease and schizophrenia. A comparison of patients matched for performance on a prefrontal-type task. *Arch Neurol*, 47, pp.418–422.

Gómez-Esteban, J.C. et al., 2006. Monozygotic Twins Suffering from Huntington's Disease Show Different Cognitive and Behavioural Symptoms. *European Neurology*, 57(1), pp.26–30. Available at: http://www.karger.com/?doi=10.1159/000097006 [Accessed November 2, 2016].

Goodman, A.O.G. & Barker, R.A., 2010. How vital is sleep in Huntington's disease? *Journal of Neurology*, 257(6), pp.882–897. Available at: http://link.springer.com/10.1007/s00415-010-5517-4 [Accessed November 2, 2016].

Graziadei, P.P., 1970. The mucous membranes of the nose. *The Annals of otology, rhinology, and laryngology*, 79(3), pp.433–42. Available at: http://www.ncbi.nlm.nih.gov/pubmed/5426874 [Accessed December 2, 2016].

Grevers, G. & Herrmann, U., 1987. Fenestrated endothelia in vessels of the nasal mucosa. *Archives of Oto-Rhino-Laryngology*, 244(1), pp.55–60. Available at: http://link.springer.com/10.1007/BF00453492 [Accessed December 2, 2016].

Groothuis, D.R. et al., 2007. Efflux of drugs and solutes from brain: the interactive roles of diffusional transcapillary transport, bulk flow and capillary transporters. *Journal of cerebral blood flow and metabolism : official journal of the International Society of Cerebral Blood Flow and Metabolism*, 27(1), pp.43–56.

Gu, M. et al., 1996. Mitochondrial defect in Huntington's disease caudate nucleus. *Annals of Neurology*, 39(3), pp.385–389.

Gusella, J.F. et al., 1983. A polymorphic DNA marker genetically linked to Huntington's disease. *Nature*, 306(5940), pp.234–238.

Gutekunst, C.A. et al., 1999. Nuclear and neuropil aggregates in Huntington's disease: relationship to neuropathology. *The Journal of neuroscience : the official journal of the Society for Neuroscience*, 19(7), pp.2522–34. Available at: http://www.ncbi.nlm.nih.gov/pubmed/10087066 [Accessed November 2, 2016].

Hackam, A.S. et al., 2000. Huntingtin interacting protein 1 induces apoptosis via a novel caspase-dependent death effector domain. *Journal of Biological Chemistry*, 275(52), pp.41299–41308.

Hadaczek, P. et al., 2006. The "Perivascular Pump" Driven by Arterial Pulsation Is a Powerful Mechanism for the Distribution of Therapeutic Molecules within the Brain. *Molecular Therapy*, 14(1), pp.69–78.

Hadley, K., Orlandi, R.R. & Fong, K.J., 2004. Basic anatomy and physiology of olfaction and taste. *Otolaryngologic Clinics of North America*, 37(6 SPEC.ISS.), pp.1115–1126.

Hahn-Barma, V. et al., 1998. Are cognitive changes the first symptoms of Huntington's disease? A study of gene carriers. *Journal of neurology, neurosurgery, and psychiatry*, 64(2), pp.172–7. Available at: http://www.ncbi.nlm.nih.gov/pubmed/9489526 [Accessed November 2, 2016].

Hanson, L.R. et al., 2013. Intranasal Administration of CNS Therapeutics to Awake Mice. *Journal of Visualized Experiments*, (74), pp.e4440–e4440. Available at: http://www.jove.com/video/4440/intranasal-administration-of-cns-therapeutics-to-awake-mice [Accessed December 5, 2016].

Hansson, O. et al., 2001. Resistance to NMDA toxicity correlates with appearance of nuclear inclusions, behavioural deficits and changes in calcium homeostasis in mice transgenic for exon 1 of the huntington gene. *The European journal of neuroscience*, 14(9), pp.1492–504. Available at: http://www.ncbi.nlm.nih.gov/pubmed/11722611 [Accessed November 21, 2016].

Harjes, P. & Wanker, E.E., 2003. The hunt for huntingtin function: interaction partners tell many different stories. *Trends in Biochemical Sciences*, 28(8), pp.425–433. Available at: http://www.ncbi.nlm.nih.gov/pubmed/12932731 [Accessed December 28, 2016].

Hassel, B. et al., 2008. Glutamate uptake is reduced in prefrontal cortex in Huntington's disease. *Neurochemical Research*, 33(2), pp.232–237.

Hayashi, H., 2011. Lipid metabolism and glial lipoproteins in the central nervous system. *Biological & pharmaceutical bulletin*, 34(4), pp.453–61. Available at: http://www.ncbi.nlm.nih.gov/pubmed/21467629 [Accessed November 6, 2016].

Hebb, M.O., Denovan-Wright, E.M. & Robertson, H.A., 1999. Expression of the Huntington's disease gene is regulated in astrocytes in the arcuate nucleus of the hypothalamus of postpartum rats. *FASEB journal : official publication of the Federation of American Societies for Experimental Biology*, 13(9), pp.1099–106. Available at: http://www.ncbi.nlm.nih.gov/pubmed/10336893 [Accessed December 26, 2016].

Hedreen, J.C. et al., 1991. Neuronal loss in layers V and VI of cerebral cortex in Huntington's disease. *Neuroscience letters*, 133(2), pp.257–61. Available at: http://www.ncbi.nlm.nih.gov/pubmed/1840078 [Accessed November 2, 2016].

Heindel, W.C., Butters, N. & Salmon, D.P., 1988. Impaired learning of a motor skill in patients with Huntington's disease. *Behav Neurosci*, 102(1), pp.141–147. Available at: http://www.ncbi.nlm.nih.gov/entrez/query.fcgi?cmd=Retrieve&db=PubMed&dopt=Citation&list_uids=2965592.

Hering, H., Lin, C. & Sheng, M., 2003. Lipid rafts in the maintenance of synapses, dendritic spines, and surface AMPA receptor stability. *The Journal of neuroscience : the official journal of the Society for Neuroscience*, 23(8), pp.3262–3271.

Herndon, E.S. et al., 2009. Neuroanatomic profile of polyglutamine immunoreactivity in Huntington disease brains. *Journal of neuropathology and experimental neurology*, 68(3), pp.250–61. Available at: http://www.ncbi.nlm.nih.gov/pubmed/19225411 [Accessed

November 2, 2016].

Hickey, M.A., Reynolds, G.P. & Morton, A.J., 2002. The role of dopamine in motor symptoms in the R6/2 transgenic mouse model of Huntington's disease. *Journal of neurochemistry*, 81(1), pp.46–59. Available at: http://www.ncbi.nlm.nih.gov/pubmed/12067237 [Accessed November 21, 2016].

Hilditch-Maguire, P. et al., 2000. Huntingtin: an iron-regulated protein essential for normal nuclear and perinuclear organelles. *Human Molecular Genetics*, 9(19), pp.2789–2797. Available at: http://eutils.ncbi.nlm.nih.gov/entrez/eutils/elink.fcgi?dbfrom=pubmed&id=11092755&retmode=ref&cmd=prlinks\npapers2://publication/uuid/BA6DB0F9-3AA5-4A1A-9066-89B6B16E18EE.

Hinton, S.C. et al., 2007. Motor timing variability increases in preclinical Huntington's disease patients as estimated onset of motor symptoms approaches. *Journal of the International Neuropsychological Society : JINS*, 13(3), pp.539–43. Available at: http://www.ncbi.nlm.nih.gov/pubmed/17445303 [Accessed August 29, 2016].

Hirsch-Reinshagen, V. et al., 2004. Deficiency of ABCA1 Impairs Apolipoprotein E Metabolism in Brain. *Journal of Biological Chemistry*, 279(39), pp.41197–41207. Available at: http://www.jbc.org/lookup/doi/10.1074/jbc.M407962200 [Accessed November 6, 2016].

Ho, A.K. et al., 2003. Profile of cognitive progression in early Huntington's disease. *Neurology*, 61(12), pp.1702–6. Available at: http://www.ncbi.nlm.nih.gov/pubmed/14694033 [Accessed November 2, 2016].

Hodges, A. et al., 2006. Regional and cellular gene expression changes in human Huntington's disease brain. *Hum Mol Genet*, 15(6), pp.965–977. Available at: http://www.ncbi.nlm.nih.gov/pubmed/16467349.

Hodgson, J.G. et al., 1999. A YAC mouse model for Huntington's disease with full-length mutant huntingtin, cytoplasmic toxicity, and selective striatal neurodegeneration. *Neuron*, 23(1), pp.181–92. Available at: http://www.ncbi.nlm.nih.gov/pubmed/10402204 [Accessed November 11, 2016].

Holbert, S. et al., 2001. The Gln-Ala repeat transcriptional activator CA150 interacts with huntingtin: Neuropathologic and genetic evidence for a role in Huntington's disease pathogenesis. *Proceedings of the National Academy of Sciences*, 98(4), pp.1811–1816. Available at: http://www.ncbi.nlm.nih.gov/pubmed/11172033 [Accessed December 28, 2016].

Hong, Y. et al., 2016. Mutant Huntingtin Impairs BDNF Release from Astrocytes by Disrupting Conversion of Rab3a-GTP into Rab3a-GDP. *The Journal of Neuroscience* , 36(34), pp.8790–8801. Available at: http://www.jneurosci.org/content/36/34/8790.abstract.

Jafek, B.W., 1983. Ultrastructure of human nasal mucosa. *The Laryngoscope*, 93(12), pp.1576–1599. Available at: http://dx.doi.org/10.1288/00005537-198312000-00011.

Janowski, B.A. et al., 1996. An oxysterol signalling pathway mediated by the nuclear receptor LXR[alpha]. *Nature*, 383(6602), pp.728–731. Available at: http://dx.doi.org/10.1038/383728a0.

Jansson, B. & Björk, E., 2002. Visualization of in vivo olfactory uptake and transfer using fluorescein dextran. *Journal of drug targeting*, 10(5), pp.379–86. Available at: http://www.tandfonline.com/doi/abs/10.1080/1061186021000001823.

Jiang, R. et al., 2016. Dysfunctional Calcium and Glutamate Signaling in Striatal Astrocytes from Huntington's Disease Model Mice. *Journal of Neuroscience*, 36(12), pp.3453–3470. Available at: http://www.ncbi.nlm.nih.gov/pubmed/27013675 [Accessed December 22, 2016].

Johnson, M.A. et al., 2006. Dopamine release is severely compromised in the R6/2 mouse model of Huntington's disease. *Journal of neurochemistry*, 97(3), pp.737–46. Available at: http://www.ncbi.nlm.nih.gov/pubmed/16573654 [Accessed November 21, 2016].

Johnson, R. & Buckley, N.J., 2009. Gene Dysregulation in Huntington's Disease: REST, MicroRNAs and Beyond. *NeuroMolecular Medicine*, pp.1–17.

Johnston, M. et al., 2004. Evidence of connections between cerebrospinal fluid and nasal lymphatic vessels in humans, non-human primates and other mammalian species. *Cerebrospinal fluid research*, 1(1), p.2. Available at: http://www.ncbi.nlm.nih.gov/pubmed/15679948 [Accessed December 2, 2016].

Kaltenbach, L.S. et al., 2007. Huntingtin Interacting Proteins Are Genetic Modifiers of Neurodegeneration. *PLoS Genetics*, 3(5), p.e82. Available at: http://dx.plos.org/10.1371/journal.pgen.0030082 [Accessed December 28, 2016].

Kandel, E.R., Schwartz, J.H. & Jessell, T.M., 2000. *Principles of Neural Science*,

Karasinska, J.M. et al., 2013. ABCA1 influences neuroinflammation and neuronal death. *Neurobiology of Disease*, 54, pp.445–455. Available at: http://linkinghub.elsevier.com/retrieve/pii/S0969996113000429 [Accessed November 6, 2016].

Karten, B. et al., 2002. Cholesterol accumulates in cell bodies, but is decreased in distal axons, of Niemann-Pick C1-deficient neurons. *Journal of neurochemistry*, 83(5), pp.1154–63. Available at: http://www.ncbi.nlm.nih.gov/pubmed/12437586 [Accessed November 14, 2016].

Karten, B., Campenot, R.B., et al., 2006. Expression of ABCG1, but not ABCA1, correlates with cholesterol release by cerebellar astroglia. *Journal of Biological Chemistry*, 281(7), pp.4049–4057.

Karten, B. et al., 2005. Generation and function of astroglial lipoproteins from Niemann-Pick type C1-deficient mice. *The Biochemical journal*, 387(Pt 3), pp.779–88. Available at: http://www.ncbi.nlm.nih.gov/pubmed/15544574 [Accessed November 14, 2016].

Karten, B., Campenot, R.B., et al., 2006. The Niemann-Pick C1 protein in recycling endosomes of presynaptic nerve terminals. *Journal of lipid research*, 47(3), pp.504–14. Available at: http://www.ncbi.nlm.nih.gov/pubmed/16340014 [Accessed November 14, 2016].

Kegel, K.B. et al., 2002. Huntingtin Is Present in the Nucleus, Interacts with the Transcriptional Corepressor C-terminal Binding Protein, and Represses Transcription. *Journal of Biological Chemistry*, 277(9), pp.7466–7476. Available at: http://www.ncbi.nlm.nih.gov/pubmed/11739372 [Accessed December 19, 2016].

Keryer, G. et al., 2011. Ciliogenesis is regulated by a huntingtin-HAP1-PCM1 pathway and is altered in Huntington disease. *The Journal of clinical investigation*, 121(11), pp.4372–82. Available at: http://www.ncbi.nlm.nih.gov/pubmed/21985783 [Accessed December 28, 2016].

Kessel, a, Ben-Tal, N. & May, S., 2001. Interactions of cholesterol with lipid bilayers: the preferred configuration and fluctuations. *Biophysical journal*, 81(2), pp.643–658.

Klapstein, G.J. et al., 2001. Electrophysiological and morphological changes in striatal spiny neurons in R6/2 Huntington's disease transgenic mice. *Journal of neurophysiology*, 86(6), pp.2667–77. Available at: http://www.ncbi.nlm.nih.gov/pubmed/11731527 [Accessed November 20, 2016].

Koos, D.S. & Fraser, S.E., 2005. The Grueneberg ganglion projects to the olfactory bulb. *Neuroreport*, 16(17), pp.1929–1932.

Kordasiewicz, H.B. et al., 2012. Sustained Therapeutic Reversal of Huntington's Disease by Transient Repression of Huntingtin Synthesis. *Neuron*, 74(6), pp.1031–1044. Available at: http://www.ncbi.nlm.nih.gov/pubmed/22726834 [Accessed December 28, 2016].

Kung, V.W.S. et al., 2007. Dopamine-dependent long term potentiation in the dorsal striatum is reduced in the R6/2 mouse model of Huntington's disease. *Neuroscience*, 146(4), pp.1571–1580. Available at: http://linkinghub.elsevier.com/retrieve/pii/S0306452207003600 [Accessed November 21, 2016].

Kwee, R.M. & Kwee, T.C., 2007. Virchow-Robin spaces at MR imaging. *Radiographics : a review publication of the Radiological Society of North America, Inc*, 27(4), pp.1071–1086. Available at: papers3://publication/doi/10.1148/rg.274065722.

de la Monte, S.M., Vonsattel, J.P. & Richardson, E.P., 1988. Morphometric demonstration of atrophic changes in the cerebral cortex, white matter, and neostriatum in Huntington's disease. *Journal of neuropathology and experimental neurology*, 47(5), pp.516–25. Available at:

http://www.ncbi.nlm.nih.gov/pubmed/2971785 [Accessed November 2, 2016].

Lahiri, D.K., 2004. Apolipoprotein E as a Target for Developing New Therapeutics for Alzheimer's Disease Based on Studies From Protein, RNA, and Regulatory Region of the Gene. *Journal of Molecular Neuroscience*, 23(3), pp.225–234. Available at: http://link.springer.com/10.1385/JMN:23:3:225 [Accessed November 6, 2016].

Lane-Donovan, C.E., Philips, G.T. & Herz, J., 2015. More Than Cholesterol Transporters : Lipoprotein Receptors in. , 83(4), pp.771–787.

Lang, T. et al., 2001. SNAREs are concentrated in cholesterol-dependent clusters that define docking and fusion sites for exocytosis. *EMBO Journal*, 20(9), pp.2202–2213.

Lange, K.W. et al., 1995. Comparison of executive and visuospatial memory function in Huntington's disease and dementia of Alzheimer type matched for degree of dementia. *Journal of neurology, neurosurgery, and psychiatry*, 58(5), pp.598–606.

Lawrence, A.D. et al., 1999. Discrimination, reversal, and shift learning in Huntington's disease: mechanisms of impaired response selection. *Neuropsychologia*, 37(12), pp.1359–74. Available at: http://www.ncbi.nlm.nih.gov/pubmed/10606011 [Accessed November 2, 2016].

Lawrence, A.D. et al., 1996. Executive and mnemonic functions in early Huntington's disease. *Brain : a journal of neurology*, pp.1633–45. Available at: http://www.ncbi.nlm.nih.gov/pubmed/8931586 [Accessed December 3, 2016].

Lawrence, A.D. et al., 1998. The relationship between striatal dopamine receptor binding and cognitive performance in Huntington's disease. *Brain : a journal of neurology*, pp.1343–55. Available at: http://www.ncbi.nlm.nih.gov/pubmed/9679785 [Accessed November 2, 2016].

Lawrence, A.D. et al., 2000. Visual object and visuospatial cognition in Huntington's disease: implications for information processing in corticostriatal circuits. *Brain : a journal of neurology*, pp.1349–64. Available at: http://www.ncbi.nlm.nih.gov/pubmed/10869048 [Accessed November 2, 2016].

Leavitt, B.R. et al., 2006. Wild-type huntingtin protects neurons from excitotoxicity. *Journal of Neurochemistry*, 96(4), pp.1121–1129.

Leavitt, B.R. et al., 2001. Wild-type huntingtin reduces the cellular toxicity of mutant huntingtin in vivo. *American journal of human genetics*, 68(2), pp.313–324.

Lee, W. et al., 2013. Enhanced Ca2+-dependent glutamate release from astrocytes of the BACHD Huntington's disease mouse model. *Neurobiology of Disease*, 58, pp.192–199. Available at: http://www.ncbi.nlm.nih.gov/pubmed/23756199 [Accessed December 26, 2016].

Legleiter, J. et al., 2010. Mutant huntingtin fragments form oligomers in a polyglutamine length-dependent manner in vitro and in vivo. *The Journal of biological chemistry*, 285(19),

pp.14777–90. Available at: http://www.ncbi.nlm.nih.gov/pubmed/20220138 [Accessed December 28, 2016].

Lehmann, J.M. et al., 1997. Activation of the nuclear receptor LXR by oxysterols defines a new hormone response pathway. *J Biol Chem*, 272(6), pp.3137–3140. Available at: http://www.ncbi.nlm.nih.gov/pubmed/9013544.

Lemiere, J. et al., 2004. Cognitive changes in patients with Huntington's disease (HD) and asymptomatic carriers of the HD mutation--a longitudinal follow-up study. *Journal of neurology*, 251(8), pp.935–42. Available at: http://www.ncbi.nlm.nih.gov/pubmed/15316797 [Accessed November 2, 2016].

Leoni, V. et al., 2002. Changes in human plasma levels of the brain specific oxysterol 24S-hydroxycholesterol during progression of multiple sclerosis. *Neuroscience letters*, 331(3), pp.163–166.

Leoni, V. et al., 2008. Plasma 24S-hydroxycholesterol and caudate MRI in pre-manifest and early Huntington's disease. *Brain*, 131(11), pp.2851–2859. Available at: http://www.brain.oxfordjournals.org/cgi/doi/10.1093/brain/awn212 [Accessed November 11, 2016].

Leoni, V. et al., 2013. Plasma 24S-hydroxycholesterol correlation with markers of Huntington disease progression. *Neurobiology of Disease*, 55, pp.37–43.

Leoni, V. et al., 2011. Whole body cholesterol metabolism is impaired in Huntington's disease. *Neuroscience Letters*, 494(3), pp.245–249. Available at: http://linkinghub.elsevier.com/retrieve/pii/S030439401100317X [Accessed November 12, 2016].

Leoni, V. & Caccia, C., 2015. The impairment of cholesterol metabolism in Huntington disease. *Biochimica et Biophysica Acta (BBA) - Molecular and Cell Biology of Lipids*, 1851(8), pp.1095–1105. Available at: http://linkinghub.elsevier.com/retrieve/pii/S1388198115000037 [Accessed November 6, 2016].

Levine, M.S. et al., 1999. Enhanced sensitivity to N-methyl-D-aspartate receptor activation in transgenic and knockin mouse models of Huntington's disease. *Journal of neuroscience research*, 58(4), pp.515–32. Available at: http://www.ncbi.nlm.nih.gov/pubmed/10533044 [Accessed November 21, 2016].

Li, S.-H. & Li, X.-J., 2004. Huntingtin–protein interactions and the pathogenesis of Huntington's disease. *Trends in Genetics*, 20(3), pp.146–154. Available at: http://www.ncbi.nlm.nih.gov/pubmed/15036808 [Accessed December 19, 2016].

Li, Y. et al., 2001. Differential Functions of Members of the Low Density Lipoprotein Receptor

Family Suggested by their Distinct Endocytosis Rates. *Journal of Biological Chemistry*, 276(21), pp.18000–18006.

Liévens, J.C. et al., 2001. Impaired glutamate uptake in the R6 Huntington's disease transgenic mice. *Neurobiology of disease*, 8(5), pp.807–821.

Liévens, J.-C. et al., 2001. Impaired Glutamate Uptake in the R6 Huntington's Disease Transgenic Mice. *Neurobiology of Disease*, 8(5), pp.807–821. Available at: http://linkinghub.elsevier.com/retrieve/pii/S0969996101904309 [Accessed November 21, 2016].

Linetti, a. et al., 2010. Cholesterol reduction impairs exocytosis of synaptic vesicles. *Journal of Cell Science*, 123(4), pp.595–605. Available at: http://jcs.biologists.org/cgi/doi/10.1242/jcs.060681.

Lingwood, D. & Simons, K., 2010. Lipid Rafts As a Membrane-Organizing Principle. *Science*, 327(5961), pp.46–50. Available at: http://www.sciencemag.org/cgi/doi/10.1126/science.1174621 [Accessed November 8, 2016].

Lione, L.A. et al., 1999. Selective discrimination learning impairments in mice expressing the human Huntington's disease mutation. *The Journal of neuroscience : the official journal of the Society for Neuroscience*, 19(23), pp.10428–37. Available at: http://www.ncbi.nlm.nih.gov/pubmed/10575040 [Accessed November 19, 2016].

Liot, G. et al., 2013. Mutant Huntingtin alters retrograde transport of TrkB receptors in striatal dendrites. *The Journal of neuroscience : the official journal of the Society for Neuroscience*, 33(15), pp.6298–309. Available at: http://www.jneurosci.org/cgi/doi/10.1523/JNEUROSCI.2033-12.2013 [Accessed December 28, 2016].

Liu, Q. et al., 2010. Neuronal LRP1 Knockout in Adult Mice Leads to Impaired Brain Lipid Metabolism and Progressive, Age-Dependent Synapse Loss and Neurodegeneration. *Journal of Neuroscience*, 30(50), pp.17068–17078. Available at: http://www.jneurosci.org/cgi/doi/10.1523/JNEUROSCI.4067-10.2010 [Accessed November 7, 2016].

Lloyd M.H. and Wofenshohn S.E. (1998) Practical use of distress scoring systems in the application of humane endpoints. In: Humane Endpoints in Animal Experiments for Biomedical Research, Proceedings of the International Conference. November 22-25 1998, Zeist, The Netherlands (Hendriksen C.F.M. and Moron D.B., eds). London UK: Royal Society of Medicine Press, pp.48-53.

London, E.D., Klemm, N. & Coyle, J.T., 1980. Phylogenetic distribution of [3H]kainic acid

receptor binding sites in neuronal tissue. *Brain Research*, 192(2), pp.463–476.

Lüesse, H.G. et al., 2001. Evaluation of R6/2 HD transgenic mice for therapeutic studies in Huntington's disease: behavioral testing and impact of diabetes mellitus. *Behavioural brain research*, 126(1–2), pp.185–95. Available at: http://www.ncbi.nlm.nih.gov/pubmed/11704263 [Accessed November 19, 2016].

Lund, E.G. et al., 2003. Knockout of the cholesterol 24-hydroxylase gene in mice reveals a brain-specific mechanism of cholesterol turnover. *Journal of Biological Chemistry*, 278(25), pp.22980–22988.

Lund, E.G., Guileyardo, J.M. & Russell, D.W., 1999. cDNA cloning of cholesterol 24-hydroxylase, a mediator of cholesterol homeostasis in the brain. *Proceedings of the National Academy of Sciences of the United States of America*, 96(13), pp.7238–7243.

Luthi-Carter, R. et al., 2003. Complex alteration of NMDA receptors in transgenic Huntington's disease mouse brain: Analysis of mRNA and protein expression, plasma membrane association, interacting proteins, and phosphorylation. *Neurobiology of Disease*, 14(3), pp.624–636.

Luthi-Carter, R. et al., 2000. Decreased expression of striatal signaling genes in a mouse model of Huntington's disease. *Human molecular genetics*, 9(9), pp.1259–71. Available at: http://www.ncbi.nlm.nih.gov/pubmed/10814708 [Accessed November 21, 2016].

Luthi-Carter, R. et al., 2002. Dysregulation of gene expression in the R6/2 model of polyglutamine disease: parallel changes in muscle and brain. *Human molecular genetics*, 11(17), pp.1911–26. Available at: http://www.ncbi.nlm.nih.gov/pubmed/12165554 [Accessed November 21, 2016].

Lütjohann, D. et al., 1996. Cholesterol homeostasis in human brain: evidence for an age-dependent flux of 24S-hydroxycholesterol from the brain into the circulation. *Proceedings of the National Academy of Sciences of the United States of America*, 93(18), pp.9799–9804.

Lütjohann, D. et al., 2000. Plasma 24S-hydroxycholesterol (cerebrosterol) is increased in Alzheimer and vascular demented patients. *Journal of Lipid Research*, 41(2), pp.195–8.

Lütjohann, D. & von Bergmann, K., 2003. 24S-hydroxycholesterol: a marker of brain cholesterol metabolism. *Pharmacopsychiatry*, 36 Suppl 2, pp.S102-6. Available at: http://www.ncbi.nlm.nih.gov/pubmed/14574622 [Accessed November 13, 2016].

Maat-Schieman, M.L. et al., 1999. Distribution of inclusions in neuronal nuclei and dystrophic neurites in Huntington disease brain. *Journal of neuropathology and experimental neurology*, 58(2), pp.129–37. Available at: http://www.ncbi.nlm.nih.gov/pubmed/10029096 [Accessed November 2, 2016].

Macdonald, V. & Halliday, G., 2002. Pyramidal cell loss in motor cortices in Huntington's disease.

Neurobiology of disease, 10(3), pp.378–86. Available at: http://www.ncbi.nlm.nih.gov/pubmed/12270698 [Accessed November 2, 2016].

Magen, I. & Hornstein, E., 2014. Oligonucleotide-based therapy for neurodegenerative diseases. *Brain Research*, 1584, pp.116–128.

Mahley, R.W., Weisgraber, K.H. & Huang, Y., 2006. Apolipoprotein E4: A causative factor and therapeutic target in neuropathology, including Alzheimer's disease. *Proceedings of the National Academy of Sciences*, 103(15), pp.5644–5651. Available at: http://www.pnas.org/cgi/doi/10.1073/pnas.0600549103 [Accessed November 6, 2016].

Maity, T., Fuse, N. & Beachy, P. a, 2005. Molecular mechanisms of Sonic hedgehog mutant effects in holoprosencephaly. *Proceedings of the National Academy of Sciences of the United States of America*, 102(47), pp.17026–17031.

Mangiarini, L. et al., 1996. Exon 1 of the HD Gene with an Expanded CAG Repeat Is Sufficient to Cause a Progressive Neurological Phenotype in Transgenic Mice. *Cell*, 87(3), pp.493–506.

Mann, R.K. & Beachy, P.A., 2000. Cholesterol modification of proteins. *Biochimica et Biophysica Acta - Molecular and Cell Biology of Lipids*, 1529(1–3), pp.188–202.

Marcora, E., Gowan, K. & Lee, J.E., 2003. Stimulation of NeuroD activity by huntingtin and huntingtin-associated proteins HAP1 and MLK2. *Proceedings of the National Academy of Sciences of the United States of America*, 100(16), pp.9578–83. Available at: http://www.ncbi.nlm.nih.gov/pubmed/12881483 [Accessed December 28, 2016].

Markianos, M. et al., 2008. Low plasma total cholesterol in patients with Huntington's disease and first-degree relatives. *Mol Genet Metab*, 93(3), pp.341–346.

Martens, J.R., O'Connell, K. & Tamkun, M., 2004. Targeting of ion channels to membrane microdomains: localization of KV channels to lipid rafts. *Trends in Pharmacological Sciences*, 25(1), pp.16–21. Available at: http://linkinghub.elsevier.com/retrieve/pii/S0165614703003559 [Accessed November 8, 2016].

Martin, M.G. et al., 2014. Constitutive hippocampal cholesterol loss underlies poor cognition in old rodents. *EMBO Molecular Medicine*, 6(7), pp.902–917. Available at: http://www.pubmedcentral.nih.gov/articlerender.fcgi?artid=4119354&tool=pmcentrez&rendertype=abstract.

Martinez-Vicente, M. et al., 2010. Cargo recognition failure is responsible for inefficient autophagy in Huntington's disease. *Nature Neuroscience*, 13(5), pp.567–576. Available at: http://www.pubmedcentral.nih.gov/articlerender.fcgi?artid=2860687&tool=pmcentrez&rendertype=abstract.

Marullo, M. et al., 2012. Pitfalls in the detection of cholesterol in Huntington's disease models.

PLoS Currents. Available at: http://currents.plos.org/hd/?p=6263 [Accessed November 11, 2016].

Mauch, D.H. et al., 2001. CNS synaptogenesis promoted by glia-derived cholesterol. *Science (New York, N.Y.)*, 294(5545), pp.1354–1357.

Maxfield, F.R. & Wüstner, D., 2002. Intracellular cholesterol transport. *Journal of Clinical Investigation*, 110(7), pp.891–898. Available at: http://www.jci.org/articles/view/16500 [Accessed November 7, 2016].

Meade, C.A. et al., 2002. Cellular localization and development of neuronal intranuclear inclusions in striatal and cortical neurons in R6/2 transgenic mice. *The Journal of comparative neurology*, 449(3), pp.241–69. Available at: http://www.ncbi.nlm.nih.gov/pubmed/12115678 [Accessed November 20, 2016].

Meaney, S. et al., 2002. On the rate of translocation in vitro and kinetics in vivo of the major oxysterols in human circulation: critical importance of the position of the oxygen function. *Journal of lipid research*, 43(26), pp.2130–2135.

Menalled, L.B. et al., 2012. Comprehensive Behavioral and Molecular Characterization of a New Knock-In Mouse Model of Huntington's Disease: zQ175 H. Okazawa, ed. *PLoS ONE*, 7(12), p.e49838. Available at: http://dx.plos.org/10.1371/journal.pone.0049838 [Accessed November 11, 2016].

Menalled, L.B., 2005. Knock-in mouse models of Huntington's disease. *NeuroRx : the journal of the American Society for Experimental NeuroTherapeutics*, 2(3), pp.465–70. Available at: http://www.ncbi.nlm.nih.gov/pubmed/16389309 [Accessed November 11, 2016].

Mena-Segovia, J. et al., 2002. Changes in sleep-waking cycle after striatal excitotoxic lesions. *Behavioural brain research*, 136(2), pp.475–81. Available at: http://www.ncbi.nlm.nih.gov/pubmed/12429410 [Accessed November 2, 2016].

Meredith, M.E., Salameh, T.S. & Banks, W. a, 2015. Intranasal Delivery of Proteins and Peptides in the Treatment of Neurodegenerative Diseases. *The AAPS journal*, 17(11), pp.780–787. Available at: http://www.ncbi.nlm.nih.gov/pubmed/25801717.

Merritt AD, Conneally PM, Rahman NF, D. AL, 1969. *Juvenile Huntington's chorea* A. Barbeau & T. Brunette, eds., Amsterdam: Excerpta Medica Foundation.

Miller, B.R. et al., 2008. Dysregulated information processing by medium spiny neurons in striatum of freely behaving mouse models of Huntington's disease. *Journal of neurophysiology*, 100(4), pp.2205–16. Available at: http://www.ncbi.nlm.nih.gov/pubmed/18667541 [Accessed December 20, 2016].

Minchin, R., 2008. Nanomedicine: sizing up targets with nanoparticles. *Nature nanotechnology*,

3(1), pp.12–13.

Mitsche, M. A., McDonald, J. G., Hobbs, H. H. & Cohen, J. C. Flux analysis of cholesterol biosynthesis in vivo reveals multiple tissue and cell-type specific pathways. *Elife* **4,** 1–21 (2015).

Miyamoto, N. et al., 2015. Astrocytes Promote Oligodendrogenesis after White Matter Damage via Brain-Derived Neurotrophic Factor. *The Journal of neuroscience : the official journal of the Society for Neuroscience*, 35(41), pp.14002–8. Available at: http://www.ncbi.nlm.nih.gov/pubmed/26468200\nhttp://www.pubmedcentral.nih.gov/articlerender.fcgi?artid=PMC4604233.

Modifiers of Huntingtons Disease Consortium, G. et al., 2015. Identification of Genetic Factors that Modify Clinical Onset of Huntington's Disease. *Cell*, 162, pp.516–526.

Molero, A.E. et al., 2009. Impairment of developmental stem cell-mediated striatal neurogenesis and pluripotency genes in a knock-in model of Huntington's disease. *Proceedings of the National Academy of Sciences*, 106(51), pp.21900–21905. Available at: http://www.ncbi.nlm.nih.gov/pubmed/19955426 [Accessed December 19, 2016].

Mondal, M. et al., 2008. Sterols Are Mainly in the Cytoplasmic Leaflet of the Plasma Membrane and the Endocytic Recycling Compartment in CHO Cells. *Molecular Biology of the Cell*, 20(2), pp.581–588. Available at: http://www.molbiolcell.org/cgi/doi/10.1091/mbc.E08-07-0785 [Accessed November 8, 2016].

Montoya, A. et al., 2006. Episodic memory impairment in Huntington's disease: a meta-analysis. *Neuropsychologia*, 44(10), pp.1984–94. Available at: http://www.ncbi.nlm.nih.gov/pubmed/16797615 [Accessed November 2, 2016].

Moreira Sousa, C. et al., 2013. The Huntington disease protein accelerates breast tumour development and metastasis through ErbB2/HER2 signalling. *EMBO Molecular Medicine*, 5(2), pp.309–325. Available at: http://www.ncbi.nlm.nih.gov/pubmed/23300147 [Accessed December 28, 2016].

Morton, A.J., 2005. Disintegration of the Sleep-Wake Cycle and Circadian Timing in Huntington's Disease. *Journal of Neuroscience*, 25(1), pp.157–163. Available at: http://www.jneurosci.org/cgi/doi/10.1523/JNEUROSCI.3842-04.2005 [Accessed November 2, 2016].

Morton, A.J., Faull, R.L. & Edwardson, J.M., 2001. Abnormalities in the synaptic vesicle fusion machinery in Huntington's disease. *Brain research bulletin*, 56(2), pp.111–7. Available at: http://www.ncbi.nlm.nih.gov/pubmed/11704347 [Accessed November 21, 2016].

Mundargi, R.C. et al., 2008. Nano/micro technologies for delivering macromolecular therapeutics

using poly(d,l-lactide-co-glycolide) and its derivatives. *Journal of Controlled Release*, 125(3), pp.193–209. Available at: http://www.ncbi.nlm.nih.gov/pubmed/18083265 [Accessed December 3, 2016].

Muratore, M., 2013. Raman spectroscopy and partial least squares analysis in discrimination of peripheral cells affected by Huntington's disease. *Analytica Chimica Acta*, 793, pp.1–10. Available at: http://linkinghub.elsevier.com/retrieve/pii/S0003267013008350 [Accessed November 13, 2016].

Murphy, K.P. et al., 2000. Abnormal synaptic plasticity and impaired spatial cognition in mice transgenic for exon 1 of the human Huntington's disease mutation. *The Journal of neuroscience : the official journal of the Society for Neuroscience*, 20(13), pp.5115–23. Available at: http://www.ncbi.nlm.nih.gov/pubmed/10864968 [Accessed November 20, 2016].

Myers, R., 2004. Huntington's disease genetics. *NeuroRx : the journal of the American Society for Experimental NeuroTherapeutics*, 1(2), pp.255–262. Available at: http://www.ncbi.nlm.nih.gov/entrez/query.fcgi?db=pubmed&cmd=Retrieve&dopt=AbstractPlus&list_uids=15717026.

Myers, R.H. et al., 1991. Decreased neuronal and increased oligodendroglial densities in Huntington's disease caudate nucleus. *Journal of neuropathology and experimental neurology*, 50(6), pp.729–42. Available at: http://www.ncbi.nlm.nih.gov/pubmed/1836225 [Accessed November 2, 2016].

Nieweg, K., Schaller, H. & Pfrieger, F.W., 2009. Marked differences in cholesterol synthesis between neurons and glial cells from postnatal rats. *Journal of neurochemistry*, 109(1), pp.125–34. Available at: http://doi.wiley.com/10.1111/j.1471-4159.2009.05917.x [Accessed December 6, 2016].

Ooi, L. & Wood, I.C., 2007. Chromatin crosstalk in development and disease: lessons from REST. *Nature reviews. Genetics*, 8(7), pp.544–54. Available at: http://dx.doi.org/10.1038/nrg2100.

Panov, a V et al., 2002. Early mitochondrial calcium defects in Huntington's disease are a direct effect of polyglutamines. *Nat Neurosci*, 5(8), pp.731–736. Available at: http://www.nature.com/neuro/journal/v5/n8/pdf/nn884.pdf.

Panyam, J. & Labhasetwar, V., 2003. Biodegradable nanoparticles for drug and gene delivery to cells and tissue. *Advanced Drug Delivery Reviews*, 55(3), pp.329–347.

Pardeshi, C. V. et al., 2012. Formulation, optimization and evaluation of spray-dried mucoadhesive microspheres as intranasal carriers for Valsartan. *Journal of Microencapsulation*, 29(2), pp.103–114.

Parsons, M.P. et al., 2016. Real-time imaging of glutamate clearance reveals normal striatal uptake

in Huntington disease mouse models. *Nature Communications*, 7, p.11251. Available at: http://www.ncbi.nlm.nih.gov/pubmed/27052848 [Accessed December 26, 2016].

Paulsen, J.S. et al., 2001. Clinical markers of early disease in persons near onset of Huntington's disease. *Neurology*, 57(4), pp.658–62. Available at: http://www.ncbi.nlm.nih.gov/pubmed/11524475 [Accessed November 2, 2016].

Paulsen, J.S. et al., 1995. Distinct cognitive profiles of cortical and subcortical dementia in advanced illness. *Neurology*, 45(5), pp.951–6. Available at: http://www.ncbi.nlm.nih.gov/pubmed/7746413 [Accessed November 2, 2016].

Paulsen, J.S. et al., fMRI biomarker of early neuronal dysfunction in presymptomatic Huntington's Disease. *AJNR. American journal of neuroradiology*, 25(10), pp.1715–21. Available at: http://www.ncbi.nlm.nih.gov/pubmed/15569736 [Accessed October 23, 2016].

Peake, K.B. & Vance, J.E., 2012. Normalization of Cholesterol Homeostasis by 2-Hydroxypropyl- -cyclodextrin in Neurons and Glia from Niemann-Pick C1 (NPC1)-deficient Mice. *Journal of Biological Chemistry*, 287(12), pp.9290–9298. Available at: http://www.jbc.org/cgi/doi/10.1074/jbc.M111.326405 [Accessed November 14, 2016].

Perutz, M.F., 1996. Glutamine repeats and inherited neurodegenerative diseases: molecular aspects. *Current opinion in structural biology*, 6(6), pp.848–58. Available at: http://www.ncbi.nlm.nih.gov/pubmed/8994886 [Accessed November 2, 2016].

Pfrieger, F.W., 2003. Cholesterol homeostasis and function in neurons of the central nervous system. *Cellular and molecular life sciences : CMLS*, 60(6), pp.1158–71. Available at: http://www.ncbi.nlm.nih.gov/pubmed/12861382.

Pfrieger, F.W. & Ungerer, N., 2011. Cholesterol metabolism in neurons and astrocytes. *Progress in Lipid Research*, 50(4), pp.357–371. Available at: http://dx.doi.org/10.1016/j.plipres.2011.06.002.

Pitas, R.E. et al., 1987. Astrocytes synthesize apolipoprotein E and metabolize apolipoprotein E-containing lipoproteins. *Biochimica et Biophysica Acta (BBA) - Lipids and Lipid Metabolism*, 917(1), pp.148–161.

Plant, K. et al., 2006. Transient incorporation of native GluR2-lacking AMPA receptors during hippocampal long-term potentiation. *Nature neuroscience*, 9(5), pp.602–604.

Poirier, J. et al., 1993. Cholesterol synthesis and lipoprotein reuptake during synaptic remodelling in hippocampus in adult rats. *Neuroscience*, 55(1), pp.81–90.

Poirier, M.A. et al., 2002. Huntingtin spheroids and protofibrils as precursors in polyglutamine fibrilization. *Journal of Biological Chemistry*, 277(43), pp.41032–41037.

Politis, M. et al., 2008. Hypothalamic involvement in Huntington's disease: an in vivo PET study.

Brain : a journal of neurology, 131(Pt 11), pp.2860–9. Available at: http://www.ncbi.nlm.nih.gov/pubmed/18829696 [Accessed October 23, 2016].

Polt, D.R. & Palian, M.M., 2001. Glycopeptide analgesics. *Drugs of the Future*, 26(6), p.561. Available at: http://journals.prous.com/journals/servlet/xmlxsl/pk_journals.xml_summary_pr?p_JournalId=2&p_RefId=668342&p_IsPs=N [Accessed December 2, 2016].

Porter, F.D., 2006. Cholesterol precursors and facial clefting. *Journal of Clinical Investigation*, 116(9), pp.2322–2325. Available at: http://www.jci.org/articles/view/29872 [Accessed November 14, 2016].

Porter, F.D. & Herman, G.E., 2011. Malformation syndromes caused by disorders of cholesterol synthesis. *The Journal of Lipid Research*, 52(1), pp.6–34. Available at: http://www.jlr.org/cgi/doi/10.1194/jlr.R009548 [Accessed November 14, 2016].

Porter, J. a, Young, K.E. & Beachy, P. a, 1996. Cholesterol modification of hedgehog signaling proteins in animal development. *Science (New York, N.Y.)*, 274(5285), pp.255–259.

Prasad, A. et al., 2000. Regional and developmental expression of the Npc1 mRNA in the mouse brain. *Journal of Neurochemistry*, 75(3), pp.1250–1257.

Pringsheim, T. et al., 2012. The incidence and prevalence of Huntington's disease: A systematic review and meta-analysis. *Movement Disorders*, 27(9), pp.1083–1091.

Puglielli, L., Tanzi, R.E. & Kovacs, D.M., 2003. Alzheimer's disease: the cholesterol connection. *Nature Neuroscience*, 6(4), pp.345–351. Available at: http://www.nature.com/doifinder/10.1038/nn0403-345 [Accessed November 6, 2016].

Van Raamsdonk, J.M. et al., 2005. Cognitive dysfunction precedes neuropathology and motor abnormalities in the YAC128 mouse model of Huntington's disease. *The Journal of neuroscience : the official journal of the Society for Neuroscience*, 25(16), pp.4169–80. Available at: http://www.ncbi.nlm.nih.gov/pubmed/15843620.

Ramirez, D.M.O., Andersson, S. & Russell, D.W., 2008. Neuronal expression and subcellular localization of cholesterol 24-hydroxylase in the mouse brain. *The Journal of comparative neurology*, 507(5), pp.1676–93. Available at: http://www.pubmedcentral.nih.gov/articlerender.fcgi?artid=4015140&tool=pmcentrez&rendertype=abstract.

Rebeck, G.W. et al., 1993. Apolipoprotein E in sporadic Alzheimer's disease: allelic variation and receptor interactions. *Neuron*, 11(4), pp.575–80. Available at: http://www.ncbi.nlm.nih.gov/pubmed/8398148 [Accessed November 6, 2016].

Reid, P.C. et al., 2004. A novel cholesterol stain reveals early neuronal cholesterol accumulation in

the Niemann-Pick type C1 mouse brain. *Journal of lipid research*, 45(3), pp.582–591.

Reiner, A. et al., 1988. Differential loss of striatal projection neurons in Huntington disease. *Proceedings of the National Academy of Sciences of the United States of America*, 85(15), pp.5733–7. Available at: http://www.ncbi.nlm.nih.gov/pubmed/2456581 [Accessed November 2, 2016].

Reiner, A. et al., 2001. Neurons lacking huntingtin differentially colonize brain and survive in chimeric mice. *The Journal of neuroscience : the official journal of the Society for Neuroscience*, 21(19), pp.7608–19. Available at: http://www.ncbi.nlm.nih.gov/pubmed/11567051.

Reiner, A. et al., 2013. Striatal parvalbuminergic neurons are lost in Huntington's disease: implications for dystonia. *Movement disorders : official journal of the Movement Disorder Society*, 28(12), pp.1691–9. Available at: http://www.ncbi.nlm.nih.gov/pubmed/24014043 [Accessed November 2, 2016].

Rennels, M.L., Blaumanis, O.R. & Grady, P.A., 1990. Rapid solute transport throughout the brain via paravascular fluid pathways. *Adv.Neurol.*, 52:431-9., pp.431–439.

Rensen, P.C.N. et al., 2000. Apolipoprotein E is resistant to intracellular degradation in vitro and in vivo. Evidence for retroendocytosis. *Journal of Biological Chemistry*, 275(12), pp.8564–8571.

Reynolds, G.P. et al., 1999. Brain neurotransmitter deficits in mice transgenic for the Huntington's disease mutation. *Journal of neurochemistry*, 72(4), pp.1773–6. Available at: http://www.ncbi.nlm.nih.gov/pubmed/10098889 [Accessed November 21, 2016].

des Rieux, A. et al., 2006. Nanoparticles as potential oral delivery systems of proteins and vaccines: A mechanistic approach. *Journal of Controlled Release*, 116(1), pp.1–27. Available at: http://www.ncbi.nlm.nih.gov/pubmed/17050027 [Accessed December 2, 2016].

Rigamonti, D. et al., 2001. Huntingtin's Neuroprotective Activity Occurs via Inhibition of Procaspase-9 Processing. *Journal of Biological Chemistry*, 276(18), pp.14545–14548.

Rigamonti, D. et al., 2000. Wild-type huntingtin protects from apoptosis upstream of caspase-3. *The Journal of neuroscience : the official journal of the Society for Neuroscience*, 20(10), pp.3705–13. Available at: http://www.ncbi.nlm.nih.gov/pubmed/10804212.

Rohrbough, J. & Broadie, K., 2005. Lipid regulation of the synaptic vesicle cycle. *Nature reviews. Neuroscience*, 6(2), pp.139–150.

Rosas, H.D. et al., 2010. Altered white matter microstructure in the corpus callosum in Huntington's disease: Implications for cortical "disconnection." *NeuroImage*, 49(4), pp.2995–3004. Available at: http://linkinghub.elsevier.com/retrieve/pii/S1053811909010866 [Accessed November 2, 2016].

Rosas, H.D. et al., 2006. Diffusion tensor imaging in presymptomatic and early Huntington's disease: Selective white matter pathology and its relationship to clinical measures. *Movement Disorders*, 21(9), pp.1317–1325. Available at: http://doi.wiley.com/10.1002/mds.20979 [Accessed November 2, 2016].

Rosas, H.D. et al., 2002. Regional and progressive thinning of the cortical ribbon in Huntington's disease. *Neurology*, 58(5), pp.695–701. Available at: http://www.ncbi.nlm.nih.gov/pubmed/11889230 [Accessed November 2, 2016].

Rosenbaum, A.I. et al., 2010. Endocytosis of beta-cyclodextrins is responsible for cholesterol reduction in Niemann-Pick type C mutant cells. *Proceedings of the National Academy of Sciences*, 107(12), pp.5477–5482. Available at: http://www.pnas.org/cgi/doi/10.1073/pnas.0914309107 [Accessed November 14, 2016].

Rosenberg, N.K., Sørensen, S.A. & Christensen, A.L., 1995. Neuropsychological characteristics of Huntington's disease carriers: a double blind study. *Journal of medical genetics*, 32(8), pp.600–4. Available at: http://www.ncbi.nlm.nih.gov/pubmed/7473650 [Accessed November 2, 2016].

Rowe, K.C. et al., 2010. Self-paced timing detects and tracks change in prodromal Huntington disease. *Neuropsychology*, 24(4), pp.435–42. Available at: http://www.ncbi.nlm.nih.gov/pubmed/20604618 [Accessed August 29, 2016].

Rui, Y.-N. et al., 2015. Huntingtin functions as a scaffold for selective macroautophagy. *Nature Cell Biology*, 17(3), pp.262–275. Available at: http://www.pubmedcentral.nih.gov/articlerender.fcgi?artid=4344873&tool=pmcentrez&rendertype=abstract.

Russell, D.W. et al., 2009. Cholesterol 24-Hydroxylase: An Enzyme of Cholesterol Turnover in the Brain. *Annual Review of Biochemistry*, 78(1), pp.1017–1040. Available at: http://www.annualreviews.org/doi/10.1146/annurev.biochem.78.072407.103859 [Accessed November 5, 2016].

Sadek, J.R. et al., 2004. Retrograde amnesia in dementia: comparison of HIV-associated dementia, Alzheimer's disease, and Huntington's disease. *Neuropsychology*, 18(4), pp.692–9. Available at: http://www.ncbi.nlm.nih.gov/pubmed/15506837 [Accessed November 2, 2016].

Saito, K. et al., 2009. Ablation of cholesterol biosynthesis in neural stem cells increases their VEGF expression and angiogenesis but causes neuron apoptosis. *Proceedings of the National Academy of Sciences of the United States of America*, 106(20), pp.8350–5. Available at: http://www.pubmedcentral.nih.gov/articlerender.fcgi?artid=2688855&tool=pmcentrez&rendertype=abstract.

Sakashita, N. et al., 2000. Localization of human acyl-coenzyme A:cholesterol acyltransferase-1 (ACAT-1) in macrophages and in various tissues. *The American Journal of Pathology*, 156(1), pp.227–236. Available at: http://dx.doi.org/10.1016/S0002-9440(10)64723-2.

Sanan, D.A. et al., 1994. Apolipoprotein E associates with beta amyloid peptide of Alzheimer's disease to form novel monofibrils. Isoform apoE4 associates more efficiently than apoE3. *Journal of Clinical Investigation*, 94(2), pp.860–869. Available at: http://www.jci.org/articles/view/117407 [Accessed November 14, 2016].

Sapp, E. et al., 2001. Early and progressive accumulation of reactive microglia in the Huntington disease brain. *Journal of neuropathology and experimental neurology*, 60(2), pp.161–72. Available at: http://www.ncbi.nlm.nih.gov/pubmed/11273004 [Accessed November 2, 2016].

Schaefer, M.L. et al., 2002. Trigeminal collaterals in the nasal epithelium and olfactory bulb: A potential route for direct modulation of olfactory information by trigeminal stimuli. *Journal of Comparative Neurology*, 444(3), pp.221–226.

Schneider, S.A. et al., 2010. Abnormal explicit but normal implicit sequence learning in premanifest and early Huntington's disease. *Movement disorders : official journal of the Movement Disorder Society*, 25(10), pp.1343–9. Available at: http://www.ncbi.nlm.nih.gov/pubmed/20544716 [Accessed November 2, 2016].

Selkoe, D.J., 2002. Alzheimer's Disease Is a Synaptic Failure. *Science*, 298(5594), pp.789–791. Available at: http://www.sciencemag.org/cgi/doi/10.1126/science.1074069 [Accessed November 14, 2016].

Seong, I.S. et al., 2009. Huntingtin facilitates polycomb repressive complex 2. *Human Molecular Genetics*, 19(4), pp.573–583.

Shankaran, M. et al., 2017. Early and brain region-specific decrease of de novo cholesterol biosynthesis in Huntington's disease: A cross-validation study in Q175 knock-in mice. *Neurobiology of Disease*, 98, pp.66–76. Available at: http://www.ncbi.nlm.nih.gov/pubmed/27913290 [Accessed December 19, 2016].

Shimohata, T. et al., 2000. Expanded polyglutamine stretches interact with TAFII130, interfering with CREB-dependent transcription. *Nature genetics*, 26(1), pp.29–36.

Shin, J.-Y. et al., 2005. Expression of mutant huntingtin in glial cells contributes to neuronal excitotoxicity. *The Journal of cell biology*, 171(6), pp.1001–12. Available at: http://www.ncbi.nlm.nih.gov/pubmed/16365166 [Accessed November 2, 2016].

Silvestri, R. et al., 1995. Sleep features in Tourette's syndrome, neuroacanthocytosis and Huntington's chorea. *Neurophysiologie Clinique/Clinical Neurophysiology*, 25(2), pp.66–77. Available at: http://linkinghub.elsevier.com/retrieve/pii/0987705396810343 [Accessed

November 2, 2016].

Simons, M. et al., 1998. Cholesterol depletion inhibits the generation of beta-amyloid in hippocampal neurons. *Proceedings of the National Academy of Sciences of the United States of America*, 95(11), pp.6460–4. Available at: http://www.ncbi.nlm.nih.gov/pubmed/9600988 [Accessed November 14, 2016].

Sipione, S. et al., 2002. Early transcriptional profiles in huntingtin-inducible striatal cells by microarray analyses. *Human molecular genetics*, 11(17), pp.1953–65. Available at: http://www.ncbi.nlm.nih.gov/pubmed/12165557.

Skotte, N.H. et al., 2014. Allele-Specific Suppression of Mutant Huntingtin Using Antisense Oligonucleotides: Providing a Therapeutic Option for All Huntington Disease Patients J. C. Glorioso, ed. *PLoS ONE*, 9(9), p.e107434. Available at: http://dx.plos.org/10.1371/journal.pone.0107434 [Accessed December 29, 2016].

Smith, R., Brundin, P. & Li, J.Y., 2005. Synaptic dysfunction in Huntington's disease: a new perspective. *Cell Mol Life Sci*, 62(17), pp.1901–1912. Available at: http://www.ncbi.nlm.nih.gov/entrez/query.fcgi?cmd=Retrieve&db=PubMed&dopt=Citation&list_uids=15968465.

Soane, R.J. et al., 1999. Evaluation of the clearance characteristics of bioadhesive systems in humans. *International Journal of Pharmaceutics*, 178(1), pp.55–65.

Soccio, R.E., 2004. Intracellular Cholesterol Transport. *Arteriosclerosis, Thrombosis, and Vascular Biology*, 24(7), pp.1150–1160. Available at: http://atvb.ahajournals.org/cgi/doi/10.1161/01.ATV.0000131264.66417.d5.

Song, C. et al., 2003. Expression of polyglutamine-expanded huntingtin induces tyrosine phosphorylation of N-methyl-D-aspartate receptors. *Journal of Biological Chemistry*, 278(35), pp.33364–33369.

Sooksawate, T. & Simmonds, M.A., 2001. Effects of membrane cholesterol on the sensitivity of the GABA A receptor to GABA in acutely dissociated rat hippocampal neurones. , 40, pp.178–184.

Squitieri, F. et al., 1994. DNA haplotype analysis of huntington disease reveals clues to the origins and mechanisms of CAG expansion and reasons for geographic variations of prevalence. *Human Molecular Genetics*, 3(12), pp.2103–2114. Available at: http://www.ncbi.nlm.nih.gov/pubmed/7881406 [Accessed August 28, 2016].

Stack, E.C. et al., 2005. Chronology of behavioral symptoms and neuropathological sequela in R6/2 Huntington's disease transgenic mice. *The Journal of Comparative Neurology*, 490(4), pp.354–370. Available at: http://doi.wiley.com/10.1002/cne.20680 [Accessed November 19,

2016].

Steffan, J.S. et al., 2001. Histone deacetylase inhibitors arrest polyglutamine-dependent neurodegeneration in Drosophila. *Nature*, 413(6857), pp.739–743.

Steffan, J.S. et al., 2000. The Huntington's disease protein interacts with p53 and CREB-binding protein and represses transcription. *Proc Natl Acad Sci U S A*, 97(12), pp.6763–6768. Available at: http://www.pubmedcentral.nih.gov/articlerender.fcgi?artid=18731&tool=pmcentrez&rendertype=abstract\nhttp://www.ncbi.nlm.nih.gov/entrez/query.fcgi?cmd=Retrieve&db=PubMed&dopt=Citation&list_uids=10823891.

Strand, A.D. et al., 2005. Gene expression in Huntington's disease skeletal muscle: A potential biomarker. *Human Molecular Genetics*, 14(13), pp.1863–1876.

Strehlow, A.N.T., Li, J.Z. & Myers, R.M., 2006. Wild-type huntingtin participates in protein trafficking between the Golgi and the extracellular space. *Human Molecular Genetics*, 16(4), pp.391–409. Available at: http://www.ncbi.nlm.nih.gov/pubmed/17189290 [Accessed December 19, 2016].

Sun, Y. et al., 2001. Polyglutamine-expanded Huntingtin Promotes Sensitization of N-Methyl-D-aspartate Receptors via Post-synaptic Density 95. *Journal of Biological Chemistry*, 276(27), pp.24713–24718. Available at: http://www.ncbi.nlm.nih.gov/pubmed/11319238 [Accessed December 19, 2016].

Susan Standring, PhD, Ds., 2009. Gray's Anatomy 40th edition. *Churchill Livingstone*, pp.196–200. Available at: http://www.us.elsevierhealth.com/anatomy/gray-anatomy-expert-consult/9780443066849/.

Suzuki, R. et al., 2013. Reduction of the Cholesterol Sensor SCAP in the Brains of Mice Causes Impaired Synaptic Transmission and Altered Cognitive Function S. O'Rahilly, ed. *PLoS Biology*, 11(4), p.e1001532. Available at: http://dx.plos.org/10.1371/journal.pbio.1001532 [Accessed November 6, 2016].

Suzuki, S. et al., 2007. Brain-Derived Neurotrophic Factor Regulates Cholesterol Metabolism for Synapse Development. *Journal of Neuroscience*, 27(24).

Tabrizi, S.J. et al., 2000. Mitochondrial dysfunction and free radical damage in the Huntington R6/2 transgenic mouse. *Annals of neurology*, 47(1), pp.80–6. Available at: http://www.ncbi.nlm.nih.gov/pubmed/10632104 [Accessed November 21, 2016].

Takano, H. & Gusella, J.F., 2002. The predominantly HEAT-like motif structure of huntingtin and its association and coincident nuclear entry with dorsal, an NF-kB/Rel/dorsal family transcription factor. *BMC neuroscience*, 3, p.15. Available at:

http://www.ncbi.nlm.nih.gov/pubmed/12379151 [Accessed December 28, 2016].

Tarditi, A. et al., 2006. Early and transient alteration of adenosine A2A receptor signaling in a mouse model of Huntington disease. *Neurobiology of disease*, 23(1), pp.44–53.

Taurin, S., Nehoff, H. & Greish, K., 2012. Anticancer nanomedicine and tumor vascular permeability; Where is the missing link? In *Journal of Controlled Release*. pp. 265–275.

Theeuwes F and Yum SI., 1976. Principles of the design and operation of generic osmotic pumps for the delivery of semisolid or liquid drug ormulations. *Ann Biomed Eng*, 4(4), pp.343–353.

Thiele, C. et al., 2000. Cholesterol binds to synaptophysin and is required for biogenesis of synaptic vesicles. *Nature cell biology*, 2(1), pp.42–49. Available at: http://dx.doi.org/10.1038/71366.

Thorne, R.G. et al., 2004. Delivery of insulin-like growth factor-I to the rat brain and spinal cord along olfactory and trigeminal pathways following intranasal administration. *Neuroscience*, 127(2), pp.481–96. Available at: http://www.ncbi.nlm.nih.gov/pubmed/15262337 [Accessed November 30, 2016].

Thorne, R.G. et al., 2008. Delivery of interferon-b to the monkey nervous system following intranasal administration. *Neuroscience*, 152(3), pp.785–797.

Thu, D.C. V et al., 2010. Cell loss in the motor and cingulate cortex correlates with symptomatology in Huntington's disease. *Brain : a journal of neurology*, 133(Pt 4), pp.1094–110. Available at: http://www.ncbi.nlm.nih.gov/pubmed/20375136 [Accessed November 2, 2016].

Tippett, L.J. et al., 2006. Striosomes and mood dysfunction in Huntington's disease. *Brain*, 130(1), pp.206–221. Available at: http://www.brain.oxfordjournals.org/cgi/doi/10.1093/brain/awl243 [Accessed November 2, 2016].

Tiwari, S. et al., 2009. Liposome in situ gelling system: Novel carrier based vaccine adjuvant for intranasal delivery of recombinant protein vaccine. *Procedia in Vaccinology*, 1(1), pp.148–163.

Tong, X. et al., 2014. Astrocyte Kir4.1 ion channel deficits contribute to neuronal dysfunction in Huntington's disease model mice. *Nature neuroscience*, 17(5), pp.694–703. Available at: http://www.ncbi.nlm.nih.gov/pubmed/24686787.

Del Toro, D. et al., 2010. Altered cholesterol homeostasis contributes to enhanced excitotoxicity in Huntington's disease. *Journal of Neurochemistry*, 115(1), pp.153–167. Available at: http://doi.wiley.com/10.1111/j.1471-4159.2010.06912.x [Accessed November 11, 2016].

del Toro, D. et al., 2009. Mutant huntingtin impairs post-Golgi trafficking to lysosomes by delocalizing optineurin/Rab8 complex from the Golgi apparatus. *Molecular biology of the cell*, 20(5), pp.1478–92. Available at: http://www.ncbi.nlm.nih.gov/pubmed/19144827 [Accessed

December 28, 2016].

Tosi, Giovanni, Barbara Ruozi, Daniela Belletti, Antonietta Vilella, Michele Zoli, Maria Angela Vandelli, and F.F., 2013. Brain-targeted polymeric nanoparticles: in vivo evidences of different routes of administration in rodents. *Nanomedicine*, 8, pp.1373–1383.

Tosi, G. et al., 2005. Conjugated poly(D,L-lactide-co-glycolide) for the preparation of in vivo detectable nanoparticles. *Biomaterials*, 26(19), pp.4189–95. Available at: http://www.ncbi.nlm.nih.gov/pubmed/15664646 [Accessed December 2, 2016].

Tosi, G. et al., 2014. Insight on the fate of CNS-targeted nanoparticles. Part II: Intercellular neuronal cell-to-cell transport. *Journal of Controlled Release*, 177, pp.96–107. Available at: http://www.ncbi.nlm.nih.gov/pubmed/24417968 [Accessed December 2, 2016].

Tosi, G. et al., 2011. Investigation on mechanisms of glycopeptide nanoparticles for drug delivery across the blood-brain barrier. *Nanomedicine (London, England)*, 6(3), pp.423–36. Available at: http://www.futuremedicine.com/doi/10.2217/nnm.11.11 [Accessed December 2, 2016].

Tosi, G. et al., 2011. NIR-labeled nanoparticles engineered for brain targeting: in vivo optical imaging application and fluorescent microscopy evidences. *Journal of Neural Transmission*, 118(1), pp.145–153. Available at: http://www.ncbi.nlm.nih.gov/pubmed/20931242 [Accessed December 2, 2016].

Tosi, G. et al., 2008. Polymeric nanoparticles for the drug delivery to the central nervous system. *Expert opinion on drug delivery*, 5(2), pp.155–174.

Tosi, G. et al., 2007. Targeting the central nervous system: In vivo experiments with peptide-derivatized nanoparticles loaded with Loperamide and Rhodamine-123. *Journal of Controlled Release*, 122(1), pp.1–9.

Tosi, G., Ruozi, B. & Belletti, D., 2012. Nanomedicine: the future for advancing medicine and neuroscience. *Nanomedicine*, 7(8), pp.1113–1116. Available at: http://www.futuremedicine.com/doi/10.2217/nnm.12.90 [Accessed December 2, 2016].

Trager, U. et al., 2014. Characterisation of immune cell function in fragment and full-length Huntington's disease mouse models. *Neurobiol Dis*, 73C, pp.388–398. Available at: http://www.ncbi.nlm.nih.gov/pubmed/25447230.

Trushina, E. et al., 2006. Mutant huntingtin inhibits clathrin-independent endocytosis and causes accumulation of cholesterol in vitro and in vivo. *Human Molecular Genetics*, 15(24), pp.3578–3591. Available at: http://www.hmg.oxfordjournals.org/cgi/doi/10.1093/hmg/ddl434 [Accessed November 11, 2016].

Turmaine, M. et al., 2000. Nonapoptotic neurodegeneration in a transgenic mouse model of Huntington's disease. *Proc Nat Acad Sci Usa*, 97(14), pp.8093–8097.

Valenza, M. et al., 2007. Cholesterol biosynthesis pathway is disturbed in YAC128 mice and is modulated by huntingtin mutation. *Human Molecular Genetics*, 16(18), pp.2187–2198. Available at: http://www.hmg.oxfordjournals.org/cgi/doi/10.1093/hmg/ddm170 [Accessed November 11, 2016].

Valenza, M. et al., 2010. Cholesterol defect is marked across multiple rodent models of Huntington's disease and is manifest in astrocytes. *The Journal of neuroscience : the official journal of the Society for Neuroscience*, 30(32), pp.10844–50. Available at: http://www.pubmedcentral.nih.gov/articlerender.fcgi?artid=3842469&tool=pmcentrez&rendertype=abstract.

Valenza, M. et al., 2015. Disruption of astrocyte-neuron cholesterol cross talk affects neuronal function in Huntington's disease. *Cell Death and Differentiation*, 22(4), pp.690–702. Available at: http://www.nature.com/doifinder/10.1038/cdd.2014.162 [Accessed November 14, 2016].

Valenza, M. et al., 2005. Dysfunction of the cholesterol biosynthetic pathway in Huntington's disease. *The Journal of neuroscience : the official journal of the Society for Neuroscience*, 25(43), pp.9932–9. Available at: http://www.jneurosci.org/content/25/43/9932.short.

Valenza, M. et al., 2007. Progressive dysfunction of the cholesterol biosynthesis pathway in the R6/2 mouse model of Huntington's disease. *Neurobiology of Disease*, 28(1), pp.133–142. Available at: http://linkinghub.elsevier.com/retrieve/pii/S096999610700143X [Accessed November 11, 2016].

van Woensel, M. et al. Formulations for Intranasal Delivery of Pharmacological Agents to Combat Brain Disease: A New Opportunity to Tackle GBM? Cancers (Basel). 5, 1020–48 (2013).

Vanier, M.T. & Millat, G., 2003. Niemann-Pick disease type C. *Clinical genetics*, 64(4), pp.269–81. Available at: http://www.ncbi.nlm.nih.gov/pubmed/12974729 [Accessed November 14, 2016].

Vaughan, A.M. & Oram, J.F., 2006. ABCA1 and ABCG1 or ABCG4 act sequentially to remove cellular cholesterol and generate cholesterol-rich HDL. *The Journal of Lipid Research*, 47(11), pp.2433–2443. Available at: http://www.jlr.org/cgi/doi/10.1194/jlr.M600218-JLR200 [Accessed November 6, 2016].

Velier, J. et al., 1998. Wild-type and mutant huntingtins function in vesicle trafficking in the secretory and endocytic pathways. *Experimental neurology*, 152(1), pp.34–40.

Vergoni, A.V. et al., 2009. Nanoparticles as drug delivery agents specific for CNS: in vivo biodistribution. *Nanomedicine: Nanotechnology, Biology, and Medicine*, 5(4), pp.369–377.

Verheijen, M.H.G. et al., 2009. SCAP is required for timely and proper myelin membrane synthesis. *Proceedings of the National Academy of Sciences*, 106(50), pp.21383–21388. Available at: http://www.pnas.org/lookup/doi/10.1073/pnas.0905633106 [Accessed November

6, 2016].

Vilella, A. et al., 2014. Insight on the fate of CNS-targeted nanoparticles. Part I: Rab5-dependent cell-specific uptake and distribution. *Journal of Controlled Release*, 174, pp.195–201. Available at: http://www.ncbi.nlm.nih.gov/pubmed/24316476 [Accessed December 2, 2016].

Vinogradov, S. V., Bronich, T.K. & Kabanov, A. V., 2002. Nanosized cationic hydrogels for drug delivery: Preparation, properties and interactions with cells. *Advanced Drug Delivery Reviews*, 54(1), pp.135–147.

Vitali, C., Wellington, C.L. & Calabresi, L., 2014. HDL and cholesterol handling in the brain. *Cardiovascular Research*, 103(3), pp.405–413.

Vonsattel, J.P. et al., 1985. Neuropathological classification of Huntington's disease. *Journal of neuropathology and experimental neurology*, 44(6), pp.559–77. Available at: http://www.ncbi.nlm.nih.gov/pubmed/2932539 [Accessed November 2, 2016].

Vonsattel, J.P. & DiFiglia, M., 1998. Huntington disease. *Journal of neuropathology and experimental neurology*, 57(5), pp.369–84. Available at: http://www.ncbi.nlm.nih.gov/pubmed/9596408 [Accessed November 2, 2016].

Vonsattel, J.P.G., Keller, C. & Pilar Amaya, M. del, 2008. Neuropathology of Huntington's Disease. In pp. 599–618. Available at: http://linkinghub.elsevier.com/retrieve/pii/S0072975207012560 [Accessed November 2, 2016].

Waelter, S. et al., 2001. The huntingtin interacting protein HIP1 is a clathrin and alpha-adaptin-binding protein involved in receptor-mediated endocytosis. *Hum.Mol.Genet.*, 10(17), pp.1807–1817.

Wahrle, S.E. et al., 2004. ABCA1 Is Required for Normal Central Nervous System ApoE Levels and for Lipidation of Astrocyte-secreted apoE. *Journal of Biological Chemistry*, 279(39), pp.40987–40993. Available at: http://www.jbc.org/lookup/doi/10.1074/jbc.M407963200 [Accessed November 6, 2016].

Wahrle, S.E. et al., 2005. Deletion of Abca1 increases Abeta deposition in the PDAPP transgenic mouse model of Alzheimer disease. *The Journal of biological chemistry*, 280(52), pp.43236–42. Available at: http://www.ncbi.nlm.nih.gov/pubmed/16207708 [Accessed November 14, 2016].

Wahrle, S.E. et al., 2008. Overexpression of ABCA1 reduces amyloid deposition in the PDAPP mouse model of Alzheimer disease. *Journal of Clinical Investigation*. Available at: http://content.the-jci.org/articles/view/33622 [Accessed November 14, 2016].

Walker, A.G. et al., 2008. Altered information processing in the prefrontal cortex of Huntington's

disease mouse models. *The Journal of neuroscience : the official journal of the Society for Neuroscience*, 28(36), pp.8973–82. Available at: http://www.pubmedcentral.nih.gov/articlerender.fcgi?artid=2597399&tool=pmcentrez&rendertype=abstract.

Walter, B.A. et al., 2006. The olfactory route for cerebrospinal fluid drainage into the peripheral lymphatic system. *Neuropathology and Applied Neurobiology*, 32(4), pp.388–396. Available at: http://www.ncbi.nlm.nih.gov/pubmed/16866984 [Accessed December 2, 2016].

Wang, R. et al., 2014. Metabolic and hormonal signatures in pre-manifest and manifest Huntington's disease patients. *Frontiers in physiology*, 5, p.231. Available at: http://www.ncbi.nlm.nih.gov/pubmed/25002850 [Accessed November 13, 2016].

Watkins, L.H. et al., 2000. Impaired planning but intact decision making in early Huntington's disease: implications for specific fronto-striatal pathology. *Neuropsychologia*, 38(8), pp.1112–25. Available at: http://www.ncbi.nlm.nih.gov/pubmed/10838146 [Accessed November 2, 2016].

Weller, R.O., Kida, S. & Zhang, E.T., 1992. Pathways of fluid drainage from the brain--morphological aspects and immunological significance in rat and man. *Brain pathology (Zurich, Switzerland)*, 2(4), pp.277–284.

Wellington, C.L. et al., 2002. ABCA1 mRNA and protein distribution patterns predict multiple different roles and levels of regulation. *Laboratory investigation; a journal of technical methods and pathology*, 82(3), pp.273–83. Available at: http://www.ncbi.nlm.nih.gov/pubmed/11896206 [Accessed November 6, 2016].

Wexler, N.S. et al., 1987. Homozygotes for Huntington's disease. *Nature*, 326(6109), pp.194–7. Available at: http://dx.doi.org/10.1038/326194a0.

Wheelock, V.L. et al., 2003. Predictors of nursing home placement in Huntington disease. *Neurology*, 60(6), pp.998–1001. Available at: http://www.ncbi.nlm.nih.gov/pubmed/12654967 [Accessed November 2, 2016].

White, J.K. et al., 1997. Huntingtin is required for neurogenesis and is not impaired by the Huntington's disease CAG expansion. *Nature genetics*, 17(4), pp.404–10. Available at: http://dx.doi.org/10.1038/ng1297-404.

Whitman, M.C. & Greer, C.A., 2009. Adult neurogenesis and the olfactory system. *Progress in Neurobiology*, 89(2), pp.162–175.

Wong, Y.C. & Holzbaur, E.L.F., 2014. The Regulation of Autophagosome Dynamics by Huntingtin and HAP1 Is Disrupted by Expression of Mutant Huntingtin, Leading to Defective Cargo Degradation. *Journal of Neuroscience*, 34(4), pp.1293–1305. Available at:

http://www.ncbi.nlm.nih.gov/pubmed/24453320 [Accessed December 28, 2016].

Wong, Y.C. & Holzbaur, E.L.F., 2014. The regulation of autophagosome dynamics by huntingtin and HAP1 is disrupted by expression of mutant huntingtin, leading to defective cargo degradation. *The Journal of neuroscience : the official journal of the Society for Neuroscience*, 34(4), pp.1293–305. Available at: http://www.pubmedcentral.nih.gov/articlerender.fcgi?artid=3898289&tool=pmcentrez&rendertype=abstract.

Ye, J. & DeBose-Boyd, R.A., 2011. Regulation of Cholesterol and Fatty Acid Synthesis. *Cold Spring Harbor Perspectives in Biology*, 3(7), pp.a004754–a004754. Available at: http://cshperspectives.cshlp.org/lookup/doi/10.1101/cshperspect.a004754 [Accessed November 7, 2016].

Yeagle, P.L., 1985. Cholesterol and the cell membrane. *Biochimica et biophysica acta*, 822(3–4), pp.267–87. Available at: http://www.ncbi.nlm.nih.gov/pubmed/3904832 [Accessed November 9, 2016].

Yoffey, J.M. & Drinker, C.K., 1938. THE LYMPHATIC PATHWAY FROM THE NOSE AND PHARYNX : THE ABSORPTION OF DYES. *The Journal of experimental medicine*, 68(4), pp.629–40. Available at: http://www.ncbi.nlm.nih.gov/pubmed/19870807 [Accessed December 2, 2016].

Yohrling IV, G.J. et al., 2002. Inhibition of tryptophan hydroxylase activity and decreased 5-HT1A receptor binding in a mouse model of Huntington's disease. *Journal of neurochemistry*, 82(6), pp.1416–23. Available at: http://www.ncbi.nlm.nih.gov/pubmed/12354289 [Accessed November 21, 2016].

Yoo, J.Y. et al., 2005. Characterization of degradation behavior for PLGA in various pH condition by simple liquid chromatography method. *Bio-medical materials and engineering*, 15(4), pp.279–88. Available at: http://www.ncbi.nlm.nih.gov/pubmed/16010036.

Young, A.B. et al., 1988. NMDA receptor losses in putamen from patients with Huntington's disease. *Science (New York, N.Y.)*, 241(4868), pp.981–3. Available at: http://www.ncbi.nlm.nih.gov/pubmed/2841762 [Accessed November 2, 2016].

Zakzanis, K.K., 1998. The Subcortical Dementia of Huntington's Disease. *Journal of Clinical and Experimental Neuropsychology (Neuropsychology, Development and Cognition: Section A)*, 20(4), pp.565–578. Available at: http://www.tandfonline.com/doi/abs/10.1076/jcen.20.4.565.1468 [Accessed November 2, 2016].

Zala, D. et al., 2013. Huntingtin's Function in Axonal Transport Is Conserved in Drosophila

melanogaster A. Bergmann, ed. *PLoS ONE*, 8(3), p.e60162. Available at: http://dx.plos.org/10.1371/journal.pone.0060162 [Accessed December 28, 2016].

Zeitlin, S. et al., 1995. Increased apoptosis and early embryonic lethality in mice nullizygous for the Huntington's disease gene homologue. *Nature Genetics*, 11, pp.155–163.

Zelcer, N. et al., 2009. LXR regulates cholesterol uptake through Idol-dependent ubiquitination of the LDL receptor. *Science (New York, N.Y.)*, 325(5936), pp.100–4. Available at: http://www.pubmedcentral.nih.gov/articlerender.fcgi?artid=2777523&tool=pmcentrez&rendertype=abstract.

Zhai, W. et al., 2005. In vitro analysis of huntingtin-mediated transcriptional repression reveals multiple transcription factor targets. *Cell*, 123(7), pp.1241–1253.

Zhang, Y. et al., 2003. Depletion of wild-type huntingtin in mouse models of neurologic diseases. *Journal of Neurochemistry*, 87(1), pp.101–106.

Zhao, C. & Dahlman-Wright, K., 2010. Liver X receptor in cholesterol metabolism. *Journal of Endocrinology*, 204(3), pp.233–240.

Zimmerberg, J. & Kozlov, M.M., 2006. How proteins produce cellular membrane curvature. *Nature reviews. Molecular cell biology*, 7(1), pp.9–19. Available at: http://www.ncbi.nlm.nih.gov/pubmed/16365634.

Zuccato, C. et al., 2003. Huntingtin interacts with REST/NRSF to modulate the transcription of NRSE-controlled neuronal genes. *Nature Genetics*, 35(1), pp.76–83. Available at: http://www.ncbi.nlm.nih.gov/pubmed/12881722 [Accessed December 19, 2016].

Zuccato, C. et al., 2001. Loss of huntingtin-mediated BDNF gene transcription in Huntington's disease. *Science*, 293(5529), pp.493–498.

Zuccato, C. et al., 2008. Systematic assessment of BDNF and its receptor levels in human cortices affected by Huntington's disease. *Brain Pathology*, 18(2), pp.225–238.

Zuccato, C. et al., 2007. Widespread Disruption of Repressor Element-1 Silencing Transcription Factor/Neuron-Restrictive Silencer Factor Occupancy at Its Target Genes in Huntington's Disease. *Journal of Neuroscience*, 27(26), pp.6972–6983. Available at: http://www.ncbi.nlm.nih.gov/pubmed/17596446 [Accessed December 19, 2016].

Zuccato, C. & Cattaneo, E., 2009. Brain-derived neurotrophic factor in neurodegenerative diseases. *Nature reviews. Neurology*, 5(6), pp.311–322. Available at: http://dx.doi.org/10.1038/nrneurol.2009.54.

Zuccato, C. & Cattaneo, E., 2007. Role of brain-derived neurotrophic factor in Huntington's disease. *Prog Neurobiol*, 81(5–6), pp.294–330. Available at: http://www.ncbi.nlm.nih.gov/pubmed/17379385.

Zuccato, C., Valenza, M. & Cattaneo, E., 2010. Molecular Mechanisms and Potential Therapeutical Targets in Huntington ' s Disease. *Physiol Rev*, 90(3), pp.905–981.

Zucker, B. et al., 2005. Transcriptional dysregulation in striatal projection- and interneurons in a mouse model of Huntington's disease: neuronal selectivity and potential neuroprotective role of HAP1. *Human molecular genetics*, 14(2), pp.179–89. Available at: http://www.ncbi.nlm.nih.gov/pubmed/15548548 [Accessed November 21, 2016].

Zwain, I.H. & Yen, S.S.C., 1999. Neurosteroidogenesis in astrocytes, oligodendrocytes, and neurons of cerebral cortex of rat brain. *Endocrinology*, 140(8), pp.3843–3852.

Published papers

Neurobiology of Disease 98 (2017) 66–76

Contents lists available at ScienceDirect

Neurobiology of Disease

journal homepage: www.elsevier.com/locate/ynbdi

Early and brain region-specific decrease of *de novo* cholesterol biosynthesis in Huntington's disease: A cross-validation study in Q175 knock-in mice

Mahalakshmi Shankaran [a], Eleonora Di Paolo [b], Valerio Leoni [c,d], Claudio Caccia [c], Costanza Ferrari Bardile [b], Hussein Mohammed [a], Stefano Di Donato [c,1], Seung Kwak [e], Deanna Marchionini [e], Scott Turner [a], Elena Cattaneo [b,*], Marta Valenza [b,*]

[a] *KineMed Inc., Emeryville, CA 94608, USA*
[b] *Department of BioSciences and Centre for Stem Cell Research, Università degli Studi di Milano, 20122 Milan, Italy*
[c] *Neurological Institute C. Besta, 20133 Milan, Italy*
[d] *Laboratory of Clinical Chemistry, Hospital of Varese, 21010 Varese, Italy*
[e] *CHDI Management/CHDI Foundation, 350 Seventh Ave, Suite 200, New York, NY 10001, USA*

ARTICLE INFO

Article history:
Received 30 September 2016
Revised 21 November 2016
Accepted 26 November 2016
Available online 30 November 2016

Keywords:
Huntington
Brain cholesterol
Lathosterol
Striatum

ABSTRACT

Cholesterol precursors and cholesterol levels are reduced in brain regions of Huntington's disease (HD) mice. Here we quantified the rate of *in vivo de novo* cholesterol biosynthesis in the HD brain. Samples from different brain regions and blood of the heterozygous knock-in mouse model carrying 175 CAG repeats (Q175) at different phenotypic stages were processed independently by two research units to quantify cholesterol synthesis rate by ^2H_2O labeling and measure the concentrations of lathosterol, cholesterol and its brain-specific cholesterol catabolite 24-hydroxy-cholesterol (24OHC) by isotope dilution mass spectrometry. The daily synthesis rate of cholesterol and the corresponding concentration of lathosterol were significantly reduced in the striatum of heterozygous Q175 mice early in the disease course. We also report that the decrease in lathosterol was inversely correlated with CAG-size at symptomatic stage, as observed in striatal samples from an allelic series of HD mice. There was also a significant correlation between the fractional synthesis rates of total cholesterol and 24OHC in brain of wild-type (WT) and Q175 mice, supporting the evidence that plasma 24OHC may reflect cholesterol synthesis in the adult brain. This comprehensive analysis demonstrates consistent cholesterol biosynthesis defects in HD mouse models and suggests that plasma 24OHC may serve as a biomarker of brain cholesterol metabolism.
© 2016 Published by Elsevier Inc.

1. Introduction

Huntington's disease (HD) is a progressive neurodegenerative disorder clinically characterized by cognitive, psychiatric and motor disturbances (Bates et al., 2015). It is caused by a CAG repeat expansion in the huntingtin (htt) gene that encodes for polyglutamine. The number of CAG repeats in htt is inversely correlated with age at symptomatic onset in HD, with variable age-dependent penetrance between 36 and 39 CAG repeats, but full penetrance at 40 or more repeats (Ross et al., 2014).

Since the discovery of the HD mutation, findings from cell and animal models have highlighted mechanisms and pathways altered in HD and have provided insights into HD pathogenesis and progression. However, there is no single model that recapitulates the full spectrum of disease pathophysiology, requiring one to select the best model dependent on the biological question of interest. On the other hand, when specific alterations are consistently observed across different models, and meet the genetic relationship of polymorphic CAG extension *vs* phenotypic onset, then such alterations may have higher relevance and highlight mechanisms more proximal to the HD mutation.

There is a wealth of data showing that brain cholesterol metabolism is affected in HD models (Valenza et al., 2005; Valenza et al., 2007b; Valenza et al., 2007a; Valenza et al., 2010; Valenza et al., 2015a). Analytical approaches based on isotope dilution mass spectrometry, in combination with other biochemical and molecular analyses, have shown that cholesterol precursors are reduced in the brain of five HD rodent models before the onset of motor defects, and cholesterol content is decreased at later time points (Valenza et al., 2007a; Valenza et al., 2010).

* Corresponding authors at: Laboratory of Stem Cell Biology, and Pharmacology of Neurodegenerative Diseases, Department of Biosciences - University of Milan, INGM Foundation - Padiglione Invernizzi, Via Francesco Sforza 35, 20122 Milano, Italy.
E-mail addresses: elena.cattaneo@unimi.it (E. Cattaneo), marta.valenza@unimi.it (M. Valenza).
[1] Deceased on 12 November 2015.
Available online on ScienceDirect (www.sciencedirect.com).

http://dx.doi.org/10.1016/j.nbd.2016.11.013
0969-9961/© 2016 Published by Elsevier Inc.

Cholesterol homeostasis may also be affected in HD patients early in the disease as the reduced levels of plasma 24-hydroxycholesterol (24OHC), the brain-specific catabolite of cholesterol, parallels the large decrease in caudate volume in gene-positive subjects from pre-manifest to HD stage (Leoni et al., 2008; Leoni et al., 2013). This suggests that cholesterol dysfunction may be linked to the HD mutation and might be relevant in the disease pathogenesis. First, a quarter of the cholesterol in humans is found in the brain and is produced locally because the blood-brain barrier (BBB) prevents its uptake from circulation (Dietschy and Turley, 2004). Secondly, although the rate of cholesterol synthesis decreases after myelination (Dietschy, 1984; Jurevics and Morell, 1995), the very small amount produced by everyday cholesterol synthesis in adulthood plays a role in neuronal function (Camargo et al., 2009). Third, the half-life of brain cholesterol is estimated to 5 years in humans (Bjorkhem et al., 1998; Saher and Simons, 2010), consistent with a late-onset disease. Fourth, to develop and maintain synapses, neurons have a high demand of cholesterol, which is supplied by astrocytes (Mauch et al., 2001; Valenza et al., 2007b; Nieweg et al., 2009; Valenza et al., 2015a). Finally, first attempts at delivering cholesterol (Valenza et al., 2015b) or at modulating cholesterol catabolism (Boussicault et al., 2016) in the mouse HD brain have been proven be beneficial. However, to date there are no direct measurements of cholesterol biosynthesis in the adult mouse HD brain and evidence of *CAG* length–dependence is missing.

Here we performed a cross-validation study aimed at measuring cholesterol biosynthesis *in vivo* in the adult mouse brain by independent methods. The tissue concentration of the cholesterol precursor, lathosterol, was compared to the fractional synthesis rate of cholesterol, and brain and plasma 24OHC measured by isotope labeling with deuterated water (Lee et al., 1994) the measures of cholesterol synthesis were then compared to the concentration of cholesterol and brain and plasma 24OHC, determined by isotope dilution mass spectrometry (Cohen et al., 1980). Control and heterozygous knock-in mice carrying 175 CAG repeats (herein referred as Q175; (Menalled et al., 2012) as well as mice carrying 20, 80, 111 CAG repeats were included in the study. The Q175 mouse model exhibits progressive and early-onset HD-related alterations, while the shorter repeat genotypes develop symptoms late in life or not at all; these mice enabled us to test whether any of the parameters measured were CAG dependent at different stages of disease. Additionally, we investigated whether the fraction of newly synthesized cholesterol, which is metabolized into 24OHC and can be measured in the blood, faithfully represents newly synthesized cholesterol in the brain, thus making this measurement potentially useful as a clinical biomarker for CNS cholesterol biosynthesis.

2. Material and methods

2.1. Deuterated water labeling and tissue collection in c57bl/6 mice

For deuterated water labeling, 4-months old animals received a priming intraperitoneal (i.p.) bolus of 49 mL/kg 0.9% NaCl in 99.9% ^2H_2O and were maintained on 8% ^2H_2O in drinking water for two weeks until sacrifice. This regimen results in steady state values of about 5% excess ^2H enrichment of body water. At the end of the labeling period, mice were euthanized and blood drawn by cardiac puncture. Samples from 5 mice were pooled and centrifuged to separate plasma and stored at −80 °C. Brain was removed and dissected into striatum, cortex and cerebellum and frozen on dry ice. Samples from 5 mice were pooled by brain region and stored at −80 °C.

2.2. Deuterated water labeling and tissue collection in WT and Q175 mice

Given that homozygosity is very rare in humans, all the analyses were performed in the heterozygous Q175 mice. Striatum, cortex, cerebellum, and blood from all animals have been provided by PsychoGenics (USA). 5 weeks old animals were labeled with ^2H_2O for one week whereas 6-months and 12-months old mice were labeled for two weeks with ^2H_2O as described above. Animals were food deprived for 4 h and perfused with saline prior to tissue collection. The number of hemizygous and age-matched WT littermates used for the experiments were indicated in the figure legends.

2.3. Myelin isolation

Individual brain region from 20 mice (tissue from 5 mice were pooled per sample for n = 4 samples per group) was weighed and homogenized with tissue homogenizer (Fastprep®24-MP Biomedical) in 10 mL of 30% sucrose solution. 10 mL of 10% sucrose solution was layered over 10 mL of brain homogenate in polycarbonate ultracentrifuge tube and centrifuged at 25000RPM for 30 min in SW-17 rotor. The myelin layer at the interface of the two sucrose solutions was collected with a Pasteur pipette and the pellet constituted the 'myelin-depleted fraction'. The procedure was repeated twice to further deplete the pellet of myelin by resolubilizing the pellet with 2.5 mL of 30% sucrose and layering with 1.9 mL of 10% sucrose solution in 4 mL tubes. The tubes were centrifuged at 2500RPM for 30 min in Ti 50.4 and the myelin at the interface was extracted with 2 mL pasture pipette. For further purification of isolated myelin, the combined myelin extract washed with water (1:1, v/v), resuspended in 2.5 mL of 30% sucrose solution and layered with 1.9 mL of 10% sucrose. The tubes were centrifuged at 25000RPM for 30 min in Ti50.4 rotor, the myelin at the interface of the two solutions removed and washed with water. The purified myelin and the myelin-depleted fraction were reconstituted in 500ul of water and stored at −20 °C.

2.4. Brain sterols (lathosterol, desmosterol cholesterol and 24OHC) synthesis rates

Lipid was extracted in 2:1 chloroform methanol from myelin-enriched and myelin-depleted fractions of each brain region. 125 μg of butylated hydroxytoluene (BHT) was added to 75 μL lipid extract and alkaline hydrolysis was performed with 2 mL of NaOH in 90% ethanol for 2 h at 50 °C. The sterols were extracted three times with 4 mL of cyclohexane and evaporated under stream of nitrogen. The dried sample was acetylated for subsequent analysis by GC/MS as described previously (Lee et al., 1994) on an Agilent Technologies GC6890N equipped with DB-17MS column (30 m × 0.25 mm × 0.25 μm) and 5973 N mass detector operated in selected ion-monitoring mode. The selected ions corresponding to M0 & M1 mass isotopomers for cholesterol were *m/z* 368 and 369, for 24OHC were *m/z* 426 and 427, for lathosterol were *m/z* 428 and 429, and for desmosterol were *m/z* 366 and 367. For each analyte, fractional synthesis was calculated as described below.

2.5. Calculation of fractional synthesis

Cholesterol and 24OHC synthesis rate are expressed as fractional synthesis (%) over the duration of label. The fractional synthesis (f) was calculated on the basis of the precursor-product, or rise-to-plateau, approach, $f = EM1/A^{\infty}$, where EM1 represents the mass + 1-labeled species in excess of natural abundance, and A^{∞} represents the theoretical plateau or asymptotic value for fully labeled moiety. The theoretical plateau or asymptotic value A^{∞} during ^2H_2O labeling was determined by mass isotomer distribution analysis (MIDA) of the combinatorial labeling pattern based on precursor 2H–enrichment (Hellerstein and Neese, 1992). When the duration of label was different for different age-groups, data for cholesterol and 24OHC are represented as synthesis rate per day, calculated as $-\ln(1-f)/t$, where (f) is fractional synthesis and (t) the duration in days of label.

2.6. Plasma 24OHC and cholesterol synthesis rates

For analysis of cholesterol, 125 μg of BHT added to 1.5 mL plasma (pooled from 5 mice per sample in the same manner as for brain tissues) and hydrolyzed with 2 mL of 1 M NaOH in 90% ethanol for 2 h at 50 °C. 1 mL of water added and the unsaponiable part was extracted three times with 4 mL of cyclohexane. The combined top organic phase was dried with stream of nitrogen. For analysis of 24-hydroxy cholesterol, the lipid extract were dissolved in 2 mL of toluene and loaded to 500 mg/3 mL strata Sl-1 SPE column (Phenomenex) preconditioned with methanol and hexane. The column was washed with hexane, cholesterol was eluted with 0.5% isopropanol in hexane, and 24-hydroxy sterol and other oxysterols were eluted with 30% isopropanol in hexane. Each fraction was dried under stream of nitrogen and acetylated for subsequent analysis by GC/MS as described above.

2.7. Isotope dilution mass spectrometry

Tissue homogenates were prepared in PBS. The weight of each sample was used to normalize raw data. Fifty microliters of homogenates were added to a screw-capped vial sealed with a Teflon-lined septum, together with 100 ng of 5a–cholest-7-en-3b-ol-1,2,5a,6a-d4 (D4-lathosterol; CDN Isotopes), 200 ng of D324S–hydroxycholesterol, and 5 μg of (D6) cholesterol internal standards. To prevent self-oxidation, 25 μL of butylated hydroxytoluene (BHT) (5 g/L) and 25 μL of EDTA (10 g/L) were added to each vial, and argon was flushed through to remove air. Alkaline hydrolysis was allowed to proceed at room temperature (22 °C) for 1 h in the presence of 1 M ethanolic potassium hydroxide solution under magnetic stirring. After hydrolysis, the neutral sterols (cholesterol, lathosterol, lanosterol and desmosterol; herein only lathosterol has been shown and oxysterol (24OHC) were extracted three times with 5 mL of cyclohexane. The organic solvents were evaporated under a gentle stream of argon, and converted into trimethylsilyl ethers with *N,O-Bis*(trimethylsilyl)trifluoroacetamide (BSTFA) at 70 °C for 30 min. Gas chromatography–mass spectrometry (GC–MS) to quantify single components was performed as described by Valenza et al. (2007a, 2007b).

2.8. Western blot analysis

Protein lysates from a small aliquot (2 μL) of the same homogenates used for *in vivo* labeling studies were prepared by adding 50 μL of RIPA buffer supplemented with PMSF (1:250; Sigma-Aldrich) and protease inhibitors (1:100; Sigma-Aldrich). Proteins were separated by SDS-polyacrylamide gel electrophoresis and then transferred to a nitrocellulose membrane using a Trans-Blot Turbo System (Bio-Rad). The membranes were next probed with mouse *anti*-MBP (1:500; Chemicon), mouse anti-SNAP25 (1:1000; Becton Dickinson), mouse anti-GFAP (1:500; Becton Dickinson) and mouse anti-α-tubulin (1:5000; Sigma-Aldrich), followed by washing, and probing with horseradish peroxidase-conjugated secondary antibodies (1:3000; Bio-Rad). Bands were visualized with enhanced chemoluminescence (Pierce) and imaged with the ChemiDoc MP Imaging System (Bio-Rad).

2.9. Real time PCR

Total RNA from tissues was isolated with TRIzol Reagent (Life Technologies). Total RNA (0.5 μg) was reverse-transcribed to single-stranded cDNA using the iScript cDNA synthesis kit (Bio-Rad). For each reverse-transcribed product, three real-time PCR analyses were performed in duplicate for each of the analyzed genes. Real time PCR was performed on an iCycler Thermal Cycler with a Multicolor Real-time PCR Detection System (Bio-Rad) using TaqMan 2× Master Mix (Bio-Rad). Taqman primer/probe sets were designed in collaboration with Bio-Rad technical service and are available upon request. Relative gene expression was determined using ΔΔCt method, normalizing to b-actin and Gapdh.

2.10. Statistics

No statistical methods were used to predetermine sample sizes. Data were expressed as mean ± S.E. M or ± S.D. as indicated. Statistical analysis was performed by two-tail Student's *t*-test, one-way ANOVA with Newman–Keuls Multiple Comparison post-hoc test or two-way ANOVA with Holm-Sidak's multiple comparison test, as indicated. Normality of the data was assessed using the Shapiro-Wilk test. Differences for which p was <0.05 were considered to be significant.

3. Results

3.1. Cholesterol, lathosterol and 24-hydroxycholesterol synthesis rates in wild-type mice

To determine the fractional synthetic rate of cholesterol, we utilized *in vivo* stable isotope labeling and Isotope Dilution mass spectrometry (ID/MS) analysis (Lee et al., 1994). Male mice were labeled with deuterated water (8% ^2H_2O) for 2 weeks added in the drinking water (see material and methods). Deuterium incorporated into newly made cholesterol and the ^2H enrichment in cholesterol and its precursor, lathosterol, as well its catabolite, 24OHC, were measured by mass spectrometry. Since labeled water freely and rapidly penetrates all tissues in the body and deuterium enrichments can be easily maintained at a constant level for days or weeks, the synthesis rate of very slowly turning over pools of cholesterol can be accurately determined.

Cholesterol biosynthesis rates were first measured in 4-month-old littermate wild-type (WT) mice. We purified myelin-enriched and myelin-depleted fractions (Zoller et al., 2008) from striatum, cortex and cerebellum of the labeled mice to characterize the contribution of *de novo* cholesterol synthesis in these two potentially distinct pools of cholesterol in the brain. To check for the efficiency of purification, we measured the levels of MBP (a marker of myelin), GFAP (a marker of astrocytes, which are regarded as the cells that produce most of the cholesterol in the adult brain; (Mauch et al., 2001)) and SNAP25 (a marker of neurons) in myelin-depleted and myelin-enriched fractions. Both preparations contained neuronal cells and astrocytes (as detected by SNAP25 and GFAP, respectively) but the myelin-depleted fractions were MBP negative, indicating that measures of cholesterol biosynthesis rates in myelin-depleted fractions had limited myelin contamination (Fig. 1A). Cholesterol synthesis rate, expressed as cholesterol fractional synthesis % for the duration of 2 weeks of label (see methods), was in general lower in myelin-enriched fractions compared to myelin-depleted fractions (Fig. 1B), consistent with the notion that myelin lipids turn over more slowly than other brain lipid pools (Aggarwal et al., 2011). In both fractions, cholesterol synthesis rate was highest in cortex with respect to striatum and the lowest rate of synthesis was found in cerebellum (Fig. 1B). The synthesis rate of lathosterol was also measured and found to be fully turned over in both myelin and myelin-depleted fractions in all brain regions (data not shown).

In order to maintain homeostasis in brain, cholesterol synthesis and degradation are equilibrated through its oxidation to 24OHC, which is catalyzed by cholesterol-24-hydroxylase (CYP46a1), a supposedly neuronal-specific enzyme prevalent in striatum and cortex (Lund et al., 1999; Ramirez et al., 2008). 24OHC, in contrast to cholesterol, crosses the blood-brain barrier (BBB) and is exported into the circulation to prevent excess accumulation of cholesterol in brain. The synthesis rate of 24OHC in the present study refers to the *de novo* synthesis of 24OHC from Acetyl CoA. Accordingly, the measure of ^2H enrichment in 24OHC reflects the proportion of newly synthesized cholesterol that was catabolized into 24OHC; this is based on the assumption that both non-labeled and labeled cholesterol contribute to 24OHC formation. If the enrichment in 24OHC and cholesterol in brain is equal, then the synthesis rate of 24OHC can be used as a surrogate for whole brain cholesterol synthesis ((Bjorkhem et al., 1998; Meaney et al., 2000). As shown in Fig. 1C, the 24OHC fractional synthesis in adult mice mirrored the

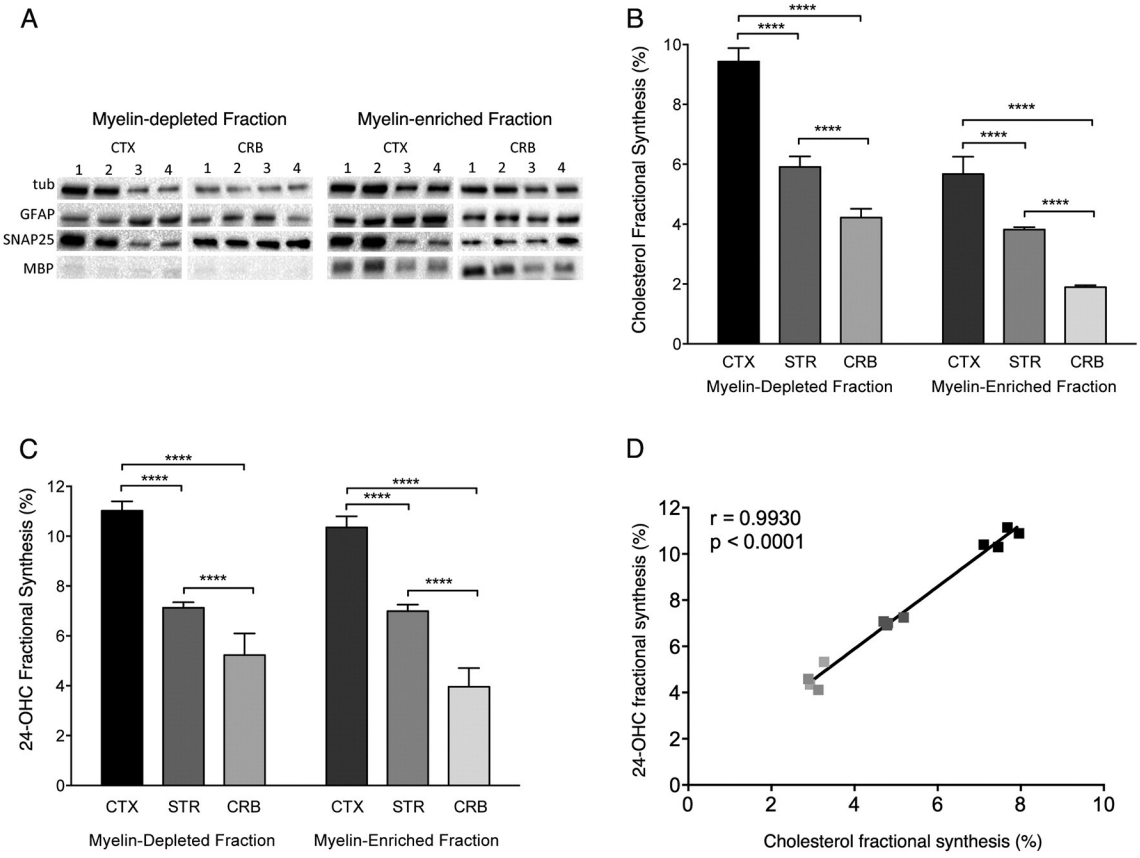

Fig. 1. Synthesis rate of brain cholesterol and 24OHC in c57bl/6 mice. (A) Representative western blot analysis for GFAP (marker of astrocytes), SNAP25 (marker of neurons) and MBP (marker of oligodendrocytes) in myelin-depleted and –enriched fractions purified from a subset of cortical and cerebellar samples, in which cholesterol biosynthesis rates were measured. Alpha-tubulin was used as loading control. (B–C) Synthesis rate of cholesterol (B), and 24OHC (C) in myelin-depleted (left) and in myelin-enriched fraction (right) from different brain regions (cortex, CTX; striatum, STR; cerebellum, CRB) in 4 month-old c57bl/6 mice. Synthesis rate is expressed as fractional synthesis % for the duration of 2 weeks of label. (D) Correlation between % new cholesterol and 24OHC synthesis in striatum of 4-month-old c57bl/6 mice. The values are the average of data obtained for myelin-enriched and myelin-depleted fractions by brain regions (black, CTX; dark grey, STR; grey, CRB) shown in Fig 1B and C. The graphs in (B, C) show the mean ± SD of fractional synthesis (%) of n = 4 samples per group, each sample was tissue pooled from 5 mice (all males). Statistics: 2-way ANOVA with post-hoc Holm-Sidak comparisons. ****$p < 0.0001$ for each brain region.

cholesterol fractional synthesis in all the brain regions tested both in myelin-enriched and myelin-depleted fractions, suggesting that 24OHC is formed from cholesterol locally and there is no bias toward conversion of newly made cholesterol into 24OHC. Cholesterol synthesis rate (Fig. 1B) and new cholesterol present in 24OHC (Fig. 1C) were also highly correlated as shown in Fig. 1D (values represent average of myelin and myelin-depleted fractions by brain region).

3.2. Cholesterol biosynthesis in the striatum of Q175 mice

The striatum is among the brain regions most affected in HD. Of note, the content of cholesterol in the striatum measured by mass spectrometry is the highest compared to other brain regions ((Runquist et al., 1995; Zhang et al., 1996; Dietschy and Turley, 2004) likely due to its richness in interconnections and synapses that require high cholesterol content. We first measured lathosterol content by isotopic dilution mass spectrometry in the striatum of WT and heterozygous Q175 mice during phenotype progression (n = 10 animals/genotype for each time point). As shown in Fig. 2A, lathosterol levels were significantly reduced in the striatum of Q175 mice since the age prior to motor deficits (5 weeks of age) with respect to WT mice, with the difference being more evident at ages with emerging motor deficits (25 weeks) and significant motor deficits (54 weeks). In agreement with what has already been reported for other HD mouse models (Valenza et al., 2007b; Valenza et al., 2007a; Valenza et al., 2010), our data here suggests that cholesterol precursor level is affected early in the Q175 mouse model.

To attribute decrease in precursor level to decreased cholesterol biosynthesis, we measured the *in vivo* cholesterol biosynthesis rate with deuterated water in the same mouse lines and at the same time points. We performed evaluations for both myelin-enriched and myelin-depleted fractions from different brain tissues of WT and Q175 mice. However, as the contribution of oligodendrocytes to cholesterol production in the adult brain is limited (Dietschy and Turley, 2004), we show data only from myelin-depleted fractions. As expected, lathosterol was completely turned over in both genotypes at all time points (data not shown). The cholesterol fractional synthesis rate, expressed as rate per day since mice of different ages had different durations of label (see methods) was reduced in the striatum of Q175 mice compared to WT mice at all ages examined, which were statistically significant at 25 and 54 weeks (10–18% reduction, Fig. 2B). Taken together, the reduced cholesterol concentration and fractional synthesis, suggest that the absolute production of cholesterol is reduced at early time points in the striatum of Q175 mice. Of note, in agreement with the notion that cholesterol biosynthesis is high during postnatal stage (up to 4 weeks of age) and low (albeit measurable) in the adult brain, we report that both lathosterol levels (Fig. 2A) and cholesterol synthesis rates (Fig. 2B) were highest in young mice but decreased in older mice, regardless of the genotype.

We next asked if reduced cholesterol synthesis rate might lead to a decrease in cholesterol content in the striatum of Q175 mice. In agreement with the literature (Jurevics and Morell, 1995; Dietschy and Turley, 2004), cholesterol levels increased steadily with age in the WT brain. In contrast, Q175 mice did not accumulate cholesterol in the

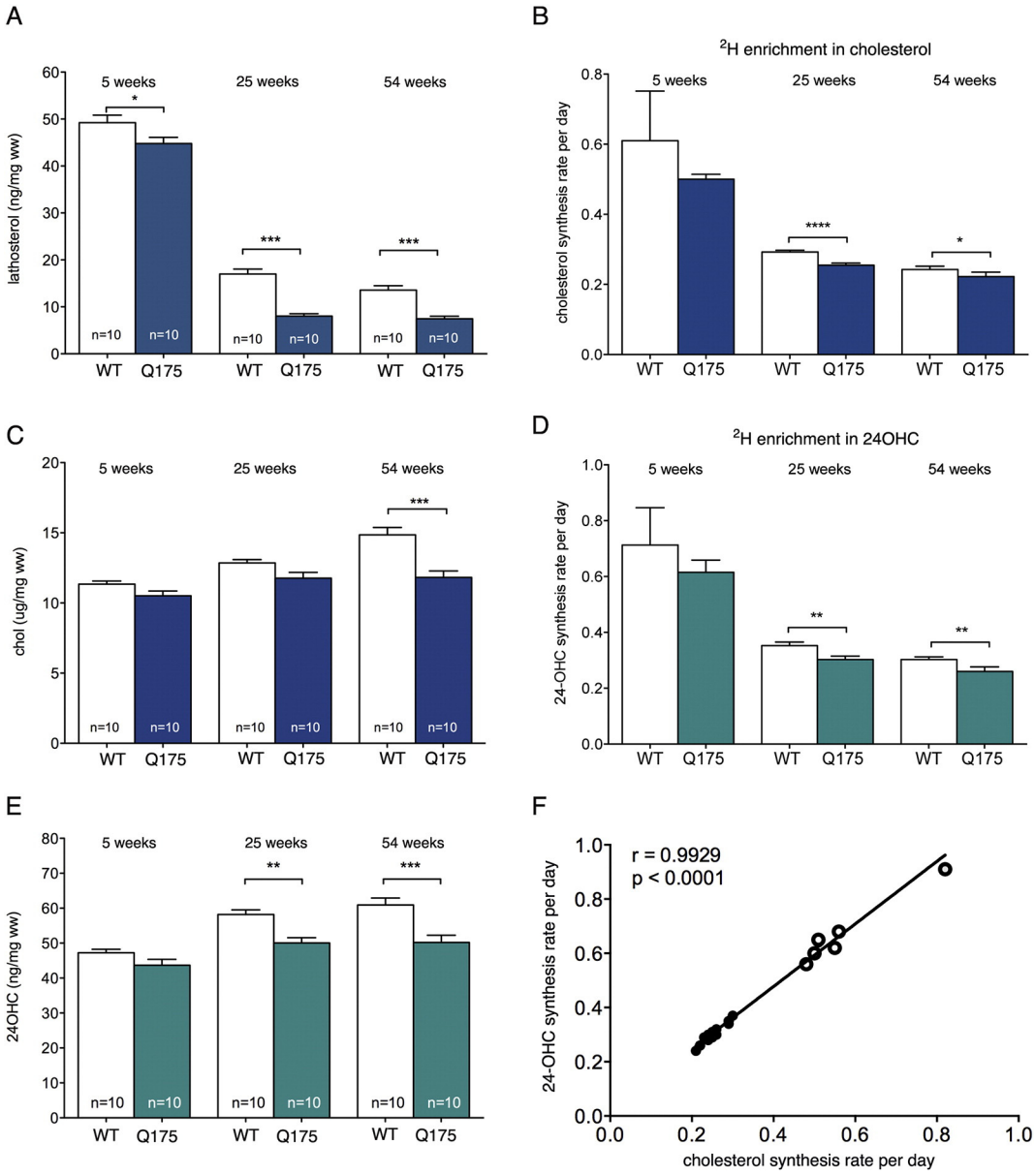

Fig. 2. Brain cholesterol homeostasis in Q175 het mice during disease progression. Lathosterol (A), cholesterol (C) and 24OHC (E) levels measured by ID-MS in striatum of WT and Q175 mice at 5, 25 and 54 weeks of age. Cholesterol synthesis rate per day (B) and 24OHC synthesis rate per day (D) in striatum of WT and Q175 mice at 5, 25 and 54 weeks of age. The 24OHC synthesis rate per day indicates the % of new cholesterol that is catabolized into 24OHC. (F) Correlation between % of new cholesterol and 24OHC synthesis in WT (white circle) and Q175 (black circle) mice in striatum at different ages. The graphs in (A, C, D) show the mean from n = 10 mice (5 males and 5 females) per group ± SEM. The graphs in (B, C, F) show the mean from 4 samples per group, each sample was tissue pooled from 5 mice (all males) per group ± SD. Statistics: two-tailed unpaired *t*-test with age-matched WT. *p < 0.05; **p < 0.01, ***p < 0.001, ****p < 0.0001.

Table 1
Concentration of lathosterol, cholesterol and 24OHC in females and males of WT and Q175 mice. Statistics. Unpaired *t*-test WT *vs* Q175, within the same age and gender group, *p < 0.05; **p < 0.01, ***p < 0.001.

Gender	Females						Males					
Age	5 weeks		25 weeks		54 weeks		5 weeks		25 weeks		54 weeks	
Genotype (n = 5/group)[a]	wt	Q175	wt	Q175	wt	Q175	wt	Q175	wt	Q175	wt	Q175
Lathosterol (ng/mg ww)	52,34 ± 2,48	43,66 ± 2.28*	17,84 ± 1,23	8,33 ± 0,675***	13,40 ± 0,87	7,77 ± 0.57***	46,11 ± 0,80	45,89 ± 1,49	16,16 ± 1,77	7,72 ± 0.77**	13,75 ± 1,74	7,12 ± 1.01*
Cholesterol (μg/mg ww)	11,65 ± 0,33	10,07 ± 0.44*	12,57 ± 0,28	10,85 ± 0.48**	14,61 ± 1,59	12,47 ± 0.54*	11,04 ± 0,25	10,95 ± 0,47	13,13 ± 0,37	12,69 ± 0,53	15,11 ± 0,81	11,16 ± 0.67**
24OHC (ng/mg ww)	48,39 ± 1,70	40,64 ± 2.60*	59,61 ± 2,27	50,75 ± 2.76*	63,20 ± 2,87	52,72 ± 0.90**	46,07 ± 0,97	46,69 ± 1,36	56,75 ± 1,34	49,36 ± 1.55**	58,67 ± 2,57	47,65 ± 3.93*

[a] Unpaired *t*-test wt *vs* Q175 (within the same age and gender groups).

brain with age; an overall reduced cholesterol content was found in the Q175 striatum, compared to WT mice, at 54 weeks of age (Fig. 2C). We also noted a gender effect as female Q175 mice showed a reduction in lathosterol and cholesterol at earlier time points (from 5 weeks of age) compared to males (from 25 to 54 weeks of age) (Table 1).

The findings of reduced cholesterol biosynthesis (at early ages; Fig. 2A,B) and cholesterol content (at ages where the mice exhibit motor deficits; Fig. 2C), together with the lack of evidence of cholesterol accumulation at any of the time points analyzed, reinforce the notion of a defect in cholesterol production in Q175 mice, and support previous findings in R6/2, YAC46, YAC72, YAC128, Q111 knock-in mice and tgHD rats carrying 51 CAG (Valenza et al., 2007b; Valenza et al., 2010). This cross-validation analysis conducted in parallel by two independent research units on the same samples supports the hypothesis that reduced cholesterol biosynthesis is the primary event that leads to a decrease in cholesterol content in mouse HD brain.

3.3. Cholesterol catabolism in the striatum of Q175 mice

To explore whether reduction rate of cholesterol synthesis can also reflected in a reduction of 24OHC production in HD mice, we measured ^{2}H enrichment in 24OHC in the striatum of WT and Q175 mice after *in vivo* stable isotope tracking experiments. As shown in Fig. 2D, a 10–14% significant reduction of 24OHC synthesis rate per day was observed starting from 25 weeks in the striatum of Q175 mice compared to WT mice. Accordingly, 24OHC level, measured by isotope dilution mass spectrometry, was reduced at 25 and 54 weeks of age in the striatum of Q175 mice compared to WT mice (Fig. 2E), an event that occurs later with respect to reduction of lathosterol level (Fig. 2A). All together these results suggest that the reduced concentration of 24OHC is reflective of reduced cholesterol synthesis, not for example, reduced formation or increased clearance of 24OHC.

Importantly, there was a significant correlation between the fractional synthesis rates of total cholesterol and 24OHC in the striatum (but also in other brain regions, see Fig. 4E,F) of both genotypes (Fig. 2F) suggesting that 24OHC can be used to track cholesterol synthesis in the brain.

3.4. Cholesterol biosynthesis and removal in other brain regions of Q175 mice

We next explored whether cholesterol biosynthesis and catabolism are also reduced in cortex and cerebellum of Q175 mice. To better appreciate differences between the brain regions tested, the striatal data from Fig. 2 were re-plotted in Fig. 3. In contrast to the early reduction in lathosterol found in the Q175 striatum, lathosterol levels were reduced in the cortex and cerebellum of Q175 mice only at 54 weeks (Fig. 3A–C). Similar levels of cholesterol were found in cortex and cerebellum of WT and Q175 mice at all the time points (Fig. 3D–F), while 24OHC mirrored lathosterol, with a significant decrease in both cortex and cerebellum only at 54 weeks (Fig. 3G–I).

In vivo measurement of cholesterol, lathosterol and 24OHC synthesis rates in the same brain regions and at the same time points revealed similar and coherent findings with respect to the isotope dilution mass spectrometry data. Similar to striatum, lathosterol was fully turned over (fractional synthesis ~100%) in cortex and cerebellum in both WT and Q175 mice (data not shown). Cholesterol synthesis rates were similar in young Q175 mice and WT mice, but there was a significant 7–10% reduction in cortex and 7–17% in cerebellum in 25- and 54-week-old Q175 mice, respectively, compared to WT mice (Fig. 4A,B). 24OHC synthesis rate in cortex and cerebellum also mirrored cholesterol with a 8–9% (in cortex) and 21–24% (in cerebellum) reduction in Q175 mice, respectively, compared to WT mice (Fig. 4C,D). Similarly to striatum, a significant correlation between the fractional synthesis rates of total cholesterol and 24OHC was found in the cortex and cerebellum from WT and Q175 mice (Fig. 4E, F).

All these findings indicate that a reduction in steady-state lathosterol and 24OHC, and cholesterol synthesis rates, in the absence of changes in cholesterol content in the CTX and CRB of Q175, suggests that these brain regions are more efficient in their compensatory responses to maintain cholesterol homeostasis, in comparison to the striatum.

3.5. SREBP-dependent cholesterol biosynthesis genes in the striatum and cortex from Q175 mice

Nearly all genes involved in cholesterol biosynthesis are transcriptionally regulated by SREBP2 (Jeon and Osborne, 2012). SREBP activity was reduced in an inducible cell model of HD, brain and primary astrocytes from the R6/2 mouse model (Valenza et al., 2005; Valenza et al., 2015a), in N171-82Q mice (Lee et al., 2015) and in postmortem HD brain (Valenza et al., 2005; Hodges et al., 2006). Here we analyzed mRNA levels of hydroxyl-methyl-glutaryil-CoA-reductase (*hmgcr*) and farnesyl-diphosphate farnesyltransferase 1 (*fdft1*) in the striatum and cortex of WT and Q175 mice. mRNA level of Fdft1, encoding for the first enzyme catalyzing the metabolic step in cholesterol biosynthesis that is exclusively committed to sterol biosynthesis, was reduced of ~20–30% in the striatum and in cortex from Q175 mice (0.82 ± 0,045 and 0.69 ± 0,064 respectively) compared to control mice (1.00 ± 0,028 and 1.00 ± 0,027 respectively). Also the mRNA level of *Hmgcr*, encoding for the rate-controlling enzyme of the upstream mevalonate pathway that produces cholesterol and other isoprenoids, was reduced of ~20% in the striatum and cortex of Q175 mice (0.81 ± 0,041 and 0.80 ± 0,025) at 54 weeks of age compared to control mice (1.00 ± 0,021 and 1.00 ± 0,020).

All these data support the hypothesis that impaired SREBP2 activation in the presence of mutant htt contributes to cholesterol dysfunction in HD.

3.6. Cholesterol related parameters in striatum and cortex from allelic series of knock-in HD mice

To test whether cholesterol dysfunction is CAG length dependent, we measured cholesterol, cholesterol precursors and 24OHC in the striatum and cortex from a mouse allelic series (Q20, Q80, Q111, Q175 – all HETs -*versus* WT control). In this experiment, samples from WT (herein defined as Q7) and Q175 mice were re-analyzed and plotted in the graphs together with the other samples. Fig. 5A shows that lathosterol level in 54-week-old striata correlates strongly ($R^2 = 0.96{,}252$) with CAG length with its level being Q175 < Q111 < Q80 < Q20 < Q7, while in 54-week-old cortical samples, we found a CAG-dependent reduction of lathosterol only in animals with Q111 and Q175 (Fig. 5B). Conversely, cholesterol content (Fig. 5C) and 24OHC level (Fig. 5E) were reduced in expanded Q striatal samples (Q80, Q111, Q175) compared to control striata (Q7 and Q20) independent from the polyQ expansion. Significant changes were observed for cholesterol (Fig. 5D) in expanded Q mice – however with the Q111 samples that did not reach significance - and a decrease of 24OHC level was found in cortical tissues of expanded Q mice (Fig. 5F) independent from the length of CAG expansion.

All together, these data suggest that lathosterol, a precursor of cholesterol biosynthesis, correlates strongly with CAG expansion in the striatal samples.

3.7. Plasma 24OHC as a marker of brain cholesterol synthesis in HD

We next asked whether 24OHC in blood might reflect brain cholesterol metabolism in Q175 and allelic series mice. Steady-state level of plasma 24OHC was similar among all samples at 5 weeks of age (Fig. 6A). However, at 54 weeks of age, there was a significant reduction in plasma 24OHC in Q80, Q111 and Q175 samples, compared to Q7(WT) samples (Fig. 6B), mirroring the levels of brain 24OHC in the same mice. In parallel, a statistically significant reduction in the plasma

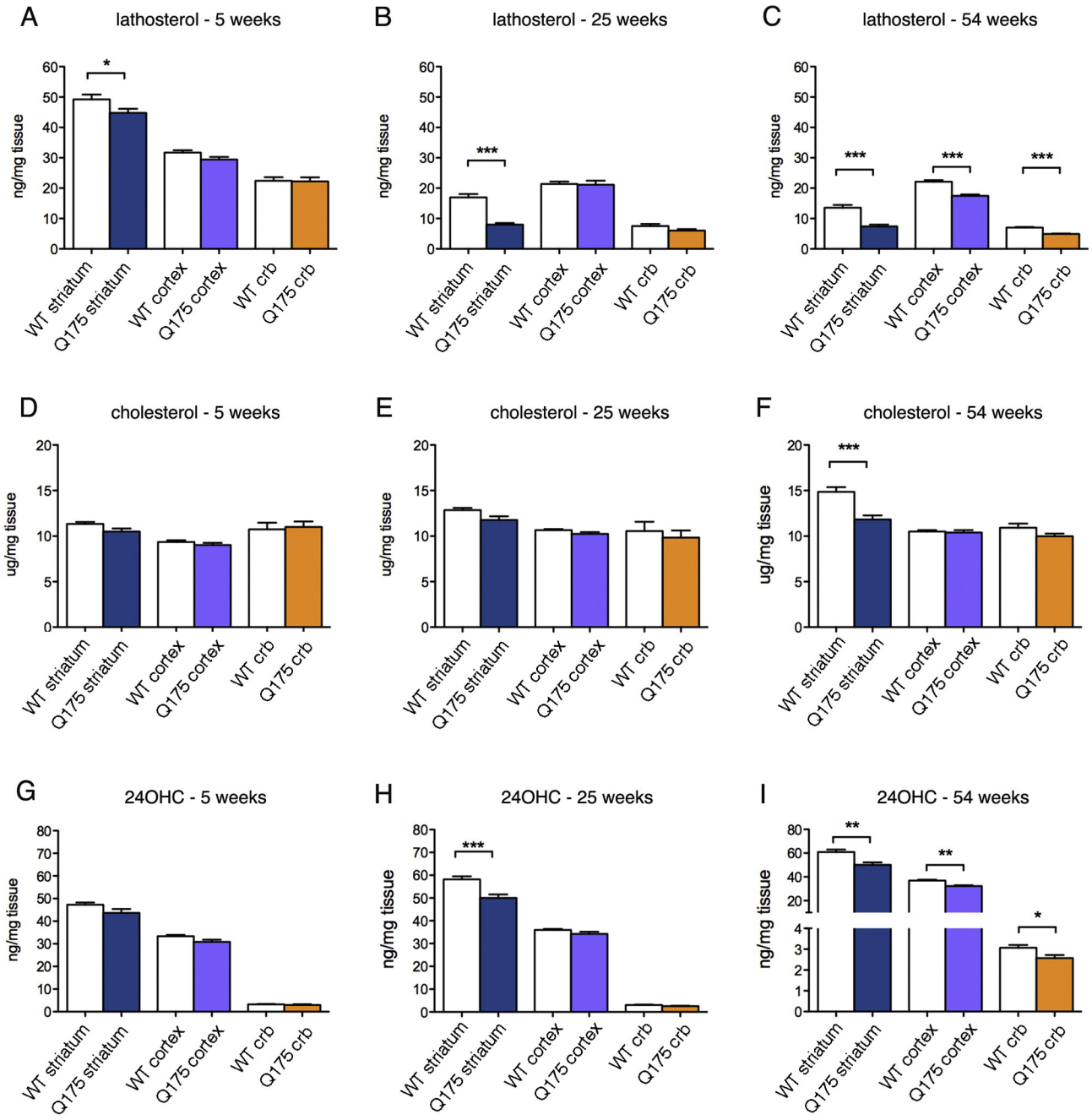

Fig. 3. Lathosterol, cholesterol and 24OHC levels in different brain regions of Q175 het mice during disease progression. Lathosterol (A-B-C), cholesterol (D-E-F) and 24OHC (G-H-I) levels measured by ID-MS in striatum, cortex and cerebellum of WT and Q175 mice at 5 weeks, 25 weeks and 54 weeks of age. The graphs show the mean from n = 10 animals/genotype ± SEM. The raw data for striatum are the same shown in Fig. 2. Statistics: two-tailed unpaired *t*-test with WT by region. *p < 0.05; **p < 0.01, ***p < 0.001.

24OHC synthesis rate was detected in Q175 mice at 25 weeks of age, although no significant changes were observed in other time points (Fig. 6C). Plasma cholesterol synthesis rate, which reflects peripheral cholesterol, was not altered in Q175 mice at all time points (Fig. 6D) suggesting that whole body *de novo* cholesterol metabolism is not affected in HD mice.

We conclude that circulating 24OHC is reduced in HD mouse models with high CAG expansion (>80Q), mirroring the brain levels, and that plasma 24OHC should be explored further for its utility as a biomarker.

4. Discussion

Our study provides a clear demonstration that a reduction in cholesterol biosynthesis is associated with HD mouse models. In particular, the uniqueness of the approach, multi-platform, isotope dilution mass spectrometry and deuterium incorporation analyses combined with *in vivo* labeling based measurements of cholesterol synthesis, in the same brain regions and time points by two independent research units, provided a rigorous cross-validation study with the best available technologies in at least one mouse model (*i.e.* Q175). Furthermore, the inclusion of brain samples from a knock-in mouse series carrying 20, 80, 111 CAG in the isotopic-dilution mass spectrometry analyses provided solid evidence of a CAG length dependence of the lathosterol level that robustly mirrors cholesterol biosynthesis rate in mouse brain.

Our previous *in vitro* and *in vivo* data have proposed that mutant huntingtin moderates the cholesterol biosynthetic pathway in the brain (Karasinska and Hayden, 2011; Valenza and Cattaneo, 2011). This is based on mass spectrometry data showing reduced level of the

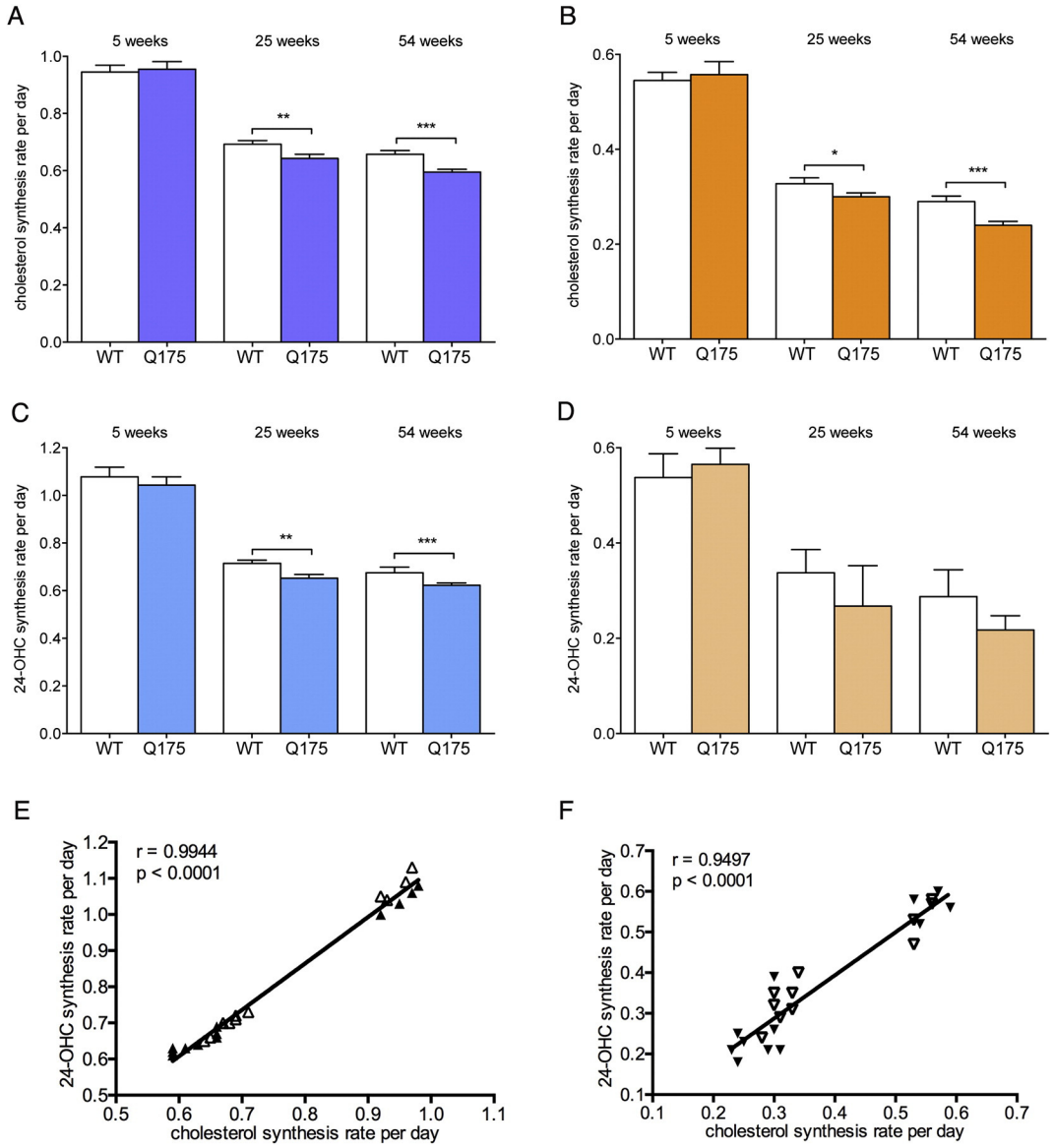

Fig. 4. Cholesterol and 24OHC synthesis rates in different brain regions of Q175 het mice during disease progression. Cholesterol synthesis rate (A–B) and percentage of new cholesterol into 24OHC (C–D) in cortex and cerebellum of WT and Q175 mice at 5 weeks, 25 weeks and 54 weeks of age. The graphs show the mean ± SD, n = 4 samples per group, each sample was tissue pooled from 5 mice (all males). Statistics: two-tailed unpaired *t*-test with age-matched WT. *p < 0.05; **p < 0.01, ***p < 0.001.

cholesterol precursor lathosterol at stages prior to onset of motor phenotypes in the brain regions from R6/2 and YAC128 mice and reduced cholesterol content at more advanced stages. However, lathosterol level is only an indirect measure of cholesterol biosynthesis (Kempen et al., 1988). Furthermore, the measure of cholesterol content in a specific tissue reflects all cholesterol present in the brain and not the pool of newly synthetized cholesterol. On the contrary, an *in vivo* labeling approach allows us to directly address questions related to synthesis rate/day of a specific metabolite. By combining indirect and direct measurements, in this report we show that cholesterol biosynthesis is significantly reduced in the striatum (and other brain regions) of the Q175 mouse model.

The cross-validation analyses performed at different time points, from young ages prior to phenotypic deficits to ages with emerging and significant phenotypic deficits, allowed us to define the timing of cholesterol dysregulation in the Q175 mouse model. Mass spectrometry data show that lathosterol levels are reduced in the striatum of Q175 mice by 5 weeks of age, followed by a decrease in 24OHC levels at 25 weeks of age. As cholesterol biosynthesis is reduced, there is likely a compensatory response to reduce cholesterol catabolism into 24OHC in order to maintain cholesterol levels in the brain. However, at 54 weeks of age, the equilibrium between synthesis and catabolism is compromised, leading to a reduced total cholesterol content compared to WT mice. *In vivo* labeling experiments are in agreement with the mass spectrometry data, indicating that reduced cholesterol biosynthesis is a primary event in the Q175 mice and is not a consequence of cholesterol catabolism. Therefore, upstream interventional strategies (*i.e.* at cholesterol synthesis) might be more impactful in HD systems. Of note, the low daily synthesis rate of cholesterol in different brain regions in Q175 mice supports the hypothesis that the availability of newly synthesized cholesterol – a small pool dedicated to synaptic transmission - is reduced in HD mouse models and might further compromise neuronal functional during disease progression. Additionally, Q175 striatum is affected at an earlier time point than cortex and other brain regions, suggesting a specific need of continuous production and/or availability of cholesterol. Accordingly, the rodent and bovine striatum has been described to contain higher levels of cholesterol compared to other regions (Jurevics and Morell, 1995; Zhang et al., 1996), which may account for its particular anatomical/functional properties.

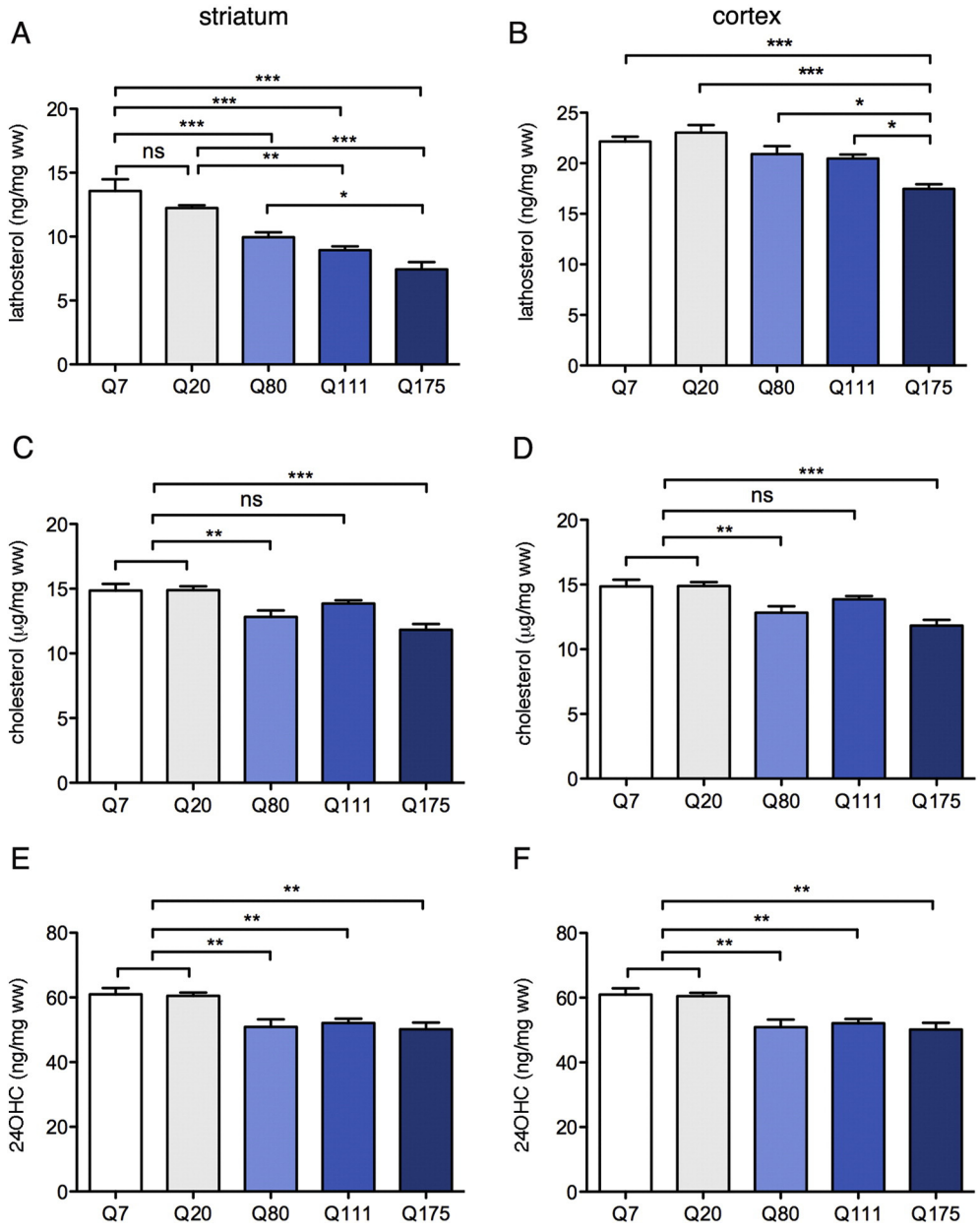

Fig. 5. Lathosterol, cholesterol and 24OHC levels in striatum and cortex from allelic series of mice expressing increasing polyQ. Lathosterol (A,B), cholesterol (C,D) and 24OHC (E,F) levels measured by ID-MS in the striatum (A,C,E) and in cortex (B,D,F) of Q7(WT) and Q20, Q80, Q111 and Q175 mice at 54 weeks of age. The graphs show the mean from n = 10 animals/genotype ± SEM. The raw data for Q7 and Q175 mice are the same shown in Fig. 2. Statistics: one-way ANOVA, Newman–Keuls multiple-comparison post-test. $^{*}p < 0.05$; $^{**}p < 0.01$, $^{***}p < 0.001$.

Recently, we have shown that cholesterol supplementation *via* nanoparticles rescues synaptic and cognitive dysfunction and partially improved global activity in the R6/2-HD mice (Valenza et al., 2015b). Another study has shown that the increase of brain cholesterol catabolism, *via* adeno-associated virus-mediated delivery of CYP46A1 into the striatum, partially improves neuropathology and motor deficits in the same mouse HD model (Boussicault et al., 2016). Whether these apparently opposed strategies act on the same molecular mechanisms is unknown. 24OHC is supposed to be the "signaling molecule" that induces the apoE-mediated cholesterol efflux from astrocytes to neurons (Abildayeva et al., 2006). We may speculate that an increase of neuronal 24OHC level stimulates cholesterol synthesis and efflux in astrocytes to supply new cholesterol to neurons. This is in agreement with the huge increase of desmosterol, the cholesterol precursor more related to astrocytic cholesterol biosynthesis (Nieweg et al., 2009), observed after CYP46A1 delivery in Boussicault work. Previous studies show that lathosterol levels are reduced in the striatum or brain of several HD mouse models in which CAG mutation in htt has been expressed in different contexts, *i.e.* over-expressed as N-terminal or full-length form (R6/2 and YAC mice respectively; (Valenza et al., 2007b; Valenza et al., 2007a) or expressed at endogenous levels in the knock-in models (Q111 and Q175; (Valenza et al., 2010) and herein described). Here we show that lathosterol level is reduced in the striatum of an allelic series of HD mice. This decrease is CAG-length dependent with the fold-decrease being higher with the increase in CAG repeats. In particular, we report that lathosterol levels are Q175 < Q111 < Q80 < Q20 < Q7, suggesting that the reduction in cholesterol biosynthesis is proximal to HD. This correlation was more evident at 54 weeks of age and in striatum, suggesting that higher CAG expansion may exacerbate cholesterol dysregulation at ages with phenotypic deficits, while compensatory mechanisms may occur at ages prior to onset of phenotypic deficits.

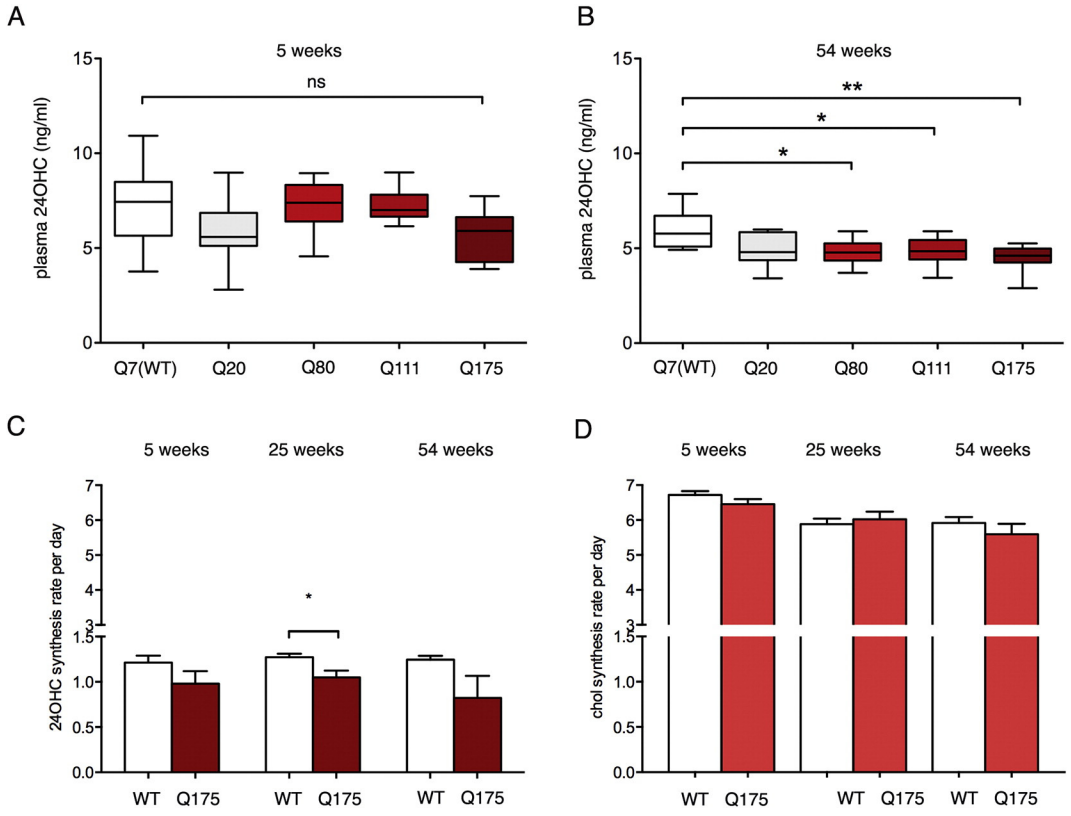

Fig. 6. Circulating 24OHC from allelic series and Q175 het mice during disease progression. (A–B) 24OHC level measured by ID-MS in blood from WT and allelic series of mice at 5 weeks and 54 weeks of age. The graphs show the mean-min-max from n = 10 animals/genotype ± SEM. (C) Cholesterol synthesis rate per day and percentage of new cholesterol into 24OHC in blood from WT and Q175 mice. The graph shows mean ± SEM of n = 4 samples per group, each sample was blood plasma pooled from 5 mice (all males). Statistics: one-way ANOVA, Newman–Keuls multiple-comparison post-test (in A–B) and two tail impaired *t*-test in (C). *p < 0.05; **p < 0.01, ***p < 0.001.

We previously proposed that reduced cholesterol biosynthesis may result as a consequence of reduced SREBP activity. Here we found that two SREBP2-dependent cholesterol genes are reduced in the striatum and cortex of Q175 mice, compared to control mice. Reduced translocation of the active form of SREBP2, rather than its sequestration into muHtt aggregates, might occur in the presence of CAG expansion, as previously suggested (Valenza et al., 2005; Valenza et al., 2015a). However, differently from that observed in the R6/2 mice (Valenza et al., 2005), we found a significant decrease of mRNA of these genes at a later time point compared to reduced lathosterol levels. Further *in vitro* and *in vivo* studies in which expression of cholesterol and lipid genes are experimentally manipulated will help to elucidate which cholesterol related genes are more proximal to mutant htt in order to identify targets of intervention to restore cholesterol biosynthesis in HD.

We also previously explored the potential of circulating 24OHC as candidate biomarker in HD mouse models and patients.

In humans, 24OHC is of cerebral origin and there is a continuous net flux of this oxysterol across the BBB from brain into the circulation (Lutjohann et al., 1996; Bjorkhem et al., 1998). In YAC128 mice, circulating 24OHC levels are reduced reflecting what is observed in the brain (Valenza et al., 2007b), while its level in plasma from HD patients mimic HD onset and progression (Leoni et al., 2008; Leoni et al., 2011; Leoni et al., 2013). Notably, 24OHC plasma level is significantly reduced in pre-manifest HD gene positive subjects and can further distinguish between pre-manifest and patients with overt motor disease. Moreover, this measure has suggested to be second only to striatal volume in its stability to distinguish among progression groups (Leoni et al., 2013). Level of circulating 24OHC is linked to brain cholesterol synthesis, but also increased clearance or reduced formation. The decrease in circulating 24OHC that we observed in mice carrying >Q80 suggests that 24OHC can be used in HD models to trace a defect in brain cholesterol biosynthesis and, eventually, a neurodegenerative process. We should consider that previous reports suggested only 50% of circulating 24OHC is of cerebral origin in mice (Meaney et al., 2000) and that the power of this measure in mice might be lower than in humans, in which almost all the 24OHC is of cerebral origin (Bjorkhem et al., 1998). A longitudinal study for 24OHC will be required to define whether 24OHC is a candidate biomarker in human HD. Using stable isotope labeling we also demonstrate for the first time the use of deuterated water labeling in plasma 24OHC as a surrogate, noninvasive measurement of *in vivo* brain cholesterol synthesis.

In conclusion, we demonstrate that reduced cholesterol synthesis is a biological pathway that is proximal to mutant huntingtin in mouse models and future studies should examine perturbations of this pathway with an eye toward therapeutic interventions in appropriate cells. Importantly, the *in vivo* labeling study conducted in mice in this study is fully translational and similar experiments could be conducted in humans. Measurement of 24OHC in the plasma of HD patients after $^{2}H2O$ labeling will help evaluate the relevance of 24OHC as a potential biomarker in HD onset and progression.

Conflict of interest

No conflicts of interest, financial or otherwise, are declared by the author(s).

Acknowledgments

This work was supported by CHDI Foundation/CHDI Management, USA to EC (no. A-5086) and to KineMed (A-5142); and by Ministero della Salute under 40 (GR-2008) to V.L. and M.V. We thank Ignacio Munoz-Sanjuan for critical reading of the manuscript. This paper is dedicated to the memory of our dear colleague, devoted scientist and well known neurologist Stefano Di Donato.

References

Abildayeva, K., Jansen, P.J., Hirsch-Reinshagen, V., Bloks, V.W., Bakker, A.H., Ramaekers, F.C., de Vente, J., Groen, A.K., Wellington, C.L., Kuipers, F., Mulder, M., 2006. 24(S)-hydroxycholesterol participates in a liver X receptor-controlled pathway in astrocytes that regulates apolipoprotein E-mediated cholesterol efflux. J. Biol. Chem. 281, 12799–12808.

Aggarwal, S., Yurlova, L., Simons, M., 2011. Central nervous system myelin: structure, synthesis and assembly. Trends Cell Biol. 21, 585–593.

Bates, G.P., Dorsey, R., Gusella, J.F., Hayden, M.R., Kay, C., Leavitt, B.R., Nance, M., Ross, C.A., Scahill, R.I., Wetzel, R., Wild, E.J., Tabrizi, S.J., 2015. Huntington disease. Nature Rev. Dis. Primers 1, 15005.

Bjorkhem, I., Lutjohann, D., Diczfalusy, U., Stahle, L., Ahlborg, G., Wahren, J., 1998. Cholesterol homeostasis in human brain: turnover of 24S-hydroxycholesterol and evidence for a cerebral origin of most of this oxysterol in the circulation. J. Lipid Res. 39, 1594–1600.

Boussicault, L., Alves, S., Lamaziere, A., Planques, A., Heck, N., Moumne, L., Despres, G., Bolte, S., Hu, A., Pages, C., Galvan, L., Piguet, F., Aubourg, P., Cartier, N., Caboche, J., Betuing, S., 2016. CYP46A1, the rate-limiting enzyme for cholesterol degradation, is neuroprotective in Huntington's disease. Brain J. Neurol. 139, 953–970.

Camargo, N., Smit, A.B., Verheijen, M.H., 2009. SREBPs: SREBP function in glia-neuron interactions. FEBS J. 276, 628–636.

Cohen, A., Hertz, H.S., Mandel, J., Paule, R.C., Schaffer, R., Sniegoski, L.T., Sun, T., Welch, M.J., White, E., 1980. Total serum cholesterol by isotope dilution/mass spectrometry: a candidate definitive method. Clin. Chem. 26, 854–860.

Dietschy, J.M., 1984. Regulation of cholesterol metabolism in man and in other species. Klin. Wochenschr. 62, 338–345.

Dietschy, J.M., Turley, S.D., 2004. Thematic review series: brain lipids. Cholesterol metabolism in the central nervous system during early development and in the mature animal. J. Lipid Res. 45, 1375–1397.

Hellerstein, M.K., Neese, R.A., 1992. Mass isotopomer distribution analysis: a technique for measuring biosynthesis and turnover of polymers. Am. J. Phys. 263, E988–1001.

Hodges, A., et al., 2006. Regional and cellular gene expression changes in human Huntington's disease brain. Hum. Mol. Genet. 15, 965–977.

Jeon, T.I., Osborne, T.F., 2012. SREBPs: metabolic integrators in physiology and metabolism. Trends Endocrinol. Metab. 23, 65–72.

Jurevics, H., Morell, P., 1995. Cholesterol for synthesis of myelin is made locally, not imported into brain. J. Neurochem. 64, 895–901.

Karasinska, J.M., Hayden, M.R., 2011. Cholesterol metabolism in Huntington disease. Nat. Rev. Neurol. 7, 561–572.

Kempen, H.J., Glatz, J.F., Gevers Leuven, J.A., van der Voort, H.A., Katan, M.B., 1988. Serum lathosterol concentration is an indicator of whole-body cholesterol synthesis in humans. J. Lipid Res. 29, 1149–1155.

Lee, W.N., Bassilian, S., Guo, Z., Schoeller, D., Edmond, J., Bergner, E.A., Byerley, L.O., 1994. Measurement of fractional lipid synthesis using deuterated water (2H2O) and mass isotopomer analysis. Am. J. Phys. 266, E372–E383.

Lee, J.H., Tecedor, L., Chen, Y.H., Monteys, A.M., Sowada, M.J., Thompson, L.M., Davidson, B.L., 2015. Reinstating aberrant mTORC1 activity in Huntington's disease mice improves disease phenotypes. Neuron 85, 303–315.

Leoni, V., Mariotti, C., Tabrizi, S.J., Valenza, M., Wild, E.J., Henley, S.M., Hobbs, N.Z., Mandelli, M.L., Grisoli, M., Bjorkhem, I., Cattaneo, E., Di Donato, S., 2008. Plasma 24S-hydroxycholesterol and caudate MRI in pre-manifest and early Huntington's disease. Brain J. Neurol. 131, 2851–2859.

Leoni, V., Mariotti, C., Nanetti, L., Salvatore, E., Squitieri, F., Bentivoglio, A.R., Bandettini di Poggio, M., Piacentini, S., Monza, D., Valenza, M., Cattaneo, E., Di Donato, S., 2011. Whole body cholesterol metabolism is impaired in Huntington's disease. Neurosci. Lett. 494, 245–249.

Leoni, V., Long, J.D., Mills, J.A., Di Donato, S., Paulsen, J.S., group P-Hs, 2013. Plasma 24S-hydroxycholesterol correlation with markers of Huntington disease progression. Neurobiol. Dis. 55, 37–43.

Lund, E.G., Guileyardo, J.M., Russell, D.W., 1999. cDNA cloning of cholesterol 24-hydroxylase, a mediator of cholesterol homeostasis in the brain. Proc. Natl. Acad. Sci. U. S. A. 96, 7238–7243.

Lutjohann, D., Breuer, O., Ahlborg, G., Nennesmo, I., Siden, A., Diczfalusy, U., Bjorkhem, I., 1996. Cholesterol homeostasis in human brain: evidence for an age-dependent flux of 24S-hydroxycholesterol from the brain into the circulation. Proc. Natl. Acad. Sci. U. S. A. 93, 9799–9804.

Mauch, D.H., Nagler, K., Schumacher, S., Goritz, C., Muller, E.C., Otto, A., Pfrieger, F.W., 2001. CNS synaptogenesis promoted by glia-derived cholesterol. Science 294, 1354–1357.

Meaney, S., Lutjohann, D., Diczfalusy, U., Bjorkhem, I., 2000. Formation of oxysterols from different pools of cholesterol as studied by stable isotope technique: cerebral origin of most circulating 24S-hydroxycholesterol in rats, but not in mice. Biochim. Biophys. Acta 1486, 293–298.

Menalled, L.B., Kudwa, A.E., Miller, S., Fitzpatrick, J., Watson-Johnson, J., Keating, N., Ruiz, M., Mushlin, R., Alosio, W., McConnell, K., Connor, D., Murphy, C., Oakeshott, S., Kwan, M., Beltran, J., Ghavami, A., Brunner, D., Park, L.C., Ramboz, S., Howland, D., 2012. Comprehensive behavioral and molecular characterization of a new knock-in mouse model of Huntington's disease: zQ175. PLoS One 7, e49838.

Nieweg, K., Schaller, H., Pfrieger, F.W., 2009. Marked differences in cholesterol synthesis between neurons and glial cells from postnatal rats. J. Neurochem. 109, 125–134.

Ramirez, D.M., Andersson, S., Russell, D.W., 2008. Neuronal expression and subcellular localization of cholesterol 24-hydroxylase in the mouse brain. J. Comp. Neurol. 507, 1676–1693.

Ross, C.A., Aylward, E.H., Wild, E.J., Langbehn, D.R., Long, J.D., Warner, J.H., Scahill, R.I., Leavitt, B.R., Stout, J.C., Paulsen, J.S., Reilmann, R., Unschuld, P.G., Wexler, A., Margolis, R.L., Tabrizi, S.J., 2014. Huntington disease: natural history, biomarkers and prospects for therapeutics. Nat. Rev. Neurol. 10, 204–216.

Runquist, M., Parmryd, I., Thelin, A., Chojnacki, T., Dallner, G., 1995. Distribution of branch point prenyltransferases in regions of bovine brain. J. Neurochem. 65, 2299–2306.

Saher, G., Simons, M., 2010. Cholesterol and myelin biogenesis. Subcell. Biochem. 51, 489–508.

Valenza, M., Cattaneo, E., 2011. Emerging roles for cholesterol in Huntington's disease. Trends Neurosci. 34, 474–486.

Valenza, M., Rigamonti, D., Goffredo, D., Zuccato, C., Fenu, S., Jamot, L., Strand, A., Tarditi, A., Woodman, B., Racchi, M., Mariotti, C., Di Donato, S., Corsini, A., Bates, G., Pruss, R., Olson, J.M., Sipione, S., Tartari, M., Cattaneo, E., 2005. Dysfunction of the cholesterol biosynthetic pathway in Huntington's disease. J. Neurosci. 25, 9932–9939.

Valenza, M., Leoni, V., Tarditi, A., Mariotti, C., Bjorkhem, I., Di Donato, S., Cattaneo, E., 2007a. Progressive dysfunction of the cholesterol biosynthesis pathway in the R6/2 mouse model of Huntington's disease. Neurobiol. Dis. 28, 133–142.

Valenza, M., Carroll, J.B., Leoni, V., Bertram, L.N., Bjorkhem, I., Singaraja, R.R., Di Donato, S., Lutjohann, D., Hayden, M.R., Cattaneo, E., 2007b. Cholesterol biosynthesis pathway is disturbed in YAC128 mice and is modulated by huntingtin mutation. Hum. Mol. Genet. 16, 2187–2198.

Valenza, M., Leoni, V., Karasinska, J.M., Petricca, L., Fan, J., Carroll, J., Pouladi, M.A., Fossale, E., Nguyen, H.P., Riess, O., MacDonald, M., Wellington, C., DiDonato, S., Hayden, M., Cattaneo, E., 2010. Cholesterol defect is marked across multiple rodent models of Huntington's disease and is manifest in astrocytes. J. Neurosci. 30, 10844–10850.

Valenza, M., Marullo, M., Di Paolo, E., Cesana, E., Zuccato, C., Biella, G., Cattaneo, E., 2015a. Disruption of astrocyte-neuron cholesterol cross talk affects neuronal function in Huntington's disease. Cell Death Differ. 22, 690–702.

Valenza, M., Chen, J.Y., Di Paolo, E., Ruozi, B., Belletti, D., Ferrari Bardile, C., Leoni, V., Caccia, C., Brilli, E., Di Donato, S., Boido, M.M., Vercelli, A., Vandelli, M.A., Forni, F., Cepeda, C., Levine, M.S., Tosi, G., Cattaneo, E., 2015b. Cholesterol-loaded nanoparticles ameliorate synaptic and cognitive function in Huntington's disease mice. EMBO Mol. Med. 7, 1547–1564.

Zhang, Y., Appelkvist, E.L., Kristensson, K., Dallner, G., 1996. The lipid compositions of different regions of rat brain during development and aging. Neurobiol. Aging 17, 869–875.

Zoller, I., Meixner, M., Hartmann, D., Bussow, H., Meyer, R., Gieselmann, V., Eckhardt, M., 2008. Absence of 2-hydroxylated sphingolipids is compatible with normal neural development but causes late-onset axon and myelin sheath degeneration. J. Neurosci. 28, 9741–9754.

Research Article

SOURCE DATA | TRANSPARENT PROCESS | OPEN ACCESS

EMBO Molecular Medicine

Cholesterol-loaded nanoparticles ameliorate synaptic and cognitive function in Huntington's disease mice

Marta Valenza[1,†], Jane Y Chen[2,†], Eleonora Di Paolo[1,‡], Barbara Ruozi[3,‡], Daniela Belletti[3], Costanza Ferrari Bardile[1], Valerio Leoni[4,5], Claudio Caccia[4], Elisa Brilli[1], Stefano Di Donato[4,§], Marina M Boido[6], Alessandro Vercelli[6], Maria A Vandelli[3], Flavio Forni[3], Carlos Cepeda[2], Michael S Levine[2], Giovanni Tosi[3] & Elena Cattaneo[1,*]

Abstract

Brain cholesterol biosynthesis and cholesterol levels are reduced in mouse models of Huntington's disease (HD), suggesting that locally synthesized, newly formed cholesterol is less available to neurons. This may be detrimental for neuronal function, especially given that locally synthesized cholesterol is implicated in synapse integrity and remodeling. Here, we used biodegradable and biocompatible polymeric nanoparticles (NPs) modified with glycopeptides (g7) and loaded with cholesterol (g7-NPs-Chol), which *per se* is not blood–brain barrier (BBB) permeable, to obtain high-rate cholesterol delivery into the brain after intraperitoneal injection in HD mice. We report that g7-NPs, in contrast to unmodified NPs, efficiently crossed the BBB and localized in glial and neuronal cells in different brain regions. We also found that repeated systemic delivery of g7-NPs-Chol rescued synaptic and cognitive dysfunction and partially improved global activity in HD mice. These results demonstrate that cholesterol supplementation to the HD brain reverses functional alterations associated with HD and highlight the potential of this new drug-administration route to the diseased brain.

Keywords cholesterol; cognition; Huntington's disease; nanoparticles; synapses

Subject Categories Metabolism; Neuroscience

DOI 10.15252/emmm.201505413 | Received 6 May 2015 | Revised 20 October 2015 | Accepted 21 October 2015 | Published online 20 November 2015

EMBO Mol Med (2015) 7: 1547–1564

Introduction

Huntington's disease (HD) is a genetic neurological disorder caused by a CAG expansion in the gene encoding the huntingtin (HTT) protein (HDCRG, 1993). Clinically, HD is characterized by motor, cognitive, and psychiatric disturbances (Ross *et al*, 2014) and is associated with neuronal dysfunction, atrophy of the striatum and other brain regions, and progressive loss of striatal medium-sized spiny neurons (MSNs) and of cortical pyramidal neurons (Vonsattel & DiFiglia, 1998). Several molecular and cellular dysfunctions have been identified (Zuccato *et al*, 2010), and one affected pathway implicates brain cholesterol.

The brain is the most cholesterol-rich organ in the body, with almost all of the cholesterol produced *in situ*, as circulating cholesterol is not able to cross the BBB (Dietschy & Turley, 2004). A large majority of cholesterol (> 70% of brain cholesterol mass) is present in myelin sheaths. Indeed, the rate of cholesterol synthesis is highest during post-natal stage to build myelin scaffolding. Cholesterol is also a structural component of glial and neuronal membranes and is concentrated in lipid rafts, specialized membrane microdomains that initiate, propagate, and maintain signal transduction events (Paratcha & Ibanez, 2002). Newly synthesized cholesterol is also required for vesicle assembly and fusion (Huttner & Zimmerberg, 2001; Lang *et al*, 2001), synapse formation, integrity, remodeling (Pfrieger, 2003), and neurotransmitter release (Thiele *et al*, 2000; Mauch *et al*, 2001). Accordingly, a breakdown of cholesterol synthesis causes brain malformations and impaired cognitive functions (Valenza & Cattaneo, 2006).

1 Department of BioSciences, Centre for Stem Cell Research, Università degli Studi di Milano, Milan, Italy
2 Intellectual and Developmental Disabilities Research Center, Semel Institute for Neuroscience, Brain Research Institute, David Geffen School of Medicine, University of California Los Angeles, Los Angeles, CA, USA
3 Department of Life Sciences, University of Modena and Reggio Emilia, Modena, Italy
4 Neurological Institute C. Besta, Milan, Italy
5 Laboratory of Clinical Chemistry, Ospedale di Circolo e Fondazione Macchi, Varese, Italy
6 Neuroscience Institute Cavalieri Ottolenghi, Neuroscience Institute of Turin, Orbassano, Turin, Italy
*Corresponding author. Tel: +39 02 50325842; E-mail: elena.cattaneo@unimi.it
†These authors share first authorship
‡These authors share second authorship
§Deceased on 12 November 2015

© 2015 The Authors. Published under the terms of the CC BY 4.0 license

HD is characterized by abnormal brain cholesterol homeostasis. Patients with HD show altered cholesterol homeostasis since pre- and early stages of disease as judged by the plasmatic measure of 24S-hydroxy-cholesterol (24OHC), the brain-specific catabolite of cholesterol able to cross the blood–brain barrier (BBB) (Leoni *et al*, 2008, 2013). Reduced cholesterol biosynthesis and levels are also found in the brain of several HD mouse models (Valenza *et al*, 2007a,b, 2010). On the contrary, others reported an increased accumulation of free cholesterol in brain tissues of HD mouse models (Trushina *et al*, 2006; del Toro *et al*, 2010) likely due to different sample preparation and less sensitive methods (colorimetric and enzymatic assays) to detect and quantify cholesterol compared to mass spectrometry (Marullo *et al*, 2012). Of note, more recently, some of the same groups have reported a decrease of lathosterol and cholesterol levels in the striatum of a HD mouse model by means of mass spectrometry (Trushina *et al*, 2014). Cholesterol dysregulation occurs in astrocytes (Valenza *et al*, 2015) and is linked to a specific action of mutant HTT on sterol regulatory-element-binding proteins (SREBPs) and its target genes, whose reduced transcription leads to less brain cholesterol produced and released and available to be uptaken by neurons (Valenza *et al*, 2005).

Accordingly, an early decrease of cholesterol production in the HD brain might be detrimental for neuronal activities. Abnormalities in synaptic communication within the striatum and between the cortex and striatum occur long before, or in the absence of, cell death in HD animal models (Milnerwood & Raymond, 2010) and cognitive disturbances have been observed decades before predicted clinical diagnosis in HD gene carriers (Levine *et al*, 2004; Paulsen & Long, 2014). Similarly, brain cholesterol biosynthesis is significantly reduced before the onset of motor symptoms in all the HD animal models analyzed so far (Valenza *et al*, 2007a,b) and synaptosomes —a compartment dedicated to impulse transmission and neurotransmitter release—carry suboptimal levels of sterols in the early stages of HD in one mouse model (Valenza *et al*, 2010). However, a link between the reduced level of cholesterol and neuronal dysfunction *in vivo* in HD is still missing.

Here, we explored the effects of cholesterol supplementation on synaptic communication and machinery, motor and cognitive behaviors, and neuropathology in the R6/2 mouse model, a well-established early onset transgenic mouse model of HD (Mangiarini *et al*, 1996). Since cholesterol does not cross the BBB, cholesterol was delivered using a new technology for drug administration in the brain (Vergoni *et al*, 2009; Tosi *et al*, 2010), that is, via biodegradable polymeric (polylactide-co-glycolide, PLGA) nanoparticles (NPs) modified with a glycopeptide (g-7) able to cross the BBB upon systemic injection in mice (Costantino *et al*, 2005; Tosi *et al*, 2007, 2011b). The development of new strategies to enhance brain delivery based on colloidal carriers is of great importance, since nanocarriers can protect drugs and deliver them across the BBB to target brain cells in a non-invasive way (Tosi *et al*, 2008). Notably, both FDA and EMA have approved PLGA in various drug delivery systems in humans (Mundargi *et al*, 2008), as confirmed by a number of market products (i.e., Lupron Depot®, Nutropin Depot ®).

We report that, in contrast to unmodified NPs, g7-NPs efficiently crossed the BBB and within a few hours after systemic injection reached glial and neuronal cells in different brain regions. Importantly, repeated systemic delivery of g7-NPs-Chol rescued synaptic communication, protected from cognitive decline and partially improved global activity in HD mice.

Results

Chemical–physical and technological optimization of unloaded and cholesterol-loaded Nanoparticles

The chemical formulation and features of unloaded NPs (u-NPs) herein employed have been largely described (Vergoni *et al*, 2009; Tosi *et al*, 2011a, 2014; Vilella *et al*, 2014). To optimize the production of NPs loaded with cholesterol (NPs-Chol), we first prepared u-NPs and NPs loaded with different amounts of cholesterol (1, 5, and 10 mg of Chol per 100 mg of polymer; herein defined as NPs-Chol1, NPs-Chol2 and NPs-Chol3, respectively) according to the nanoprecipitation procedure (Minost *et al*, 2012) (see Materials and Methods). The composition of different NPs is described in Appendix Table S1, and details about their optimization and characterization are described in the Appendix.

NPs were characterized by their chemical–physical properties, summarized in Appendix Table S2. The average diameter (Z-average) of u-NPs ranged from 170 to 192 nm. Z-average for NPs-Chol1 and NPs-Chol2 was lower than 210 nm, while size of NPs-Chol3 ranged between 200 nm and 300 nm. The polydispersity index (PDI value), a measure of the heterogeneity of NPs, was 0.08 ± 0.01 for u-NPs, suggesting a homogeneous and monomodal distribution population around the mean size. NPs-Chol1 and NPs-Chol2 showed a PDI value of 0.09 ± 0.01 and 0.11 ± 0.02, respectively, and a narrow dimension distribution, indicating that they are monomodal and monodisperse systems. On the contrary, NPs-Chol3 was characterized by a PDI value close to 0.3, accounting for a marked increase in sample heterogeneity. Zeta-potential (ζ-pot), a function of particle surface charges that influences cell interaction, was negative for all the NPs-Chol samples and similar to those of u-NPs. Moreover, ζ-pot of NPs-Chol3 displayed higher standard deviation (-12 ± 10 mV) with respect to those of NPs-Chol1 (-9 ± 4 mV) and NPs-Chol2 (-8 ± 4 mV), further highlighting the higher heterogeneity of this sample.

To evaluate whether and how the incorporation of cholesterol influences the morphology, architecture and surface properties of NPs, atomic force microscopy (AFM) and transmission electron microscopy (TEM) analyses were performed on u-NPs and NPs-Chol (Fig 1A–C). In agreement with the chemical–physical properties (Appendix Table S2), the "height" AFM image (Fig 1A, left column), 3D reconstruction (Fig 1A, middle column), and TEM micrograph (Fig 1A, right column) of u-NPs highlighted well compact and defined spherical structures (Belletti *et al*, 2012). The AFM analysis for NPs-Chol1 confirmed the spherical shape, but shape and size were less homogeneous if compared with those of u-NPs (Fig 1B). Particles adopted an irregular frame, evident in the AFM 3D reconstruction, supporting the hypothesis that alteration of polymer organization and intimate interplay between cholesterol and PLGA occurred when cholesterol was added to the formulation. The greater complexity of these samples was confirmed by TEM microphotographs (right columns) emphasizing the less dense and compact structures of NPs-Chol1 with respect to

 © 2015 The Authors

u-NPs. NPs-Chol2 showed similar morphology and architecture of NPs-Chol1 (data not shown). Instead, the AFM images of NPs-Chol3 showed the presence of irregular structures and unformed material and a remarkable tendency to aggregate (Fig 1C). With respect to u-NPs and NPs-Chol1, NPs-Chol3 seemed to promote the formation of disorganized clusters characterized by heterogeneous dimensions (242 ± 52 nm) and by a roughness surface with evident fissuring. Similarly, TEM microphotographs showed the complexity of NPs-Chol3 that appeared with abundant adsorbed unformed material (likely unloaded cholesterol) and modified NPs' morphology.

We also evaluated the content of cholesterol into NPs (loading capacity, LC%) and the encapsulation efficiency (EE%) (Appendix Table S2). About 0.7 ± 0.1 mg/100 mg of formulation, corresponding to an EE of 68%, were loaded in the NPs-Chol1, indicating that an important fraction of the initial cholesterol was stably incorporated into the NPs-Chol1. On the contrary, a decrease in EE value was observed as the amount of cholesterol used in the preparation increased. In NPs-Chol2 and NPs-Chol3, the EE remarkably decreased (about 20%) although the highest value of drug loading was observed in NPs-Chol3 (2.5 mg of Chol/100 mg of NPs). However, as previously pointed out, cholesterol in NPs-Chol3 was

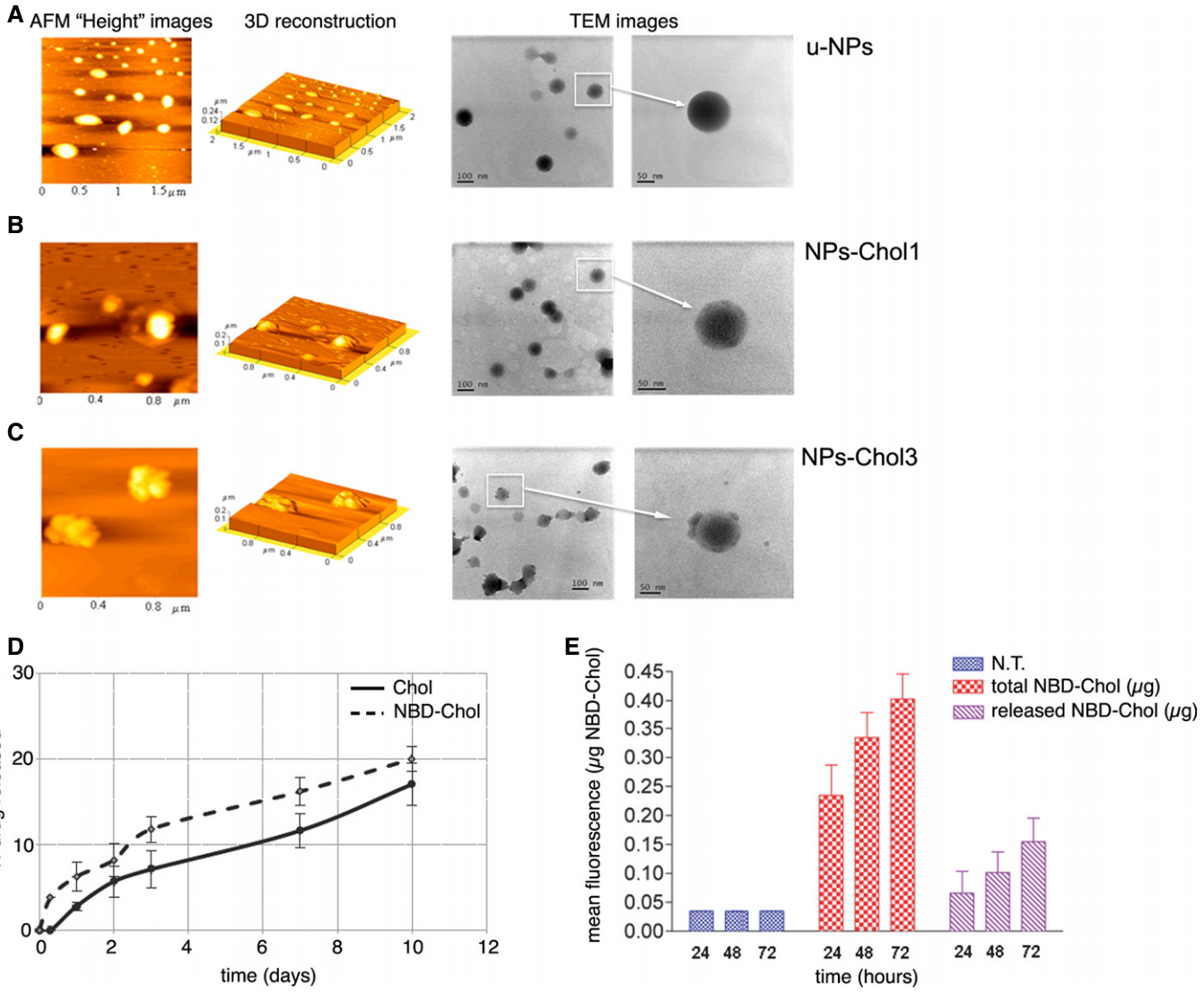

Figure 1. Characterization of NPs loaded with different concentrations of cholesterol.

A–C AFM and TEM analysis of unloaded (u-NPs) and cholesterol-loaded NPs (NPs-Chol). AFM "height" images (left column), 3D reconstruction (middle column), and TEM micrograph (right column) of u-NPs (A), NPs-Chol1 (B), and NPs-Chol3 (C).

D Release profile in water of cholesterol (continuous line, —) and NBD-Chol (dotted line, - - -) from NPs-Chol1 and NPs-NBD-Chol1, respectively. The graph represents mean ± SEM. Data are from three independent experiments.

E *In vitro* release of NBD-Chol from NPs at different time intervals in NS cells. Data in the graph represent mean (μg) ± SEM of total NBD-Chol (embedded into and released from NPs; red columns) and NBD-Chol released after NPs degradation (purple columns) present in the homogenates of NS cells treated with NPs-NBD-Chol1. Data obtained from four independent experiments. N.T.: not treated cells.

© 2015 The Authors

not completely embedded, but a remarkable fraction was absorbed onto the surface. Based on these analyses, NPs-Chol1 formulation was used in all experiments.

Controlled release of cholesterol from NPs in physiological conditions and *in vitro*

To explore the ability of the system to release cholesterol, we first carried out release studies in deionized water for 10 days (Fig 1D). The release profile of cholesterol from NPs-Chol1 (hereafter referred as NPs-Chol; solid line) showed an initial "burst release" (< 8%) during the first 3 days, followed by a second slow release phase. Chol release was detected close to values of 18% over 10 days owing to the poor water solubility of cholesterol (estimated to be 2 μg/ml). Moreover, during the second phase, the slow linear release kinetic of Chol from NPs-Chol between day 5 and day 10 could be ascribed to NPs degradation.

In specific experiments, we also adopted a lead formulation prepared by replacing cholesterol with the fluorescent cholesterol derivative NBD-Chol to discriminate between endogenous and exogenous cholesterol released from NPs. We therefore characterized also the NBD-Chol-loaded NPs (NPs-NBD-Chol) in terms of their chemical–physical and technological properties (Appendix Table S2) and morphological features (Appendix Fig S1). The release of NBD-Chol from NPs in water showed a slow kinetic profile (Fig 1D, dotted line) similar to that observed for native cholesterol (Fig 1D, solid line). Similar findings were observed when the kinetic profile of drug release was evaluated in experiments conducted in cultured cells (Fig 1E). Spectrophotometric quantification of NBD-Chol in neural stem (NS) cells treated with 3 μg of NPs-NBD-Chol revealed that only 20% of the total NBD-Chol taken by the cells was released after 24 h (0.05 μg vs. 0.23 μg; Fig 1E, seventh and fourth columns, respectively). At 72 h, the amount of NBD-Chol released increased to about 35% of the total NBD-Chol taken up by cells (0.14 μg vs. 0.39 μg; Fig 1E, ninth and sixth columns, respectively), confirming the slow kinetic profile of cholesterol release from NPs.

g7-NPs distribution in HD cells and brain

The g7-NPs used in this study are designed to cross the BBB, and previous studies indicated that about 10% are estimated to penetrate the brain (Costantino *et al*, 2005; Tosi *et al*, 2007, 2011a,b, 2014). To verify that g7-NPs could penetrate HD cells, primary neurons from R6/2 mice and neurons and astrocytes from mouse NS cells carrying 140 CAG repeats (NS Q140/7) were exposed to g7-NPs labeled with rhodamine to allow their detection with fluorescence microscopy. Appendix Fig S2 shows that g7-NPs are taken up *in vitro* by different brain cells expressing mutant Htt. Importantly, 4 h after a single intraperitoneal (ip) injection into 8-week-old R6/2 mice and wild-type (WT) littermates, both control (unmodified) NPs (C-NPs) and g7-NPs were detected in the liver (Fig 2A) and in other peripheral tissues (Appendix Fig S3), but only g7-NPs were detected in the brain (Fig 2B). Quantification of g7-NPs yielded an approximate ratio of ~10:1 in the WT liver compared to striatum and cortex (Fig 2C). This quantification also revealed a reduced propensity of g7-NPs to reach the R6/2 brain compared to the WT brain, while g7-NPs were more prevalent in R6/2 liver compared to WT liver, suggesting that HD-related mechanisms may influence the BBB crossing of g7-NPs. g7-NPs were also found 24 h and 2 weeks after a single (Fig 2D) or multiple ip injections performed in the same week (Fig 2E). High-magnification confocal images indicated the presence of g7-NPs in different brain regions and in IBA1 immunoreactive microglial cells (Fig 2F) and in GFAP positive astrocytes (Fig 2G). Notably, g7-NPs were also detected in neuronal cells, as demonstrated by immunostaining against calbindin (Fig 2H; Appendix Fig S4) and DARPP-32 (Fig 2I).

Delivery and release of cholesterol *in vivo* in the R6/2 brain

To track the delivery and intracellular release of cholesterol from g7-NPs, we employed rhodamine-labeled g7-NPs (Vergoni *et al*, 2009) loaded with the fluorescent cholesterol derivative NBD-Chol (g7-NPs-NBD-Chol). NBD-Chol closely resembles the structure of native cholesterol and is normally used to study cholesterol trafficking (Gimpl & Gehrig-Burger, 2007). Accordingly, NBD-Chol, injected into brain ventricles of mice, co-localizes with PMCA ATPase, a marker of plasma membrane, suggesting that exogenous cholesterol is incorporated on brain cells' membranes *in vivo* (Appendix Fig S5). We next monitored the distribution of g7-NPs as red spots and the distribution of released NBD-Chol as green signal. *In vivo*, at 12 and 24 h after a single ip injection of g7-NPs-NBD-Chol, g7-NPs and NBD-Chol co-localized in brain cells (Fig 3A and B). In particular, Fig 3B shows the distribution of g7-NPs (red signal) and NBD-Chol (green signal) in a brain section of a R6/2 mouse injected ip with g7-NPs-NBD-Chol and sacrificed 24 h later. Both g7-NPs and NBD-Chol signals co-localized as indicated by the scatterplot of red and green pixel intensities. However, g7-NPs and NBD-Chol were no longer co-localized after 14 days as demonstrated in Fig 3C. Similar results were found at 7 days after ip injection (data not shown). These findings indicate that NBD-Chol was partially released from NPs 1–2 weeks after injection, in parallel with a reduction in the signal from g7-NPs, probably due to their degradation. Quantification of g7-NPs in brain slices from injected mice confirmed a decreased number of NPs over time as determined after normalizing the red spots on the mean size of NPs (Fig 3D). In the liver, the kinetics of NBD-Chol release and g7-NPs degradation was faster (< 24 h) than in brain (Appendix Fig S6).

g7-NPs-Chol rescue synaptic activity in HD mice

As synaptic transmission in striatal MSNs is altered in R6/2 mice during disease progression (Cepeda *et al*, 2003, 2004), we next explored whether cholesterol supplementation to the brain via systemic injection of g7-NPs-Chol restored synaptic parameters in HD mice. Pilot experiments with R6/2 animals that received only 1 or 2 injections of g7-NPs-Chol did not show any significant modifications in electrophysiological properties (data not shown). We therefore designed our trials in order to provide sustained and prolonged delivery of cholesterol to the HD brain. Treatment started at the pre-symptomatic stage (5 weeks of age) and continued until the symptomatic stage (9 weeks of age) under

 © 2015 The Authors

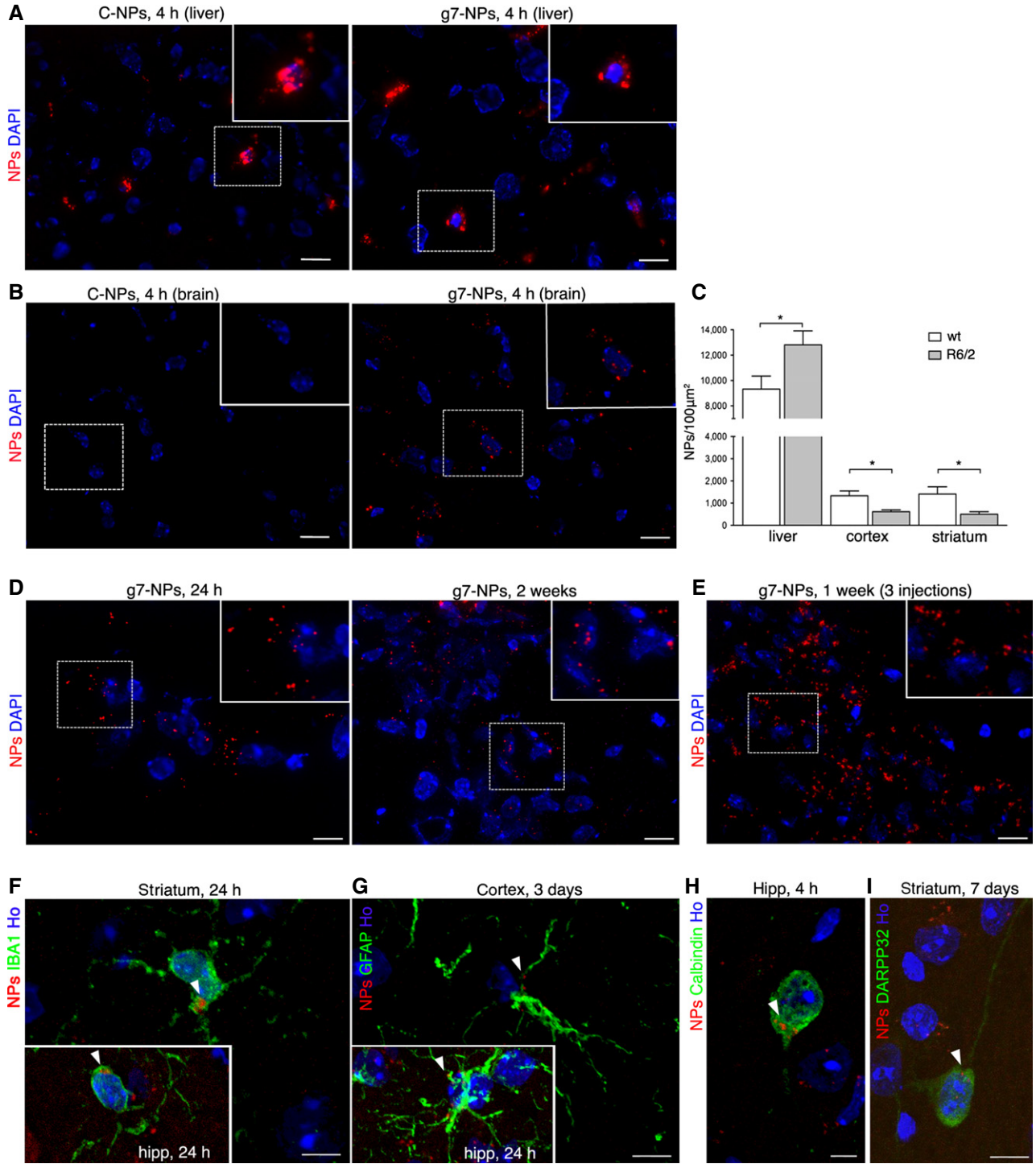

Figure 2. g7-NPs reach different brain cells and release cholesterol in R6/2 mice.

A, B Representative confocal images of liver (A) and brain (B) slices from R6/2 mice ip injected with C-NPs (left) or with g7-NPs (right) and sacrificed after 4 h.

C Quantification of g7-NPs localized in the liver, striatum, and cortex of WT (n = 3) and R6/2 mice (n = 3). Data are expressed as the number of g7-NPs for 100 µm^2 ± SEM. Statistics: *P < 0.05 determined by Student's t-test.

D, E g7-NPs in brain slices from R6/2 mice administered with a single ip injection and sacrificed after 24 h (D, left) or 2 weeks (D, right) and after multiple ip injections within 1 week (E).

F–I Representative confocal images of immunostaining against IBA1 (F), GFAP (G), calbindin (H), and DARPP-32 (I) on coronal sections of brains isolated from R6/2 mice ip injected with g7-NPs and sacrificed at the indicated time points. White arrowheads indicate intracellular g7-NPs.

Data information: DAPI (A, B, D) or Hoechst 33258 (Ho) (F–I) was used to counterstain nuclei. Scale bars: 20 µm (A); 10 µm (B, D, E); 5 µm (F–I).

© 2015 The Authors

two experimental regimens. One group of R6/2 mice and WT littermates were administered 0.15 mg g7-NPs/g body weight for each injection, once every two weeks (three injections total) while the second experimental group was injected twice a week (ten injections total) accounting for a total estimated amount of 6.3 μg or 21 μg of cholesterol injected, respectively. Four groups were compared: WT mice administered with saline (referred to as WT), R6/2 mice administered with saline (referred to as R6/2), R6/2 injected with empty g7-NPs (referred to as R6/2-emp), and R6/2 mice receiving three or ten injections (referred to as R6/2-Chol). At sacrifice, the presence of g7-NPs was analyzed by fluorescence microscopy in liver sections from each animal and in cortical samples taken from the brains before the electrophysiological recordings (Appendix Fig S7). At the end of the analyses, data from the two experimental paradigms were pooled together as no significant differences were found.

HD mouse models have been extensively analyzed for their basic striatal electrophysiological phenotypes. Similar and robust defects have been described in striatal MSNs, namely a reduced membrane capacitance, a decrease in spontaneous excitatory postsynaptic current (EPSC), and an increase in spontaneous inhibitory postsynaptic current (IPSC) frequencies (Cepeda *et al*, 2003). The consistency of these phenotypes across different HD mouse models suggests that these changes are a result of the mutant huntingtin gene. We therefore tested whether our experimental scheme for cholesterol supplementation could reverse any of these phenotypes. Our whole-cell patch-clamp recordings of MSNs in brain slices showed that membrane capacitance, a reflection of membrane area, was significantly reduced in R6/2 mice treated with saline or empty g7-NPs (R6/2-untreated; data were pooled as no differences were found), compared to WT mice (WT, treated with saline) (Appendix Table S3). In contrast, in neurons from R6/2 mice treated with g7-NPs-Chol (R6/2-Chol), cell capacitance was not significantly reduced compared to WT cells, suggesting a mild rescue of cell membrane area (Appendix Table S3). Input resistance was found increased in both R6/2-untreated and R6/2-Chol neurons compared to WT neurons. Additionally, a significant decrease in the decay time constant in cells from R6/2-Chol mice compared with cells from WT or R6/2 mice treated with saline or empty g7-NPs was observed (Appendix Table S3). This effect may be attributed to changes in membrane fluidity induced by cholesterol supplementation.

The average frequency of spontaneous IPSCs was also significantly higher in MSNs from R6/2-untreated mice compared to WT mice (Fig 4A and B, inset), as previously observed (Cepeda *et al*, 2004). In contrast, R6/2-Chol mice displayed a significant reduction in the frequency of IPSCs compared to R6/2-untreated (Fig 4B, inset), in particular for small-amplitude events (< 40 pA; Fig 4B), while the cumulative inter-event interval histogram showed a decreased release probability in R6/2-Chol compared to R6/2-untreated cells (Fig 4C). Similar to MSNs from R6/2-untreated mice, IPSCs from R6/2-Chol mice had faster kinetics than cells from WT mice as judged by shorter decay time and half-amplitude duration of the current events compared to WTs (Appendix Table S4A).

The frequency of spontaneous excitatory postsynaptic currents (EPSCs) (Fig 4D) was significantly reduced in R6/2-untreated mice compared to WT mice (Fig 4E, inset). Although the decrease in the average frequency of EPSCs was not significantly rescued in R6/2-Chol mice, the cumulative inter-event interval indicated a significantly increased release probability in R6/2-Chol cells versus R6/2-untreated cells (Fig 4F). EPSC kinetics was similar among groups, except for half-amplitude duration, which was significantly shorter in R6/2-chol cells than in WT cells (Appendix Table S4B). Altogether, these findings indicate that specific membrane and synaptic alterations observed in MSNs from R6/2 mice can be rescued by *in vivo* cholesterol supplementation through g7-NPs.

Cholesterol supplementation ameliorates cognitive dysfunction in HD

We next assessed the impact of cholesterol supplementation on the behavior of HD mice by using motor and cognitive tasks. The injections regimen used in the behavioral studies, described in Fig 5A, is the same employed for electrophysiological studies. In the rotarod test, R6/2 mice treated with saline or empty g7-NPs exhibited typical impaired coordination compared to WT mice, as indicated by a shorter latency to fall from an accelerating rotarod. This deficit was not improved in R6/2-Chol mice (Fig 5B). Similarly, in the open field test, reduced rearing activity, which is a form of vertical exploration, was not rescued by cholesterol supplementation at 10 weeks of age (Fig 5C). At the same age, the hypokinetic phenotype shown in R6/2 mice (measured as global activity in the open field) was still apparent in R6/2-Chol, but the phenotype was less dramatic compared to R6/2-untreated mice and significance reached $P < 0.05$ (Fig 5D), suggesting that cholesterol supplementation partially ameliorates locomotion-related behavior in a novel environment. Other parameters (stereotyped movements, locomotion, resting time, mean velocity) showed similar changes (Appendix Fig S8A). Accordingly, R6/2-untreated mice worsened over time more than R6/2-Chol mice (Appendix Fig S8B) as indicated by the significant difference reached at later time points when the two groups were compared at 8 and 10 weeks of age. These findings suggest that sustained and repeated cholesterol supplementation might slow the disease progression.

As changes in cholesterol synthesis/levels are associated with cognitive decline (Suzuki *et al*, 2013), we next evaluated cognitive tasks in HD mice after cholesterol supplementation. To evaluate cognitive performance, we used the novel object recognition test, a low-stress task aimed at evaluating recognition memory. Importantly, object memory is impaired in patients with HD. In a pattern recognition task, subjects have to remember and touch the abstract patterns they are shown during training and that are paired with a novel pattern during testing. Early HD patients and clinically symptomatic subjects performed significantly worse than control subjects (Lawrence *et al*, 1996, 2000). R6/2-untreated mice showed a pronounced inability to discriminate novel from familiar objects from 8 weeks of age and worsened over time (Fig 5E). Notably, R6/2-Chol mice performed as well as WT mice, indicating that cholesterol supplementation rescued memory deficits at all time points (Fig 5E). Importantly, the time-course analysis also revealed that the benefit on recognition memory in R6/2-Chol mice was still present at 12 weeks of age, that is, 3 weeks after the last injection (Fig 5E).

 © 2015 The Authors

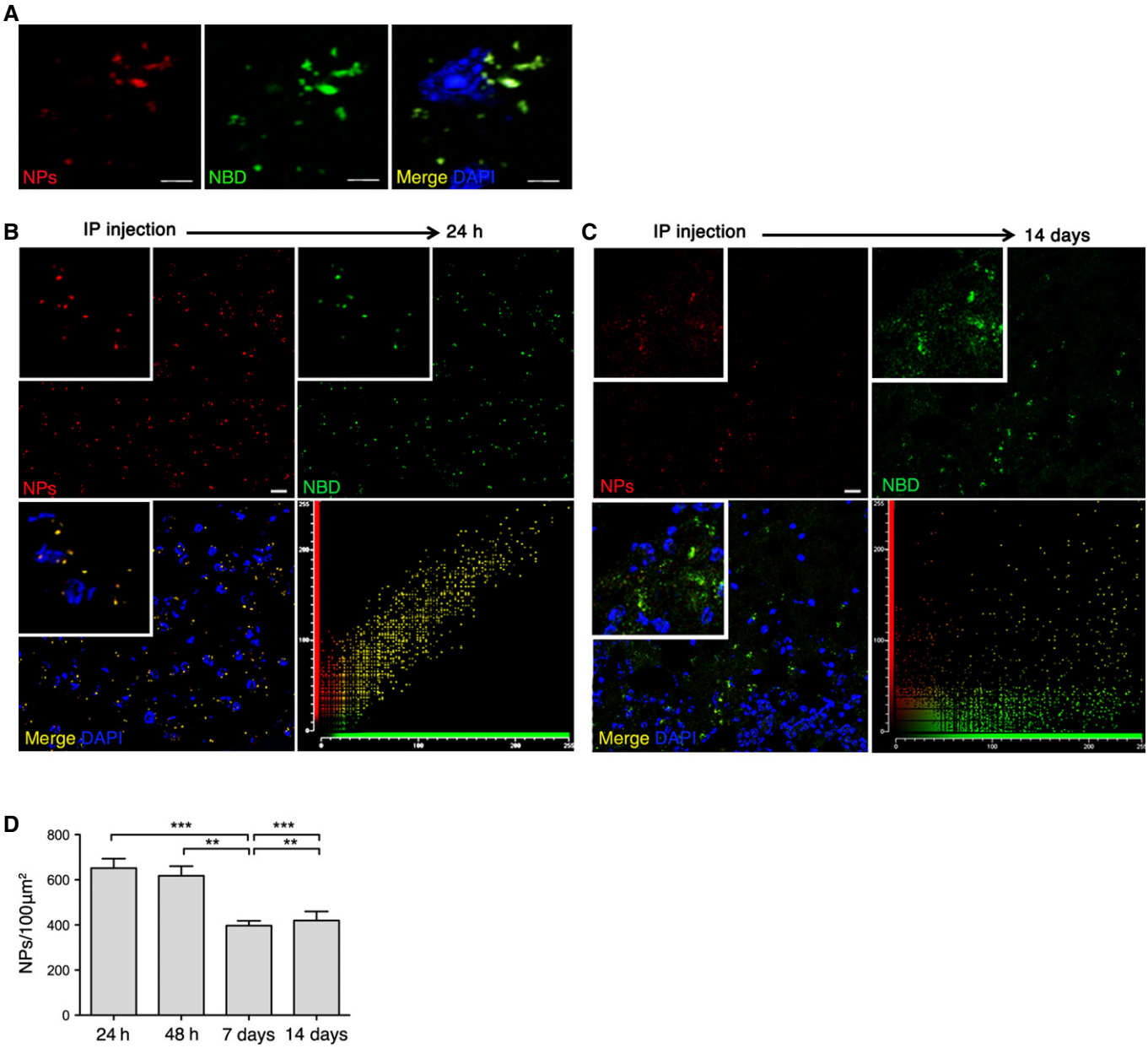

Figure 3. Cholesterol delivery and release *in vivo* in the R6/2 brain.

A Representative confocal image (crop) of brain slices from R6/2 mice ip injected with rhodamine-labeled g7-NPs-NBD-Chol and sacrificed after 12 h, showing co-localization of NBD-Chol (green) and rhodamine (NPs, red). Scale bar: 5 µm.

B, C Representative confocal image (low magnification) of brain slices from R6/2 mice ip injected with g7-NPs-NBD-Chol and sacrificed after 24 h (B) or 2 weeks (C) and relative co-localization of NBD-Chol and g7-NPs. Scale bar: 10 µm.

D g7-NPs quantification in brain slices at the same time points in (B, C). Data are expressed as number of g7-NPs (evaluated based their size) for 100 μm^2 ± SEM. Statistics: $^{**}P < 0.01$ (48 h vs. 7 days; 7 days vs. 14 days), $^{***}P < 0.001$ (24 h vs. 7 days; 7 days vs. 14 days) determined by one-way ANOVA followed by Newman–Keuls multiple comparison test.

Data information: DAPI was used to counterstain nuclei.

Cholesterol supplementation restores levels of synaptic components but not neuropathology

To determine whether cholesterol supplementation modulates synaptic protein machinery, we used biochemically purified triton-insoluble fractions (TIF) from the brain of WT ($n = 5$), R6/2-untreated ($n = 6$) and R6/2-Chol ($n = 3$) mice and performed semiquantitative Western blotting for scaffolding proteins such as PSD95 and gephyrin and NMDA receptor subunits (GluN1 and GluN2B) (Fig 6A). Reduced PSD95, as well as a reduction in GluN1 and GluN2B, were found in R6/2-untreated mice compared to WTs, as expected (Fig 6B). Importantly, cholesterol supplementation

© 2015 The Authors

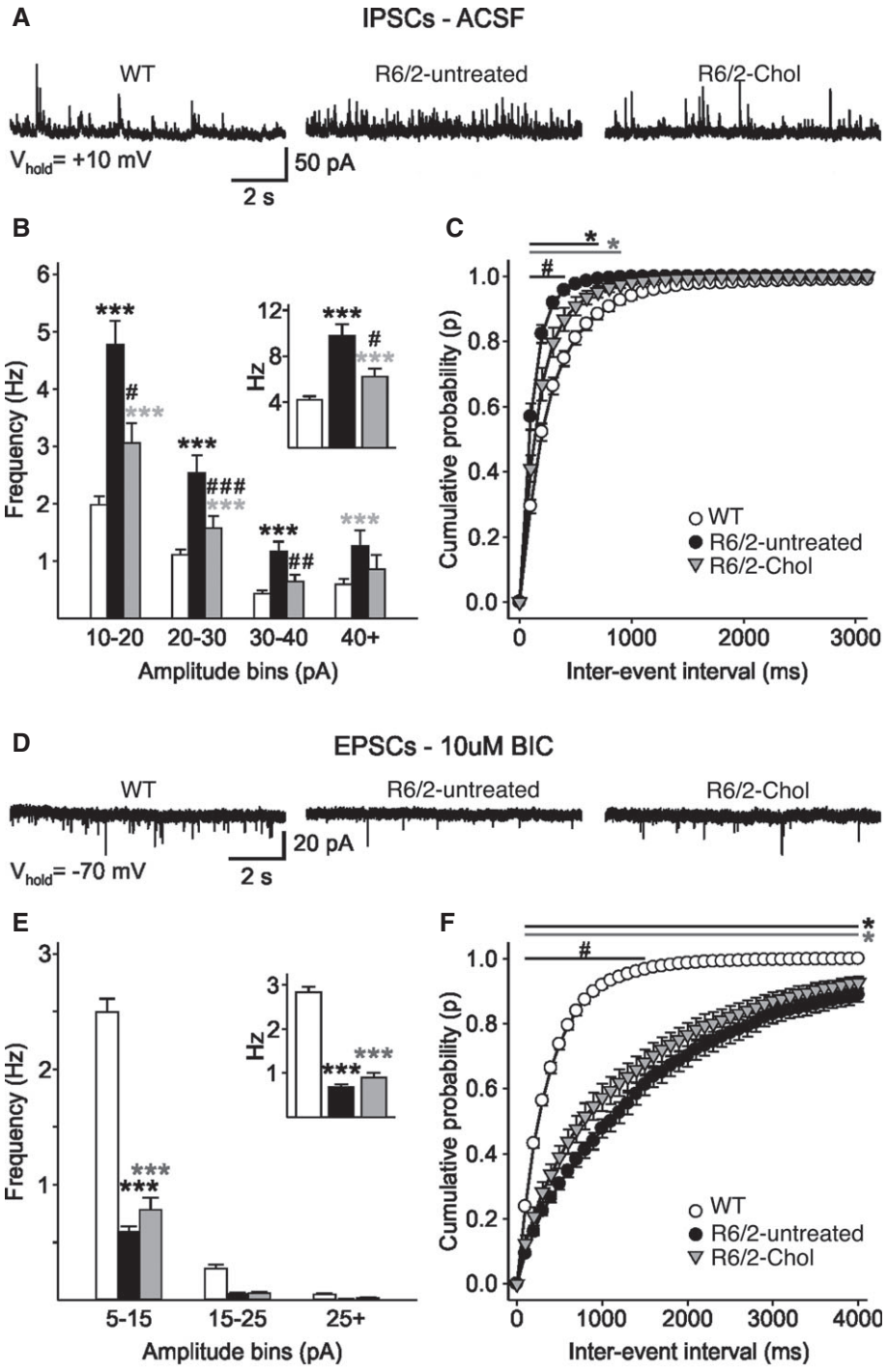

Figure 4. Systemic injections of g7-NPs-Chol rescue synaptic alteration in R6/2 mice.

A Spontaneous IPSCs were recorded from striatal MSNs (WTs = 52; R6/2-untreated = 27; R6/2-Chol = 29) at a holding potential of +10 mV. As no differences were found between R6/2 mice treated with saline (R6/2) or with empty g7-NPs (R6/2-emp), data were pooled.

B Amplitude–frequency histogram and average frequency (inset) of IPSCs from R6/2-Chol, R6/2-untreated, and WT MSNs.

C Cumulative inter-event histogram showing the release probability of IPSCs in all groups.

D Spontaneous EPSCs were recorded from striatal MSNs (WTs = 52; R6/2-untreated = 27; R6/2-Chol = 29) at a holding potential of −70 mV. As no differences were found between R6/2 mice treated with saline (R6/2) and with empty g7-NPs (R6/2-emp), data were pooled.

E Amplitude–frequency histogram and average frequency (inset) of EPSCs from R6/2-Chol, R6/2-untreated, and WT MSNs.

F Cumulative inter-event histogram showing the release probability of EPSCs in all groups.

Data information: (B, D–F) Data represent mean ± SEM. $P < 0.05$ was determined by one-way ANOVA followed by Newman–Keuls multiple comparison tests ($^{\#}P < 0.05$, $^{\#\#}P < 0.01$, $^{\#\#\#}P < 0.001$ R6/2-untreated mice vs. R6/2-Chol mice; $^{*}P < 0.05$, $^{**}P < 0.01$, $^{***}P < 0.001$ WT mice vs R6/2-untreated or R6/2-Chol mice).

 © 2015 The Authors

normalized or increased the levels of these proteins (Fig 6B), suggesting a rescue of the molecular composition of the synaptic machinery contributing to synaptic structure.

To evaluate whether cholesterol supplementation also influences the expression of synaptic genes, we performed qRT–PCR for a panel of synaptic genes known to be reduced in HD. BDNF mRNA is reduced in brain of several HD mice and is considered a critical hallmark in HD (Zuccato and Cattaneo (2014). Unpaired *t*-test between R6/2-untreated and R6/2-Chol groups revealed a slight but significant increase of *bdnf* expression in HD cortex after cholesterol supplementation (Fig 6C). We also evaluated the expression of *snap25* and *complexin II* (Fig 6D and E), the latter being a gene encoding for a presynaptic protein involved in neurotransmitter release (Reim *et al*, 2001). Similarly to *bdnf*, mRNA levels of snap25 were significantly increased in cortex of HD mice after cholesterol supplementation (Fig 6D). mRNA level of *complexin II* was strongly reduced in cortex, hippocampus, and striatum of R6/2-untreated mice compared to WTs. Cholesterol supplementation significantly increased *complexin II* expression in hippocampus and striatum from R6/2-Chol mice compared to R6/2-untreated mice (Fig 6E). These findings suggest that cholesterol supplementation partially ameliorates transcriptional abnormalities in the synaptic machinery in HD mice.

We also quantified mRNA levels of genes considered to be MSN markers, that is, darpp32, dopamine receptor D2 (drd2), and muscarinic acetylcholine receptor M4 (chmr4). As expected, all these genes were reduced in the striatum from R6/2-untreated mice compared to WTs, but cholesterol supplementation did not significantly influence their expression (Appendix Fig S9).

To investigate whether cholesterol supplementation counteracts striatal atrophy and MSN degeneration, we performed unbiased stereological analyses at 12 weeks of age. Reduced striatal volume and enlargement of ventricles, both measures of striatal atrophy, were observed in R6/2 mice treated with saline (R6/2) compared to WTs (Appendix Fig S10; Fig 6F), as already reported in the literature. The administration of empty g7-NPs or g7-NPs-Chol did not influence striatal volume in R6/2 mice (Appendix Fig S10). A statistically significant reduction in ventricular volume was evident in R6/2-Chol in comparison with R6/2 mice, similar to that observed in WTs (Fig 6F). However, R6/2 mice treated with empty g7-NPs (R6/2-emp) also showed a similar rescue, suggesting that the administration of g7-NPs *per se*, likely due to degradation of PLGA in lactic and glycolic acids, might influence this neuropathological parameter.

Altogether, these findings suggest that cholesterol supplementation via g7-NPs is not sufficient to counteract brain atrophy and neurodegeneration in R6/2 mice, at least with this experimental paradigm, although it does increase the expression of specific genes and synaptic proteins.

In vivo evaluation of safety of g7-NPs in HD mice

Cholesterol supplementation to the brain might lead to a further reduction in cholesterol synthesis, already compromised in R6/2 mice (Valenza *et al*, 2007b). We therefore measured cholesterol precursors and the brain-specific cholesterol catabolite 24OHC in the brain of the treated mice at 12 weeks of age. Lathosterol, a marker of cholesterol synthesis, was equally reduced in both R6/2-untreated and R6/2-Chol mice compared to WTs (Fig 7A), suggesting that exogenous cholesterol supplemented via g7-NPs does not further decrease the endogenous biosynthetic pathway. Similarly, 24OHC, an indicator of brain cholesterol catabolism that usually mirrors cholesterol biosynthesis in brain (Lund *et al*, 2003), was found similarly reduced in both R6/2 groups compared to WTs (Fig 7B).

As it is known that most of the NPs (90%) localize in periphery, we also measured mRNA levels of cholesterol biosynthetic genes (*hmgcr* and *fdft1*) in liver and lung. The mRNA expression of both cholesterol genes was similar in both tissues in all groups, even in the presence of g7-NPs-Chol (Fig 7C and D). All these results suggest that the exogenous cholesterol delivered to the brain or accumulated in peripheral tissues does not lead to alterations of endogenous cholesterol homeostasis in the time frame analyzed in this study.

Although the NPs employed in this study are considered biocompatible and biodegradable as made of PLGA, which is approved by the FDA and EMA, an immunogenicity study of these NPs *in vivo* is missing. Both PLGA, released after degradation of empty or cholesterol-loaded g7-NPs, and cholesterol itself might influence immune responses. Therefore, we analyzed mRNA levels of two pro-inflammation genes encoding for TNF-alpha and IL6, in peripheral tissues from our cohorts. As shown in Fig 7E and F, *Tnf-alpha* and *Il6* mRNA levels were significantly increased in the liver and in lung of R6/2 mice treated with saline (R6/2) compared to WTs, supporting the available evidence that peripheral inflammation is associated with HD condition (Trager *et al*, 2014; Chang *et al*, 2015). Similar activation of inflammatory genes was also observed in R6/2 mice treated with empty g7-NPs (R6/2-emp) or g7-NPs-Chol (R6/2-Chol), suggesting that multiple administrations of g7-NPs (empty or loaded with cholesterol) do not affect *per se* peripheral inflammation in R6/2 mice.

Discussion

Synaptic dysfunction is an attractive target for possible HD therapies as it occurs early in the disease process when cell death in HD models is not obvious (Cepeda *et al*, 2004; Cummings *et al*, 2006; Joshi *et al*, 2009; Milnerwood *et al*, 2010) and paralleling the evidence that cognitive disturbances in patients with HD occur long before onset of overt motor manifestations (Levine *et al*, 2004; Paulsen *et al*, 2008; Schippling *et al*, 2009; Orth *et al*, 2010). We show that exogenous cholesterol supplementation to the HD mouse brain restores normal synaptic communication and protects mice from cognitive decline. This study provides the missing link between the reduction in brain cholesterol in the mouse HD brain and some of the neuronal abnormalities in the disease state. The data herein reported are in line with our recent *in vitro* studies, suggesting that strategies aimed at supplying cholesterol to HD neurons can ameliorate neuronal and synaptic dysfunction (Valenza *et al*, 2015).

Cholesterol supplementation via ip injection of cholesterol-loaded NPs normalizes GABAergic and, partially, glutamatergic synaptic activity in striatal MSNs of R6/2 mice (Fig 4), supporting the relevance of cholesterol in synaptic integrity and neuronal

© 2015 The Authors

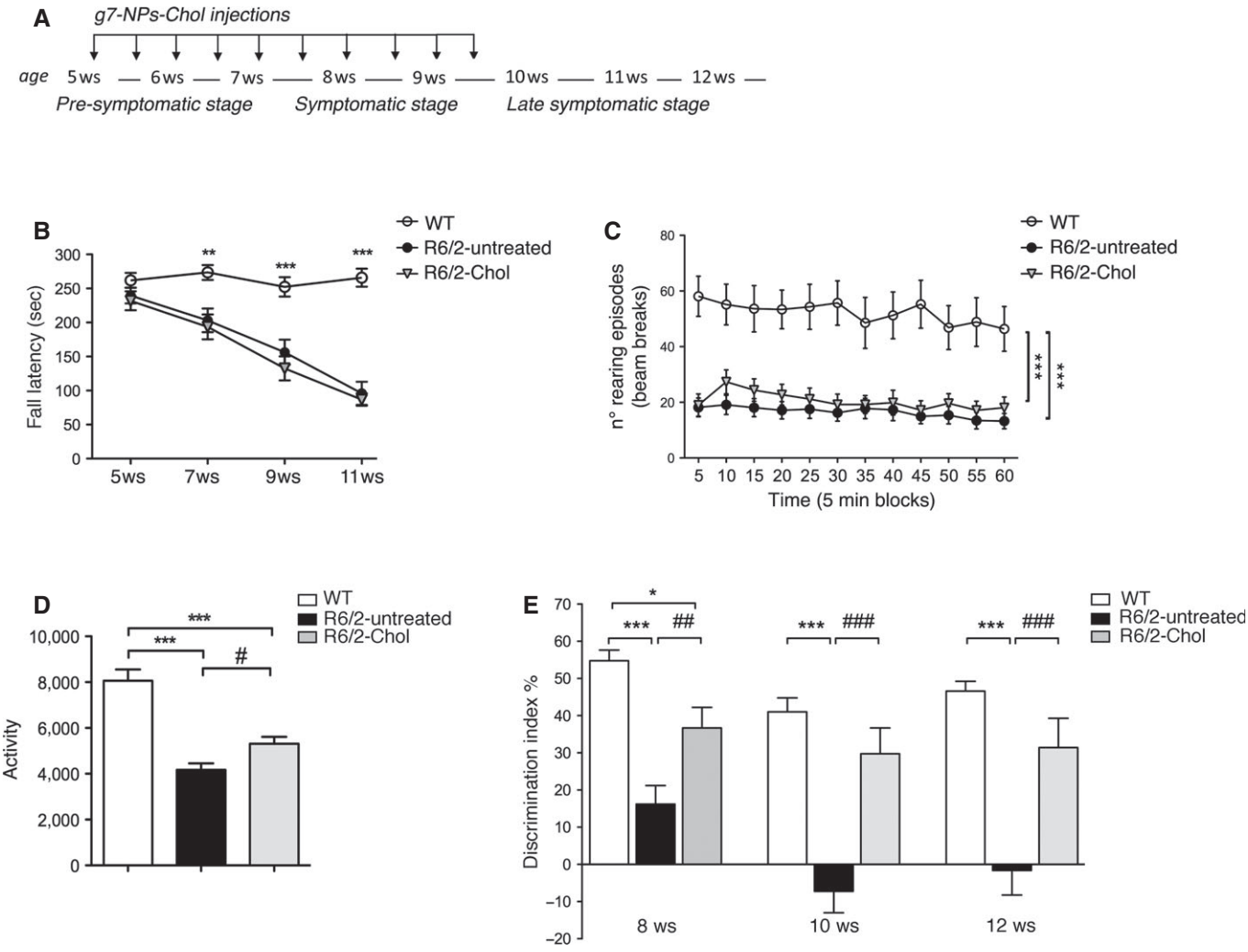

Figure 5. Systemic injections of g7-NPs-Chol ameliorate cognitive defects in R6/2 mice.

A Experimental paradigm performed in all the trials.

B Fall latency from an accelerating rotarod for 5- to 11-week-old WT and R6/2 mice during cholesterol supplementation (WT = 17; R6/2-untreated = 21; R6/2-Chol = 13).

C Rearing activity in open field at 10 weeks of age (WT = 14; R6/2-untreated = 21; R6/2-Chol = 15).

D Global activity in the open field test at 10 weeks of age (WT = 14; R6/2-untreated = 21; R6/2-Chol = 15).

E Index of discrimination (%) in WT, R6/2-untreated, and R6/2-Chol mice during disease progression, at 8 weeks of age (WT = 24; R6/2-untreated = 36; R6/2-Chol = 21), at 10 weeks of age (WT = 25; R6/2-untreated = 35; R6/2-Chol = 20), and at 12 weeks of age (WT = 24; R6/2-untreated = 30; R6/2-Chol = 19); the index above zero indicates a preference for the novel object; the index below zero indicates a preference for the familiar object. As no differences were found between R6/2 mice treated with saline (R6/2) or treated with empty g7-NPs (R6/2-emp), data were pooled.

Data information: Data in (B–E) are from three independent trials and represent mean ± SEM. $P < 0.05$ was determined by two-way ANOVA (in B, C) and by one-way ANOVA (in D, E) followed by Newmann–Keuls multiple comparison tests ($^{\#}P < 0.05$, $^{\#\#}P < 0.01$, $^{\#\#\#}P < 0.001$ R6/2-untreated mice vs. R6/2-Chol mice; $^{*}P < 0.05$, $^{**}P < 0.01$, $^{***}P < 0.001$ WT mice vs. R6/2-untreated or R6/2-Chol mice).

function (Pfrieger, 2003). Cholesterol supplementation also protects R6/2 mice from cognitive decline as measured by recognition memory recovery (Fig 5E). Novel object preference has been often associated with the hippocampus; however, it also depends on functional interaction between hippocampus and cortex (Barker & Warburton, 2011) and, more recently, it has been linked to the striatum (Darvas & Palmiter, 2009). Consistently, reduction of the cholesterol sensor SCAP in the brains of mice leads to a decrease in brain cholesterol synthesis and causes impaired synaptic transmission and altered cognitive function assessed by novel object recognition test (Suzuki *et al*, 2013). Of note, cognitive decline has been recently associated with hippocampal cholesterol loss and cholesterol infusion in aged mice improved learning and memory in aged rodents (Martin *et al*, 2014a).

Several *in vitro* findings indicate that synaptic transmission is sensitive to cholesterol levels both at pre-synaptic and post-synaptic levels. Indeed, cholesterol depletion affects vesicle recycling and fusion (Thiele *et al*, 2000; Dason *et al*, 2010, 2014; Linetti *et al*, 2010), AMPARs mobility (Hering *et al*, 2003; Renner *et al*, 2009; Martin *et al*, 2014b), and the distribution and

 © 2015 The Authors

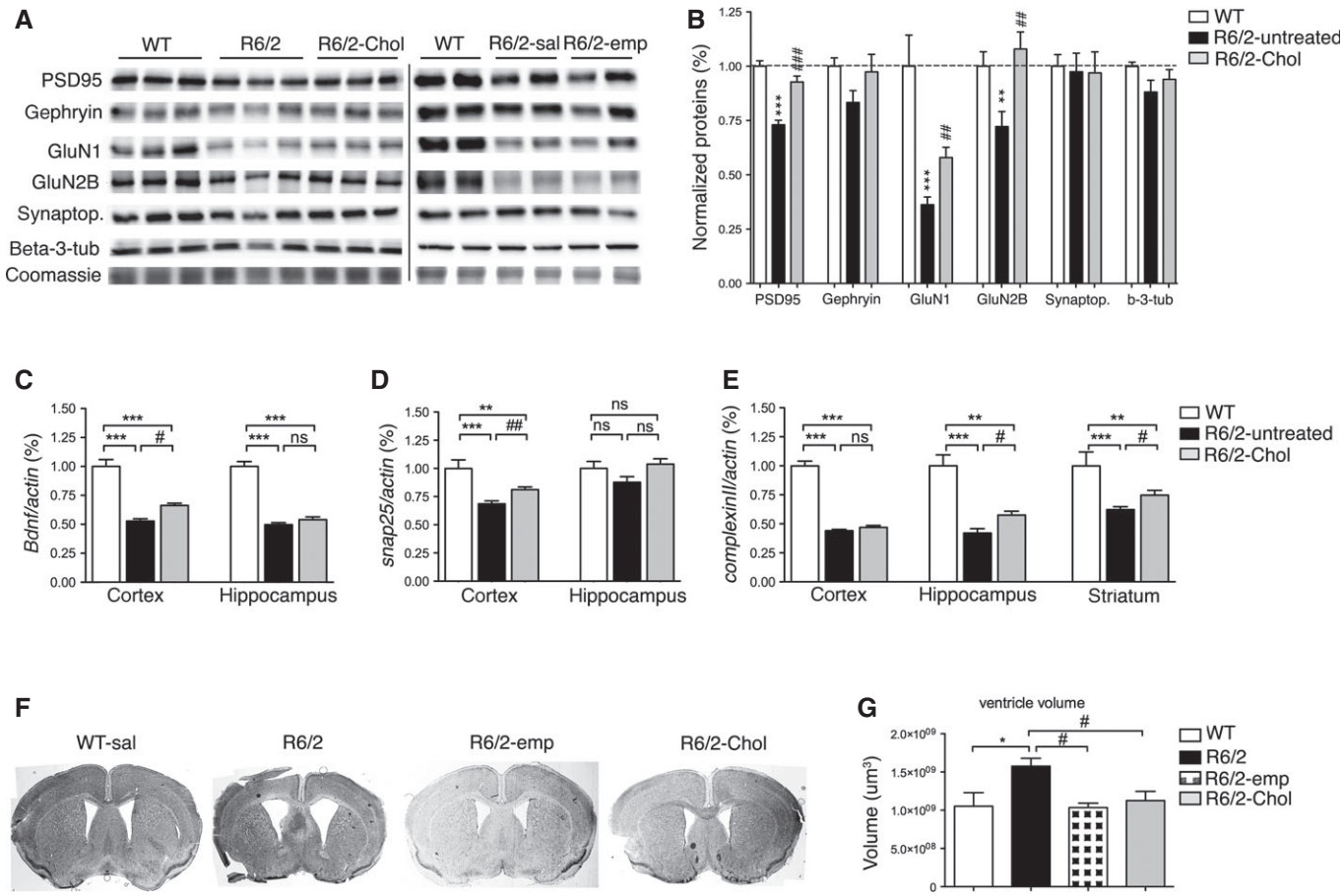

Figure 6. Systemic injections of g7-NPs-Chol positively influence synaptic protein network but not neuropathology.

A, B Protein levels (A) and relative densitometry quantification (B) of several synaptic proteins in triton-insoluble (synaptic enriched) fractions purified from total brains from WT (n = 5), R6/2-untreated (n = 5) and R6/2-Chol (n = 3). Levels of PSD95 and NMDA receptor subunits GluN1 and GluN2B are rescued in R6/2 mice by cholesterol supplementation.

C–E mRNA levels for Bdnf (C), and Snap25 (D) in cortex and hippocampus; Complexin II (E) in cortex, hippocampus, and striatum from a subset of WT (n = 4), R6/2-untreated (n = 7), and R6/2-chol animals (n = 3). As no differences were found between R6/2 mice treated with saline or treated with empty g7-NPs, data were pooled.

F, G Representative images of Nissl staining (F) and ventricle volume revealed by Neurolucida analysis at 12 weeks of age in WT (n = 7), R6/2 (n = 7), R6/2-emp (n = 6), and R6/2-Chol (n = 8) mice.

Data information: Data in (B–E, G) represent mean ± SEM. $P < 0.05$ was determined by one-way ANOVA followed by Newman–Keuls multiple comparison tests (in B, E) and by Student's t-test between R6/2-untreated and R6/2-Chol (in C, D) ($^{\#}P < 0.05$, $^{\#\#}P < 0.01$, $^{\#\#\#}P < 0.001$ R6/2-untreated mice vs. R6/2-Chol mice; $^{*}P < 0.05$, $^{**}P < 0.01$, $^{***}P < 0.001$ WT mice vs. R6/2-untreated or R6/2-Chol mice).
Source data are available online for this figure.

function of NMDAR (Frank *et al*, 2004, 2008). Accordingly, we found that cholesterol supplementation increases the levels of the scaffold synaptic protein PSD95 and NMDARs in synaptic protein-enriched fractions of HD mice (Fig 6A and B), suggesting that *in vivo* delivery of cholesterol contributes to preserve the structure and integrity of the synaptic machinery. In agreement with the biochemical findings, the partial but significant increase of mRNA levels of *bdnf*, *snap25,* and *complexin II* (all involved in synaptic transmission) in different brain regions of HD mice after cholesterol supplementation (Fig 6C–E) suggests that cholesterol may act at different levels in improving synaptic and cognitive functions. In particular, mRNA levels of complexin II, a key player in the mechanisms underlying cognitive processes (Reim *et al*, 2001; Glynn *et al*, 2003), are reduced in R6/2 mice and in human HD striatum and cortex (Morton & Edwardson, 2001; Freeman & Morton, 2004) and complexin II knockout mice show selective cognitive deficits that reflect those seen in R6/2 mice (Glynn *et al*, 2003). The cognitive benefits might be also related to an effect of exogenous cholesterol on hormone steroids (Hara *et al*, 2015), but further studies are needed to address this issue.

Cholesterol is also required to establish proper membrane permeability, fluidity, and thickness, and it stabilizes membranes and provides order to membranes. The partial rescue of membrane capacitance and the decrease in the decay time constant that we have observed in striatal MSNs from R6/2 mice treated with g7-NPs-Chol (Appendix Table S4) suggest that cholesterol supplementation

© 2015 The Authors

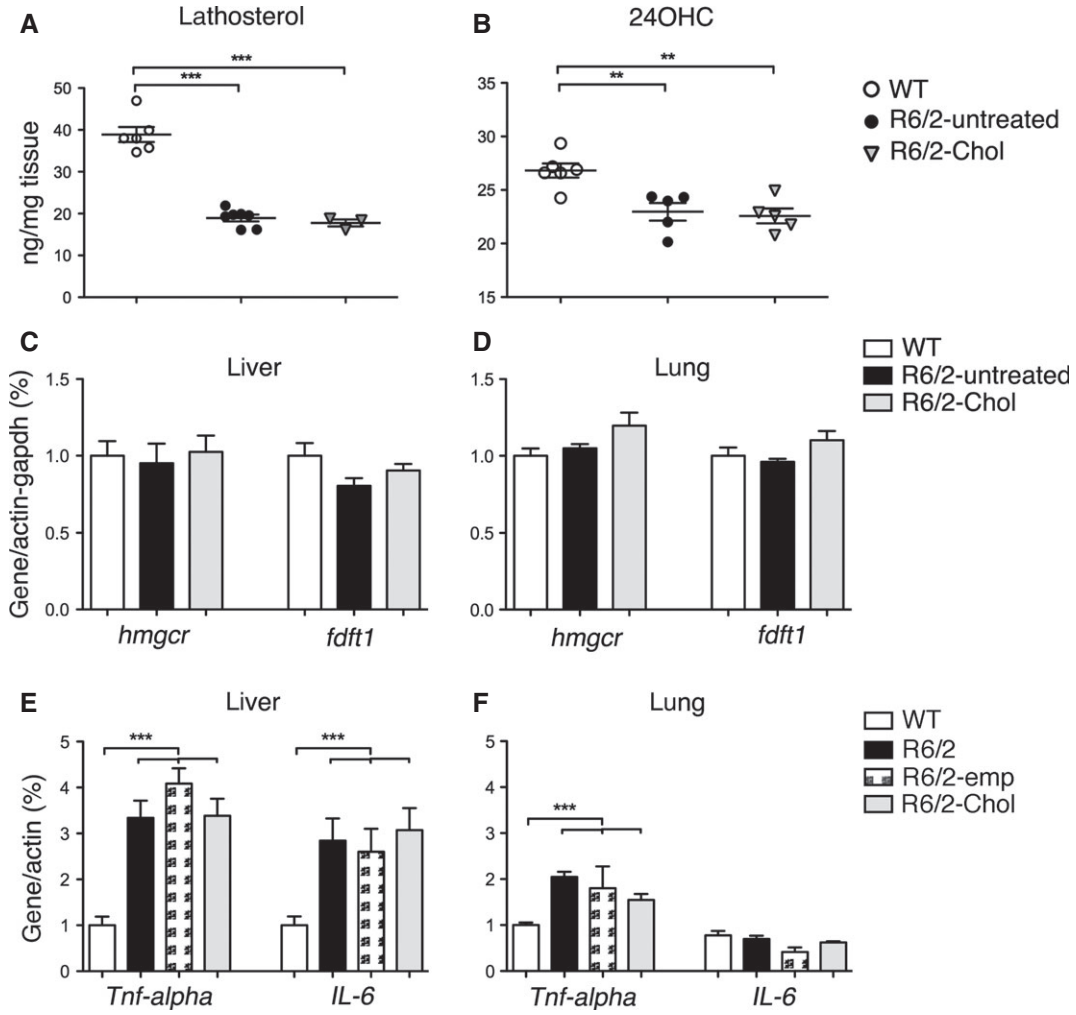

Figure 7. Exogenous cholesterol or g7-NPs *per se* do not influence endogenous cholesterol synthesis or induce inflammatory response.

A, B Lathosterol and 24OHC measured by mass spectrometry in the brain of WT (n = 6), R6/2-untreated (n = 7) and R6/2-Chol (n = 5) mice.

C, D mRNA levels of hmgcr and fdft1 in liver and lung of WT (n = 7), R6/2-untreated (n = 8) and R6/2-Chol (n = 4) mice. As no differences were found between R6/2 mice treated with saline or treated with empty g7-NPs, data were pooled.

E, F mRNA levels of inflammatory genes in liver and lung of the of WT (n = 7), R6/2 (n = 4), R6/2-emp (n = 4) and R6/2-Chol (n = 5) mice.

Data information: Data in (A–F) represent mean ± SEM. *$P < 0.05$, **$P < 0.01$, ***$P < 0.001$ was determined by one-way ANOVA followed by Newman–Keuls multiple comparison tests.

induces changes in membrane fluidity. However, other than showing its incorporation into the membrane (Appendix Fig S5), we were not able to establish where exactly the exogenous cholesterol, once released by g7-NPs, localizes in brain cells, and more refined methods to visualize exogenous cholesterol at subcellular levels are needed.

We also reported that cholesterol supplementation does not rescue motor defects and restores only partially the global activity of HD mice (Fig 5B and D). The dichotomy that we observed in rescuing cognitive but not motor functions might be associated with specific roles of cholesterol in neuronal function. Similarly, neuropathological hallmarks such as striatal volume and MSN markers (Appendix Figs S9 and S10) do not significantly change after cholesterol supplementation in R6/2 mice, suggesting that cholesterol alone, at least within this experimental paradigm, is not sufficient to prevent brain atrophy or to improve neuropathology. Of note, both empty g7-NPs and g7-NPs-Chol seem to counteract the enlargement of ventricle volume observed in R6/2 mice (Fig 6F and G) likely due to degradation of PLGA in lactic and glycolic acids that might influence metabolic pathways related to energy. However, the significance of this effect is unknown and cannot be ascribed to cholesterol. We should also consider that the content of cholesterol delivered to the brain through g7-NPs is estimated to be 21 μg (for the ten injections) and, although we started the treatment at 5 weeks of age, cholesterol was released after 1–2 weeks as shown by the co-localization studies (Fig 3). Both low dose and slow timing of cholesterol release might not be sufficient to reverse motor performance and brain atrophy in HD mice. Further studies, by

 © 2015 The Authors

employing mini-pump-based strategies for early and continuous delivery of well-defined concentrations of cholesterol, will allow to gain more information about the possible impact of cholesterol delivery on motor defects.

Recent advances in nanotechnology and growing needs in biochemical applications have driven the development of multifunctional nanoparticles. Nanodrugs in liposome- or albumin-based formulations are already used in the clinic for some forms of cancers (Barenholz, 2012; Sethi *et al*, 2013; Von Hoff *et al*, 2013), and others are being tested in pre-clinical trials (Tasciotti *et al*, 2008; Shen *et al*, 2013). This is the first study in which g7-NPs have been applied to a disease model for CNS targeting of molecules that are not able to cross the BBB (such as cholesterol). g7-NPs reach different brain regions 2–4 h after a single systemic injection and localize in different brain cells, including striatal neurons (Figs 1 and 2). Previous pharmacological and biodistribution studies estimated that the percentage of g7-NPs that reaches the brain is > 10% of the injected dose (Tosi *et al*, 2007) and that multiple non-receptor-mediated mechanisms are implicated (Tosi *et al*, 2011b). Other NPs carrying ligands, antibodies, or peptides for specific receptors that enter into the brain by receptor-mediated endocytosis usually reach the brain compartment as maximum level values ranging from 0.1 to 1% of the injected dose (Gabathuler, 2010; Tosi *et al*, 2012; Gosk *et al*, 2004) owing to a possible saturation of the receptor or by the competiveness of endogenous ligands. Therefore, g7-NPs may represent a novel tool that can be used for brain delivery of several molecules. However, from a therapeutic prospective, we are conscious that additional quantitative studies of g7-NPs alone and loaded with cholesterol are needed to increase the knowledge about biodistribution and pharmacokinetics.

The polymeric NPs used in this study are made of PLGA, a copolymer approved by the FDA as drug delivery system for parenteral administration (Danhier *et al*, 2012). PLGA is considered biodegradable and biocompatible as it degrades completely into its original monomers, lactic and glycolic acid, which are easily metabolized in the body via the Krebs cycle and then eliminated (Shive & Anderson, 1997). However, specific studies concerning immune reactivity of g7-NPs are missing. Similarly, depending on the molecule delivered, specific studies should be performed in order to exclude any immune reaction or other side effects in different tissues. Our studies suggest that g7-NPs and cholesterol itself do not induce inflammatory response in liver and lungs, where almost all g7-NPs are localized. A more extensive biochemical study to evaluate the impact of g7-NPs degradation (and of the molecule released) is needed to accelerate preclinical testing and translational developments of these NPs.

A limitation of g7-NPs in this current study is the low drug loading (1%) that does not allow the delivery of elevated amounts of cholesterol. Presumably, a high amount of cholesterol, its strong affinity for hydrophobic interactions, and the rigidity of the sterane ring lead to the disruption of the PLGA organization as observed for NPs-Chol3 formation (Fig 1), with a marked increase in sample heterogeneity and low quality of nanoparticles. The identification of strategies aimed at increasing the amount of cholesterol encapsulated into g7-NPs without affecting chemical–physical properties of NPs will allow to reduce the number of injections/week while increasing the amount of cholesterol that reaches the brain cells. From another prospective, the low content and the slow release of cholesterol by g7-NPs might be advantageous as cholesterol accumulation is dangerous for the brain. Further studies are needed to identify the threshold of cholesterol increase that is beneficial for HD brain/neurons and beyond which negative effects may occur.

The very low dose of exogenous cholesterol delivered in the brain of HD mice in our experimental paradigm (21 μg) does not allow to discriminate it from the large content of endogenous cholesterol even by mass spectrometry. However, the demonstration of a rescue in specific electrophysiological and behavioral phenotypes support the notion that the exogenous cholesterol delivered to the adult brain is sufficient to ameliorate neuronal dysfunction in HD. A similar concentration of cholesterol infused via osmotic pumps in aged mice has recently been able to improve learning and memory in aged rodents (Martin *et al*, 2014a).

In conclusion, these results emphasize the beneficial effects of cholesterol supplementation in reversing synaptic alterations and delaying cognitive defects in the HD mouse brain. Additionally, this study demonstrates the validity of a new technology based on g7-NPs to administer drugs (besides cholesterol) to the HD brain and lays the ground for future therapeutic approaches.

Materials and Methods

NPs formulation and characterization

Gly-L-Phe-D-Thr-Gly-L-Phe-L-Leu-L-Ser(O-β-D-Glucose)-$CONH_2$ (g7) was prepared as previously described (Tosi *et al*, 2011b) and conjugated with PLGA to obtain g7-PLGA. PLGA derivatization yields were confirmed by nuclear magnetic resonance to be 30–40 μmol peptide/g of polymer. PLGA conjugated with rhodamine (Sigma-Aldrich) was prepared as previously described (Costantino *et al*, 2005; Tosi *et al*, 2005). In all NPs, a fraction of polyvinyl alcohol (PVA) (about 12.5 mg PVA/100 mg NPs) remains stably associated with the NPs despite the repeated purification. The residual PVA forms a connected network with the PLGA chains becoming a "secondary" constituent of the NPs and partially masking the exposed acidic groups of the polymer. This explanation justifies the less negative values of ζ-pot with respect to those of the NPs prepared in the absence of PVA. Details related to the production and characterization of NPs and related to Fig 1 are listed in the Appendix Supplementary Methods.

Cell culture and glial and neuronal differentiation

Neural stem (NS) cells carrying normal (Q7/7) or mutant htt (Q140/7) employed in this study and protocols for their differentiation were previously described (Conforti *et al*, 2013; Valenza *et al*, 2015). Primary neuronal cultures were prepared from the cortex of R6/2 mice embryos (day 18 of gestation) as previously described (Valenza *et al*, 2015).

Animals and treatments

Experiments at the University of Milan were carried out in accordance with the European Communities Council Directive

© 2015 The Authors

2010/63/EU revising Directive 86/609/EEC regarding the care and use of animals for experimental procedures. All procedures at UCLA were performed in accordance with the U.S. Public Health Service Guide for Care and Use of Laboratory Animals and were approved by the Institutional Animal Care and Use Committee at UCLA. Genotyping of R6/2 mouse colonies (~150 CAG repeats) was performed by PCR of DNA obtained from tail samples, once at weaning and again following sacrifice for verification. The lifespan of this R6/2 mouse colony is approximately 12–14 weeks, with HD-like phenotypes evident from 8 weeks of age. All the mice have been randomly assigned to experimental groups, and the investigators have been blinded to the sample group allocation during the treatments and experiments. For each injection, the mice were administered 0.15 mg g7-NPs/g body weight (NPs stock concentration is 12.5 mg/ml; 0.7 mg in 100 mg of NPs), which corresponds to 1 μg of cholesterol/g. The chemical–physical characterization and drug content in the g7-NPs used in the pre-clinical trials is summarized in Appendix Table S5. The complete list of WT and R6/2 animals used for each experiment is described in Appendix Table S6. An initial trial was performed in WT and R6/2 mice treated with control NPs loaded with cholesterol (without g7, i.e., not able to cross the BBB). No changes were found in terms of behavioral tasks and molecular signature (Appendix Fig S11). Therefore, we decided to not include these groups in subsequent trials with g7-NPs-Chol.

Immunohistochemistry

The animals were deeply anesthetized and transcardially perfused with 4% PFA. When only NPs were detected, cells or tissues were fixed in cold methanol at −20°C for 10 min, since fixation with paraformaldehyde reduced rhodamine-related NP fluorescence. Immunohistochemistry was performed on 15–30 μm coronal sections with the following primary antibodies: rabbit anti-IBA1 (1:500; Wako), rabbit anti-GFAP (1:250; Dako), rabbit anti-calbindin28 kDa (1:100; Swant), mouse anti-DARPP32 or rabbit anti-DARPP32 (1:100, Epitomics; S. Cruz), and mouse anti-PMCA ATPase (clone 5F10, 1:500; Thermo Scientific). Alexa Fluor 488-conjugated goat secondary antibodies (1:1,000; Invitrogen) were used for detection. Sections were counterstained with the nuclear dye Hoechst 33258 or 4′,6-diamidino-2-phenylindole (DAPI) (Invitrogen). Confocal images were acquired with a ZEISS LSM 510 or a LEICA SP5 laser scanning confocal microscopes.

NPs quantification

To quantify NPs in different tissues, we used ImageJ software to measure the fluorescence derived from the rhodamine used to label the NPs. NPs were counted in 10 images for each tissue taken from three WT and three R6/2 mice. Images were divided into three color channels to set a threshold for the red produced by the NPs, and we calculated the percentage of red signal for each image. Knowing the total area of the field and the size of the NPs, we calculated the approximate number of NPs in the selected area. The count of NPs in the liver and in the brain was made at 20× and 60×, respectively, and the data were normalized to compare the results. Ten images for each animal/condition were analyzed. The images were acquired with a Leica AF6000LX microscope.

Electrophysiology

At 10–11 weeks of age, mice were anesthetized with isoflurane and decapitated, and the brain was rapidly removed to ice-cold dissection artificial cerebrospinal fluid (ACSF) containing 130 mM NaCl, 3 mM KCl, 26 mM $NaHCO_3$, 1.25 mM $NaHPO_4$, 10 mM glucose, 5 mM $MgCl_2$, and 1 mM $CaCl_2$ oxygenated with 95% O_2/5% CO_2 (pH 7.2–7.4, osmolality 290–310 mOsm/l). Coronal slices (300 μm) of the striatum were cut with a microtome (Model VT 1000S, Leica Microsystems) and transferred to an incubating chamber containing oxygenated standard ACSF (with 2 mM $CaCl_2$ and 2 mM $MgCl_2$) for 1 h before electrophysiological recordings.

Whole-cell patch-clamp recordings were obtained from MSNs visualized in slices with the aid of infrared video microscopy and identified by somatic size and basic membrane properties (membrane capacitance, input resistance, and time constant). The patch pipette (3–5 MΩ) was filled with solution containing 125 mM Cs-methanesulfonate, 4 mM NaCl, 3 mM KCl, 1 mM $MgCl_2$, 9 mM EGTA, 8 mM HEPES, 5 mM MgATP, 1 mM Tris-GTP, 10 mM disodium phosphocreatine, and 0.1 mM leupeptin (pH 7.2, osmolality 270–280 mOsm/l).

Spontaneous postsynaptic currents were recorded in standard ACSF. The membrane current was filtered at 1 kHz and digitized at 100–200 μs using Clampex 10.2 (gap-free mode). Cells were voltage-clamped at −70 mV to assess basic membrane properties. Membranes were stepped to a holding potential of +10 mV to assess $GABA_A$ receptor-mediated IPSCs. Bicuculline methiodide (10 μM) was added to block $GABA_A$ receptor-mediated currents, and spontaneous glutamate receptor-mediated EPSCs were recorded at a holding potential of −70 mV. Spontaneous synaptic currents and event kinetics were analyzed offline using the automatic detection protocol within the MiniAnalysis Program (Synaptosoft) and checked manually for accuracy. Event counts were performed blind to genotype and treatment. The threshold amplitude for the detection of an event (5 pA for glutamatergic currents and 10 pA for GABAergic currents) was set above the root mean square background noise level (1–2 pA at V_{hold} = −70 mV and 2–3 pA at V_{hold} = +10 mV). Amplitude–frequency and inter-event interval distributions were constructed to evaluate differences in events at each amplitude and interval.

Behavioral characterization

Rotarod: Mice were first trained at a fixed speed of 4 rpm on the apparatus (model 47600, Ugo Basile). After 1 h, the mice were tested in an accelerating task (from 4 to 40 rpm) over 5 min, for three trials per day for three consecutive days with an inter-trial interval of 30 min. Latency to fall was recorded for each trial and averaged. Open Field: The animals were placed individually into the center of a transparent, square, activity-cage arena (45 cm × 45 cm) (2Biological Instrument). Both horizontal and vertical activities were assessed, monitoring mice allowed to freely move for 60 min using the Actitrack software (2Biological Instrument) connected to infrared sensors placed all around the square cage. Novel Object Recognition Test: The device consisted of a Plexiglass square arena (dimensions: 40 × 40 × 40 cm). All phases of the test were conducted in the presence of low-intensity light. Mice were first habituated to the arena in the absence of objects for 15 min (on one

 © 2015 The Authors

day, in the morning). On the same day, in the afternoon, two similar objects were presented to each mouse for 10 min (A′ and A″), after which the mice were returned to their home cage. Twenty-four hours later, the same animals were tested for 10 min in the arena with a familiar object (A″) and a new object (B). The index of discrimination was calculated as (time exploring the novel object − time exploring the familiar object) / (time exploring both objects) × 100. Object preference was measured as (time exploring each object) / (time exploring both objects) × 100. All experiments were done blind to genotypes.

Triton-insoluble protein fraction preparation and Western blot

Triton-insoluble fractions of the brain were prepared as described in the study by Gardoni *et al* (2009), separated on SDS–PAGE and probed with specific antibodies. Antibodies used in these experiments include anti-PSD-95 (1:1,000; #124011 SySy), NMDAR1 (GluN1) (1:500; #AB9864, Millipore), NMDAR2B (GluN2B) (1:500; #MAB57578, Millipore), gephyrin (1:1,000; #147111, SySy), synaptophysin (1:1,000, S. Cruz), and beta-3-tubulin (1:3,000; #G7121, Promega). Horseradish peroxidase-conjugated secondary antibodies were then used (1:3,000; Bio-Rad). Bands were visualized with enhanced chemoluminescence (Pierce) and imaged with the ChemiDoc MP Imaging System (Bio-Rad). The bands were densitometrically quantified (Image Lab, Bio-Rad) and normalized for Coomassie staining. Beta-3-tubulin was used as an additional loading control.

RNA isolation, retrotranscription, and real-time quantitative PCR

Total RNA from tissues was isolated with TRIzol reagent (Life Technologies). Total RNA (0.25–1 μg) was reverse-transcribed to single-stranded cDNA using the iScript cDNA synthesis kit (Bio-Rad). For each reverse-transcribed product, three real-time PCR analyses were performed in duplicate for each of the analyzed genes. An iCycler thermal cycler with a Multicolor Real-time PCR Detection System (Bio-Rad) was used to evaluate gene expressions. Taqman probes with a FAM dye label (for cholesterol genes) or EVA Green Supermix (for inflammatory genes) was used, as previously described (Valenza *et al*, 2015).

Nissl staining and Neurolucida analysis

Animals were perfused and brains dissected, frozen and serially cut (30 μm-thick coronal sections) on the cryostat. One 30-μm-thick section every five was stained with cresyl violet (Nissl staining). Briefly, sections were dried overnight. Then, they were dehydrated with a scale alcoholic of ethanol and xylene, than rehydrated, and immersed in 1% cresyl violet and 1% glacial acetic acid aqueous solution for 5 min. The staining was followed by a new dehydration in ascending ethanol and xylene. Sections were cover-slipped with Leica CV mounting media (Cat#14046430011). Brain, ventricle, and striatum perimeters (relative to one hemisphere) were reconstructed in a cerebral segment included between plates 19 and 39 of the Franklin K. and Paxinos G. atlas (Paxinos & Franklin, 2008). They were drawn at 40× at a microscope with a motorized stage interfaced to the computer, using the Neurolucida software (Microbrightfield Inc., VT, USA). The obtained volumes were analyzed with the Neuroexplorer software (Microbrightfield Inc.) using the Cavalieri formula for volume reconstruction.

Measurement of sterols

Samples were prepared and analyzed by isotopic dilution mass spectrometry as previously described (Valenza *et al*, 2010).

Statistics

SigmaPlot 12.3 (Systat software) or Prism 5 (GraphPad software) was used to perform all statistical analyses. Data are presented as means ± standard error of the mean (SEM). Grubbs' test was applied to identify outliers. For each set of data to be compared, we determined in Prism whether data were normally distributed or not. As they were all normally distributed, we used parametric tests.

The paper explained

Problem
Huntington's disease is a genetic neurodegenerative disorder characterized by progressive motor, cognitive, and psychiatric disturbances. Cholesterol biosynthesis and content are reduced in the brain of multiple animal models of HD. This dysfunction—of cerebral origin—is measurable in blood of patients with HD since pre-symptomatic stages of disease. However, a link between reduced synthesis/level of cholesterol and neuronal dysfunction *in vivo* in HD is missing. As circulating or dietary cholesterol is not able to cross the blood–brain barrier (BBB) and cholesterol in the brain depends largely on endogenous biosynthesis, this dysfunction may be detrimental for neuronal function especially given that locally synthesized cholesterol is implicated in synapses formation, integrity, and remodeling.

Results
To address the relationship between cholesterol dysfunction and synaptic and cognitive deficits in HD mouse models, we delivered cholesterol into the brain by using a novel technology based on cholesterol-loaded polymeric nanoparticles further modified with a peptide (g7) to cross the BBB after systemic injection in the mice. We showed that these nanoparticles (g7-NPs) reach different brain regions and different brain cells and gradually release cholesterol after their degradation. We also showed that repeated systemic administration of cholesterol-loaded g7-NPs in HD mice: (i) rescues synaptic communication in striatal medium-sized spiny neurons, (ii) prevents cognitive decline and partially improves global activity, and (iii) restores the levels of proteins that compose the synaptic machinery.

Impact
Neuronal and synaptic dysfunction is an attractive target for possible HD therapies because it occurs long before cell death in mouse models and in humans with HD. An intervention at this stage could, in theory, slow or stop neuron loss before it starts. Our conclusions highlight the relevance of cholesterol deficits in cognitive impairment associated with HD and the benefits of cholesterol supplementation with a broad impact for other brain disorders.
In parallel, the evidence that g7-NPs can be used as vectors for the delivery of therapeutic molecules (besides cholesterol) to the brain opens new and medically very relevant scenarios for the treatment of several CNS disorders. Importantly, the nanoparticles employed are made of PLGA, which is approved by FDA in various drug delivery systems in humans as it is considered biodegradable and biocompatible.

© 2015 The Authors

Indeed, differences between group means were assessed with an unpaired Student's *t*-test, and two-way or one-way ANOVA followed by Bonferroni or Newman–Keuls *post hoc* tests, as indicated in the text. Differences were considered statistically significant if $P < 0.05$. No statistical methods were used to pre-determine sample sizes, but our sample sizes are similar to those reported in the literature. For details, see also Appendix Table S7 showing statistical analyses and *P*-values for the main figures.

Expanded View for this article is available online.

Acknowledgements
We thank Luca Pignata and Chiara Orciani for technical assistance and Elisa Battaglia for help with the behavioral tests. We also thank Miriam Ascagni (CIMA, an advanced microscopy facility established by Università degli Studi Milano, Milan), Valeria Berno and Silvia Tartari (Imaging Facility in INGM, Milan), and Centro Grandi Strumenti (University of Modena and Reggio Emilia) for technical assistance and support with confocal analysis. This work was partially supported by Neuromics European grant (305121) to E.C. and by Ministero della Salute under 40 (GR-2008-1145270) to M.V and V.L.. The electrophysiology studies were supported by USPHS NS41574, HD004612, and NS081335 to M.S.L. and C.C. The Hereditary Disease Foundation (to M.L. and G.T.) supported the preparation of g7-NPs for the electrophysiological studies.

This paper is dedicated to the memory of our dear colleague, devoted scientist and well known neurologist Stefano Di Donato.

Author contributions
EC and MV developed the study, conceived the experimental plans, and analyzed the data. JYC, CCe, and MSL developed and performed the electrophysiological experiments and analyzed the data. GT, BR, DB, MAV, and FF developed the NP-based strategy, produced, and characterized all NPs used in this work. MV, EB, and GT performed the immunostaining experiments and provided most of the confocal images. MV performed biochemical analyses and with CFB all the molecular analyses; MV, EDP, and CFB performed the behavioral tests. VL, CCa and SDD performed all the mass spectrometry analyses. MMB and AV performed all reconstruction analyses with Neurolucida. MV, GT, BR, and EC interpreted the data and wrote the manuscript. All authors read and edited the manuscript. EC supervised the entire work and gave final approval of the manuscript version to be published.

Conflict of interest
The authors declare that they have no conflict of interest.

References

Barenholz Y (2012) Doxil(R)–the first FDA-approved nano-drug: lessons learned. *J Control Release* 160: 117 – 134

Barker GR, Warburton EC (2011) When is the hippocampus involved in recognition memory? *J Neurosci* 31: 10721 – 10731

Belletti D, Tosi G, Forni F, Gamberini MC, Baraldi C, Vandelli MA, Ruozi B (2012) Chemico-physical investigation of tenofovir loaded polymeric nanoparticles. *Int J Pharm* 436: 753 – 763

Cepeda C, Hurst RS, Calvert CR, Hernandez-Echeagaray E, Nguyen OK, Jocoy E, Christian LJ, Ariano MA, Levine MS (2003) Transient and progressive electrophysiological alterations in the corticostriatal pathway in a mouse model of Huntington's disease. *J Neurosci* 23: 961 – 969

Cepeda C, Starling AJ, Wu N, Nguyen OK, Uzgil B, Soda T, Andre VM, Ariano MA, Levine MS (2004) Increased GABAergic function in mouse models of Huntington's disease: reversal by BDNF. *J Neurosci Res* 78: 855 – 867

Chang KH, Wu YR, Chen YC, Chen CM (2015) Plasma inflammatory biomarkers for Huntington's disease patients and mouse model. *Brain Behav Immun* 44: 121 – 127

Conforti P, Camnasio S, Mutti C, Valenza M, Thompson M, Fossale E, Zeitlin S, MacDonald ME, Zuccato C, Cattaneo E (2013) Lack of huntingtin promotes neural stem cells differentiation into glial cells while neurons expressing huntingtin with expanded polyglutamine tracts undergo cell death. *Neurobiol Dis* 50: 160 – 170

Costantino L, Gandolfi F, Tosi G, Rivasi F, Vandelli MA, Forni F (2005) Peptide-derivatized biodegradable nanoparticles able to cross the blood-brain barrier. *J Control Release* 108: 84 – 96

Cummings DM, Milnerwood AJ, Dallerac GM, Waights V, Brown JY, Vatsavayai SC, Hirst MC, Murphy KP (2006) Aberrant cortical synaptic plasticity and dopaminergic dysfunction in a mouse model of Huntington's disease. *Hum Mol Genet* 15: 2856 – 2868

Danhier F, Ansorena E, Silva JM, Coco R, Le Breton A, Preat V (2012) PLGA-based nanoparticles: an overview of biomedical applications. *J Control Release* 161: 505 – 522

Darvas M, Palmiter RD (2009) Restriction of dopamine signaling to the dorsolateral striatum is sufficient for many cognitive behaviors. *Proc Natl Acad Sci USA* 106: 14664 – 14669

Dason JS, Smith AJ, Marin L, Charlton MP (2010) Vesicular sterols are essential for synaptic vesicle cycling. *J Neurosci* 30: 15856 – 15865

Dason JS, Smith AJ, Marin L, Charlton MP (2014) Cholesterol and F-actin are required for clustering of recycling synaptic vesicle proteins in the presynaptic plasma membrane. *J Physiol* 592: 621 – 633

Dietschy JM, Turley SD (2004) Thematic review series: brain Lipids. Cholesterol metabolism in the central nervous system during early development and in the mature animal. *J Lipid Res* 45: 1375 – 1397

Frank C, Giammarioli AM, Pepponi R, Fiorentini C, Rufini S (2004) Cholesterol perturbing agents inhibit NMDA-dependent calcium influx in rat hippocampal primary culture. *FEBS Lett* 566: 25 – 29

Frank C, Rufini S, Tancredi V, Forcina R, Grossi D, D'Arcangelo G (2008) Cholesterol depletion inhibits synaptic transmission and synaptic plasticity in rat hippocampus. *Exp Neurol* 212: 407 – 414

Freeman W, Morton AJ (2004) Regional and progressive changes in brain expression of complexin II in a mouse transgenic for the Huntington's disease mutation. *Brain Res Bull* 63: 45 – 55

Gabathuler R (2010) Approaches to transport therapeutic drugs across the blood-brain barrier to treat brain diseases. *Neurobiol Dis* 37: 48 – 57

Gardoni F, Mauceri D, Malinverno M, Polli F, Costa C, Tozzi A, Siliquini S, Picconi B, Cattabeni F, Calabresi P *et al* (2009) Decreased NR2B subunit synaptic levels cause impaired long-term potentiation but not long-term depression. *J Neurosci* 29: 669 – 677

Gimpl G, Gehrig-Burger K (2007) Cholesterol reporter molecules. *Biosci Rep* 27: 335 – 358

Glynn D, Bortnick RA, Morton AJ (2003) Complexin II is essential for normal neurological function in mice. *Hum Mol Genet* 12: 2431 – 2448

Gosk S, Vermehren C, Storm G, Moos T (2004) Targeting anti-transferrin receptor antibody (OX26) and OX26-conjugated liposomes to brain capillary endothelial cells using in situ perfusion. *J Cereb Blood Flow Metab* 24: 1193 – 1204

Hara Y, Waters EM, McEwen BS, Morrison JH (2015) Estrogen Effects on Cognitive and Synaptic Health Over the Lifecourse. *Physiol Rev* 95: 785 – 807

 © 2015 The Authors

HDCRG (1993) A novel gene containing a trinucleotide repeat that is expanded and unstable on Huntington's disease chromosomes. The Huntington's Disease Collaborative Research Group. *Cell* 72: 971 – 983

Hering H, Lin CC, Sheng M (2003) Lipid rafts in the maintenance of synapses, dendritic spines, and surface AMPA receptor stability. *J Neurosci* 23: 3262 – 3271

Huttner WB, Zimmerberg J (2001) Implications of lipid microdomains for membrane curvature, budding and fission. *Curr Opin Cell Biol* 13: 478 – 484

Joshi PR, Wu NP, Andre VM, Cummings DM, Cepeda C, Joyce JA, Carroll JB, Leavitt BR, Hayden MR, Levine MS *et al* (2009) Age-dependent alterations of corticostriatal activity in the YAC128 mouse model of Huntington disease. *J Neurosci* 29: 2414 – 2427

Lang T, Bruns D, Wenzel D, Riedel D, Holroyd P, Thiele C, Jahn R (2001) SNAREs are concentrated in cholesterol-dependent clusters that define docking and fusion sites for exocytosis. *EMBO J* 20: 2202 – 2213

Lawrence AD, Sahakian BJ, Hodges JR, Rosser AE, Lange KW, Robbins TW (1996) Executive and mnemonic functions in early Huntington's disease. *Brain* 119(Pt 5): 1633 – 1645

Lawrence AD, Watkins LH, Sahakian BJ, Hodges JR, Robbins TW (2000) Visual object and visuospatial cognition in Huntington's disease: implications for information processing in corticostriatal circuits. *Brain* 123(Pt 7): 1349 – 1364

Leoni V, Mariotti C, Tabrizi SJ, Valenza M, Wild EJ, Henley SM, Hobbs NZ, Mandelli ML, Grisoli M, Bjorkhem I *et al* (2008) Plasma 24S-hydroxycholesterol and caudate MRI in pre-manifest and early Huntington's disease. *Brain* 131: 2851 – 2859

Leoni V, Long JD, Mills JA, Di Donato S, Paulsen JS, Group P-Hs (2013) Plasma 24S-hydroxycholesterol correlation with markers of Huntington disease progression. *Neurobiol Dis* 55: 37 – 43

Levine MS, Cepeda C, Hickey MA, Fleming SM, Chesselet MF (2004) Genetic mouse models of Huntington's and Parkinson's diseases: illuminating but imperfect. *Trends Neurosci* 27: 691 – 697

Linetti A, Fratangeli A, Taverna E, Valnegri P, Francolini M, Cappello V, Matteoli M, Passafaro M, Rosa P (2010) Cholesterol reduction impairs exocytosis of synaptic vesicles. *J Cell Sci* 123: 595 – 605

Lund EG, Xie C, Kotti T, Turley SD, Dietschy JM, Russell DW (2003) Knockout of the cholesterol 24-hydroxylase gene in mice reveals a brain-specific mechanism of cholesterol turnover. *J Biol Chem* 278: 22980 – 22988

Mangiarini L, Sathasivam K, Seller M, Cozens B, Harper A, Hetherington C, Lawton M, Trottier Y, Lehrach H, Davies SW *et al* (1996) Exon 1 of the HD gene with an expanded CAG repeat is sufficient to cause a progressive neurological phenotype in transgenic mice. *Cell* 87: 493 – 506

Martin MG, Ahmed T, Korovaichuk A, Venero C, Menchon SA, Salas I, Munck S, Herreras O, Balschun D, Dotti CG (2014a) Constitutive hippocampal cholesterol loss underlies poor cognition in old rodents. *EMBO Mol Med* 6: 902 – 917

Martin MG, Pfrieger F, Dotti CG (2014b) Cholesterol in brain disease: sometimes determinant and frequently implicated. *EMBO Rep* 15: 1036 – 1052

Marullo M, Valenza M, Leoni V, Caccia C, Scarlatti C, De MA, Zuccato C, Di Donato S, Carafoli E, Cattaneo E (2012) Pitfalls in the detection of cholesterol in Huntington's disease models. *PLoS Curr* 4: e505886e505889a501968

Mauch DH, Nagler K, Schumacher S, Goritz C, Muller EC, Otto A, Pfrieger FW (2001) CNS synaptogenesis promoted by glia-derived cholesterol. *Science* 294: 1354 – 1357

Milnerwood AJ, Gladding CM, Pouladi MA, Kaufman AM, Hines RM, Boyd JD, Ko RW, Vasuta OC, Graham RK, Hayden MR *et al* (2010) Early increase in extrasynaptic NMDA receptor signaling and expression contributes to phenotype onset in Huntington's disease mice. *Neuron* 65: 178 – 190

Milnerwood AJ, Raymond LA (2010) Early synaptic pathophysiology in neurodegeneration: insights from Huntington's disease. *Trends Neurosci* 33: 513 – 523

Minost A, Delaveau J, Bolzinger MA, Fessi H, Elaissari A (2012) Nanoparticles via nanoprecipitation process. *Recent Pat Drug Deliv Formul* 6: 250 – 258

Morton AJ, Edwardson JM (2001) Progressive depletion of complexin II in a transgenic mouse model of Huntington's disease. *J Neurochem* 76: 166 – 172

Mundargi RC, Babu VR, Rangaswamy V, Patel P, Aminabhavi TM (2008) Nano/micro technologies for delivering macromolecular therapeutics using poly(D, L-lactide-co-glycolide) and its derivatives. *J Control Release* 125: 193 – 209

Orth M, Schippling S, Schneider SA, Bhatia KP, Talelli P, Tabrizi SJ, Rothwell JC (2010) Abnormal motor cortex plasticity in premanifest and very early manifest Huntington disease. *J Neurol Neurosurg Psychiatry* 81: 267 – 270

Paratcha G, Ibanez CF (2002) Lipid rafts and the control of neurotrophic factor signaling in the nervous system: variations on a theme. *Curr Opin Neurobiol* 12: 542 – 549

Paulsen JS, Langbehn DR, Stout JC, Aylward E, Ross CA, Nance M, Guttman M, Johnson S, MacDonald M, Beglinger LJ *et al* (2008) Detection of Huntington's disease decades before diagnosis: the Predict-HD study. *J Neurol Neurosurg Psychiatry* 79: 874 – 880

Paulsen JS, Long JD (2014) Onset of Huntington's disease: can it be purely cognitive? *Mov Disord* 29: 1342 – 1350

Paxinos G, Franklin KBJ (2008) *Paxinos and Franklin's the Mouse Brain in Stereotaxic Coordinates*, 3rd edn. Waltham, MA: Academic Press

Pfrieger FW (2003) Role of cholesterol in synapse formation and function. *Biochim Biophys Acta* 1610: 271 – 280

Reim K, Mansour M, Varoqueaux F, McMahon HT, Sudhof TC, Brose N, Rosenmund C (2001) Complexins regulate a late step in Ca2 + -dependent neurotransmitter release. *Cell* 104: 71 – 81

Renner M, Choquet D, Triller A (2009) Control of the postsynaptic membrane viscosity. *J Neurosci* 29: 2926 – 2937

Ross CA, Aylward EH, Wild EJ, Langbehn DR, Long JD, Warner JH, Scahill RI, Leavitt BR, Stout JC, Paulsen JS *et al* (2014) Huntington disease: natural history, biomarkers and prospects for therapeutics. *Nat Rev Neurol* 10: 204 – 216

Schippling S, Schneider SA, Bhatia KP, Munchau A, Rothwell JC, Tabrizi SJ, Orth M (2009) Abnormal motor cortex excitability in preclinical and very early Huntington's disease. *Biol Psychiatry* 65: 959 – 965

Sethi A, Sher M, Akram MR, Karim S, Khiljee S, Sajjad A, Shah SN, Murtaza G (2013) Albumin as a drug delivery and diagnostic tool and its market approved products. *Acta Pol Pharm* 70: 597 – 600

Shen H, Rodriguez-Aguayo C, Xu R, Gonzalez-Villasana V, Mai J, Huang Y, Zhang G, Guo X, Bai L, Qin G *et al* (2013) Enhancing chemotherapy response with sustained EphA2 silencing using multistage vector delivery. *Clin Cancer Res* 19: 1806 – 1815

Shive MS, Anderson JM (1997) Biodegradation and biocompatibility of PLA and PLGA microspheres. *Adv Drug Deliv Rev* 28: 5 – 24

Suzuki R, Ferris HA, Chee MJ, Maratos-Flier E, Kahn CR (2013) Reduction of the cholesterol sensor SCAP in the brains of mice causes impaired synaptic transmission and altered cognitive function. *PLoS Biol* 11: e1001532

Tasciotti E, Liu X, Bhavane R, Plant K, Leonard AD, Price BK, Cheng MM, Decuzzi P, Tour JM, Robertson F *et al* (2008) Mesoporous silicon particles

© 2015 The Authors

as a multistage delivery system for imaging and therapeutic applications. *Nat Nanotechnol* 3: 151 – 157

Thiele C, Hannah MJ, Fahrenholz F, Huttner WB (2000) Cholesterol binds to synaptophysin and is required for biogenesis of synaptic vesicles. *Nat Cell Biol* 2: 42 – 49

del Toro D, Xifro X, Pol A, Humbert S, Saudou F, Canals JM, Alberch J (2010) Altered cholesterol homeostasis contributes to enhanced excitotoxicity in Huntington's disease. *J Neurochem* 115: 153 – 167

Tosi G, Rivasi F, Gandolfi F, Costantino L, Vandelli MA, Forni F (2005) Conjugated poly(D, L-lactide-co-glycolide) for the preparation of in vivo detectable nanoparticles. *Biomaterials* 26: 4189 – 4195

Tosi G, Costantino L, Rivasi F, Ruozi B, Leo E, Vergoni AV, Tacchi R, Bertolini A, Vandelli MA, Forni F (2007) Targeting the central nervous system: in vivo experiments with peptide-derivatized nanoparticles loaded with Loperamide and Rhodamine-123. *J Control Release* 122: 1 – 9

Tosi G, Costantino L, Ruozi B, Forni F, Vandelli MA (2008) Polymeric nanoparticles for the drug delivery to the central nervous system. *Expert Opin Drug Deliv* 5: 155 – 174

Tosi G, Vergoni AV, Ruozi B, Bondioli L, Badiali L, Rivasi F, Costantino L, Forni F, Vandelli MA (2010) Sialic acid and glycopeptides conjugated PLGA nanoparticles for central nervous system targeting: in vivo pharmacological evidence and biodistribution. *J Control Release* 145: 49 – 57

Tosi G, Bondioli L, Ruozi B, Badiali L, Severini GM, Biffi S, De Vita A, Bortot B, Dolcetta D, Forni F *et al* (2011a) NIR-labeled nanoparticles engineered for brain targeting: in vivo optical imaging application and fluorescent microscopy evidences. *J Neural Transm* 118: 145 – 153

Tosi G, Fano RA, Bondioli L, Badiali L, Benassi R, Rivasi F, Ruozi B, Forni F, Vandelli MA (2011b) Investigation on mechanisms of glycopeptide nanoparticles for drug delivery across the blood-brain barrier. *Nanomedicine* 6: 423 – 436

Tosi G, Badiali L, Ruozi B, Vergoni AV, Bondioli L, Ferrari A, Rivasi F, Forni F, Vandelli MA (2012) Can leptin-derived sequence-modified nanoparticles be suitable tools for brain delivery? *Nanomedicine* 7: 365 – 382

Tosi G, Vilella A, Chhabra R, Schmeisser MJ, Boeckers TM, Ruozi B, Vandelli MA, Forni F, Zoli M, Grabrucker AM (2014) Insight on the fate of CNS-targeted nanoparticles. Part II: intercellular neuronal cell-to-cell transport. *J Control Release* 177: 96 – 107

Trager U, Andre R, Magnusson-Lind A, Miller JR, Connolly C, Weiss A, Grueninger S, Silajdzic E, Smith DL, Leavitt BR *et al* (2014) Characterisation of immune cell function in fragment and full-length Huntington's disease mouse models. *Neurobiol Dis* 73C: 388 – 398

Trushina E, Singh RD, Dyer RB, Cao S, Shah VH, Parton RG, Pagano RE, McMurray CT (2006) Mutant huntingtin inhibits clathrin-independent endocytosis and causes accumulation of cholesterol in vitro and in vivo. *Hum Mol Genet* 15: 3578 – 3591

Trushina E, Canaria CA, Lee DY, McMurray CT (2014) Loss of caveolin-1 expression in knock-in mouse model of Huntington's disease suppresses pathophysiology in vivo. *Hum Mol Genet* 23: 129 – 144

Valenza M, Rigamonti D, Goffredo D, Zuccato C, Fenu S, Jamot L, Strand A, Tarditi A, Woodman B, Racchi M *et al* (2005) Dysfunction of the cholesterol biosynthetic pathway in Huntington's disease. *J Neurosci* 25: 9932 – 9939

Valenza M, Cattaneo E (2006) Cholesterol dysfunction in neurodegenerative diseases: is Huntington's disease in the list? *Prog Neurobiol* 80: 165 – 176

Valenza M, Carroll JB, Leoni V, Bertram LN, Bjorkhem I, Singaraja RR, Di Donato S, Lutjohann D, Hayden MR, Cattaneo E (2007a) Cholesterol biosynthesis pathway is disturbed in YAC128 mice and is modulated by huntingtin mutation. *Hum Mol Genet* 16: 2187 – 2198

Valenza M, Leoni V, Tarditi A, Mariotti C, Bjorkhem I, Di Donato S, Cattaneo E (2007b) Progressive dysfunction of the cholesterol biosynthesis pathway in the R6/2 mouse model of Huntington's disease. *Neurobiol Dis* 28: 133 – 142

Valenza M, Leoni V, Karasinska JM, Petricca L, Fan J, Carroll J, Pouladi MA, Fossale E, Nguyen HP, Riess O *et al* (2010) Cholesterol defect is marked across multiple rodent models of Huntington's disease and is manifest in astrocytes. *J Neurosci* 30: 10844 – 10850

Valenza M, Marullo M, Di Paolo E, Cesana E, Zuccato C, Biella G, Cattaneo E (2015) Disruption of astrocyte-neuron cholesterol cross talk affects neuronal function in Huntington's disease. *Cell Death Differ* 22: 690 – 702

Vergoni AV, Tosi G, Tacchi R, Vandelli MA, Bertolini A, Costantino L (2009) Nanoparticles as drug delivery agents specific for CNS: in vivo biodistribution. *Nanomedicine* 5: 369 – 377

Vilella A, Tosi G, Grabrucker AM, Ruozi B, Belletti D, Vandelli MA, Boeckers TM, Forni F, Zoli M (2014) Insight on the fate of CNS-targeted nanoparticles. Part I: Rab5-dependent cell-specific uptake and distribution. *J Control Release* 174: 195 – 201

Von Hoff DD, Ervin T, Arena FP, Chiorean EG, Infante J, Moore M, Seay T, Tjulandin SA, Ma WW, Saleh MN *et al* (2013) Increased survival in pancreatic cancer with nab-paclitaxel plus gemcitabine. *N Engl J Med* 369: 1691 – 1703

Vonsattel JP, DiFiglia M (1998) Huntington disease. *J Neuropathol Exp Neurol* 57: 369 – 384

Zuccato C, Valenza M, Cattaneo E (2010) Molecular mechanisms and potential therapeutical targets in Huntington's disease. *Physiol Rev* 90: 905 – 981

Zuccato C, Cattaneo E (2014) Huntington's disease. *Handb Exp Pharmacol* 220: 357 – 409

License: This is an open access article under the terms of the Creative Commons Attribution 4.0 License, which permits use, distribution and reproduction in any medium, provided the original work is properly cited.

 © 2015 The Authors

Appendix PDF

Cholesterol-loaded nanoparticles ameliorate synaptic and cognitive function in Huntington's disease mice

Marta Valenza[1§], Jane Y. Chen[2§], Eleonora Di Paolo[1¶], Barbara Ruozi[3¶], Daniela Belletti[3], Costanza Ferrari Bardile[1], Valerio Leoni[4,5], Claudio Caccia[4], Elisa Brilli[1], Stefano Di Donato[4], Marina M. Boido[6], Alessandro Vercelli[6], Maria A. Vandelli[3], Flavio Forni[3], Carlos Cepeda[2], Michael S. Levine[2] , Giovanni Tosi[3], Elena Cattaneo[1]

[1]Department of BioSciences and Centre for Stem Cell Research, Università degli Studi di Milano, Milan, Italy; [2]Intellectual and Developmental Disabilities Research Center, Semel Institute for Neuroscience, Brain Research Institute, David Geffen School of Medicine, University of California Los Angeles, Los Angeles, CA; [3]Department of Life Sciences, University of Modena and Reggio Emilia, Modena, Italy. [4]Neurological Institute C. Besta, Milan, Italy. [5]Laboratory of Clinical Chemistry, Ospedale di Circolo e Fondazione Macchi, Varese, Italy. [6]Neuroscience Institute Cavalieri Ottolenghi Neuroscience Institute of Turin, Orbassano (Turin), Italy.
§co-first authors. ¶co-second authors

Content:

Appendix Figure S1

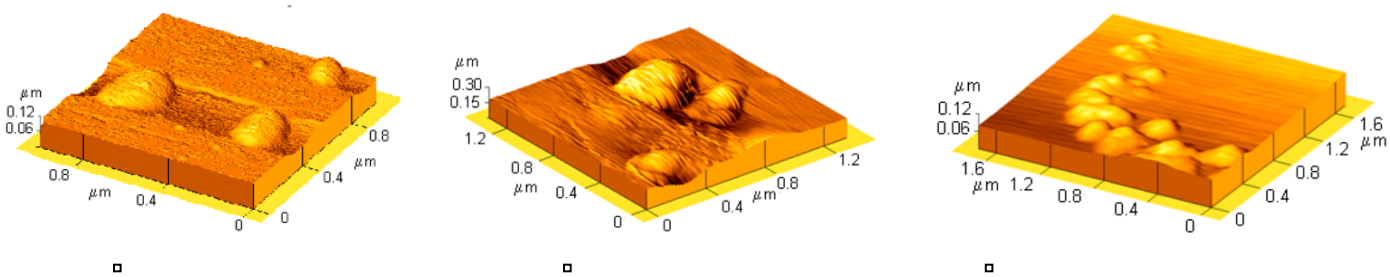

Rhod-NPs Rhod-g7-NPs Rhod-g7-NPs-NBD-Chol1

Appendix Figure S1. AFM analysis (3D elaboration) of Rhodamine Samples (Rhod-NPs, Rhod-g7-NPs, Rhod-g7-NPs-NBD-Chol1). The chemico-physical properties have been described in Appendix Table 2.

Appendix Figure S2

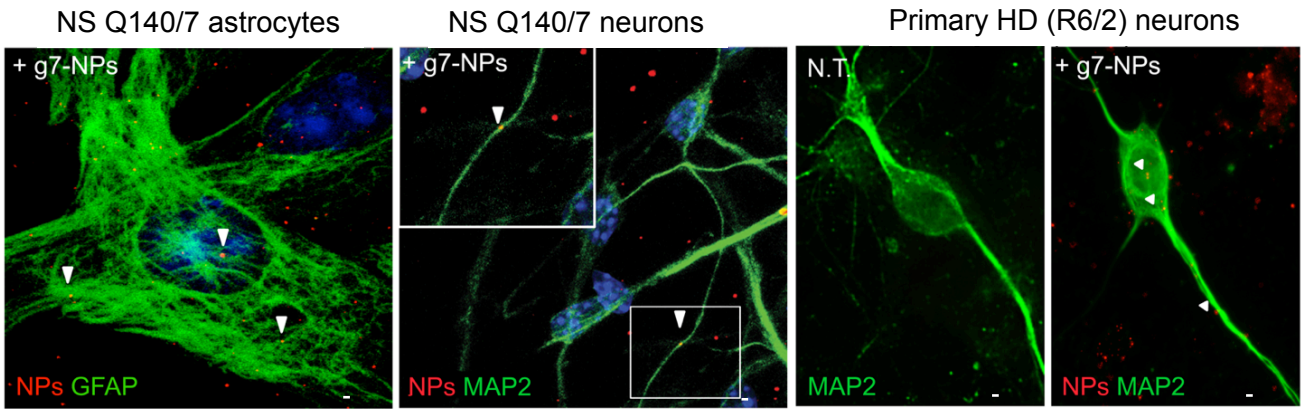

Appendix Figure S2. g7-NPs are taken up *in vitro* by different brain cells expressing mutant huntingtin. (a) high-magnification confocal image (cropped) of astrocytes at day 14 of glial differentiation derived from NS Q140/7 cells incubated with g7-NPs for 6 hrs and immunostained for GFAP. Original magnification: 63x. (b) Representative high-magnification confocal image (cropped) of neurons at day 7 of neuronal differentiation derived from NS Q140/7 cells incubated with g7-NPs for 6 hrs and immunostained for MAP2. The boxed region is shown at higher magnification in the inset. Original magnification: 63x. (c) Representative high-magnification confocal image (cropped) of primary cortical neurons generated from R6/2 embryos at 18 days of gestation, not treated (N.T.) or treated with g7-NPs (+g7-NPs) for 6 hrs and immunostained for MAP2. Original magnification: 63x. Hoechst 33258 was used to counterstain the nuclei. White arrowheads indicate intracellular g7-NPs. Scale bar: 5 μm.

Appendix Figure S3

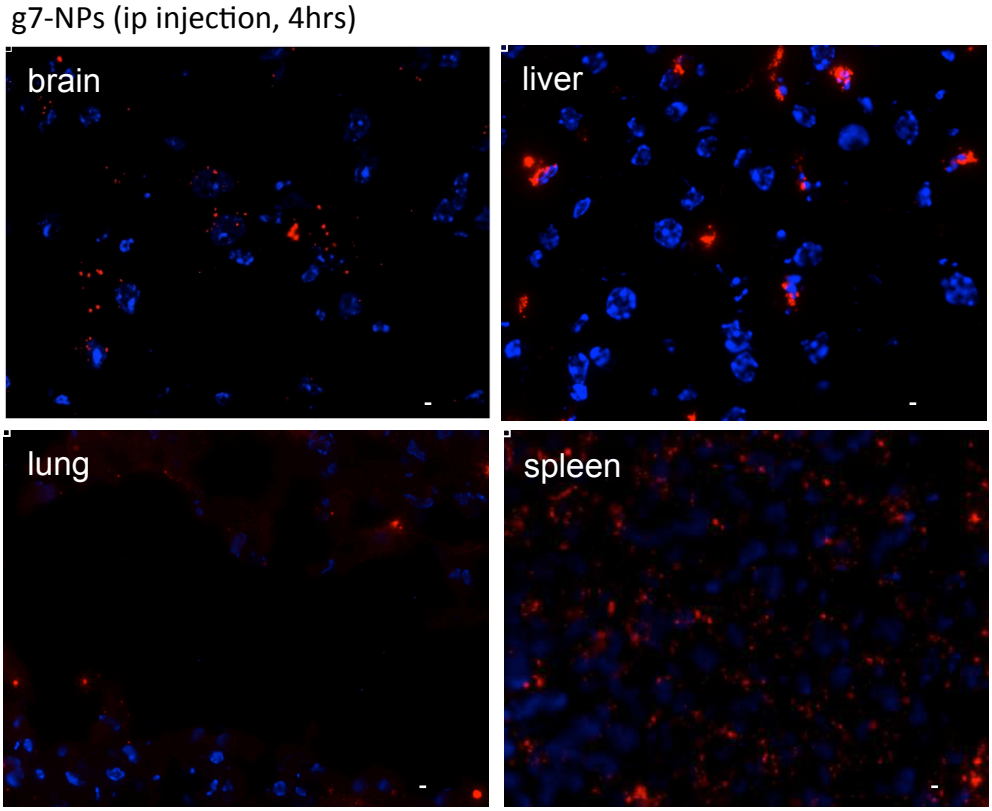

Appendix Figure S3. Distribution of g7-NPs in brain and peripheral tissues in mice. Representative high-magnification confocal images of brain, liver, lung, and spleen slices from WT mice ip injected with g7-NPs and sacrificed after 4 hrs. 4',6-diamidino-2-phenylindole was used to counterstain nuclei. Original magnification: 63x (scale bar: 10μm).

Appendix Figure S4

Hippocampus, 24h post-injection – low magnification

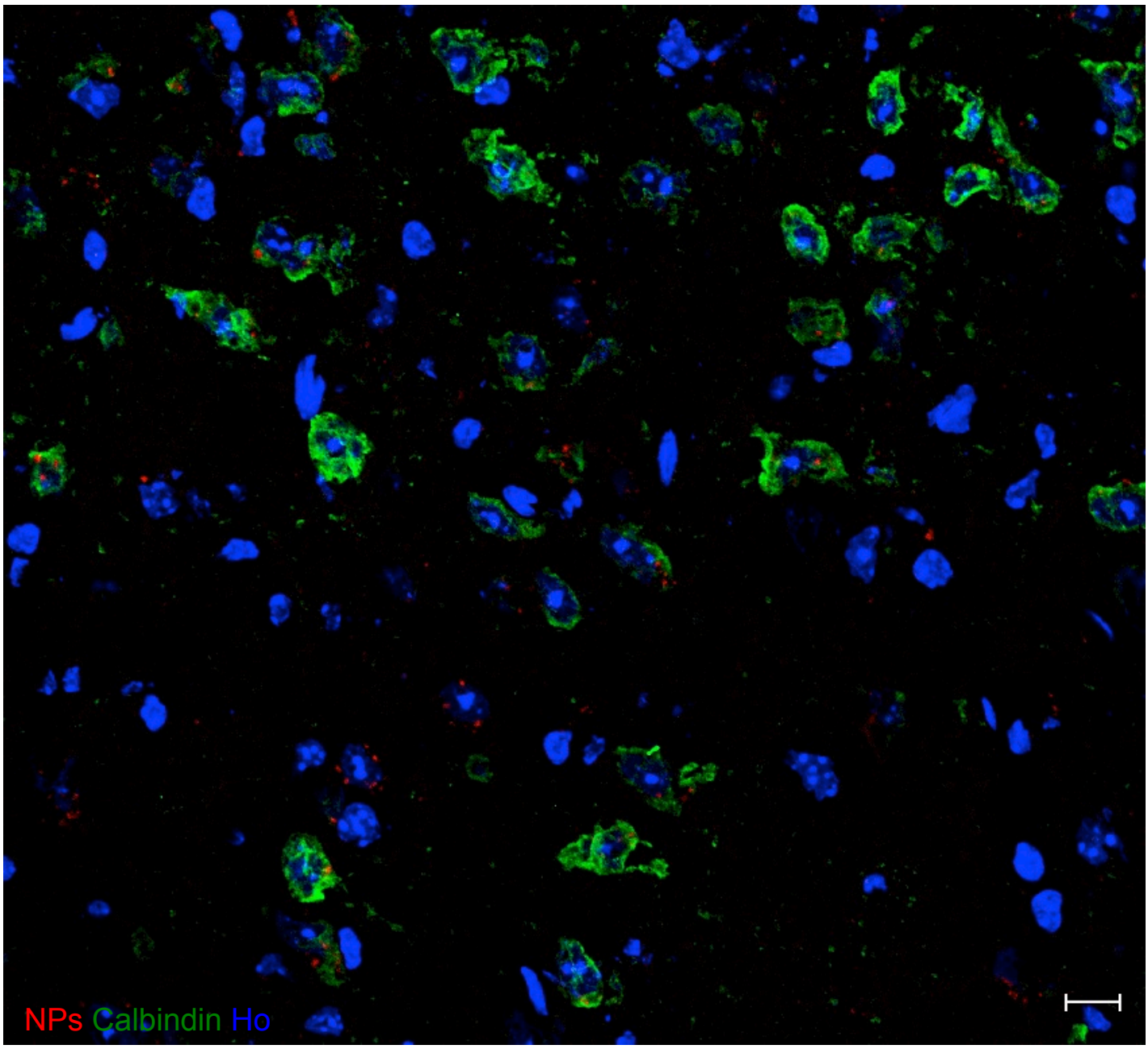

Appendix Figure S4. Distribution of g7-NPs in calbindin-positive neurons in hyppocampus. Representative confocal image of brain slice from R6/2 mice ip injected with g7-NPs and sacrificed after 24 hrs. 4',6-diamidino-2-phenylindole was used to counterstain nuclei. Scale bar: 5 μm.

Appendix Figure S5

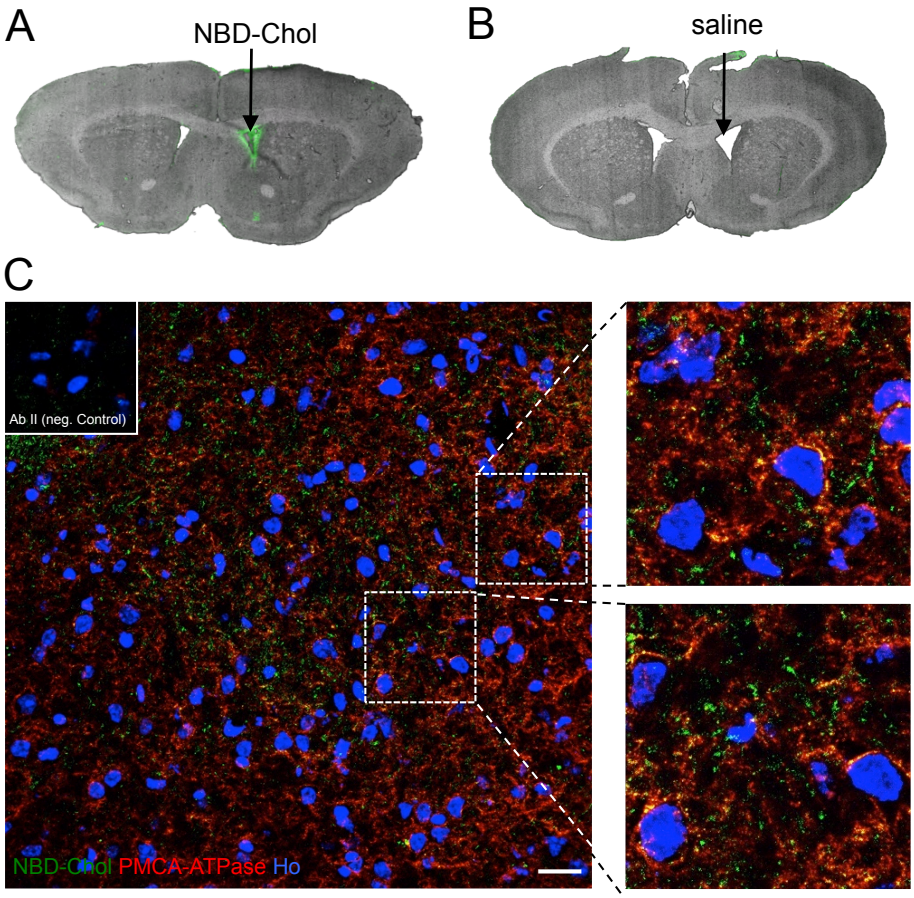

Appendix Figure S5. Co-localization of NBD-Chol with PMCA ATPase *in vivo*. Representative confocal images of brain slice from WT mice injected with NBD-Chol (10ug) into the brain ventricles and sacrificed after 7 hrs. A-B) low-magnification images of brain slices of mice injected with NBD-Chol (A) or with saline (B) into the ventricle (see arrows). C) Representative 63x confocal image of brain slices of WT mice injected with NBD-Chol (green) and immunostained against PMCA ATPase (red), a marker for plasma membrane (scale bar: 10μm). In the crops, it is possible to appreciate the distribution of NBD-Chol into brain cells' membrane (yellow signal). The **Hoechst** 33342 dye (Ho; blue) was used to counterstain nuclei.

Appendix Figure S6

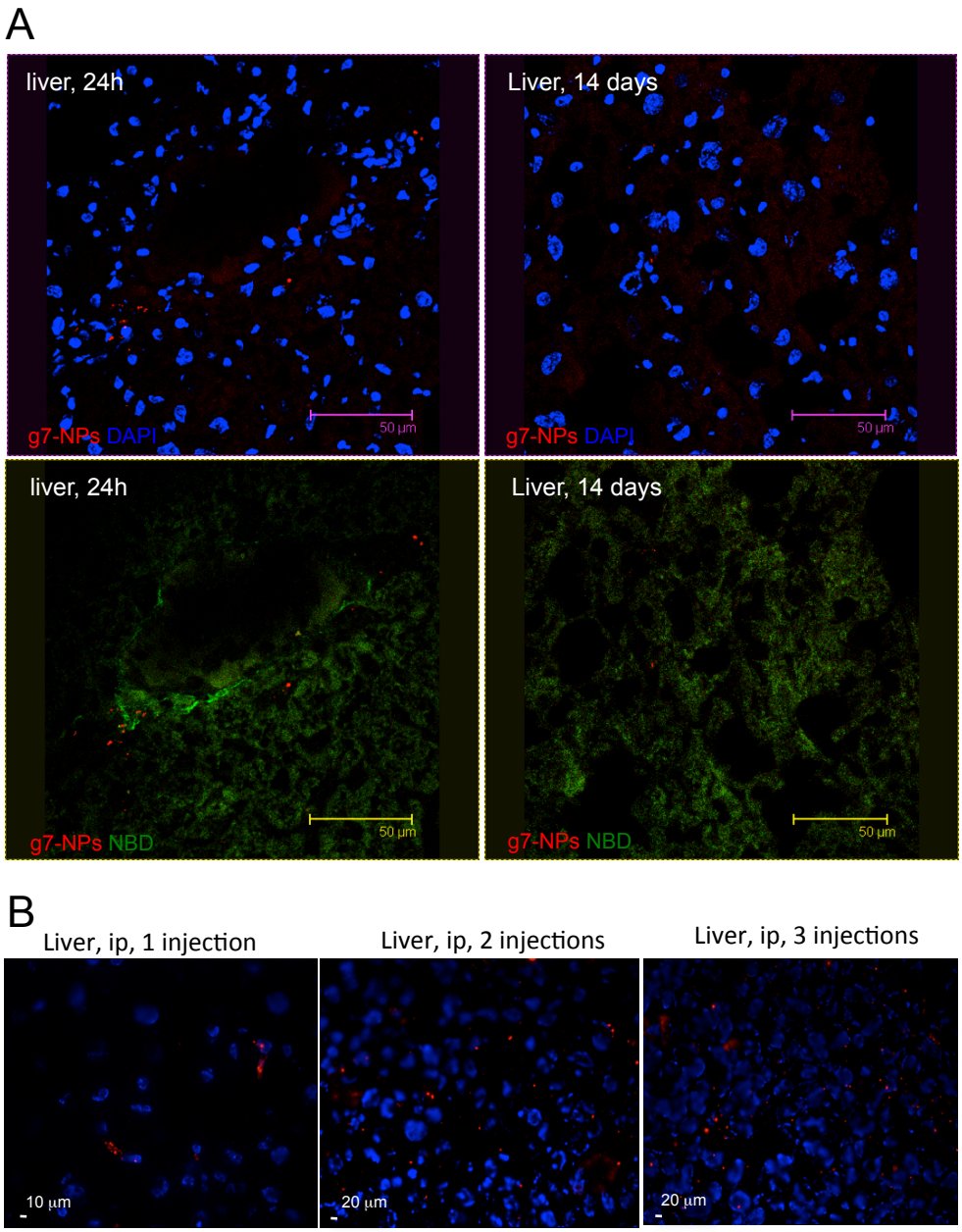

Appendix Figure S6. Kinetics of g7-NPs in the brain and liver. (a-b) Representative confocal images of brain slices (a) and of liver slices (b) from R6/2 mice ip injected with NBD-chol-g7-NPs and sacrificed after 7 days (a) or after 24 hrs or 14 days (in b; the same experiment described in Fig. 1i-l). (c) Confocal images of liver slices from WT mice after a single or multiple injections of g7-NPs and sacrificed after 1 week. Scale bars: 10 µm (in a), 50 µm (in b), and 10-20 µm (in c). All images suggest a faster degradation of g7-NPs in the liver than in the brain. 4',6-diamidino-2-phenylindole (DAPI) was used to counterstain nuclei.

Appendix Figure S7

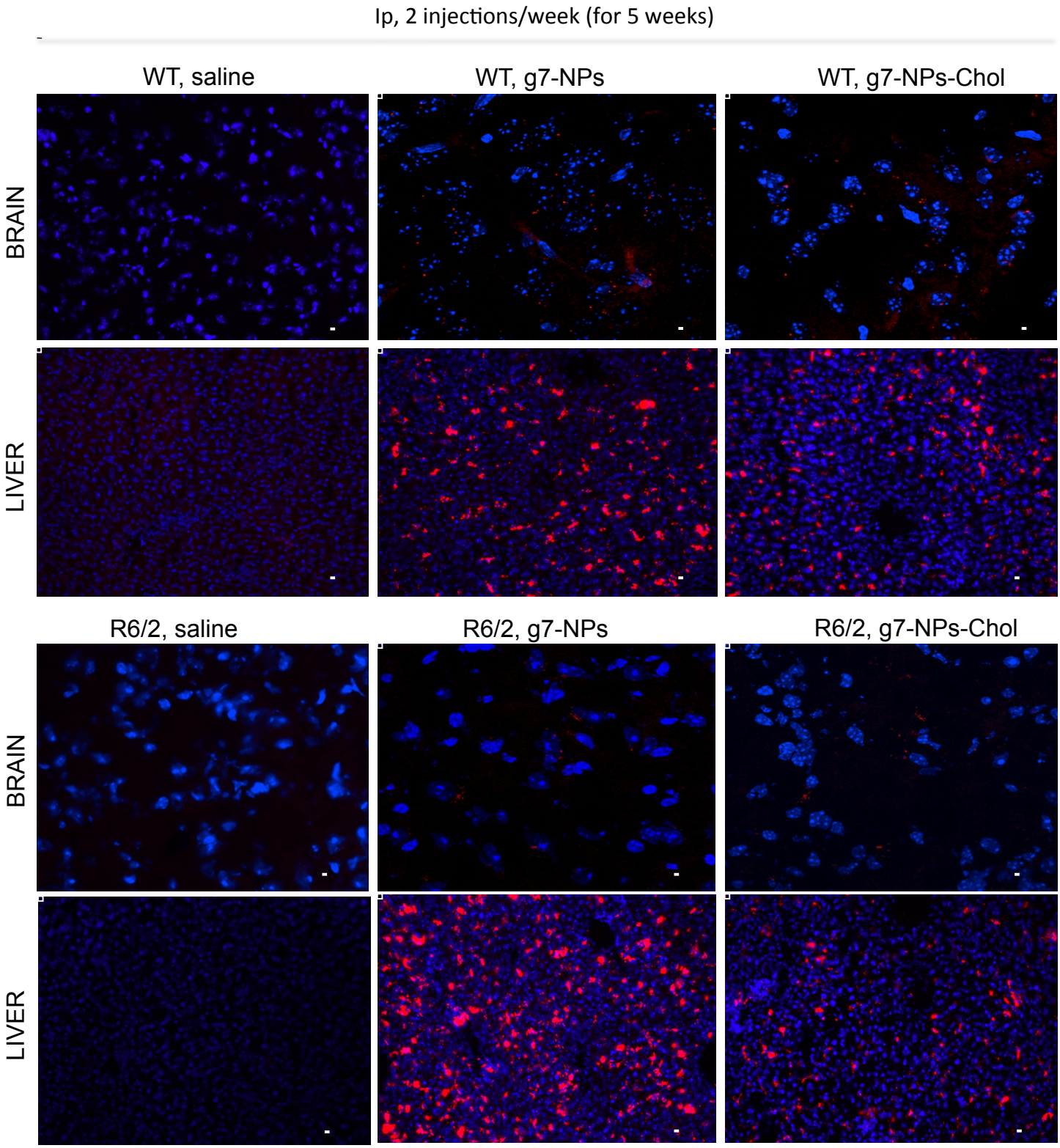

Appendix Figure S7. Distribution of g7-NPs-Chol or empty g7-NPs in the brain and liver of WT and HD mice in which electrophysiological parameters were analyzed. The presence of g7-NPs was analyzed by fluorescent microscopy in the liver and in cortical pieces taken from brains before electrophysiological analysis. 4',6-diamidino-2-phenylindole was used to counterstain nuclei. Scale bars: 10μm (brain) and 50μm (liver).

Appendix Figure S8

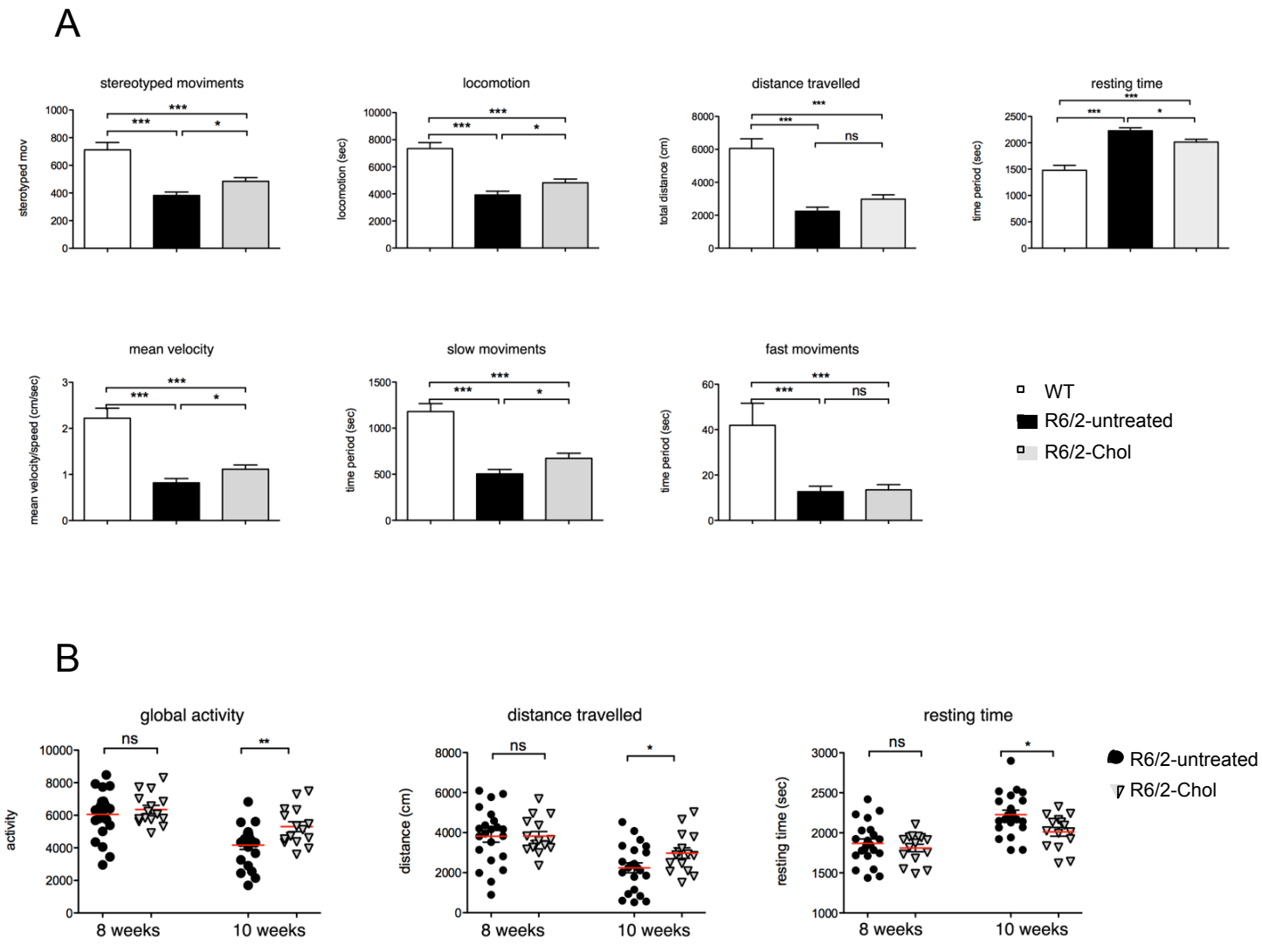

Appendix Figure S8. A) Open field parameters in WT (n=14), R6/2-untreated (n=22) and R6/2-Chol (n=15) mice. Stereotyped moviments, locomotion, total distance travelled, resting time, mean velocity, slow moviments and fast moviments at 10 weeks of age. **B)** Global activity, distance, resting time in R6/2-untreated (n=22) and R6/2-Chol mice (n=15). Data were combined to highlight the differences between R6/2 groups at each time points. All data are presented as mean ± s.e.m.; $P<0.05$ was determined by one-way ANOVA followed by Newmann-Keuls multiple comparison test or t-student test .

Appendix Figure S9

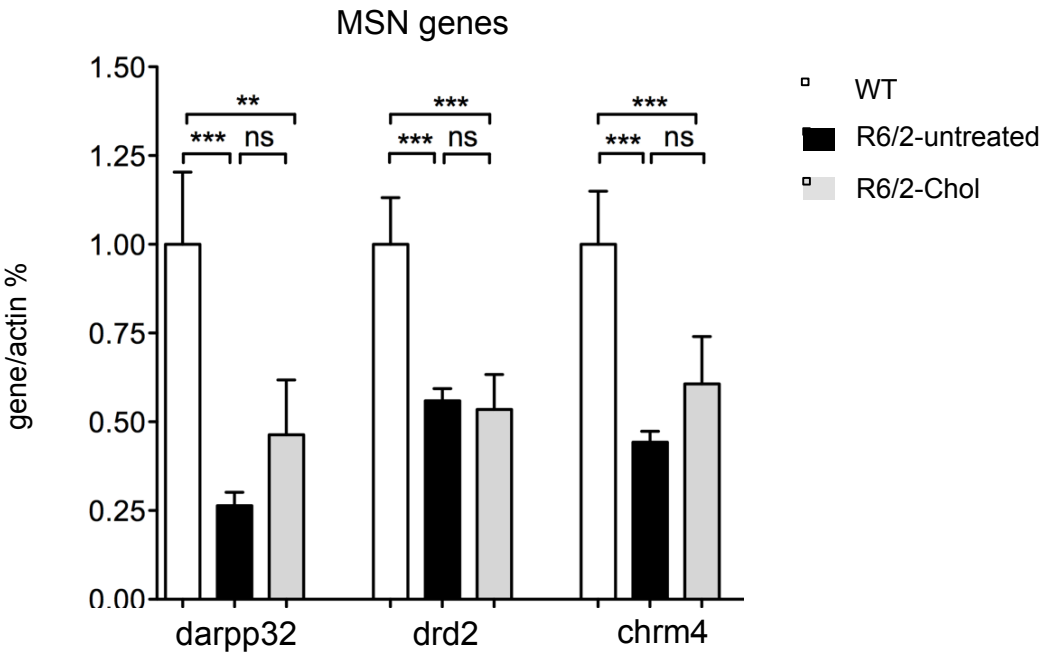

Appendix Figure S9. mRNA levels of striatal genes considered hallmarks of Medium Spiny Neurons (MSNs), such as darpp32, drd2 and chrm4. Data are presented as mean ± s.e.m.; WT (n=4), R6/2-untreated (n=7) and R6/2-Chol animals (n=3) at 12 weeks of age. $P<0.05$ was determined by one-way ANOVA followed by Newmann-Keuls multiple comparison tests.

Appendix Figure S10

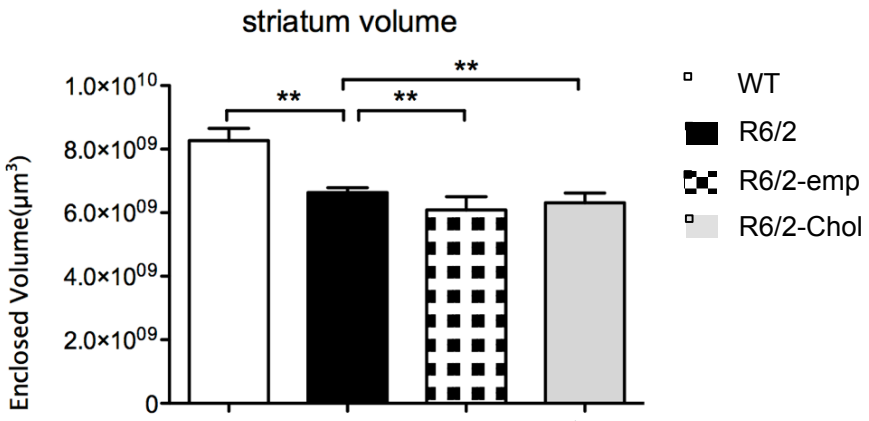

Appendix Figure S10. Striatal volume was evaluated by Neurolucida Analysis at 12 weeks of age in WT (n= 7), R6/2 (n=7), R6/2-emp (n=6), R6/2-Chol (n=8). Data represent mean ± SEM. $P<0.05$ was determined by one-way ANOVA followed by Newmann-Keuls multiple comparison tests.

Appendix Figure S11

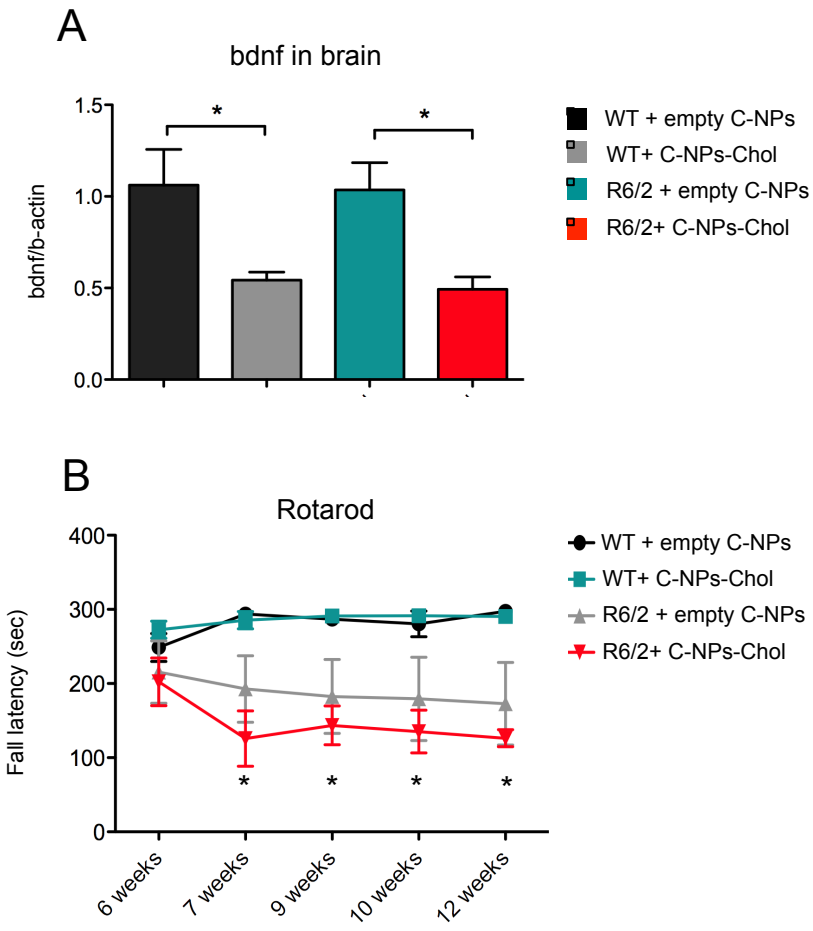

Appendix Figure S11. Initial trial performed in WT and R6/2 mice treated with unmodified control NPs (not able to cross the BBB) loaded with cholesterol (C-NPs-Chol) (n=4/genotype) or with empty C-NPs (n=4/genotype) according to the same experimental paradigm shown in Figure 5. **A)** mRNA levels of BDNF, a brain-specific hallmark of HD, were found reduced in the brain of R6/2 mice independently from the treatment, suggesting that peripheral cholesterol supplementation did not influence BDNF expression in the HD brain, differently from that observed in R6/2 mice treated with g7-NPs-Chol (Figure 6C). **B)** behavioral performance, as measured by rotarod test, was not improved in R6/2 treated with C-NPs-Chol compared to WTs; similarly, peripheral cholesterol supplementation via C-NPs-Chol injection did not influence rotarod performance in R6/2 mice (see R6/2+C-NPs-Chol line versus R6/2+ empty C-NPs). Data represent mean ± SEM. $P<0.05$ was determined by one-way ANOVA followed by Newmann-Keuls multiple comparison tests. On this basis, the unmodified control NPs loaded with cholesterol (C-NPs-Chol) group was no longer included in subsequent trials with g7-NPs-Chol.

Appendix Table S1. Composition of NPs involved in the study.

The amounts (mg) of polymers (PLGA503H; Rhod-PLGA502H; g7-PLGA), of cholesterol (Chol) and of labeled cholesterol (NDB-Chol) used as starting materials are reported for each formulation.

Sample	description	defined in the text as	PLGA503H (mg)	Rhod-PLGA502H (mg)	g7-PLGA503H (mg)	Chol (mg)	NBD-Chol (mg)
u-NPs	unloaded (empty) NPs	u-NPs	100				
NPs-Chol1	NPs loaded with 1mg Chol	NPs-Chol1	100			1	
NPs-Chol2	NPs loaded with 5mg Chol	NPs-Chol2	100			5	
NPs-Chol3	NPs loaded with 10mg Chol	NPs-Chol3	100			10	
NPs-NBD-Chol1	NPs loaded with 1mg NBD-Chol	NPs-NBD-Chol	100				1
Rhod-u-NPs	unloaded (empty) NPs labelled with Rhodamine (used in vivo experiments)	C-NPs	80	20			
Rhod-g7-NPs	unloaded (empty) NPs modified with g7 and labelled with Rhodamine (used in vivo experiments)	g7-NPs	70	10	20		
Rhod-g7-NPs-Chol1	NPs modified with g7, labelled with Rhodamine and loaded with NBD-chol (used in vivo experiments)	g7-NPs-NBD-Chol	70	10	20	1	
Rhod-g7-NPs-NBDChol1	NPs modified with g7, labelled with Rhodamine and loaded with NBD-chol (used in vivo experiments)	g7-NPs-Chol	70	10	20		1

Appendix Table S2. chemical-physical properties of NPs involved in the study

Dimensions of samples is expressed with Z-Average values (nm); Homegeneity of the samples is expressed as Polydispersity Index (PDI); intensity distribution is expressed as Di (nm); surface charge is expressed as ζ-pot (mV); percentage of polyvynyl alchol residual is expressed as percentage as %PVA; drug loading is expressed as mg of Chol per 100 mg of formulation (LC%) and as percentual encapsulation efficiency (EE%). Standard Deviation is reported as SD.

Sample	Chol/PLGA (mg/mg)	Z-Average nm (± S.D.)	PDI value (± S.D.)	D(i)10 nm (± S.D.)	D(i)50 nm (± S.D.)	D(i)90 nm (± S.D.)	ζ-pot mV (± S.D.)	% PVA residual (± S.D.)	mg Chol/100 mg form. LC%	EE%
u-NPs		181±11	0.08±0.01	139±12	187±12	205±12	-12±3	4.8±1.2		
NPs-Chol1	1:100	192±15	0.09±0.01	136±11	195±12	283±23	-9±4	5.1±0.4	0.7±0.1	68±5
NPs-Chol2	5:100	187±17	0.11±0.02	118±13	177±15	269±28	-8±4	4.5±1.8	0.8±0.03	17±1
NPs-Chol3	10:100	242±52	0.28±0.03	111±21	256±76	378±78	-12±10	5.8±1.0	2.4±0.3	24±3
NPs-NBD-Chol1	1:100	178±19	0.07±0.02	125±3	186±10	280±7	-6±3	5.7±0.2	0.4±0.1	44±1

Appendix Table S3 - passive membrane properties of MSNs from WT, R6/2-untreated and R6/2-chol mice

Capacitance (pF), Input Resistance (MΩ) and Time constant (ms) registered in MSNs from WT mice treated with saline (WT), R6/2 mice treated with saline or with empty g7-NPs (R6/2-untreated) and R6/2 treated with g7-NPs-Chol (R6/2-Chol).

group	Capacitance (pF)	Input Resistance (MΩ)	Time constant (ms)
WT	68.7 ± 2.27	51.6 ± 2.73	1.9 ± 0.07
R6/2-untreated	59.8 ± 2.40*	179.3 ± 14.91***	1.9 ± 0.09
R6/2-Chol	62.9 ± 3.60	180.2 ± 24.27***	1.4 ± 0.12***###

***R6/2-Chol vs WT; ### R6/2-chol vs R6/2-untreated

Appendix Table S4 - kinetics of IPSCs (A) and of EPSCs (B) in MSNs from WT, R6/2-untreated and R6/2-chol mice

A. IPSC event kinetics

group	Rise time (ms)	Decay time (ms)	Half-amplitude duration (ms)
WT-sal	3.1 ± 0.09	19.0 ± 0.62	18.3 ± 0.42
R6/2-untreated	2.7 ± 0.12	16.1 ± 0.82*	15.8 ± 0.5***
R6/2-Chol	2.5 ± 0.14***	14.2 ± 1.09***	14.7 ± 0.73***

B. EPSC event kinetics

group	Rise time (ms)	Decay time (ms)	Half-amplitude duration (ms)
WT-sal	1.0 ± 0.03	3.5 ± 0.08	4.9 ± 0.12
R6/2-untreated	1.1 ± 0.06	3.5 ± 0.15	4.7 ± 0.17
R6/2-Chol	1.0 ± 0.06	3.3 ± 0.14	4.4 ± 0.22*

***R6/2-Chol or R6/2-untreated vs WT

Appendix Table S5 - chemico-physical characterization and drug content in the NPs in the preclinical trials

NPs	tyoe of experiments	Rhod	g7	Chol administered (mg/g)	Size (nm) (PDI)	Z-potential (mV)
g7-NPs	first pre-clinical trial (electrophysiology)	✓	✓	-	192 (0.06)	-11.7
g7-NPs-Chol		✓	✓	0,7	199 (0.06)	-12.5
g7-NPs	second pre-clinical trial (electrophysiology)	✓	✓	-	176 (0.09)	-12.2
g7-NPs-Chol		✓	✓	0,7	174 (0.08)	-9.1
g7-NPs	third preclinical trial (behaviour)	✓	✓	-	210 (0.11)	-5.7
g7-NPs-Chol		✓	✓	0,7	190 (0.08)	-9.2
g7-NPs	fourth preclinical trial (behaviour)	✓	✓	-	187 (0.09)	-6.4
g7-NPs-Chol		✓	✓	0,7	210 (0.12)	-7.3
g7-NPs	fifth preclinical trial (behaviour)	✓	✓	-	147 (0.09)	-16.4
g7-NPs-Chol		✓	✓	0,7	151 (0.10)	-17.3

Appendix Table S6 - summary all animals used in this study

	n° exp	date	Nps	n° WT mice	n° R6/2 mice	injection	n° injections	sacrifice after first injection	
characterization and distribution of g7-NPs	1	28/04/10	g7-NPs	2		iv	1	2 hrs	ip vs. iv injection Nps kinetics in the mouse brain
			g7-NPs	4		iv	1	4 hrs	
			g7-NPs	3		iv	1	12 hrs	
			C-NPs	2		iv	1	2 hrs	
			C-NPs	2		iv	1	4 hrs	
			g7-NPs	2		ip	1	4 hrs	
			g7-NPs	2		ip	1	12 hrs	
	2	07/06/10	g7-NPs-NBD-Chol	3		ip	1	4 hrs	NPs kinetics in the mouse brain NBD and g7-NPs co-localization IHC different brain cells
			g7-NPs-NBD-Chol	3		ip	1	24 hrs	
			g7-NPs-NBD-Chol	3		ip	1	48 hrs	
			g7-NPs-NBD-Chol	3		ip	1	1 week	
			g7-NPs-NBD-Chol	2	2	ip	2	48 hrs	
			g7-NPs-NBD-Chol	2	2	ip	3	1 week	
			saline	2	2	ip	1	48 hrs	
			saline	2	2	ip	3	1 week	
	3	12/07/10	g7-NPs-NBD-Chol	1	3	ip	1	1 week	NPs kinetics in the mouse brain first co-localization study
			g7-NPs-NBD-Chol		3	ip	1	2 weeks	
			g7-NPs-NBD-Chol		3	ip	1	3 weeks	
			saline	1	3	ip	1	3 weeks	
			g7-NPs-NBD-Chol	1	3	ip	2	2 weeks	
			g7-NPs-NBD-Chol	1	3	ip	3	3 weeks	
			saline	1	3	ip	3	3 weeks	
			g7-NPs-NBD-Chol	1		ip	1	5 months	
	4	08/07/12	g7-NPs	3	3	ip	1	4 hrs	IHC different brain cells g7-NPs counts in liver, striatum and cortex
	5	01/07/12	empty-C-NPs	4	4	ip	2/week	5 weeks	effect of cholesterol supplementation only in periphery
			C-NPs-Chol	4	4	ip	2/week	5 weeks	
	6	01/08/12	g7-NPs-NBD-Chol		3	ip	1	24 hrs	IHC different brain cells; second co-localization study; g7-NPs counts in brain
			g7-NPs-NBD-Chol		3	ip	1	48 hrs	
			g7-NPs-NBD-Chol		3	ip	1	7 days	
			g7-NPs-NBD-Chol		3	ip	1	14 days	
	7	28/05/13	g7-NPs		2	ip	1	24 hrs	IHC different brain cells
			g7-NPs-NBD-Chol		2	ip	1	24 hrs, 1 week	
			saline	2	2	ip	1	24 hrs	
pre-clinical trials	8	01/10/10	g7-NPs	4	4	ip	3	5 weeks	first pilot study (UCLA), electrophysiological studies; rotarod test
			g7-NPs-Chol	10	10	ip	3	5 weeks	
	9	01/05/11	g7-NPs	5	5	ip	2/week	5 weeks	second pilot study (UCLA), for electrophysiological studies
			g7-NPs-Chol	5	5	ip	2/week	5 weeks	
			saline	5	5	ip	2/week	5 weeks	
	10	01/07/13	g7-NPs		3	ip	2/week	5 weeks	third pilot study (UNIMI), for behavioral tests (rotarod and NORT); neurophatology, biochemestry
			g7-NPs-Chol		6	ip	2/week	5 weeks	
			saline	8	7	ip	2/week	5 weeks	
	11	01/11/13	g7-NPs		4	ip	2/week	5 weeks	forth pilot study (UNIMI), for behavioral tests (rotarod, NORT, open field); neurophatology, biochemestry
			g7-NPs-Chol		8	ip	2/week	5 weeks	
			saline	8	8	ip	2/week	5 weeks	
	12	01/06/14	g7-NPs		6	ip	2/week	5 weeks	fifth pilot study (UNIMI), for behavioral tests (NORT, open field); neurophatology, biochemestry, qRTPCR (injections until 11 ws)
			g7-NPs-Chol		8	ip	2/week	5 weeks	
			saline	8	8	ip	2/week	5 weeks	

Appendix Table S7 - summary of statistics for the main figures

Figure	Statistical Analysis				
Figure 2C	unpaired t test				
	WT liver vs R6/2 liver				
	P value	0,0104			
	P value summary	*			
	Are means signif. different? (P < 0.05)	Yes			
	One- or two-tailed P value?	Two-tailed			
	t, df	t=2.859 df=18			
	WT cortex vs R6/2 cortex				
	P value	< 0.0001			
	P value summary	***			
	Are means signif. different? (P < 0.05)	Yes			
	One- or two-tailed P value?	Two-tailed			
	t, df	t=9.559 df=18			
	WT striatum vs R6/2 striatum				
	P value	< 0.0001			
	P value summary	***			
	Are means signif. different? (P < 0.05)	Yes			
	One- or two-tailed P value?	Two-tailed			
	t, df	t=8.309 df=18			

Figure 3D	One-way analysis of variance				
	P value	< 0.0001			
	P value summary	***			
	Are means signif. different? (P < 0.05)	Yes			
	Number of groups	4			
	F	12,34			
	R squared	0,5069			
	Bonferroni's Multiple Comparison Test	Mean Diff.	t	Significant? P < 0.05?	Summary
	brain 24h vs brain 48h	34,06	0,6415	No	ns
	brain 24h vs brain 7d	255,0	4,804	Yes	***
	brain 24h vs brain 14d	232,1	4,371	Yes	***
	brain 48h vs brain 7d	221,0	4,162	Yes	**
	brain 48h vs brain 14d	198,0	3,730	Yes	**
	brain 7d vs brain 14d	-22,97	0,4326	No	ns

Figure 4B	One-way analysis of variance				
	P value	< 0.0001			
	P value summary	***			
	Are means signif. different? (P < 0.05)	Yes			
	Number of groups	3			
	F	39,46			
	R squared	0,4315			
	Newman-Keuls Multiple Comparison Test	Mean Diff.	q	Significant? P < 0.05?	Summary
	WT (n=52) vs R6/2-untreated (n=27)	-6,793	12,39	Yes	***
	WT (n=52) vs R6/2-Chol (n=29)	-3,396	6,338	Yes	***
	R6/2-untreated (n=27) vs R6/2-Chol (n=29)	-3,397	5,514	Yes	*

Figure 4E	One-way analysis of variance				
	P value	< 0.0001			
	P value summary	***			
	Are means signif. different? (P < 0.05)	Yes			
	Number of groups	3			
	F	78,23			
	R squared	0,6197			
	Newman-Keuls Multiple Comparison Test	Mean Diff.	q	Significant? P < 0.05?	Summary
	WT (n=52) vs R6/2-untreated (n=27)	-1,990	15,37	Yes	***
	WT (n=52) vs R6/2-Chol (n=29)	-0,1656	1,047	No	ns
	R6/2-untreated (n=27) vs R6/2-Chol (n=29)	-1,824	13,09	Yes	***

Figure 5B	two-way ANOVA test				
	WT vs R6/2-untreated				
	time	Difference	t	P value	Summary
	5 ws	-22,27	1,107	P > 0.05	ns
	7 ws	-70,36	3,496	P<0.01	**
	9 ws	-95,94	4,768	P<0.001	***
	11 ws	-169,9	8,030	P<0.001	***
	WT vs R6/2-Chol				
	time	Difference	t	P value	Summary
	5 ws	-29,99	1,320	P > 0.05	ns
	7 ws	-79,95	3,518	P<0.01	**
	9 ws	-119,7	5,268	P<0.001	***
	11 ws	-179,0	7,878	P<0.001	***
Figure 5C	two-way ANOVA test				
	WT vs R6/2-untreated				
	treatment	Difference	t	P value	Summary
	5	-39,91	5,890	P<0.001	***
	10	-36,07	5,324	P<0.001	***
	15	-35,53	5,244	P<0.001	***
	20	-36,26	5,352	P<0.001	***
	25	-36,77	5,426	P<0.001	***
	30	-39,44	5,821	P<0.001	***
	35	-30,75	4,538	P<0.001	***
	40	-33,94	5,009	P<0.001	***
	45	-40,27	5,944	P<0.001	***
	50	-31,47	4,645	P<0.001	***
	55	-35,39	5,223	P<0.001	***
	60	-33,13	4,890	P<0.001	***

	WT vs R6/2-Chol				
	treatment	Difference	t	P value	Summary
	5	-39,08	5,241	P<0.001	***
	10	-27,82	3,732	P<0.01	**
	15	-29,22	3,919	P<0.01	**
	20	-30,65	4,111	P<0.001	***
	25	-33,11	4,441	P<0.001	***
	30	-36,49	4,895	P<0.001	***
	35	-29,34	3,935	P<0.01	**
	40	-31,36	4,207	P<0.001	***
	45	-38,03	5,101	P<0.001	***
	50	-27,25	3,655	P<0.01	**
	55	-31,71	4,254	P<0.001	***
	60	-28,32	3,798	P<0.01	**

Figure 5D	one-way ANOVA test				
	P value	< 0.0001			
	P value summary	***			
	Are means signif. different? (P < 0.05)	Yes			
	Number of groups	3			
	F	32,65			
	R squared	0,5763			
	Newman-Keuls Multiple Comparison Test	Mean Diff.	q	Significant? P < 0.05?	Summary
	R6/2-untreated vs WT	-3890	11,36	Yes	***
	R6/2-untreated vs R6/2-Chol	-1133	3,379	Yes	*
	R6/2-Chol vs WT	-2757	7,408	Yes	***

Figure 5E					
NORT - 8 weeks	One-way analysis of variance				
	P value	< 0.0001			
	P value summary	****			
	Are means signif. different? (P < 0.05)	Yes			
	Number of groups	3			
	F	17,42			
	R square	0,3087			
	Newman-Keuls Multiple Comparison Test	Mean Diff.	q	Significant? P < 0.05?	Summary
	R6/2-untreated vs WT	-38,54	8,271	Yes	***
	R6/2-untreated vs R6/2-Chol	-20,46	4,213	Yes	**
	R6/2-Chol vs WT	-18,09	3,423	Yes	*
NORT - 10 weeks	One-way analysis of variance				
	P value	< 0.0001			
	P value summary	****			
	Are means signif. different? (P < 0.05)	Yes			
	Number of groups	3			
	F	22,32			
	R square	0,3669			
	Newman-Keuls Multiple Comparison Test	Mean Diff.	q	Significant? P < 0.05?	Summary
	R6/2-untreated vs WT	-48,29	8,904	Yes	***
	R6/2-untreated vs R6/2-Chol	-37,02	6,377	Yes	***
	R6/2-Chol vs WT	-11,27	1,813	No	ns
NORT - 12 weeks	One-way analysis of variance				
	P value	< 0.0001			
	P value summary	****			
	Are means signif. different? (P < 0.05)	Yes			
	Number of groups	3			
	F	18,27			
	R square	0,3430			
	Newman-Keuls Multiple Comparison Test	Mean Diff.	q	Significant? P < 0.05?	Summary
	R6/2-untreated vs WT	-48,22	8,299	Yes	***
	R6/2-untreated vs R6/2-Chol	-33,04	5,311	Yes	***
	R6/2-Chol vs WT	-15,18	2,330	No	ns

Figure 6A					
PSD95	One-way analysis of variance				
	P value	< 0.0001			
	P value summary	***			
	Are means signif. different? (P < 0.05)	Yes			
	Number of groups	3			
	F	36,39			
	R squared	0,5740			
	Newman-Keuls Multiple Comparison Test	Mean Diff.	q	Significant? P < 0.05?	Summary
	R62-untreated vsWT	-0,2700	11,60	Yes	***
	R62-untreated vs R6/2-Chol	-0,1973	7,916	Yes	***
	R6/2-Chol vs WT	-0,07268	2,802	No	ns
Gephryin	One-way analysis of variance				
	P value	0,0739			
	P value summary	ns			
	Are means signif. different? (P < 0.05)	No			
	Number of groups	3			
	F	2,873			
	R squared	0,1755			
	Newman-Keuls Multiple Comparison Test	Mean Diff.	q	Significant? P < 0.05?	Summary
	R62-untreated vsWT	-0,1670	3,161	No	ns
	R62-untreated vs R6/2-Chol	-0,1409	---	No	ns
	R6/2-Chol vs WT	-0,02604	---	No	ns

GluN1	One-way analysis of variance				
	P value	< 0.0001			
	P value summary	***			
	Are means signif. different? (P < 0.05)	Yes			
	Number of groups	3			
	F	16,54			
	R squared	0,5416			
	Newman-Keuls Multiple Comparison Test	Mean Diff.	q	Significant? P < 0.05?	Summary
	R62-untreated vsWT	-0,6375	8,111	Yes	***
	R62-untreated vs R6/2-Chol	-0,2169	2,760	No	ns
	R6/2-Chol vs WT	-0,4206	4,923	Yes	**
GluN2B	One-way analysis of variance				
	P value	0,0028			
	P value summary	**			
	Are means signif. different? (P < 0.05)	Yes			
	Number of groups	3			
	F	7,188			
	R squared	0,3240			
	Newman-Keuls Multiple Comparison Test	Mean Diff.	q	Significant? P < 0.05?	Summary
	R62-untreated vs R6/2-Chol	-0,3574	4,921	Yes	**
	R62-untreated vsWT	-0,2780	4,051	Yes	**
	R6/2-Chol vs WT	-0,07939	1,055	No	ns
beta-3-tub	One-way analysis of variance				
	P value	0,1550			
	P value summary	ns			
	Are means signif. different? (P < 0.05)	No			
	Number of groups	3			
	F	1,956			
	R squared	0,09117			
	Newman-Keuls Multiple Comparison Test	Mean Diff.	q	Significant? P < 0.05?	Summary
	R62-untreated vsWT	-0,1177	2,796	No	ns
	R62-untreated vs R6/2-Chol	-0,05825	---	No	ns
	R6/2-Chol vs WT	-0,05946	---	No	ns

Figure 6C	R6/2-Chol vs R6/2-untreated				
	bdnf cortex				
	Unpaired t test				
	P value	0,0001			
	P value summary	***			
	Are means signif. different? (P < 0.05)	Yes			
	One- or two-tailed P value?	Two-tailed			
	t, df	t=4.475 df=25			
	bdnf hippocampus				
	Unpaired t test				
	P value	0,1607			
	P value summary	ns			
	Are means signif. different? (P < 0.05)	No			
	One- or two-tailed P value?	Two-tailed			
	t, df	t=1.441 df=28			

Figure 6D	snap25 cortex				
	Unpaired t test				
	P value	0,0092			
	P value summary	**			
	Are means signif. different? (P < 0.05)	Yes			
	One- or two-tailed P value?	Two-tailed			
	t, df	t=2.920 df=18			
	snap25 hippocampus				
	Unpaired t test				
	P value	0,0729			
	P value summary	ns			
	Are means signif. different? (P < 0.05)	No			
	One- or two-tailed P value?	Two-tailed			
	t, df	t=1.905 df=18			

Figure 6E	complexin cortex				
	Unpaired t test				
	P value	0,1774			
	P value summary	ns			
	Are means signif. different? (P < 0.05)	No			
	One- or two-tailed P value?	Two-tailed			
	t, df	t=1.404 df=18			
	complexin hippocampus				
	Unpaired t test				
	P value	0,0169			
	P value summary	*			
	Are means signif. different? (P < 0.05)	Yes			
	One- or two-tailed P value?	Two-tailed			
	t, df	t=2.666 df=16			
	complexin striatum				
	Unpaired t test				
	P value	0,0151			
	P value summary	*			
	Are means signif. different? (P < 0.05)	Yes			
	One- or two-tailed P value?	Two-tailed			
	t, df	t=2.687 df=18			

Figure 6G	One-way analysis of variance				
	P value	0,0180			
	P value summary	*			
	Are means signif. different? (P < 0.05)	Yes			
	Number of groups	4			
	F	4,071			
	R squared	0,3372			
	Newman-Keuls Multiple Comparison Test	Mean Diff.	q	Significant? P < 0.05?	Summary
	R6/2-emp vs R6/2	-541900000	4,141	Yes	*
	R6/2-emp vs R6/2-Chol	-92100000	0,7250	No	ns
	R6/2-emp vs WT	-18000000	---	No	ns
	WT vsR6/2-Chol	-74100000	---	No	ns
	R6/2-Chol vs R6/2	-449800000	3,695	Yes	*

Figure 7A	One-way analysis of variance				
	P value	< 0.0001			
	P value summary	***			
	Are means signif. different? (P < 0.05)	Yes			
	Number of groups	3			
	F	79,31			
	R squared	0,9243			
	Newman-Keuls Multiple Comparison Test	Mean Diff.	q	Significant? P < 0.05?	Summary
	r62 chol vs wt saline	-21,12	13,53	Yes	***
	r62 chol vs r62 saline	-1,197	0,7860	No	ns
	r62 saline vs wt saline	-19,92	16,22	Yes	***
Figure 7B	One-way analysis of variance				
	P value	0,0016			
	P value summary	**			
	Are means signif. different? (P < 0.05)	Yes			
	Number of groups	3			
	F	11,02			
	R squared	0,6290			
	Newman-Keuls Multiple Comparison Test	Mean Diff.	q	Significant? P < 0.05?	Summary
	R6/2-Chol vs WT	-4,237	5,916	Yes	**
	R6/2-Chol vs R6/2	-0,3880	0,5187	No	ns
	R6/2 vs WT	-3,849	5,374	Yes	**

Figure 7E	One-way analysis of variance				
	P value	< 0.0001			
	P value summary	***			
	Are means signif. different? (P < 0.05)	Yes			
	Number of groups	4			
	F	24,89			
	R squared	0,5586			
	Newman-Keuls Multiple Comparison Test	Mean Diff.	q	Significant? P < 0.05?	Summary
TNF-alpha	WT vs R6/2-emp	-3,087	9,294	Yes	***
	WT vs R6/2-Chol	-2,386	8,344	Yes	***
	WT vs R6/2	-2,339	8,820	Yes	***
IL6	WT vs R6/2-emp	-0,7488	2,064	No	ns
	WT vs R6/2-Chol	-0,04721	---	No	ns
	WT vs R6/2	-0,7016	---	No	ns
Figure 7F	One-way analysis of variance				
	P value	< 0.0001			
	P value summary	***			
	Are means signif. different? (P < 0.05)	Yes			
	Number of groups	4			
	F	11,98			
	R squared	0,3786			
	Newman-Keuls Multiple Comparison Test	Mean Diff.	q	Significant? P < 0.05?	Summary
TNF-alpha	WT vs R6/2	-1,049	7,972	Yes	***
	WT vs R62-emp	-0,8024	4,866	Yes	**
	WT vs R6/2-Chol	-0,5491	3,869	Yes	**
IL6	R6/2-Chol vs R6/2	-0,5000	3,139	No	ns
	R6/2-Chol vs R62-emp	-0,2533	---	No	ns
	R62-emp vs R6/2	-0,2467	---	No	ns

Appendix Methods

Details about formulation and characterization of NPs employed in this study are herein described.

Purification and collection of the NPs

To purify the loaded NPs from the unloaded Chol, NBD-Chol and PVA residuals, all the samples were centrifuged at 17,000 rpm for 10 min (Sorvall RC28S, Dupont, Brussels, Belgium), washed several times with water and re-suspended in water. The purified NP suspensions were freeze-dried (-60°C, $1 \cdot 10^{-3}$ mm/Hg, for 48 h; LyoLab 3000, Heto-Holten, Allerod, Denmark) using trehalose as cryoprotectant (1:0.5 w:w polymer/trehalose ratio). After the liophylisation process, all the samples were stored at 4°C in N_2 atmosphere. The yield of NPs (Yield %) was calculated as the percentage of NPs recovered after the freeze-drying procedure compared to the weight of PLGA and Chol used for the preparation as follows: Yield (%) = (NPs recovered after the freeze-dried process – anidre trehalose - PVA residual) weight x100/ (PLGA+Chol) weight. Before their use, freeze-dried NPs were weighed, re-suspended in water at the concentration of 10 mg/mL by bath sonication for 3 min at r.t.

Determination of the amount of PVA residual

As the residual PVA associated with the NPs could affect the physical properties and the uptake by cells, the residual PVA was determined by a colorimetric method based on the formation of the colored complex between two adjacent hydroxyl groups of PVA and an iodine molecule. Briefly, freeze-dried NPs (5 mg) were solubilized in dichloromethane (1 mL). Then, water (2 mL) was added and the organic solvent was evaporated at r.t. under stirring (2 h). The suspension was filtered (cellulose nitrate filter, porosity 0.45 μm, Sartorius, Florence, Italy) to remove the polymeric residue and the aqueous solution (1 mL) was treated with 0.5 M NaOH (2 mL) for 15 min at 60°C. The solution was neutralized with 1 N HCl (900 μL) and the volume adjusted to 5 mL with water. Then, a solution of I_2/KI (0.5 mL) (0.05 M/0.15 M) and water (1.5 mL) was added to a solution of boric acid (0.65 M; 3 mL). PVA concentration was determined measuring the absorbance at 690 nm after 15 min of incubation at r.t. in comparison with a standard plot of PVA prepared under the same experimental conditions.

Chemico-physical characterization

The surface morphology of both unloaded and loaded NPs was evaluated by means of the atomic force microscope (AFM, Park Instruments, Sunnyvale, CA, USA) analysis at r.t. (about 25°C) operating in air and in non-contact mode using triangular silicon tips. The resonant frequencies of the cantilever were found to be about 160 kHz. Before the analysis, a drop (20 μL) of a water-diluted suspension of the NPs (about 0.01 mg/mL) was applied on a small mica disk (1 cm × 1 cm); after 2 min, the excess of water was removed using paper filter. The topographical images obtained, also called "height" images, were flattened using second-order fitting to remove sample tilt.

Architecture and internal structure of NPs was studied by using the transmission electron microscope (TEM) operating at an acceleration voltage of 200 KV (model JEM 2010; JEOL, Oxford Instruments, Abingdon, England). Briefly, a drop of a water-diluted suspension of the samples (about 0.03 mg/mL) was placed on a 200-mesh copper grid (TABB Laboratories Equipment, Berks, UK), allowed to adsorb and the suspension surplus was removed by filter paper.

Mean particle size (Z-Average) and polydispersivity index (PDI) of the NPs (in distilled water) were determined at 25°C by PCS using a Zetasizer Nano ZS (Malvern, UK; Laser 4 mW He–Ne, 633 nm, Laser attenuator Automatic, transmission 100–0.0003%, Detector Avalanche photodiode, Q.E. > 50% at 633 nm, T = 25 ◦C). The results were normalized with respect to a polystirene standard suspension. The zeta potential (ζ-pot) was measured by using the same

equipment with a combination of laser Doppler velocimetry and phase analysis light scattering (PALS). All the data are expressed as means of at least three determinations carried out for each preparation lot (three lots for each sample).

Drug entrapment efficiency (EE%) and loading capacity (LC%)

To quantify the amount of Chol loaded into NPs, an exact amount of loaded NPs (5 mg) was dissolved in chloroform (0.5 mL). Then, isopropyl alcohol (1mL) (in which Chol, but not PLGA, is soluble) was added. The mixture was then vortexed (15 Hz for 1 min; ZX3, VelpScientifica, Usmate, Italy) to promote the precipitation of the polymer and then filtered (polytetrafluoroethylene filter, porosity 0.20 µm, Sartorius). The amount of Chol loaded in the NPs was quantified by RP-HPLC. The HPLC apparatus (JASCO Europe, Cremella, Italy) comprised a Model PU980 pump provided with an injection valve with a 50 µL sample loop (Jasco, Model 7725i) and the UV detector (Jasco UV975). Chromatography separation was carried out on a Syncronics C18 (250x4.6 mm; porosity 5 µm; Thermo Fisher Scientific, Waltham, MA, USA) at r.t., flow rate of 1.2 mL/min, by operating in an isocratic mode using 50:50 v/v acetonitrile:ethanol as mobile phase. Before the use, mobile phase eluents were filtered through a 0.45 µm hydrophilic polypropylene membrane filters (Sartorius). The eluent absorbance was monitored at 220 nm using the UV detector (Jasco UV975). Chromatographic peak area of the standard solution were collected and used for the generation of calibration curve. Linearity was assumed in the range of 18-300 µg/mL (r^2=0.995).

The entrapment efficiency (EE) and the loading capacity (LC), expressed as percentage, were calculated using the following formula: EE%= D/Td×100; LC%= D/W×100 where D is the amount of Chol loaded in the NPs, Td is the amount of drug used for the preparation and W is the weight of the NPs (polymer + drug). All the data are expressed as the mean of at least three determinations.

Release of Chol and NBD-Chol from loaded NPs under simulated conditions

Figure 1D shows the % of Chol and NBD-Chol released in water. The initial "burst effect" can be attributed to the fraction of Chol adsorbed or in close contact with the surface of the NPs. This surface Chol fraction dissolved into the surrounding liquid, leading to the fast initial release profile. Moreover, during the second phase, Chol embedded in the NPs could significantly delay the *in vitro* release. The slow linear release kinetic of Chol from NPs-Chol between day 5 and day 10 could be ascribed to NPs degradation. While hydrophilic drugs with high solubility could increase the rate of water diffusion into the biodegradable matrix, accelerating the release and the (bulk) erosion, hydrophobic molecules with low water solubility (as Chol) may hinder water diffusion into the matrix, slowing the release rate as the consequence of the NPs surface erosion with a consequent release.

An exact amount of lyophilized NPs-Chol1 or NPs-NBD-Chol1 (0.5 mg) were suspended in water under perfect sink conditions (6 mL) into a well closed glass vial that was incubated into a water bath at 37±0.2°C under magnetic stirring (250 rpm). At fixed time intervals, the loaded NPs were centrifuged (40,000 rpm for 30 min at 10°C) and the surnatant (1 mL) was collected to be lyophilized (-60°C, $1 \cdot 10^{-3}$ mm/Hg, for 48 h; LyoLab 3000, Heto-Holten). To evaluate the amount of Chol released from NPs-Chol1, the freeze dried residual was dissolved in water and derivatized with 50 µL of N,O-bis(trimethylsilyl) trifluoroacetamide/trimethylchlorosilane (BSTFA/TMCS) (Sigma–Aldrich).The mixture was heated at 60°C for 30 min. Then, the sample was equilibrated at 25°C and diluted with n-exane. The quantification of the derivatized-Chol was performed by gas chromatography (GC) with selected ion monitoring mass spectrometric (SIM-MSD) using Agilent (Santa Clara, CA, USA) 7890A gas chromatography interfaced with an 5975C Series GC/MSD with Triple-Axis HED-EM Detector and equipped with an Agilent 190915-433 column (30m∗250µm∗0.25µm). The chromatographic conditions were as follow: initial oven temperature 240°C which was

increased by 15°C/min to 315°C. The temperature of the injector was set at 280°C. Helium was used as the carrier gas in a splitless mode injection (3 µL). In selected ion monitoring (SIM) mode three characteristic ions were analyzed (329, 353 and 368 m/z) and the most representative 329 m/z was used for the calibration.

Calibration was achieved starting from stock solution of Chol (1mg/mL) properly diluted with chloroform, evaporated to dryness and analyzed in the manner previously described. Linearity was assured in the range 0.1-2.7 ppm (r^2=0.998).

To evaluate the amount of NBD-Chol released from NPs-NBD-Chol1, the lyophilized residual was solubilized in 1:5 v/v chloroform:isopropyl alcohol mixture and injected in a chromatographic system. The HPLC apparatus (Jasco, Model PU 2089 pump, injection valve model 7725i with a 20 µl sample loop) was correlated with a fluorimetric detector (Jasco FP 2020). Chromatographic separation was carried out on a Syncronis C18 column (250*4.6 µm; 5µm; ThermoScientific) at 30°C and at a flow-rate of l mL/min. Elution was performed in an isocratic mode using as mobile phase a 90:10 v/v acetonitrile:isopropyl alcohol mixture. Mobile phase eluents were filtered through a 0.45 µm of hydrophilic polypropylene membrane filters (Sartorius) before the use. The fluorescence of the eluent was monitored by excitation at 484 nm detecting the emission at 539 nm. A calibration curve was done by analyzing standard solution assuring linearity in the range 0.4-16 µg/ml (r^2=0.995).

In vitro release studies and NBD-Chol quantification

For quantitative studies, NS cells were plated in proliferation medium in 6-mwell plates at 300,000 cells/well. Cells were treated for different time points (24-48-72 h) with 165 µL NPs-NBD-Chol1 suspension (4 mg/mL, 440 µg NBD-Chol/100mg NPs) to receive 3 µg NBD-Chol. After the treatment, the cells were washed with PBS, collected in tubes and centrifuged for 5 min at 1000xg. The centrifuged cell pellets were re-suspended in 400 µl of Lysis Buffer [10 mM TRIS HCl pH 7.5, 150 mM NaCl, 5 mM EDTA, supplemented with PMSF (phenylmethylsulfonyl fluoride) 1:200 and Protease inhibitor 1:100] to obtain a homogenate containing total NBD-Chol (released and still encapsulated into NPs). A fraction of the homogenate (200 µL) was centrifuged for 15 min at 19000xg to separate NBD-Chol still encapsulated into NPs (pellet) from NBD-Chol released after NPs degradation (surnatant). NBD-Chol was quantified in duplicate in both fractions (pellet and surnatant) and in total homogenate by spectrophotometry at 488 nm. NBD-Chol release was calculated by subtracting the NBD fluorescence detected in the pellet (containing the intact NPs) to NBD fluorescence detected in the homogenate (total NBD-Chol present into cells).

Cell Death and Differentiation (2015) 22, 690–702
© 2015 Macmillan Publishers Limited All rights reserved 1350-9047/15
www.nature.com/cdd

Disruption of astrocyte-neuron cholesterol cross talk affects neuronal function in Huntington's disease

M Valenza[1,3], M Marullo[1,3], E Di Paolo[1], E Cesana[2], C Zuccato[1], G Biella[2] and E Cattaneo*[,1]

In the adult brain, neurons require local cholesterol production, which is supplied by astrocytes through apoE-containing lipoproteins. In Huntington's disease (HD), such cholesterol biosynthesis in the brain is severely reduced. Here we show that this defect, occurring in astrocytes, is detrimental for HD neurons. Astrocytes bearing the huntingtin protein containing increasing CAG repeats secreted less apoE-lipoprotein-bound cholesterol in the medium. Conditioned media from HD astrocytes and lipoprotein-depleted conditioned media from wild-type (wt) astrocytes were equally detrimental in a neurite outgrowth assay and did not support synaptic activity in HD neurons, compared with conditions of cholesterol supplementation or conditioned media from wt astrocytes. Molecular perturbation of cholesterol biosynthesis and efflux in astrocytes caused similarly altered astrocyte–neuron cross talk, whereas enhancement of glial SREBP2 and ABCA1 function reversed the aspects of neuronal dysfunction in HD. These findings indicate that astrocyte-mediated cholesterol homeostasis could be a potential therapeutic target to ameliorate neuronal dysfunction in HD.
Cell Death and Differentiation (2015) **22,** 690–702; doi:10.1038/cdd.2014.162; published online 10 October 2014

Huntington's disease (HD) is an adult-onset neurodegenerative disorder characterized by cell loss mainly in the striatum and cortex. Its pathophysiology is linked to an expanded CAG repeat in the IT-15 gene, which leads to an elongated polyQ tract in huntingtin (HTT) protein. No disease-modifying treatment is available for HD and novel pathophysiological insights and therapeutic strategies are needed.[1]

Lipids are vital to brain health and function. Accordingly, the brain has a local source of cholesterol,[2] and a breakdown of cholesterol synthesis causes brain malformations and impaired cognitive function.[3,4] Cholesterol metabolism is disrupted in HD[5,6] as revealed by transcriptional, biochemical, and mass spectrometry analyses in HD rodent models.[7,8] This dysregulation is linked to a specific action of mutant HTT on sterol-regulatory-element-binding proteins (SREBPs) and on its target genes, whose reduced transcription leads to lower brain cholesterol levels.[7] In HD humans, brain cholesterol homeostasis is affected since pre-symptomatic stages, as determined by measurement of the brain-specific cholesterol catabolite 24-S-hydroxy-cholesterol (24OHC).[9,10] However, it remains unclear how reduced brain cholesterol would become pathological for HD neurons.

In adulthood, astrocytes produce cholesterol, which is secreted as a complex with apolipoprotein (apo) E lipoproteins and delivered to neurons.[11,12] Mutant HTT is expressed in glial cells,[13,14] and transgenic mice overexpressing mutant HTT in astrocytes show age-dependent neurological symptoms.[15,16] Additionally, primary astrocytes overexpressing full-length human mutant HTT show reduced mRNA levels of cholesterol biosynthetic genes, along with impaired cellular production and secretion of apoE.[8]

Here we employed molecular and cellular tools to test the impact of cholesterol perturbation between astrocytes and neurons in HD. Reduced secretion of cholesterol bound to apoE lipoproteins by HD astrocytes negatively influenced neurite outgrowth and neuronal synaptic properties. Furthermore, gain-of-function experiments revealed that this non-cell-autonomous mechanism can be overridden through molecular enhancement of cholesterol biosynthesis in HD astrocytes.

Results

Astrocytes bearing mutant HTT protein display cholesterol dysfunction. To test whether and how cholesterol dysfunction in HD astrocytes impacted neuronal function, we took advantage of neural stem (NS) cells that are capable of differentiating into neurons or astrocytes depending on culture conditions[17] (Supplementary Figures 1a and e). We first found that mRNA levels of hydroxyl-methyl-glutaryl-CoA reductase (*hmgcr*) were similar between wild-type (wt) and HD NS cells under self-renewal conditions, but were severely reduced in GFAP$^+$ NS-derived astrocytes carrying mutant HTT with 140 CAG repeats (Q140/7 astrocytes) compared with wt NS-derived astrocytes (Q7/7 astrocytes) (Figure 1a). Accordingly, following 6–8 h of pre-incubation with serum-free medium, the Q140/7 astrocytes secreted less

[1]Department of Biosciences and Centre for Stem Cell Research, Università degli Studi di Milano, Milano, Italy and [2]Department of Biology and Biotechnology, Università degli Studi di Pavia, Pavia, Italy
*Corresponding author: E Cattaneo, Department of Biosciences and Centre for Stem Cell Research, Università degli Studi di Milano, Via Viotti 3/5, Milan, 20133, Italy. Tel: +39 02 50325830; Fax: +39 02 50325843; E-mail: elena.cattaneo@unimi.it
[3]These authors contributed equally to this work
Abbreviations: 24OHC, 24-S-hydroxy-cholesterol; Bsn, Bassoon; CAG, cytosine-adenine-guanine; fdft1, farnesyl-diphosphate farnesyltransferase; GCM, glial-conditioned medium; HD, Huntington's disease; Hmgcr, hydroxyl-methyl-glutaryl-CoA reductase; HTT, huntingtin; LRP1, LDL receptor-related protein; NS, neural stem; SRE, sterol regulatory element; SREBPs, sterol regulatory element-binding proteins; Wt, wild-type
Received 20.5.14; revised 13.8.14; accepted 03.9.14; Edited by M Piacentini; published online 10.10.14

apoE in the media compared with Q7/7 astrocytes (Figure 1b). ApoE level was also significantly decreased in the media from an allelic series of Hdh CAG knock-in NS cells carrying 50 or 111 CAG repeats (Q50/7 and Q111/7 astrocytes) in a CAG length-dependent manner (Q7/7 > Q50/7 > Q111/7) (Figure 1c).[17] HTT-depleted astrocytes displayed the same reduction in apoE level as in Q111/7 (Figure 1c), supporting the hypothesis that normal HTT has a role in cholesterol synthesis.[18] Furthermore, primary astrocytes from a transgenic HD mouse model (R6/2; Supplementary Figure 1f) secreted lower apoE levels compared with primary wt astrocytes (Figure 1d). Quantitative assays confirmed that concentrations of apoE (Figure 1e) and cholesterol (Figure 1f) were significantly reduced in conditioned media from Q140/7 astrocytes and from primary R6/2 astrocytes compared with their respective controls. The impairment in apoE release is likely due to reduced synthesis of intracellular apoE as indicated by reduced mRNA and protein levels in YAC128 astrocytes[8] and in R6/2 and HD NS-derived astrocytes (Supplementary Figure 1g).

Although apoE level was reduced in the media from R6/2 astrocytes, the sizes of apoE lipoproteins, as judged by non-denaturing gel electrophoresis, were similar in the media from the control and HD cultures (Figure 1g). This finding suggests that the total content of cholesterol bound to apoE lipoproteins secreted by HD astrocytes was lower because of reduced apoE level and not as a consequence of inefficient lipoprotein lipidation. Together, these results indicate that HD astrocytes produce and secrete less cholesterol bound to apoE lipoproteins *in vitro,* with possible consequences for neuronal function.

Neurite outgrowth is reduced in HD neurons and is rescued by exogenous cholesterol. Upon exposure to a pan-neuronal differentiation protocol, NS cells can be converted into generic $MAP2^+$ neurons.[17,19] Here, we first differentiated wt and HD NS cell lines towards neurons, and after 7 days, the cells were fixed and immunostained with an anti-MAP2 antibody to visualize the neurites. Not surprisingly, neurite outgrowth was reduced in Q140/7 neurons compared with Q7/7 neurons, as shown by MAP2 staining (Figure 1h) and relative quantification using an automated neurite tracing (*NeuriteTracer*[20]) (Figure 1i). Flow cytometric analysis also showed a reduced number of MAP2-positive cells in Q140/7 (28.3%) compared with Q7/7 neurons (44.1%; Supplementary Figure 2a). Notably, addition of cholesterol improved neurite outgrowth in Q140/7 neurons (Figures 1h and i) with maximal effect at 7–10 μg/ml (Figure 1j). Above this concentration, cholesterol failed to promote neurite outgrowth, as depicted by the bell-shaped curves for Q140/7 neurons (Figure 1j) and, to a lesser extent, for Q7/7 neurons (Supplementary Figure 2b). In the same experimental paradigm, cholesterol treatment did not influence cell survival/proliferation in control or HD neurons (Supplementary Figure 2c). Overall, these results highlight a relationship between neurite outgrowth and cholesterol administration, demonstrating that exogenous cholesterol application is beneficial to HD neurons *in vitro*.

Glial-conditioned medium from HD astrocytes does not support neurite outgrowth in HD neurons. To test whether glial-conditioned media (GCM) influenced HD neurons, we quantified neurite outgrowth following exposure to GCM from wt and HD astrocytes. First, GCM from primary and NS-derived astrocytes were prepared (see Method section) and used to supplement the regular growth medium of Q140/7 neurons, starting from day 4 of neuronal differentiation. As observed for exogenous cholesterol administration, GCM from primary wt astrocytes (GCM wt) or from Q7/7 astrocytes (GCM Q7/7) promoted neurite outgrowth in Q140/7 neurons with respect to the cells under glial-free condition (not treated, NT) (Figures 2a and b). Conversely, GCM from primary astrocytes generated from R6/2 mice (GCM R6/2), or from Q50/7 or Q140/7 astrocytes (GCM Q50/7 and GCM Q140/7), did not promote neurite outgrowth (Figures 2a and b). Not surprisingly, all GCMs (except for R6/2) performed better than NT, although the difference was not significant, suggesting that other glial components, not affected in the HD condition, contribute to neurite outgrowth.

To test whether lipoproteins in the GCM were responsible for promoting neurite outgrowth, we cultured Q140/7 neurons with lipoprotein-depleted GCM from wt astrocytes (GCM_{wt}delip) or GCM from primary astrocytes generated from apoE knock-out mice (GCM $apoE^{-/-}$). Neither GCM stimulated neurite outgrowth in Q140/7 neurons (Supplementary Figure 3a,b). Notably, neither GCM contained a detectable apoE level (Supplementary Figure 3c) whereas GCM $apoE^{-/-}$ contained higher levels of apoD (Supplementary Figure 3d), another lipoprotein expressed in the brain, which is increased in $apoE^{-/-}$ mice to carry out some of the apoE-dependent functions.[21] These data indicate that apoE lipoproteins in GCM are key factors in stimulating neurite outgrowth by supplying cholesterol to HD neurons.

Genetic perturbation of astrocytic cholesterol production and release influences neurite outgrowth in HD neurons. To further test the impact of cholesterol perturbation on neurite outgrowth in HD neurons, we performed gain- and loss-of-function experiments. We first silenced *abca1*, the gene encoding ATP-binding cassette transporter ABCA1, the major regulator of cellular cholesterol homeostasis. Transfection of wt primary astrocytes with small interfering RNAs (siRNA) against *abca* reduced the level of *abca1* mRNA (abca-i) by 40% compared with wt astrocytes transfected with the scrambled siRNA control (scrambled) (Figure 3a). This led to a 50% decrease of apoE levels secreted in the GCM (GCM_{wt}abca-i) compared with GCM from scrambled astrocytes (GCM_{wt}scrambled) (Figure 3b). Importantly, neurite outgrowth was severely impaired when Q140/7 neurons were cultured with GCM_{wt}abca-i, but not with GCM_{wt}scrambled (Figures 3c and d). Overexpression of ABCA1 in R6/2 astrocytes (Figure 3e) did not lead to increased apoE level in the GCM ($GCM_{R6/2}$ABCA1) compared with $GCM_{R6/2}$pcDNA (Figure 3f, left), in agreement with the evidence that greater than sixfold overexpression of ABCA1 in the mouse brain is required to alter apoE levels.[22] However, ABCA1 overexpression stimulated R6/2 astrocytes to release larger apoE lipoproteins into the medium

(Figure 3f, right, arrows), suggesting increased lipidation. When HD neurons were cultured with GCM from R6/2 astrocytes overexpressing ABCA1 ($GCM_{R6/2}ABCA1$), we observed stimulated neurite outgrowth compared with untreated HD neurons or treated with $GCM_{R6/2}$ pcDNA (Figures 3g and h).

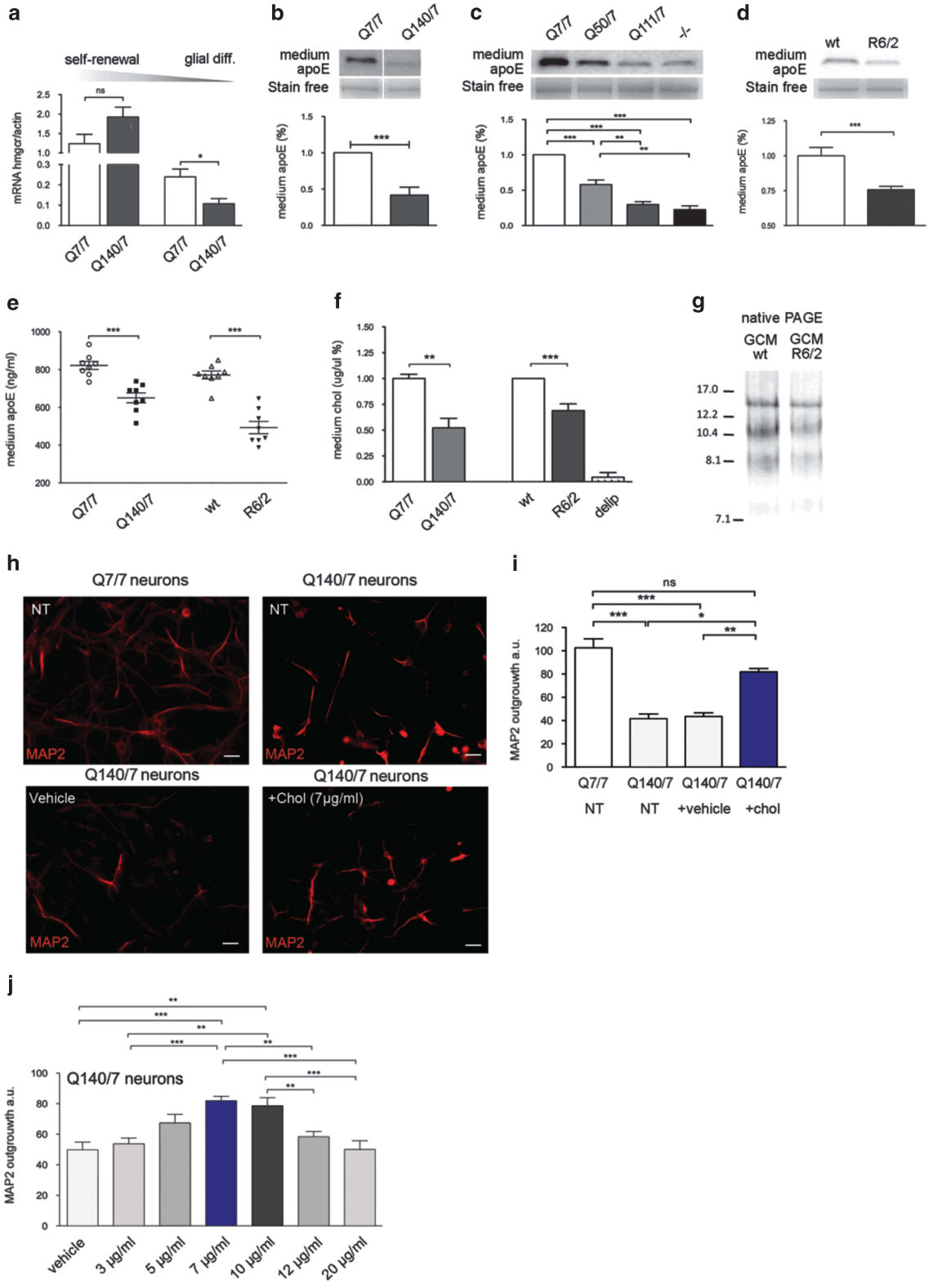

We also silenced in HD neurons the gene encoding for LDL receptor-related protein (LRP1), the major neuronal apoE receptor[23] (Supplementary Figure 4a). As expected, GCM wt and GCM Q7/7 both promoted neurite outgrowth in HD neurons transfected with the scrambled siRNA compared with the same NT neurons and both failed to promote neurite outgrowth when *lrp1* had been silenced (Supplementary Figures 4b and c). However, the reduced lrp1 mRNA level is not mechanistically linked to cholesterol dysfunction, because the *lrp1* mRNA level was indistinguishable between wt and R6/2 brains at pre- and late-symptomatic stages (Supplementary Figure 4d). These data indicate that the cholesterol uptake system is intact in HD neurons, but a defect in cholesterol synthesis reduces the amount of astrocyte-derived cholesterol available for neuronal function.

SREBP2 is the master transcription factor that activates the expression of nearly all cholesterol biosynthesis genes by binding to the sterol regulatory element (SRE) in target gene promoters. Previous studies reported that SREBP activity and its nuclear translocation were reduced in an inducible cell model of HD and in R6/2 brains.[7] Reduced nuclear levels of the N-terminal active fragment of SREBP2 (Nt-BP2) were also found in R6/2 astrocytes compared with wt astrocytes (Supplementary Figure 5a) and mRNA levels of SREBP2, but not of SREBP1, were decreased in HD NS-derived astrocytes compared with controls (Supplementary Figure 5b). Notably, a SRE sequence is present in the promoter region of SREBP2,[24] suggesting that reduced SREBP2 activation may in turn affect *srebp2* gene expression. Knock-down of *srebp2* expression in primary wt astrocytes (Figure 4a) led to decreased apoE levels in the GCM (GCM_{wt}srebp2-i) compared with in GCM from wt astrocytes nucleofected with the scrambled-siRNA (GCM_{wt}scrambled) (Figure 4b). The presence of GCM_{wt}srebp2-i elicited a robust phenotype in HD neurons, which included the inability to promote neurite outgrowth with respect to GCM_{wt}scrambled (Figures 4c and d). In contrast, overexpression of Nt-BP2 in primary R6/2 astrocytes stimulated an increase of mRNA levels of hmgcr and farnesyl-diphosphate farnesyltransferase (fdft1), followed by an increase in *abca1* mRNA at 67 h of nucleofection (Figure 4e). At this time point, the relative GCM consisted of larger apoE lipoproteins (Figure 4f). Similarly to ABCA1 overexpression, we found that neurite outgrowth was increased when Q140/7 neurons were cultured with $GCM_{R6/2}$Nt-BP2 compared with NT neurons or to neurons cultured with $GCM_{R6/2}$pcDNA (Figures 4g and h). Similar findings were obtained with Q50/7 neurons (Supplementary Figure 6). ApoE, albeit at low levels, is essential along with newly cholesterol to rescue neuritic defects in HD neurons. Indeed, GCM from $apoE^{-/-}$ astrocytes overexpressing Nt-BP2 failed to rescue neurite outgrowth in HD neurons (Supplementary Figure 7).

Together, these data indicate that cholesterol biosynthesis modulation in HD astrocytes influences the secretion of cholesterol bound to apoE-containing lipoproteins and neurite outgrowth in HD neurons.

GCM from HD astrocytes reduces synaptic properties in HD neurons. As cholesterol secreted by astrocytes is crucial for synaptic formation and maintenance,[25] we looked at the synaptic-promoting capacities of GCM wt and GCM HD in HD neurons. We cultured striatal or cortical primary neurons of R6/2 mice in the presence of GCM wt (from primary wt astrocytes) or GCM HD (from primary R6/2 astrocytes), starting from 4 *days in vitro* (*div*). At 11 *div*, we counted the number of *bona fide* synaptic contacts by double-staining the cultures for the pre-synaptic scaffold Bassoon (Bsn) and for vGLUT2 or GABA. We then counted the number of Bsn/GABA or Bsn/vGLUT2 puncta to define glutamatergic or GABAergic synapses, respectively (Figures 5a and b). Under glial-free conditions, HD striatal neurons displayed significantly reduced numbers of *bona fide* synaptic contacts compared with wt neurons (Figures 5c). The presence of GCM wt reversed the defect in HD striatal neurons, and increased the number of synaptic contacts in HD cortical neurons (Figures 5c and d). However, GCM HD and GCM_{wt}delip failed to do so. The ability of GCM wt, but not of GCM HD or GCM_{wt}delip, to positively influence this parameter in HD neurons was also confirmed by western blot analyses showing increased levels of post-synaptic density protein PSD95 in HD neurons only when exposed to GCM wt (Figures 5e and f).

GCM HD impedes synaptic activity in HD neurons. We then assayed the electrophysiological properties of HD neurons through whole-cell patch-clamp technique after the different treatments. Most of the recorded primary striatal neurons from R6/2 mice (Figure 6a) exposed to GCM wt or GCM HD were functionally mature, as demonstrated by the presence of consistent families of inward and outward currents (mediated by voltage-dependent sodium and potassium channels, respectively) and by their ability to generate overshooting action potentials in response to suitable current step injections (Figures 6b and c). To test whether the

Figure 1 Cholesterol dysfunction in HD astrocytes and rescue of neuritic defects in HD neurons by cholesterol. (**a**) *Hmgcr* mRNA levels in $Hdh^{Q7/7}$ and $Hdh^{Q140/7}$ NS cell lines (herein, Q7/7 and Q140/7) during self-renewal and after glial differentiation. Beta-actin was used as the housekeeping gene. The graph shows the mean ± S.E.M. of three real-time PCR runs from two independent differentiations. (**b–d**) Representative western blot and densitometry for apoE levels in GCM (medium apoE) from Q7/7 and Q140/7 astrocytes (**b**), from allelic series of NS-derived astrocytes (Q7/7, Q50/7, and Q111/7) and HTT-depleted astrocytes (**c**), and from primary wt and R6/2 astrocytes (**d**). Stain-free imaging (Bio-Rad) was used as a loading control and for normalization. Graph shows mean % above control ± S.E.M. for six independent experiments. (**e** and **f**) ApoE quantification by ELISA assay (**e**) and cholesterol quantification by enzymatic assay (**f**) in a subset of GCMs ($n = 3–8$). The graphs show the mean absolute values (**e**) or % above control (**f**) ± S.E.M. (**g**) Representative western blot under non-denaturing conditions for evaluating size of apoE-containing lipoproteins. (**h** and **i**) Representative immunofluorescence staining with an antibody against MAP2 (**h**), and neurite outgrowth quantification (**i**) of Q7/7 and Q140/7 neurons under glial-free conditions (NT or vehicle) or in the presence of cholesterol (+ chol). The graph in (**i**) shows the mean of an arbitrary value (a.u.) ± S.E.M. from one experiment in which 10 fields were analyzed for each condition. Similar results were obtained with four other independent differentiations. (**j**) Neurite outgrowth quantification in Q140/7 neurons under glial-free conditions (vehicle) or in the presence of increasing doses of cholesterol (3, 5, 7, 10, 12, and 20 μg/ml) immunostained for MAP2. The graph shows the mean (a.u.) ± S.E.M. of 10 fields for each condition. Statistics: two-tailed unpaired *t*-test (**a**, **b**, **d**, **e**, and **f**) or one-way ANOVA, Newman–Keuls multiple-comparison post test (**c**, **i**, and **j**). $^{*}P < 0.05$; $^{**}P < 0.01$; $^{***}P < 0.001$. See Supplementary Figure 9 for full-length pictures of the blots shown in **b**, **c**, and **d**

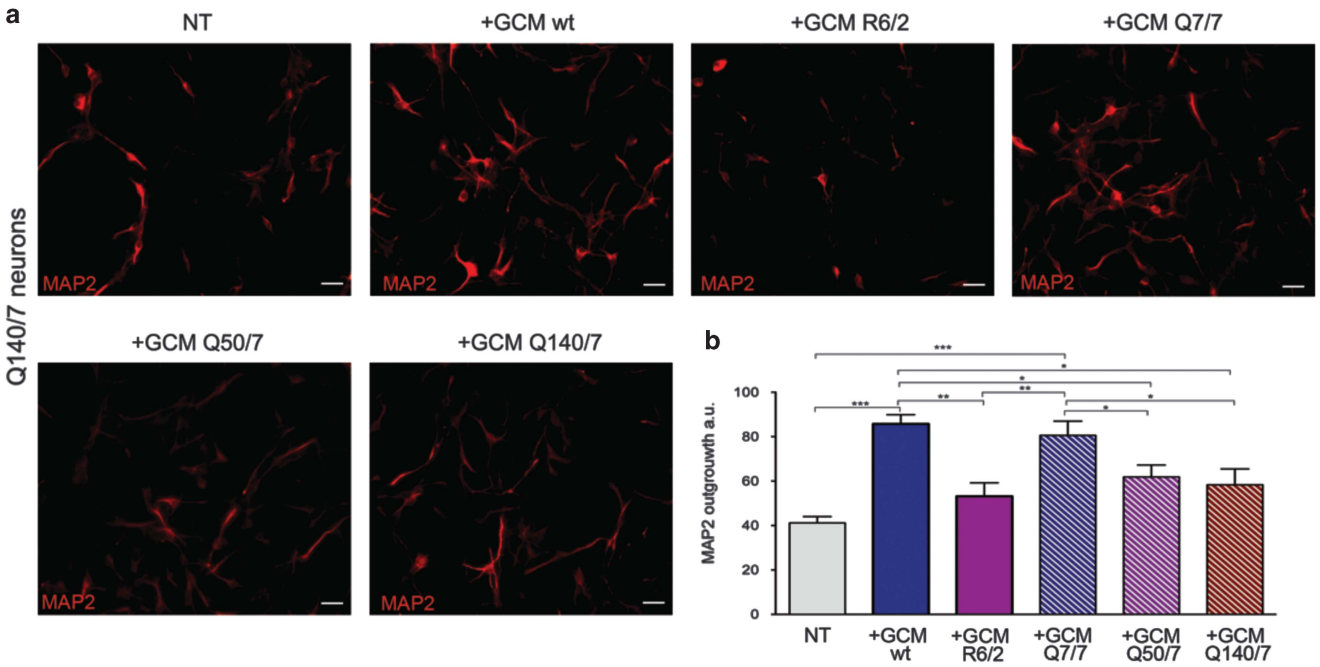

Figure 2 GCM from R6/2 astrocytes does not promote neurite outgrowth in HD NS-derived neurons. (**a**) Representative immunofluorescence staining for MAP2 in Q140/7 neurons under glial-free conditions (NT) or in the presence of GCM from primary astrocytes from wt mice (+GCM wt) or from R6/2 mice (+GCM R6/2), or GCM from Q7/7 (+GCM Q7/7), Q50/7 (+GCM Q50/7), and Q140/7 (+GCM Q140/7) NS-derived astrocytes. Scale bars: 25 μm. (**b**) Relative neurite outgrowth quantification. The graph shows the mean (a.u.) $\pm$ S.E.M. of one experiment in which 10 fields were analyzed for each condition. Similar results were obtained in two other independent differentiations. Statistics: one-way ANOVA, Newman–Keuls multiple-comparison post test (**b**). $^{*}P<0.05$; $^{**}P<0.01$; $^{***}P<0.001$

reduced cholesterol complexed to apoE lipoproteins in GCM HD had an impact on synaptic activity in HD neurons, we performed whole-cell recordings at 9–12 *div*, following incubation with GCM wt or GCM HD for 5–6 days. HD striatal neurons exhibited increased input resistance (Rin) under glial-free conditions compared with wt neurons. Importantly, exogenous cholesterol administration in the presence of GCM HD restored Rin in HD neurons to wt level (Figures 6d). Although the difference between HD and wt neurons in basal conditions was not statistically significant, application of neither GCM wt or GCM HD in HD neurons led to a significant increase in the membrane capacitance (Cm), a parameter directly correlated with cell size (Figure 6e). These results suggest that exogenous cholesterol may influence input resistance, but that other glial-derived molecules might influence the charge storing in HD neurons.

Finally, we tested the capability of the cells to develop *in vitro* a functional synaptic network, by analyzing post-synaptic activity (Figures 6f and i). Under NT conditions, only 4 out of 27 HD neurons (14.8%) produced post-synaptic currents compared with 10 out of 22 wt neurons (45.4%), suggesting that HD neurons had lower spontaneous activity (Figure 6g), consistently with a loss of synaptic contacts and a reduced post-synaptic expression. Notably, 15 out of 22 (68.2%) of HD neurons showed spontaneous synaptic activity in the presence of GCM wt, and 9 out of 28 (32.1%) in the presence of GCM HD. Cholesterol administration to HD neurons, even in the presence of GCM HD, stimulated spontaneous activity in 7 out of 10 (70%) of the recorded cells (Figure 6g), even with a higher mean frequency (2.475 ± 0.99 Hz) compared with untreated HD cells (0.42 ± 0.15 Hz; $P=0.0238$) or in the presence of GCM HD (0.29 ± 0.06 Hz; $P=0.002$) (Figure 6h). Additionally, the mean amplitude was significantly increased in the presence of GCM wt compared with GCM HD (34.7 ± 4.7 pA *versus* 17.30 ± 4.47 pA; $P=0.017$), even in the presence of exogenous cholesterol (20.93 ± 4.1 pA) (Figure 6i), suggesting that other glial molecules might influence this parameter in HD neurons. These findings indicate that a reduced supply of glial-derived cholesterol affects synaptic activity in HD neurons and this may be reversed by cholesterol supplementation.

Discussion

Astrocytes, the major cellular component of the CNS,[26] supply neurons with energy metabolites, growth factors, neurotransmitter recycling functions, and structural support. Cholesterol and glial-conditioned medium have a well-documented role in promoting axonal outgrowth *in vitro* under physiological conditions. Glial-derived lipoproteins containing cholesterol stimulate axon growth[27] and transcription of genes involved in dendrite and synapse development[28] in primary rat retinal ganglion cells; their co-culture with glial cells enhances synaptic activity and neurite outgrowth and branching in Purkinje neurons,[29] and cholesterol deficiency inhibits dendrite outgrowth in primary cortical and hippocampal neurons.[30] Impairments in astrocytic function are increasingly recognized as a culprit in neuronal dysfunction in neurodegenerative diseases,[31] such as amyotrophic lateral sclerosis,[32] Rett's syndrome,[33,34] lysosomal disorders,[35] Alzheimer's disease,[36] and HD.[16] Accordingly, astrocyte kir4.1 ion channel deficits contribute to neuronal dysfunction in

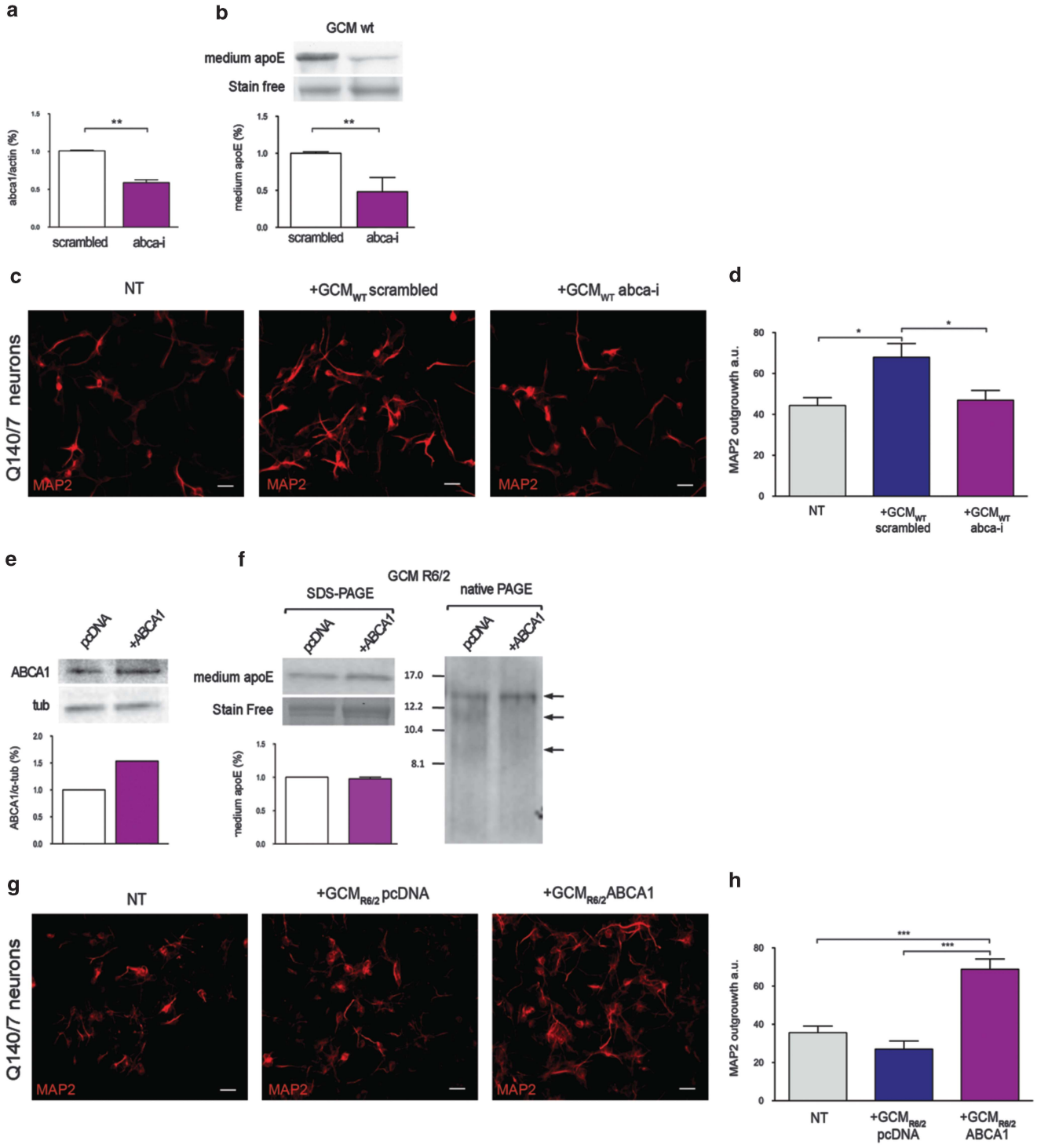

Figure 3 Genetic modulation of ABCA1 in astrocytes influences neurite outgrowth in HD neurons. (**a**) mRNA levels of *abca1* in primary wt astrocytes after transfection with siRNA against *abca1* (abca-i) compared with the same cells transfected with scramble siRNA as a control (scrambled). (**b**) ApoE levels released in the corresponding GCMs. (**c**) Representative immunofluorescence staining for MAP2 in Q140/7 neurons under glial-free conditions (NT), in the presence of GCM_{wt}scrambled, and in the presence of GCM_{wt}abca-i. (**d**) Relative neurite outgrowth quantification. (**e**) Western blot analysis for ABCA1 in primary R6/2 astrocytes after overexpression of ABCA1 (+ABCA1) or an empty vector (pcDNA). (**f**) Relative apoE levels (left) and sizes (right) in the corresponding GCM. (**g**) Representative immunofluorescence staining for MAP2 in Q140/7 neurons under glial-free conditions (NT), in the presence of $GCM_{R6/2}$ pcDNA, and in the presence of $GCM_{R6/2}$ ABCA1. (**h**) Relative neurite outgrowth quantification. Graphs in **a**, **b**, **e**, and **f** show the mean % above relative controls ± S.E.M. Scale bars: 25 μm. Graphs in **d** and **h** show the mean (a.u.) ± S.E.M. of one experiment in which 10 fields were analyzed for each condition. Similar results were obtained in two (**d**) and three (**h**) other independent differentiations. Statistics: two-tailed unpaired *t*-test (**a** and **b**) or one-way ANOVA with Newman–Keuls multiple-comparison post test (**d** and **h**). $^{*}P<0.05$; $^{**}P<0.01$; $^{***}P<0.001$. The samples in **b** were run together with GCM_{wt}srebp2-i shown in Figure 4b. The control sample (GCM_{wt}scrambled) shown in **b** and in Figure 4b is the same. See Supplementary Figure 9 for full-length pictures of the blots shown in **b**, **e**, and **f**

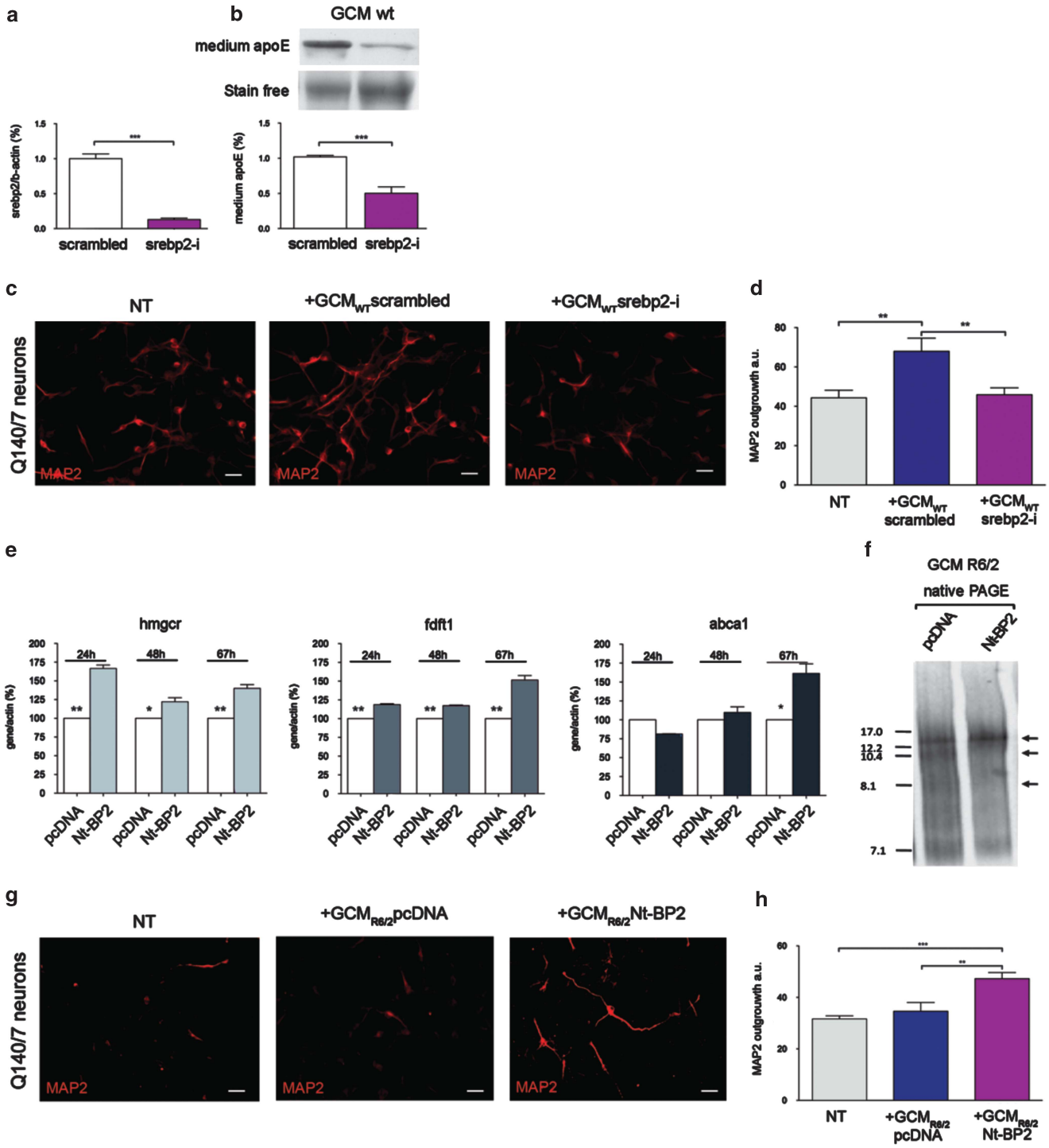

Figure 4 Genetic modulation of SREBP2 in astrocytes influences neurite outgrowth in HD neurons. (**a**) mRNA levels of *srebp2* in wt primary astrocytes after transfection with siRNA against srebp2 (srebp2-i) compared with the same cells transfected with a scramble as control (scrambled) and (**b**) apoE levels released in the corresponding GCMs. (**c**) Representative immunofluorescence staining for MAP2 in Q140/7 neurons in glial-free condition (NT), in the presence of GCM_{wt} scrambled or in the presence GCM_{wt} srebp2-i and (**d**) relative neurite outgrowth quantification. Scale bars: 25 μm. (**e**) mRNA levels of *hmgcr*, *fdft1*, and *abca1* in primary R6/2 astrocytes overexpressing the N-terminal fragment of SREBP2 (Nt-BP2) or an empty vector (pcDNA) at different time points from the nucleofection. (**f**) ApoE-containing lipoproteins size in non-denaturing condition in the corresponding GCM from R6/2 astrocytes overexpressing an empty vector (pcDNA) or Nt-BP2. (**g**) Representative immunofluorescence staining for MAP2 in Q140/7 neurons in glial-free condition (NT), in the presence of $GCM_{R6/2}$pcDNA and in the presence $GCM_{R6/2}$Nt-BP2, and (**h**) relative neurite outgrowth quantification. Graphs in **a**, **b**, and **e** show mean as % above relative controls ± S.E.M. Graphs in **d** and **h** show the mean (a.u.) ± S.E.M. for one experiment in which 10 fields were analyzed for each condition. Similar results were obtained in other two independent differentiations. Statistics: two-tailed, unpaired *t* test (**a**, **b**, and **e**) or one-way ANOVA with Newman–Keuls multiple-comparison post test (**d** and **h**). $^{*}P<0.05$; $^{**}P<0.01$; $^{***}P<0.001$. The samples in **b** were run together with GCM_{wt}abca-i shown in Figure 3b. The control sample (GCM_{wt}scrambled) shown in **b** and in Figure 3b is the same. See Supplementary Figure 9 for full-length pictures of the blots shown in **b**

HD,[37] highlighting that some electrophysiological features of striatal dysfunction in HD can be secondary to glial disturbances. Here, we demonstrate that HD astrocytes affect neuronal function through their reduced synthesis and secretion of cholesterol bound to apoE lipoproteins.

We found that HD NS-derived neurons displayed neurite outgrowth defects at day 7 of neuronal differentiation when compared with control neurons. Conditioned media from wt astrocytes, but not from HD astrocytes, rescued the neuritic defect, suggesting that cholesterol dysfunction in glial cells may contribute to neuritic morphology defects, thereby compromising neuron function. Although several glial-derived factors may contribute to neurite outgrowth in cultured neurons,[38] we demonstrated a direct link between glial cholesterol and neurite outgrowth in HD neurons. First, we showed that cholesterol administration rescued neuritic defects in HD neurons during early stages of differentiation. This effect was specifically observed with cholesterol concentrations of 7–10 μg/ml, suggesting that HD neurons depend on exogenous cholesterol for their activities and that cholesterol concentration is critical for this effect. Notably, this is the same concentration at which cholesterol is found in GCM.[11] Second, we found that lipoprotein-depleted GCM from wt astrocytes did not support neurite outgrowth and synaptic properties in HD neurons, pointing out a role of lipoproteins in neuronal function. Third, media conditioned by primary astrocytes from apoE$^{-/-}$ mice did not improve neuronal properties in HD neurons, despite the presence of higher levels of apoD, supporting the unique role of cholesterol bound to apoE lipoproteins present in GCM. Finally, *abca1* silencing in wt astrocytes negatively influenced neurite outgrowth in HD neurons, whereas its overexpression in HD astrocytes had the opposite effect. This is in agreement with the critical role of ABCA1 in brain cholesterol metabolism and neuronal function.[39] The evidence that *lrp1* mRNA levels are similar in wt and R6/2 brains also confirms that HD astrocytes are the mediators of cholesterol dysfunction in HD. Modulation of cholesterol efflux might be an alternative strategy for targeting cholesterol-dependent neuronal defects in HD. Agonists of liver-X receptors induced transcription of ABCA1 and apoE, reduced amyloid-β levels and improved cognition in Alzheimer's disease,[40] and may reduce neuroinflammation.[41] Moreover, an liver-X receptor agonist partially rescued HTT knockdown phenotypes in Zebrafish.[42] However, further studies are needed to evaluate the potential of these drugs in HD and to develop more brain-specific liver-X receptor agonists.

Our findings suggest a prominent role of glial SREBP2 in neuronal function. SREBP2 is expressed in glial cells and its activity likely controls the synthesis of lipids involved in various glia–neuron interactions, thereby affecting a range of neuronal functions.[43–45] SREBP1 and SREBP2 activities are reduced in the presence of mutant HTT, both *in vitro* and *in vivo*.[7] Although the details of the underlying molecular mechanism are unknown, mutant HTT likely interferes with the Golgi-to-nucleus translocation of the active SREBP.[7] The effects on neurite outgrowth in HD neurons following the silencing or overexpression of active SREBP2 in astrocytes demonstrate a link between cholesterol synthesis in astrocytes and subsequent efflux likely under the regulating effect of oxysterols, such as 24OHC.[46] Reduced levels of 24OHC in HD[8–10] may therefore exacerbate cholesterol unbalance between astrocytes and neurons.

In the absence of cell death, HD animal models exhibit abnormalities in synaptic communication[47,48] and neuronal dysfunction precedes cell death by many years in HD humans.[49] Similarly, cholesterol biosynthesis disruption in HD animal models and patients occurs before the onset of motor defect.[9,10,18,50] Additionally, synaptosomes carry suboptimal levels of sterols in early R6/2 model.[8] Here, we showed that a non-cell autonomous cholesterol-handling defect in astrocytes affects cholesterol shuttling between astrocytes and neurons, which has a reversible detrimental effect on synaptic-related parameters in HD neurons.

How does reduced glial cholesterol contribute to neuronal dysfunction in HD? Cholesterol promotes different aspects of synapse development and maintenance, including dendrite differentiation, synaptic vesicle formation and release, and receptor clustering and stability.[12–53] Of note, proteome-wide mapping of cholesterol-interacting proteins in mammalian cells reveals that most of these proteins are linked to neurological disorders.[54] Neurons produce cholesterol less efficiently than glial cells[55] and the appearance of most synapses in the developing brain is temporally and spatially coincident with astrocyte development, suggesting that synapse formation may depend on astrocytes-derived cholesterol.[56] Changes in cholesterol pathways and in apoE expression have been also associated to NMDA-mediated excitotoxicity.[57–59] Of note, 24OHC is a potent and specific modulator of NMDA receptors.[60] Although cholesterol homeostasis has been reported to contribute to enhanced excitotoxicity in HD,[61] however, further studies are needed to address this relationship.

In conclusion, our results indicate that HD astrocytes are responsible for cholesterol dysfunction in the HD brain, by supplying less cholesterol to the surrounding neurons. Glial SREBP2 might be a candidate target for *in vivo* approaches aiming to explore the contribution of glial cholesterol dysfunction in HD. Its enhancement may contribute to attenuating neurite degeneration and synaptic defects in HD neurons.

Materials and Methods

Neural stem cell lines and neuronal differentiation. The NS cell lines employed in this study were grown and differentiated towards neurons for 7 days, as previously described.[17]

Primary cultures of neurons. We used primary neurons to measure synaptic properties because NS-derived neurons did not reach complete functional maturation *in vitro* (data not shown). Primary cultures of striatal neurons were generated from transgenic R6/2 mice that overexpress exon 1 of the human HTT gene containing 150 CAG repeats. At embryonic day (E) 16.5, tails from each embryo were used to extract genomic DNA and to perform PCR for genotype determination. Next, the brain was dissected and tissue was placed into ice-cold HIBERNATE MEDIA (Life Technologies Italia, Monza, Italy). Cells were obtained first through an enzymatic disaggregation with 0.5 mg/ml papain (Worthington biochemical Corporation, Lakewood, NJ, USA) for 15 min at 37 °C, and then by mechanical dissociation. The dissociated cells were resuspended in DMEM (Invitrogen, Life Tecnhologies Italia) supplemented with 10% fetal bovine serum, 0.5 mM L-glutamine (Invitrogen), and 100 U/ml of penicillin-streptomycin (Invitrogen). They were then seeded at a density of 400 000 cells per well in 12-well plates or 1 000 000 cells per well in 6-well plates. After 1 *div*, the medium was totally replaced with DMEM/F12 supplemented with B27 1× (Life Technologies), 0.5 mM

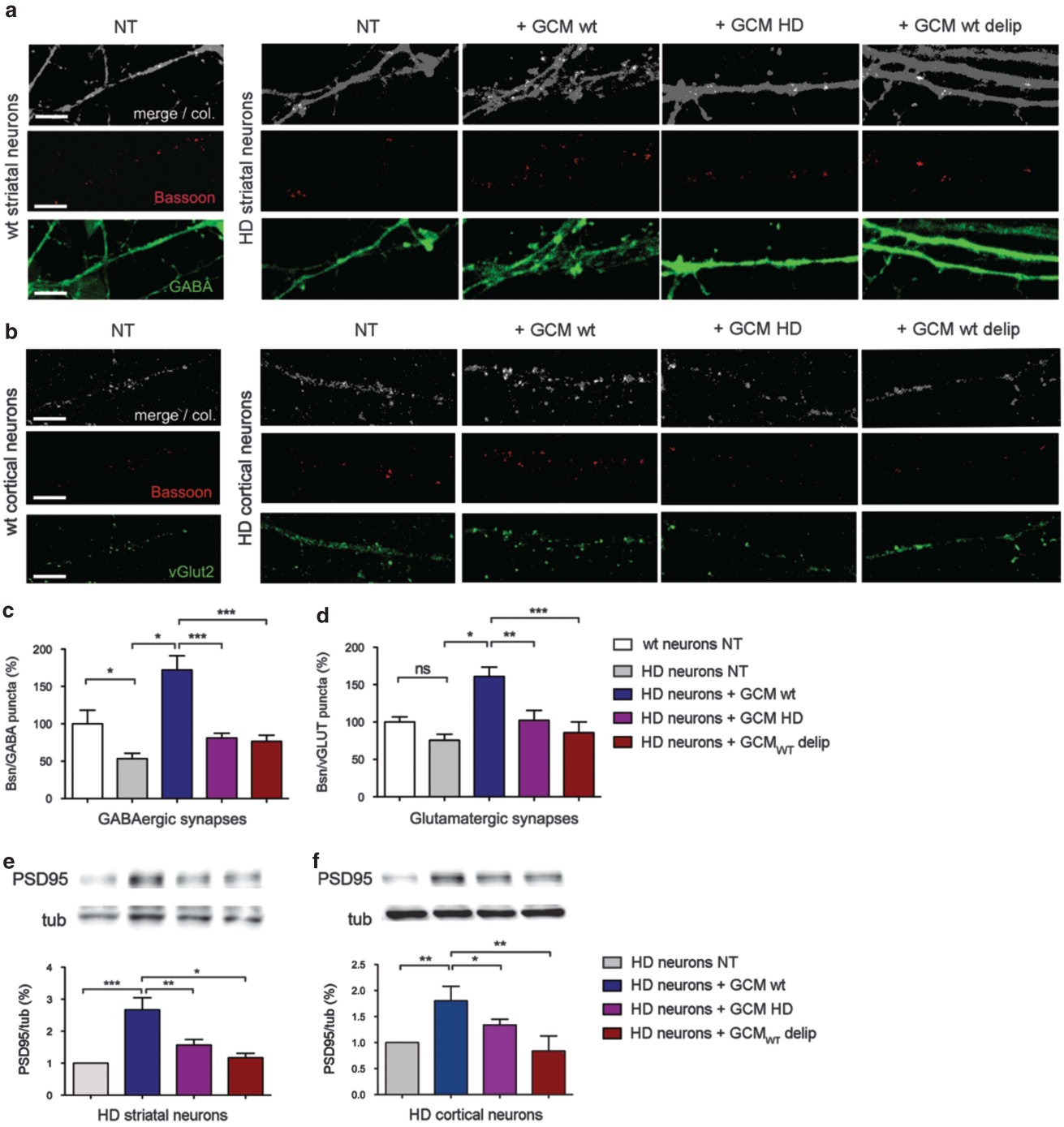

Figure 5 GCM HD does not promote synaptic properties in HD neurons. (**a** and **b**) Fluorescence images of primary cortical and striatal neurons under glial-free conditions (NT) or in the presence of GCM wt, GCM R6/2, or GCM delip, double-immunostained with Bassoon (red, middle panels) and either VGLUT-2 or GABA (green, bottom panels), along with the relative co-localization (merge; col.). (**c** and **d**) Quantification of puncta that are double-positive for Bassoon and either VGLUT-2 or GABA to identify glutamatergic and GABAergic bona-fide synapses, respectively. Scale bars: 5 μm. (**e** and **f**) Western blot analysis for PSD95 in protein lysates from primary R6/2 (HD) striatal and cortical neurons under glia-free conditions (NT) or in the presence of GCM wt, GCM R6/2, or GCM delip. (**c** and **d**) Graphs show the mean % above relative controls $\pm$ S.E.M. from 10 fields each for three independent experiments. Statistics: one-way ANOVA with Newman–Keuls multiple-comparison post test. $^{*}P<0.05$; $^{**}P<0.01$; $^{***}P<0.001$. See Supplementary Figure 9 for full-length pictures of the blots shown in **e** and **f**

L-glutamine (Invitrogen), and 100 U/ml of penicillin-streptomycin (Invitrogen). Cells were cultured for 11 *div* with multiple medium changes.

Glial-conditioned medium preparation. NS-derived astrocytes were obtained by plating NS cells on uncoated 25-cm^2 flasks, and exposing them to Glasgow Minimum Essential Medium (Celbio, Euroclone S.p.a., Milan, Italy) in the presence of 10% fetal bovine serum, 0.5 mM L-glutamine (Invitrogen), and 100 U/ml of penicillin-streptomycin (Invitrogen) for 14 days, with the medium changed every 3 days. Primary astrocytes were generated from postnatal day 1 pups as previously described.[8] Astrocytes were seeded in six-well plates

(1 600 000/well) and, 24 h later, were exposed to serum-free DMEM/F12 (Invitrogen) for 6–8 h. Conditioned medium was collected, centrifuged at 1000 × *g* for 4 min, and then concentrated 10-fold using Amicon Ultra-4 filter devices (Millipore, Billerica, MA, USA). Lipoprotein-depleted GCM was prepared by mixing 5 ml of GCM with 50 mg of colloidal silica that avidly binds lipoproteins (Cab-o-sil, Sigma-Aldrich, St Louis, MO, USA). After 30 min of mixing, the Cab-o-sil (which contained bound lipoproteins) was removed from the medium by centrifugation for 5 min at 1000 × *g*. Immunoblotting showed that the Cab-o-sil-treated GCM contained no detectable

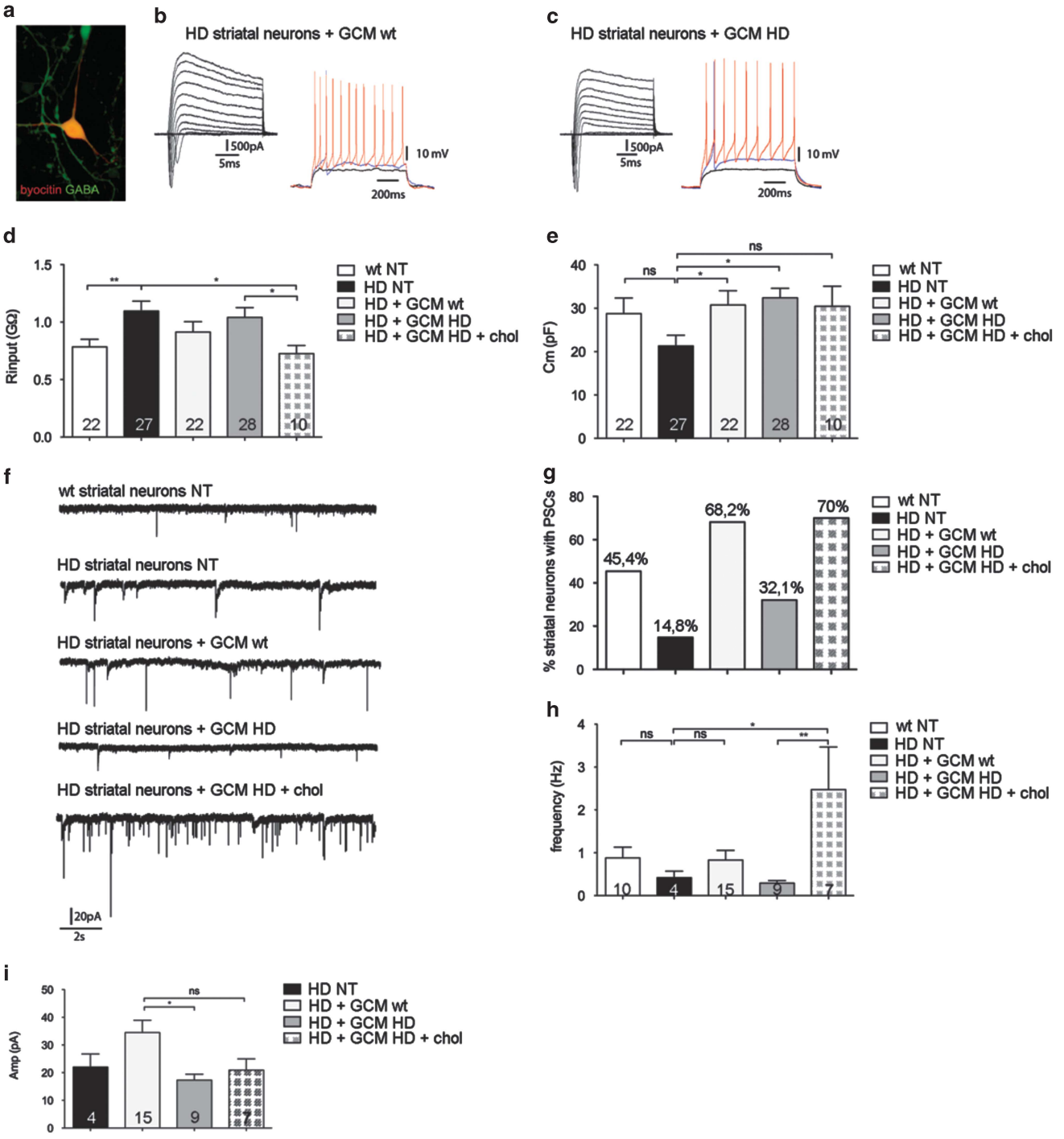

Figure 6 GCM wt, but not GCM HD, stimulates synaptic activity in HD neurons. (**a**) Representative fluorescent image of a recorded primary striatal neuron immunostained for biocytin and GABA. (**b** and **c**) Family of fast inward (negative) and outward (positive) currents, reflecting the presence of sodium (Na+) and potassium (K+) channels, respectively, recorded in response to depolarizing 10 mV voltage step (from − 90 to +50 mV) and sample traces of repetitive action potentials in primary R6/2 (HD) striatal neurons recorded in response to increasing current step injection from a holding potential of − 70 mV in the presence of GCM wt or GCM HD. (**d** and **e**) Histograms showing the input resistance (Rin) (**d**) and the membrane capacitance (Cm) (**e**) in primary wt and HD striatal neurons under different medium conditions. (**f**) Sample current traces of spontaneous synaptic activity recorded in voltage-clamp at − 70 mV. (**g**–**i**) Histograms showing the % of neurons able to produce spontaneous PSCs (**g**), the mean frequency (**h**), and the mean amplitude (**i**) of synaptic events. Data in **d**, **e**, **g**, **h**, and **i** are shown as mean ± S.E.M. Numbers inside the columns represent the number of recorded cells (**d** and **e**) or recorded cells showing PSCs (**h**). *P* values were determined by non-parametric Mann–Whitney test. **P* < 0.05; ***P* < 0.01; ****P* < 0.001; ns = not statistically significant

apoE. Each stock of GCMs used for subsequent experiments was first checked for apoE levels.

Medium apoE analysis. Equal volumes of concentrated media were resolved on Criterion TGX Stain-Free Gels (Bio-Rad, Hercules, CA, USA) with SDS. These stain-free gels contain proprietary trihalo compounds that react with tryptophan residues, producing fluorescent light through an ultraviolet light-induced reaction. Stain-free imaging of the gels and membranes, corresponding to proteins in the samples, was used as loading control and for normalization.[62] Proteins were transferred to a nitrocellulose membrane using a Trans-Blot Turbo system (Bio-Rad). They were then probed with a polyclonal goat anti-apoE antibody (1 : 800; AB947, Millipore), washed, and probed with HRP-conjugated horse anti-goat IgG (1 : 3000; Bio-Rad). Bands were visualized with enhanced chemoluminescence (Pierce, Thermo Scientific, Rockford, IL, USA) and imaged with ChemiDoc MP Imaging System (Bio-Rad).

Nondenaturing gradient gel electrophoresis. GCM samples were mixed 1 : 1 with native sample buffer (Bio-Rad) and electrophoresed on Criterion TGX Stain-Free 4–15% Gels (Bio-Rad). Proteins were transferred to a nitrocellulose membrane and probed with apoE antibody as described above. Proteins with known hydrated diameters were used as size standards (GE Healthcare, Buckinghamshire, UK).

ApoE ELISA. For *in vitro* quantitative determination of mouse apoE concentration in GCMs, we used the Mouse apoE ELISA Kit (MyBioSource, San Diego, CA, USA) following the manufacturer's procedures. Only fresh media were used for the analyses.

Measurement of total cholesterol. Total cholesterol content was evaluated in 10-fold concentrated GCMs. A colorimetric assay was performed using the Cholesterol Kit (Amplex Red Cholesterol Assay Kit, Invitrogen) following the manufacturer's instructions.

Immunofluorescence. Cells were fixed in 4% paraformaldehyde for 15 min at room temperature, and washed three times with PBS. The cells were permeabilized with Triton 0.5% (Sigma) and blocked with 5% fetal bovine serum (Euroclone S.p.a.) for 1 h at room temperature. Cells were then incubated overnight at 4 °C with one of the following primary antibodies: mouse anti-MAP2 (1 : 500; Becton Dicknson, Franklin Lakes, NJ, USA), rabbit anti-VGLUT2 (1 : 500; Synaptic Systems GmbH, Goettinger, Germany), rabbit anti-GABA (1 : 500; Sigma-Aldrich), mouse anti-GFAP (1 : 500; Becton Dickinson), and rabbit anti-S100β (1 : 200; Sigma-Aldrich). Next, the cells were washed three times with PBS, followed by a 1-h incubation at room temperature with the appropriate secondary antibodies conjugated to 488 or 568 Alexa-fluorophores (Molecular Probes, Life Technologies). Finally, the cells were washed three times with PBS, and the nuclei were stained with Hoechst 33258 (5 mg/ml; Molecular Probes, Life Technologies). Images were acquired with a Leica DMI 6000B microscope (Leica microsystems, Wetzlar, Germany) with × 10 and × 20 objectives, using LAS-AF imaging software (Leica microsystems). Adobe Photoshop CS3 (Adobe Systems Incorporated, San Jose, CA, USA) was used to increase the image quality by applying the same values of luminosity and contrast to all images being compared.

Neurite outgrowth quantification. Total neurite length was estimated using the ImageJ plugin Neurite Tracer[20] in combination with a modified macro for counting neuronal nuclei that was developed in the lab. The analysis was performed blind to the experimental conditions. In the main figures, the data are represented as the mean (a.u.) ± S.E.M. of one experiment in which 10 fields were analyzed for each condition. Graphs showing neurite outgrowth quantification expressed as % above the relative controls, as mean of all the independent experiments performed in this work have been showed in Supplementary Figure 8.

Flow cytometry. Detached cells were fixed in 0.1% paraformaldehyde, permeabilized for 15 min in a 0.2% Tween20 solution, and resuspended in fetal bovine serum. We then added a solution containing primary antibodies (anti-MAP2, 1 : 500, Becton Dickinson; anti-GFAP, 1 : 500, Becton Dickinson; anti-S100β, 1 : 200, Sigma-Aldrich). After washing, appropriate Alexa488- and 647-conjugated secondary antibodies were used (1 : 1000). Primary isotypic antibodies were used as controls. Analyses were performed using a FACS Canto II analyzer (BD Biosciences, San Jose, CA, USA) and BD FACSDiva v6.1.3 software. For each condition, 10 000 cells were analyzed.

Cell proliferation assays. On day 3 of neuronal differentiation, NS cells were plated on laminin-coated (3 μg/ml for 3–5 h at 37 °C) 96-well microplates, at 30×10^3 cells/well. The CyQuant NF Cell Proliferation Assay Kit (Molecular Probes, Invitrogen) was used to assay cell viability after treatment of the cells for 24, 48, 72, and 96 h with different doses of cholesterol, following the manufacturer's procedures.

Nucleofection. The Amaxa Cell Line Optimization Nucleofector Kit (Lonza, Basel, Switzerland) was used to modulate gene expressions in different cell lines. Electroporation was performed using pre-set programs: T-020 for the nucleofection of primary astrocytes, and A-033 for NS-derived neurons. The following constructs were used: specific siRNA for *abca*, *srebp2 and lrp1* (Santa Cruz Biotechnology, Inc., Santa Cruz, CA, USA), plasmid overexpressing ABCA1 (gift by S. Calandra, University of Modena) and plasmid overexpressing the active fragment of SREBP2 (as described previously[6]).

RNA isolation, retrotranscription, and real-time PCR for gene expression. Total RNA from cell cultures was isolated with TRIZOL Reagent (Invitrogen). Total RNA (0.25–0.5 μg) was reverse-transcribed to single-stranded cDNA using the iScript cDNA synthesis kit (Bio-Rad). For each reverse-transcribed product, three real-time PCR analyses were performed in duplicate for each of the analyzed genes. An iCycler Thermal Cycler with a Multicolor Real-time PCR Detection System (Bio-Rad) was used to evaluate gene expressions. All reactions were performed in a total volume of 15 μl, containing 60 ng cDNA, 50 mM KCl, 20 mM Tris-HCl (pH 8.4), 0.2 mM dNTPs, 25 U/ml iTaq DNA polymerase, 3 mM $MgCl_2$, SYBR Green I, 10 nM fluorescein, stabilizers (iQ EVA Green Supermix; Bio-Rad), and 0.2 μM forward and reverse primers. Amplification cycles consisted of an initial denaturing cycle at 95 °C for 3 min, followed by 45 cycles of 30 s at 95 °C, 30 s at 60 °C (for all analyzed genes), and 30 s at 72 °C. Fluorescence was quantified during the annealing step, primer specificity and product formation were confirmed by melting curve analysis (55–94 °C), and the amounts of target gene mRNA were normalized to β-actin as reference gene and by using the calibration curve method. The following primer sequences were used: *Hmgcr* fwd, GGAGCATAGGCGGCTACA; *Hmgcr* rev, ACCACCCACGGTTCCTATCT; *Fdft* fwd, ACTCAGCAGCAGCTTGAAGACC; *Fdft* rev, TGTCATCCTCCACTGTATCCAG; *Abca1* fwd, GTCAGCTGTTACTGGAAGTGG; *Abca1* rev, CGCCGGGAGTTGGATA ACGG; *lrp1* fwd, AGGCCACCTCTGCAGCTGT; *lrp1* rev, GCTGCGGATCTCGTTG TCATC; *Actin* fwd, AGTGTGACGTTGACATCCGTA; *Actin* rev, GCCAGAGCAGTA ATCTCCTTCT; *Srebp2* fwd, GCCTCTCCTTTAACCCCTTG; and *Srebp2* rev, CCAGTCAAACCAGCCCCCAG.

Quantification of *bona fide* synapses. Following the above-described procedures, we performed standard immunofluorescence on primary neuronal cultures with a mouse anti-Bassoon antibody (1 : 400; Stressgen Biotechnologies, Collegeville, PA, USA) and with the specific neuronal markers v-GLUT2 and GABA. Confocal images were acquired with a Zeiss LSM 510 laser-scanning confocal microscope with AIM4.2 software (Zeiss, Oberkochen, Germany). The number of co-localizations was quantified using the 'Red and Green Puncta Colocalization' macro under the ImageJ analysis software platform (U.S. National Institutes of Health, Bethesda, MD, USA).

Western blot analysis. Cells were lysed by adding 50 μl of RIPA buffer supplemented with PMSF (1 : 250; Sigma-Aldrich) and protease inhibitors (1 : 100; Sigma-Aldrich). After centrifugation at 10 000 × *g* for 5 min, the supernatant was collected and the protein concentration was determined by BCA assay (Thermo Scientific). Nuclear extracts to evaluate the active form of SREBP2 were prepared as previously described.[7] Proteins were separated by SDS-polyacrylamide gel electrophoresis and then transferred to a nitrocellulose membrane using a Trans-Blot Turbo System (Bio-Rad). The membranes were next probed with mouse anti-PSD95 (1 : 1000; Synaptic Systems), rabbit anti-ABCA1 (1 : 500; gift from M. Hayden), goat anti-apoE (1 : 800; AB947, Millipore), mouse anti-α-tubulin (1 : 5000; Sigma-Aldrich), rabbit anti-SREBP2 (1 : 200; Abcam, Cambridge, MA, USA) followed by washing, and probing with horseradish peroxidase-conjugated secondary antibodies (1 : 3000; Bio-Rad). Bands were visualized with enhanced chemoluminescence (Pierce) and imaged with the ChemiDoc MP Imaging System (Bio-Rad).

Electrophysiological analyses. We recorded 157 primary striatal neurons, of which 127 (80.9%) showed Na^+ currents with amplitude larger than 500 pA, suggesting that most of the recorded cells were functionally mature and potentially able to generate action potentials. Cells were visualized using an inverted microscope (Eclipse TE200, Nikon, Tokyo, Japan) equipped with both $\times 10$ and $\times 40$ objectives. During recording, primary neurons were maintained at room temperature in a bath solution containing 140 mM NaCl, 2 mM $CaCl_2$, 1 mM $MgCl_2$, 3 mM KCl, 10 mM glucose, and 10 mM HEPES, adjusted to pH 7.4 with NaOH. Patch pipettes with a resistance of 3–5 MΩ were fabricated from thick-walled borosilicate glass capillaries using a Sutter P-97 horizontal puller (Sutter Instruments, Novato, CA, USA), and filled with the following intracellular solution: 130 mM potassium gluconate, 4 mM NaCl, 10 mM HEPES, 1 mM EGTA, 2 mM $MgCl_2$, 5 mM CP, adjusted to pH 7.3 with KOH.

Recordings were obtained in the whole-cell configuration, both in voltage- and current-clamp mode, using an Axoclamp 200B amplifier (Molecular Devices) and a Digidata converter AD/DA (Molecular Devices). Signals were low-pass filtered at 10 kHz, and acquired at 10–50 kHz with Clampex software (Molecular Devices, Sunnyvale, CA, USA). To appreciate the morphology, cells were filled either with biocytin (3 mg/ml) or Alexa Fluor 488 (Molecular Probes, Invitrogen), routinely added to the intracellular solution. In voltage-clamp configuration, passive membrane properties were measured immediately after the break-in. The input resistance (Rin) was calculated from the current trace at the end (mean of the last 5 ms) of the 180-ms-long voltage step from -70 mV to -80 mV. Using the same protocol, the membrane capacitance (Cm) was measured by subtracting the time-integral of the steady-state current from the total time-integral of the current transient developing during the 10 mV voltage step and dividing by the same voltage step. Spontaneous synaptic activity was recorded in the voltage-clamp configuration at -70 mV. Negative deflections of current trace were acknowledged as spontaneous synaptic events, and the peak amplitude was evaluated as the mean over 300 μs around a local minimum. Frequency was calculated as the ratio between the number of synaptic events and the time window of 30–60 s, and the mean amplitude was calculated by selecting a sufficient number (>30) of well-isolated events. In current-clamp configuration an appropriate holding current was applied to maintain the membrane potential at -70 mV and 1-s-long positive current steps of increasing amplitude were injected to investigate the ability to generate an action potential or a repetitive firing. All chemicals were from Sigma-Aldrich.

Statistical analysis. No statistical methods were used to predetermine sample sizes, but our sample sizes were similar to those reported in literature. Data were expressed as mean $\pm$ S.E.M. Statistical analysis was performed by two-tail Student's *t*-test or one-way ANOVA with Newman–Keuls Multiple Comparison post-hoc test. The Mann–Whitney test was used to assess the input resistance, membrane capacitance, and post-synaptic current frequency and amplitude—all variables for which normality of the data could not be assumed. Normality of the data was assessed using the Shapiro-Wilk test. Outliers were identified with Grubbs' test, and were excluded from the analyses. Differences for which P was <0.05 were considered to be significant.

Conflict of Interest

The authors declare no conflict of interest.

Acknowledgements. This work was supported by the Cure Huntington Disease Initiative (CHDI, USA, no. A-5086), the Telethon Foundation (Italy, no. GGP12122), and, partially, by Neuromics (Integrated European –omics research project for diagnosis and therapy in rare neuromuscular and neurodegenerative diseases no. 305121) to EC; by Fondazione Cariplo (Italy, no. 2008/2406) to MV; and by PRIN (Ministero dell'Istruzione, della Università e della Ricerca, Italy, no. 2010JMMZLY) to GB. We thank Sebastiano Calandra (University of Modena) for providing us with the ABCA1 plasmid, Alessandro Ieraci (University of Milan) for technical support in the initial generation of primary neurons, and Giulia Chiesa and Marco Busnelli (University of Milan) for providing us with apoE$^{-/-}$ pups.

Author contributions

EC, MV, and MM developed the study, conceived the experimental plans, and analyzed the data. MM, MV, and EDP performed most of the biological, biochemical, and molecular experiments. ECe and GB were involved in all of the electrophysiological experiments and the interpretation of the results. CZ provided suggestions for some biological experiments. MV, MM, and EC interpreted the data and wrote the manuscript. All of the authors read and edited the manuscript. EC supervised the entire work, directed the strategies, and gave final approval of the version to be published.

1. Zuccato C, Valenza M, Cattaneo E. Molecular mechanisms and potential therapeutical targets in Huntington's disease. *Physiol Rev* 2010; **90**: 905–981.
2. Dietschy JM, Turley SD. Thematic review series: brain Lipids. Cholesterol metabolism in the central nervous system during early development and in the mature animal. *J Lipid Res* 2004; **45**: 1375–1397.
3. Porter FD, Herman GE. Malformation syndromes caused by disorders of cholesterol synthesis. *J Lipid Res* 2011; **52**: 6–34.
4. Suzuki R, Ferris HA, Chee MJ, Maratos-Flier E, Kahn CR. Reduction of the cholesterol sensor SCAP in the brains of mice causes impaired synaptic transmission and altered cognitive function. *PLoS Biol* 2013; **11**: e1001532.
5. Valenza M, Cattaneo E. Emerging roles for cholesterol in Huntington's disease. *Trends Neurosci* 2011; **34**: 474–486.
6. Karasinska JM, Hayden MR. Cholesterol metabolism in Huntington disease. *Nat Rev Neurol* 2011; **7**: 561–572.
7. Valenza M, Rigamonti D, Goffredo D, Zuccato C, Fenu S, Jamot L *et al.* Dysfunction of the cholesterol biosynthetic pathway in Huntington's disease. *J Neurosci* 2005; **25**: 9932–9939.
8. Valenza M, Leoni V, Karasinska JM, Petricca L, Fan J, Carroll J *et al.* Cholesterol defect is marked across multiple rodent models of Huntington's disease and is manifest in astrocytes. *J Neurosci* 2010; **30**: 10844–10850.
9. Leoni V, Mariotti C, Tabrizi SJ, Valenza M, Wild EJ, Henley SM *et al.* Plasma 24S-hydroxycholesterol and caudate MRI in pre-manifest and early Huntington's disease. *Brain* 2008; **131**: 2851–2859.
10. Leoni V, Long JD, Mills JA, Di Donato S, Paulsen JS. PREDICT-HD study group Plasma 24S-hydroxycholesterol correlation with markers of Huntington disease progression. *Neurobiol Dis* 2013; **55**: 37–43.
11. Mauch DH, Nagler K, Schumacher S, Goritz C, Muller EC, Otto A *et al.* CNS synaptogenesis promoted by glia-derived cholesterol. *Science* 2001; **294**: 1354–1357.
12. Pfrieger FW, Ungerer N. Cholesterol metabolism in neurons and astrocytes. *Prog Lipid Res* 2011; **50**: 357–371.
13. Hebb MO, Denovan-Wright EM, Robertson HA. Expression of the Huntington's disease gene is regulated in astrocytes in the arcuate nucleus of the hypothalamus of postpartum rats. *FASEB J* 1999; **13**: 1099–1106.
14. Shin JY, Fang ZH, Yu ZX, Wang CE, Li SH, Li XJ. Expression of mutant huntingtin in glial cells contributes to neuronal excitotoxicity. *J Cell Biol* 2005; **171**: 1001–1012.
15. Bradford J, Shin JY, Roberts M, Wang CE, Li XJ, Li S. Expression of mutant huntingtin in mouse brain astrocytes causes age-dependent neurological symptoms. *Proc Natl Acad Sci USA* 2009; **106**: 22480–22485.
16. Bradford J, Shin JY, Roberts M, Wang CE, Sheng G, Li S *et al.* Mutant huntingtin in glial cells exacerbates neurological symptoms of Huntington disease mice. *J Biol Chem* 2010; **285**: 10653–10661.
17. Conforti P, Camnasio S, Mutti C, Valenza M, Thompson M, Fossale E *et al.* Lack of huntingtin promotes neural stem cells differentiation into glial cells while neurons expressing huntingtin with expanded polyglutamine tracts undergo cell death. *Neurobiol Dis* 2013; **50**: 160–170.
18. Valenza M, Carroll JB, Leoni V, Bertram LN, Bjorkhem I, Singaraja RR *et al.* Cholesterol biosynthesis pathway is disturbed in YAC128 mice and is modulated by huntingtin mutation. *Hum Mol Genet* 2007; **16**: 2187–2198.
19. Spiliotopoulos D, Goffredo D, Conti L, Di Febo F, Biella G, Toselli M *et al.* An optimized experimental strategy for efficient conversion of embryonic stem (ES)-derived mouse neural stem (NS) cells into a nearly homogeneous mature neuronal population. *Neurobiol Dis* 2009; **34**: 320–331.
20. Pool M, Thiemann J, Bar-Or A, Fournier AE. NeuriteTracer: a novel ImageJ plugin for automated quantification of neurite outgrowth. *J Neurosci Methods* 2008; **168**: 134–139.
21. Jansen PJ, Lutjohann D, Thelen KM, von Bergmann K, van Leuven F, Ramaekers FC *et al.* Absence of ApoE upregulates murine brain ApoD and ABCA1 levels, but does not affect brain sterol levels, while human ApoE3 and human ApoE4 upregulate brain cholesterol precursor levels. *J Alzheimers Dis* 2009; **18**: 319–329.
22. Wahrle SE, Jiang H, Parsadanian M, Kim J, Li A, Knoten A *et al.* Overexpression of ABCA1 reduces amyloid deposition in the PDAPP mouse model of Alzheimer disease. *J Clin Invest* 2008; **118**: 671–682.
23. Herz J, Bock HH. Lipoprotein receptors in the nervous system. *Annu Rev Biochem* 2002; **71**: 405–434.
24. Miserez AR, Cao G, Probst LC, Hobbs HH. Structure of the human gene encoding sterol regulatory element binding protein 2 (SREBF2). *Genomics* 1997; **40**: 31–40.
25. Pfrieger FW. Role of glial cells in the formation and maintenance of synapses. *Brain Res Rev* 2010; **63**: 39–46.
26. Eroglu C, Barres BA. Regulation of synaptic connectivity by glia. *Nature* 2010; **468**: 223–231.
27. Hayashi H, Campenot RB, Vance DE, Vance JE. Glial lipoproteins stimulate axon growth of central nervous system neurons in compartmented cultures. *J Biol Chem* 2004; **279**: 14009–14015.

28. Goritz C, Thiebaut R, Tessier LH, Nieweg K, Moehle C, Buard I *et al.* Glia-induced neuronal differentiation by transcriptional regulation. *Glia* 2007; **55**: 1108–1122.
29. Buard I, Steinmetz CC, Claudepierre T, Pfrieger FW. Glial cells promote dendrite formation and the reception of synaptic input in Purkinje cells from postnatal mice. *Glia* 2010; **58**: 538–545.
30. Fan QW, Yu W, Gong JS, Zou K, Sawamura N, Senda T *et al.* Cholesterol-dependent modulation of dendrite outgrowth and microtubule stability in cultured neurons. *J Neurochem* 2002; **80**: 178–190.
31. Ilieva H, Polymenidou M, Cleveland DW. Non-cell autonomous toxicity in neurodegenerative disorders: ALS and beyond. *J Cell Biol* 2009; **187**: 761–772.
32. Tong J, Huang C, Bi F, Wu Q, Huang B, Liu X *et al.* Expression of ALS-linked TDP-43 mutant in astrocytes causes non-cell-autonomous motor neuron death in rats. *EMBO J* 2013; **32**: 1917–1926.
33. Ballas N, Lioy DT, Grunseich C, Mandel G. Non-cell autonomous influence of MeCP2-deficient glia on neuronal dendritic morphology. *Nat Neurosci* 2009; **12**: 311–317.
34. Lioy DT, Garg SK, Monaghan CE, Raber J, Foust KD, Kaspar BK *et al.* A role for glia in the progression of Rett's syndrome. *Nature* 2011; **475**: 497–500.
35. Di Malta C, Fryer JD, Settembre C, Ballabio A. Astrocyte dysfunction triggers neurodegeneration in a lysosomal storage disorder. *Proc Natl Acad Sci USA* 2012; **109**: E2334–E2342.
36. Furman JL, Sama DM, Gant JC, Beckett TL, Murphy MP, Bachstetter AD *et al.* Targeting astrocytes ameliorates neurologic changes in a mouse model of Alzheimer's disease. *J Neurosci* 2012; **32**: 16129–16140.
37. Tong X, Ao Y, Faas GC, Nwaobi SE, Xu J, Haustein MD *et al.* Astrocyte Kir4.1 ion channel deficits contribute to neuronal dysfunction in Huntington's disease model mice. *Nat Neurosci* 2014 Mar: 30.
38. Hughes EG, Elmariah SB, Balice-Gordon RJ. Astrocyte secreted proteins selectively increase hippocampal GABAergic axon length, branching, and synaptogenesis. *Mol Cell Neurosci* 2010; **43**: 136–145.
39. Karasinska JM, Rinninger F, Lutjohann D, Ruddle P, Franciosi S, Kruit JK *et al.* Specific loss of brain ABCA1 increases brain cholesterol uptake and influences neuronal structure and function. *J Neurosci* 2009; **29**: 3579–3589.
40. Jiang Q, Lee CY, Mandrekar S, Wilkinson B, Cramer P, Zelcer N *et al.* ApoE promotes the proteolytic degradation of Abeta. *Neuron* 2008; **58**: 681–693.
41. Cermenati G, Brioschi E, Abbiati F, Melcangi RC, Caruso D, Mitro N. Liver X receptors, nervous system, and lipid metabolism. *J Endocrinol Invest* 2013; **36**: 435–443.
42. Futter M, Diekmann H, Schoenmakers E, Sadiq O, Chatterjee K, Rubinsztein DC. Wild-type but not mutant huntingtin modulates the transcriptional activity of liver X receptors. *J Med Genet* 2009; **46**: 438–446.
43. Camargo N, Smit AB, Verheijen MH. SREBPs: SREBP function in glia-neuron interactions. *FEBS J* 2009; **276**: 628–636.
44. Verheijen MH, Camargo N, Verdier V, Nadra K, de Preux Charles AS, Medard JJ *et al.* SCAP is required for timely and proper myelin membrane synthesis. *Proc Natl Acad Sci USA* 2009; **106**: 21383–21388.
45. Camargo N, Brouwers JF, Loos M, Gutmann DH, Smit AB, Verheijen MH. High-fat diet ameliorates neurological deficits caused by defective astrocyte lipid metabolism. *FASEB J* 2012; **26**: 4302–4315.
46. Bjorkhem I. Do oxysterols control cholesterol homeostasis? *J Clin Invest* 2002; **110**: 725–730.
47. Cummings DM, Cepeda C, Levine MS. Alterations in striatal synaptic transmission are consistent across genetic mouse models of Huntington's disease. *ASN neuro* 2010; **2**: e00036.
48. Milnerwood AJ, Raymond LA. Early synaptic pathophysiology in neurodegeneration: insights from Huntington's disease. *Trends Neurosci* 2010; **33**: 513–523.
49. Orth M, Schippling S, Schneider SA, Bhatia KP, Talelli P, Tabrizi SJ *et al.* Abnormal motor cortex plasticity in premanifest and very early manifest Huntington disease. *J Neurol Neurosurg Psychiatry* 2010; **81**: 267–270.
50. Valenza M, Leoni V, Tarditi A, Mariotti C, Bjorkhem I, Di Donato S *et al.* Progressive dysfunction of the cholesterol biosynthesis pathway in the R6/2 mouse model of Huntington's disease. *Neurobiol Dis* 2007; **28**: 133–142.
51. Pfrieger FW. Role of cholesterol in synapse formation and function. *Biochim Biophys Acta* 2003; **1610**: 271–280.
52. Christopherson KS, Ullian EM, Stokes CC, Mullowney CE, Hell JW, Agah A *et al.* Thrombospondins are astrocyte-secreted proteins that promote CNS synaptogenesis. *Cell* 2005; **120**: 421–433.
53. Funfschilling U, Jockusch WJ, Sivakumar N, Mobius W, Corthals K, Li S *et al.* Critical time window of neuronal cholesterol synthesis during neurite outgrowth. *J Neurosci* 2012; **32**: 7632–7645.
54. Hulce JJ, Cognetta AB, Niphakis MJ, Tully SE, Cravatt BF. Proteome-wide mapping of cholesterol-interacting proteins in mammalian cells. *Nature methods* 2013; **10**: 259–264.
55. Nieweg K, Schaller H, Pfrieger FW. Marked differences in cholesterol synthesis between neurons and glial cells from postnatal rats. *J Neurochem* 2009; **109**: 125–134.
56. Ullian EM, Sapperstein SK, Christopherson KS, Barres BA. Control of synapse number by glia. *Science* 2001; **291**: 657–661.
57. Sodero AO, Vriens J, Ghosh D, Stegner D, Brachet A, Pallotto M *et al.* Cholesterol loss during glutamate-mediated excitotoxicity. *EMBO J* 2012; **31**: 1764–1773.
58. Taghibiglou C, Martin HG, Lai TW, Cho T, Prasad S, Kojic L *et al.* Role of NMDA receptor-dependent activation of SREBP1 in excitotoxic and ischemic neuronal injuries. *Nat Med* 2009; **15**: 1399–1406.
59. Aono M, Lee Y, Grant ER, Zivin RA, Pearlstein RD, Warner DS *et al.* Apolipoprotein E protects against NMDA excitotoxicity. *Neurobiol Dis* 2002; **11**: 214–220.
60. Paul SM, Doherty JJ, Robichaud AJ, Belfort GM, Chow BY, Hammond RS *et al.* The major brain cholesterol metabolite 24(S)-hydroxycholesterol is a potent allosteric modulator of N-methyl-D-aspartate receptors. *J Neurosci* 2013; **33**: 17290–17300.
61. del Toro D, Xifro X, Pol A, Humbert S, Saudou F, Canals JM *et al.* Altered cholesterol homeostasis contributes to enhanced excitotoxicity in Huntington's disease. *J Neurochem* 2010; **115**: 153–167.
62. Colella AD, Chegenii N, Tea MN, Gibbins IL, Williams KA, Chataway TK. Comparison of stain-free gels with traditional immunoblot loading control methodology. *Anal Biochem* 2012; **430**: 108–110.

Supplementary Information accompanies this paper on Cell Death and Differentiation website (http://www.nature.com/cdd)